NASA/CR—2017-219567

Screening of High Temperature Organic Materials for Future Stirling Convertors

Euy-sik E. Shin and Daniel A. Scheiman
Ohio Aerospace Institute, Brook Park, Ohio

October 2017

NASA STI Program . . . in Profile

Since its founding, NASA has been dedicated to the advancement of aeronautics and space science. The NASA Scientific and Technical Information (STI) Program plays a key part in helping NASA maintain this important role.

The NASA STI Program operates under the auspices of the Agency Chief Information Officer. It collects, organizes, provides for archiving, and disseminates NASA's STI. The NASA STI Program provides access to the NASA Technical Report Server—Registered (NTRS Reg) and NASA Technical Report Server—Public (NTRS) thus providing one of the largest collections of aeronautical and space science STI in the world. Results are published in both non-NASA channels and by NASA in the NASA STI Report Series, which includes the following report types:

- TECHNICAL PUBLICATION. Reports of completed research or a major significant phase of research that present the results of NASA programs and include extensive data or theoretical analysis. Includes compilations of significant scientific and technical data and information deemed to be of continuing reference value. NASA counter-part of peer-reviewed formal professional papers, but has less stringent limitations on manuscript length and extent of graphic presentations.

- TECHNICAL MEMORANDUM. Scientific and technical findings that are preliminary or of specialized interest, e.g., "quick-release" reports, working papers, and bibliographies that contain minimal annotation. Does not contain extensive analysis.

- CONTRACTOR REPORT. Scientific and technical findings by NASA-sponsored contractors and grantees.

- CONFERENCE PUBLICATION. Collected papers from scientific and technical conferences, symposia, seminars, or other meetings sponsored or co-sponsored by NASA.

- SPECIAL PUBLICATION. Scientific, technical, or historical information from NASA programs, projects, and missions, often concerned with subjects having substantial public interest.

- TECHNICAL TRANSLATION. English-language translations of foreign scientific and technical material pertinent to NASA's mission.

For more information about the NASA STI program, see the following:

- Access the NASA STI program home page at http://www.sti.nasa.gov

- E-mail your question to help@sti.nasa.gov

- Fax your question to the NASA STI Information Desk at 757-864-6500

- Telephone the NASA STI Information Desk at 757-864-9658

- Write to:
  NASA STI Program
  Mail Stop 148
  NASA Langley Research Center
  Hampton, VA 23681-2199

NASA/CR—2017-219567

Screening of High Temperature Organic Materials for Future Stirling Convertors

Euy-sik E. Shin and Daniel A. Scheiman
Ohio Aerospace Institute, Brook Park, Ohio

Prepared under Contract NNC13BA10B

National Aeronautics and
Space Administration

Glenn Research Center
Cleveland, Ohio 44135

October 2017

Acknowledgments

This report presented an overview of extensive work started at 2012 which involved numerous dedicated collaborators and contributors of whom are greatly appreciated by the authors. They include Paula Heimann and Andrew Ring from Ohio Aerospace Institute/NASA Glenn Research Center (GRC) on-site contractor; Chris Burke from SLI/GRC on-site contractor, D. Jordan McCrone, GRC LMA/VPL; Robert Pelaez, Sal Oriti from GRC; Tim Ubienski, Tony Kapucinski, GRC FTH/SLI; Mike Gorbulja from KOL-CAP Manuf.; Kerry Arnold, Cliff Fralick et al., from Sunpower, Inc.; Mike Booker, CTL Inc.; Steve Hassman, Long-Lok Corporation; and Samuel Slingluff, summer interns at GRC. The authors also thank Scott Wilson, Wayne Wong, Terry O'Malley, Jim Withrow, Lee Mason for project guidance and management, and a special thanks to Tiffany S. Williams for reviewing various reports and this paper. This work has been sponsored by the GRC RPS program office with funding from Science Mission Directorate (SMD).

Available from

NASA STI Program
Mail Stop 148
NASA Langley Research Center
Hampton, VA 23681-2199

National Technical Information Service
5285 Port Royal Road
Springfield, VA 22161
703-605-6000

This report is available in electronic form at http://www.sti.nasa.gov/ and http://ntrs.nasa.gov/

Contents

Screening of High Temperature Organic Materials for Future Stirling Convertors

Euy-sik E. Shin and Daniel A. Scheiman
Ohio Aerospace Institute
Brook Park, Ohio 44142

Abstract

Along with major advancement of Stirling-based convertors, high temperature organics are needed to develop future higher temperature convertors for much improved efficiencies as well as to improve the margin of reliability for the current SOA convertors. The higher temperature capabilities would improve robustness of the convertors and also allow them to be used in additional missions, particularly ones that require a Venus fly by for a gravity assist. Various organic materials have been employed as essential components in the convertor for their unique properties and functions such as bonding, potting, sealing, thread locking, insulation, and lubrication. The Stirling convertor radioisotope generators have been developed for potential future space applications including Lunar/Mars surface power or a variety of spacecraft and vehicles, especially with a long mission cycle, sometimes up to 17 years, such as deep space exploration. Thus, performance, durability, and reliability of the organics should be critically evaluated in terms of every possible material structure-process-service environment relations based on the potential mission specifications. The initial efforts in screening the high temperature candidates focused on the most susceptible organics, such as adhesive, potting compound, o-ring, shrink tubing, and thread locker materials in conjunction with commercially available materials. More systematic and practical test methodologies that were developed and optimized based on the extensive organic evaluations and validations performed for various Stirling convertor types were employed to determine thermal stability, outgassing, and material compatibility of the selected organic candidates against their functional requirements. Processing and fabrication conditions and procedures were also optimized. This report presents results of the three-step candidate evaluation processes, their application limitations, and the final selection recommendations.

Nomenclature

ATR	attenuated total reflectance
BC	baked-control
C_B	compression set expressed as percentage of the original deflection
CHS	cross head speed
CS	cross section
ΔH_R	residual heat of reaction or transition/cure
ΔH_T	total heat of reaction or full cure
Δl	displacement in lap shear test
DAQ	data acquisition
DMA	dynamic mechanical analysis
$\Delta\sigma$	static strength, extrapolated strength from initial SN curve, psi
ΔWt%	weight change in percent
E' or G'	tensile or shear storage modulus from DMA
E_Y	Young’s modulus

E_T	tangent modulus
ε	strain or elongation
ε_f	strain-to-failure or ultimate elongation
FT-IR	Fourier transform-infrared spectroscopy
FS	fatigue strength
GC/TCD	gas chromatography/thermal conductivity detector
GSC	gas sampling cylinder
H	overlap height of lap shear specimen
HT	high temperature
ID	inside or inner diameter
mDSC	modulated differential scanning calorimetry
MS	mass spectroscopy
Mw	molecular weight
OD	outside or outer diameter
sOM	stereo optical microscopy
PET	polyethylene terephthalate
PV	pressure vessel
RGA	residual gas analysis
RT	room temperature
RVDT	rotary variable differential transformer
SDA	synergistic durability aging
SDLT	synergistic durability life testing
SN	stress-number of cycle at failure
SOA	state-of-the-art
SOP	Standardized Operating Procedure
ST	shrink tubing
σ_f	tensile strength
T	temperature or bondline thickness of lap shear specimen
T_β	sub T_g transition temperature
T_d	thermal degradation on-set temperature
T_{end}	endothermic peak temperature
T_{exo}	exothermic peak temperature
T_g	glass transition temperature
T_m	melting temperature
$T_{\max}$	maximum temperature
T_r	relaxation temperature
T_t	transition temperature
TCIOP	temperature-alone combined in-situ outgassing with premix gas
TGA	thermogravimetric analysis
TL	thread locker
TMA	thermomechanical analyzer
TML	total mass loss
UHP	ultra high purity, 99.999w%

1.0 Introduction

Development of the Stirling radioisotope generator has been a key part of recent NASA's Radioisotope Power Systems (RPS) Program mainly due to its high fuel efficiency (Refs. 1 and 2). For the latest SOA advanced generator designed and manufactured under the joint sponsorship of the Department of Energy (DOE) and NASA, Lockheed Martin Corporation of Valley Forge, NASA Glenn Research Center (GRC), and Sunpower, Inc., reliability and durability of every components and materials used in the convertor have been extensively and systematically evaluated for a potential flight hardware development, subsequently the organic materials used were successfully validated for such convertor application (Refs. 3 to 6). Even though the flight project was terminated prematurely due to budget constraints, the overall successful performance demonstrations of the system encouraged NASA to continue the development of Stirling RPS technology, especially for higher temperature and more efficient convertors for future space science and exploration missions. As a part of this continued development activities at GRC, selection of potential high temperature organic materials was initiated.

In a typical convertor, various organic materials have been used for specific functional requirements, such as adhesives for bonding and potting, thread locking compounds for fasteners, shrink tubing for electrical insulations, o-rings for sealing, and lubrication or frictionless coatings and so on. While they had been used successfully for the current SOA convertors, due to their inherent susceptibility to temperature and radiation as well as less predictable time-dependency on their properties and performance, a new class of organic materials has to be selected for upcoming high temperature convertors, targeting long-term use at ~ 165 °C or higher. Their selection should be particularly focusing on thermal stability, durability, radiation hardness, outgassing behavior, and synergistic effects of various combined in-service conditions. Typically, thermal stability and durability of the organics were assessed by accelerated thermal aging experiments at a few elevated temperatures in conjunction with longer-term life testing. The rate of aging processes was normally accelerated by temperature, thus temperature was often used as an accelerator for the accelerated aging test to predict longer term thermal stability of the organics. However, it could be only valid when the degradation mechanisms were not altered within the test temperature range. Systematic and practical test methodologies developed and optimized based on the extensive organic evaluations and validations performed for various Stirling convertor types for more than a decade (Refs. 6 to 11) were employed to determine thermal stability, radiation hardness, outgassing, and material compatibility of the selected organic candidates in terms of their functional requirements while their process and fabrication conditions and procedures were also being optimized. Figure 1 shows the overall program plan employed in selecting the best high temperature organic candidates with the optimized test methodologies. For the four most susceptible organics identified for the initial phase of the program, the plan has been completed up to the final candidate selection, but the SDLT step has been postponed due to replanning of the overall Stirling technology development research at GRC. The test results and key findings to date are discussed in this report in the sequence of the program steps for every organic material types.

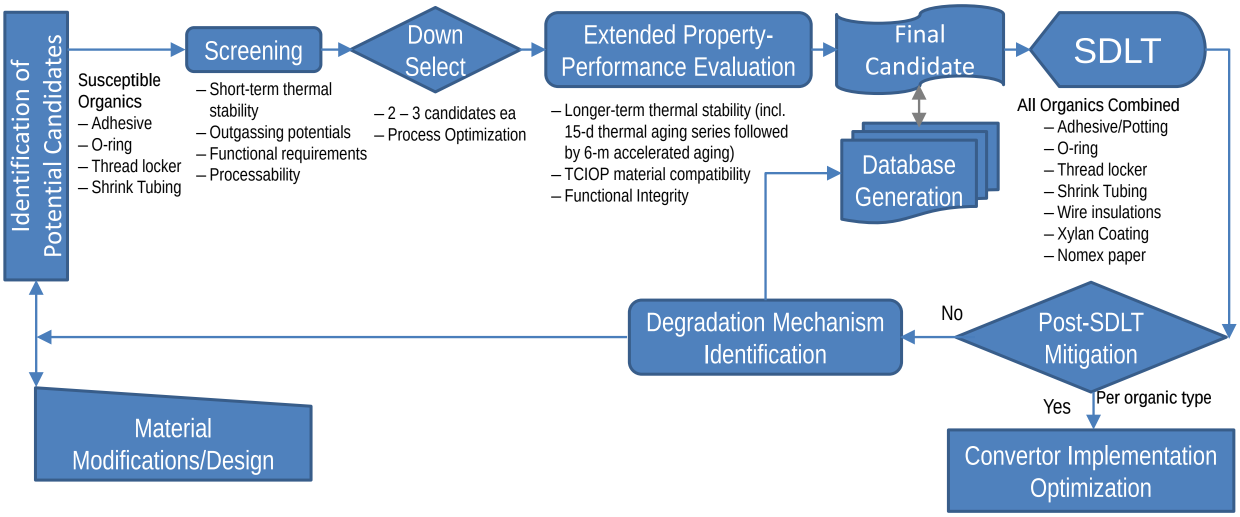

Figure 1.—Overall program plan to down-select high temperature organic materials.

2.0 Materials

The initial efforts in screening the high temperature candidates focused on the most susceptible organics, such as adhesive, potting compound, o-ring, shrink tubing, and thread locker. Initially targeting long-term use at ~ 165 °C or higher, several potential candidates per organic material type were identified from commercially available products that were mostly based on the manufacturer's data sheet or recommendations, in terms of maximum use temperature, processing/installation temperature, and processability. All materials investigated are summarized in Table 1.

Adhesive/potting candidates were either processed in a hot press or autoclave after conventional vacuum-bagging. The standard cure conditions initially employed were based on manufacturer's recommendations as summarized in Table 2. The two part Hysol EA9394C-2 epoxy was mixed in a Thinky mixer (ARE-250, THINKY CORP) using the following conditions: 1 min hand mixing; 3 min defoaming at 2200 rpm; 3 min mixing at 2000 rpm for ~6 gram total in 12 mL jar, which was the optimum mixing condition determined for the regular EA9394 epoxy previously in terms of void content, thermal properties, and bonding performance. For adhesive/potting materials, various sheet samples were fabricated using a hot-press with the standard or optimized cure/postcure conditions, typically including a thick (~ 1.5 mm), a thin (~0.1 mm), or thin sample laminated between a metal substrate, to mimic the potting or bonding application. The laminated thin film specimens were fabricated by vacuum-bagging and autoclave cure. However, for the AF131-2 epoxy which was only available in the scrim (Style 1299 Glass cloth, 0.082 - 0.10 oz/yd^2, ~ 2 mils thick) supported film adhesive form, the neat resin was squeezed out from a 20-ply stack of the film adhesive first at 90 to 100 °C based on the experimentally determined viscosity-temperature-cure relation, Figure 2. The neat resin was then degassed at 100 °C under 28 inHg vacuum and molded to the sheet samples for more controlled characterizations and meaningful comparisons between both candidates without interferences, such as weight or thermal property changes from the scrim material. The sheet samples were typically used for most physical-thermal property measurements, but for mechanical properties, more sophisticated test specimens were designed.

TABLE 1.—LIST OF COMMERCIAL CANDIDATES IDENTIFIED FOR EACH ORGANIC TYPE

Organic type	Material	Brand	Maker	Max. T, °C	Install T, °C	Product properties
Adhesive/ Potting	Epoxy	Hysol EA9394C-2	Henkel	232	93 +115	Two part epoxy paste filled with aluminum particle, long pot-life (8 hr at 25 °C)
	Cyanate ester	FM2555	Cytec	232	177 +227	Supported film adhesive on structural carrier,0.06 psf film
	Cyanate ester	RS-4A	YLA		177	Unsupported film adhesive, 0.03 psf film
	Epoxy	L-313U	JD Lincoln	204	135+213	Unsupported film adhesive, 0.05 psf film
	Epoxy	AF191K AF191U	3M	204	177 + 204	Supported (0.08 psf) and unsupported (0.055 psf) film adhesive
	Epoxy	AF131-2	3M	232	177	Flexible scrim supported film adhesive, 0.075 psf
Thread Locker	Dimethacrylate ester	Loctite 266	Henkel	232	25–40	One part, surface insensitive, high strength, high temperature anaerobic thread locking material
	Dimethacrylate ester	Loctite 294	Henkel	204	25–40	One part, low viscosity, high temperature anaerobic thread locking and sealing material
	Epoxy	Resbond 507TS	Cotronics	260	25	Two parts epoxy-based thread locker and sealant but filled with PTFE particle for lubricity
	Ceramic	Resbond 907TS	Cotronics	1148	25 + 121	Water based proprietary material, cured by moisture removal
	Polyethylene terephthalate	Poly-Lok Patch	Long-Lok Fasteners	204	25	Solidified plastic locker patched on fasteners at predetermined locations with optimum amount
Shrink tubing	Polyimide	208X	Dunstone	220–400	350	Shrink ratio > 1.12:1, highest temperature shrinkable film commercially available
	PEEK	PEEK	ZEUS	260	330	Shrink ratio > 1.4:1, excellent abrasion resistance and radiation resistance
	Teflon copolymer	PFA	ZEUS	260	340	Shrink ratio > 1.4:1, improved thermal stability and radiation resistance
	ETFE	RT-555	Raychem	200	220	Shrink ratio > 2:1, extremely resistant to hydrocarbons, low outgassing
	Silicone	SRFR	Raychem	200	175	Shrink ratio > 1.5:1, extremely flexible
O-ring	Silicone	70SLR	Marco	200	N/A	Baseline material for current SOA convertors
		S1151	Marco	315	N/A	High temperature formulation
	Perfluoroelastomer/ Fluorocarbon Rubber (FFKM)	Kalrez	DuPont	260	N/A	Excellent chemical and temperature resistance
		Markez Z1028	Marco	300	N/A	Black, excellent chemical compatibility and high temperature capabilities
		Markez Z1307	Marco	275	N/A	Translucent, semi-crystalline nano-filled, low out-gassing, high temp capabilities

TABLE 2.—STANDARD CURE CONDITIONS OF ADHESIVE CANDIDATES

Candidate	Cure condition				Postcure condition		Heating rate, °C/min
	Temperature, °C	Pressure, psi	Vacuum, inHg	Time, hr	Temperature, °C	Time, hr	
EA9394C-2	93	45	15	1	115	2	2.8
FM2555	177	45	26	4	227	2	2.8
RS-4A	177	45	15	2	232	6	2.8
L-313U	135	45	26	3	213	5	2.8
AF191K or U	177	45	26	1	204	4	2.8
AF131-2	177	45	26	1.5	N/A	N/A	2.8

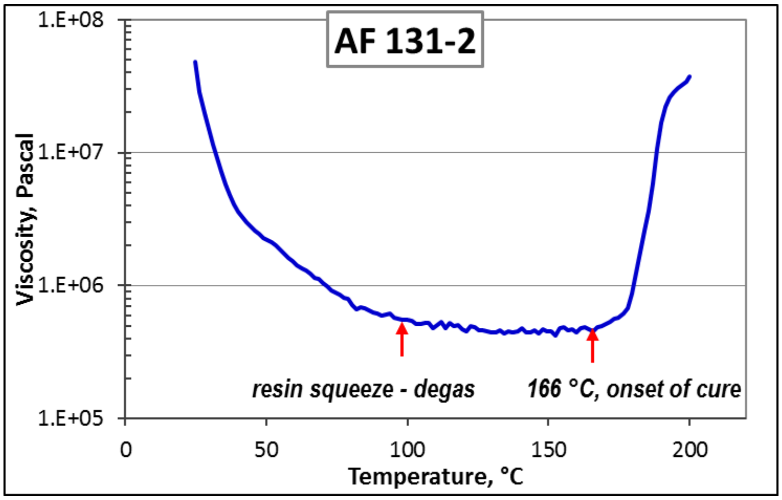

Figure 2.—Typical viscosity-temperature relation of AF131-2 adhesive.

The optimum cure conditions of the TL candidates were determined during their initial screening evaluations and down-selection. It should be noted that the Loctite 266 and 294 from Henkel were a one-part anaerobic cure system in which cure initiates by contact with metallic ions when confined in the absence of air between close fitting metal surfaces. Other materials were either thermally cured or cured by moisture removal or patched thermoplastic.

Shrink tubing materials were received in expanded form but were tested in fully recovered or shrunken form. Typical test samples were 3/16-in. OD by 1.12-in. (30 mm) long sections and shrunk snugly without metal core. A loose fit was recommended by manufacturers using the optimized conditions determined during their initial screening evaluations and down-selection.

All o-ring samples were tested as purchased. The type of o-ring used was AS568-013; Nominal, 7/16-in. ID by 9/16-in. OD by 1/16-in. CS (actual, 0.426-in. ID by 0.070-in. CS).

3.0 Experimental

3.1 Material Property Testing

Extensive material properties and behavior of the organics were systematically monitored and characterized not only for comparison among the candidates, but also to identify the degree of degradation and mechanisms involved in various thermal aging experiments. Most properties were identified by their performance or functional requirements of the organic materials, and were categorized by (i) physical properties; (ii) thermal properties; (iii) molecular/chemical structural properties; and (iv) mechanical properties. It should be noted that in the case of the 6-month accelerated thermal aging experiment, typically the samples of the controls, 15-, 50- and 100-day aging were tested all together at the same time right after the 100-day aging while the 180-day samples were tested at the end of the aging. This was to minimize unwanted effects of instrument baseline calibration and other test variations, especially for those properties sensitive to testing time and conditions, thus to improve consistency while minimizing in delay of test schedule.

3.1.1 Physical Properties

Changes in weight, dimension, color, and surface morphology or microstructure of test specimens were systematically monitored after various thermal aging or TCIOP exposures.

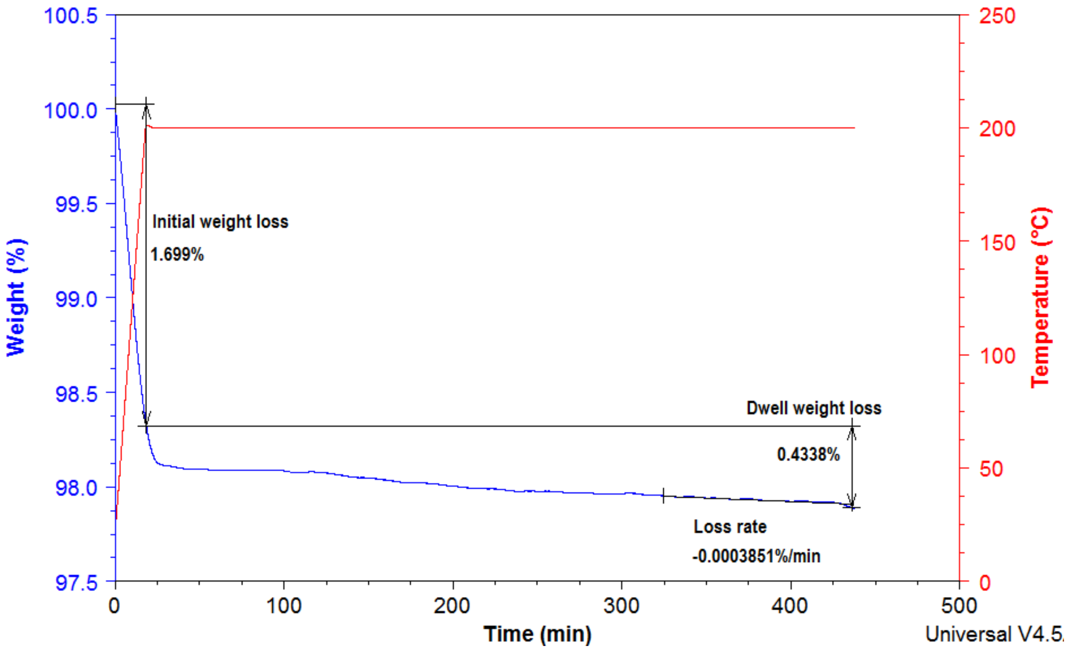

Figure 3.—Typical plot of the isothermal TGA scan showing three outgassing characteristics.

3.1.2 Thermal Properties

Typical thermal properties monitored were T_m, T_g, T_β, T_r, T_t, T_{end}, T_{exo}, and ΔH by mDSC or DMA; storage modulus and loss modulus as a function of temperature by DMA; T_d by TGA and various weight loss characteristics, such as Δwt% occurring from RT to 100 °C normally due to evaporation of water, from 100 to 200 °C which is typically associated with thermally-induced outgassing, or from RT to 700 °C representing char yield. Other outgassing characteristics observed by isothermal TGA analyses included Δwt% during the temperature ramp, Δwt% during the 7 hr dwell, and weight loss rate calculated at the last 100 min of the test as shown in Figure 3. The weight loss and outgassing characteristics were presented in terms of a normalized weight by the outgas-able phase, typically Δwt% at 700 °C from that of a normal TGA scan for more practical and meaningful comparison. These outgassing characteristics from various organic materials were comparable to the ASTM outgassing database, thus used initially for acceptability in the Stirling convertor applications. TGA and mDSC were typically run under dry nitrogen at a heating rate 5 and 10 °C/min, respectively, while DMA was run under air at 5 °C/min heating rate. In the case of the adhesives, the degree of cure or % cure was calculated by the residual ΔH of their exothermic peak based on the ΔH_T.

3.1.3 Molecular Structural Properties

In most cases, FT-IR in ATR mode was used to assess the changes in molecular structure. For the specimens with controlled thicknesses, the IR spectra were quantified via intensities of the peaks. In the case of the TL materials, a noncontact IR scanning method via reflection mode (Nicolet NEXUS 670 with Thermo Nicolet Continuum microscope) was employed on the fasteners that were removed from the torque specimen assembly after torque testing since ATR mode was not suitable. The noncontact IR scanning via reflection mode had a zooming capacity up to ~200X. Semi-quantitative assessment of thermal degradation and molecular structural changes were monitored mostly via IR peak shape and location analyses.

3.1.4 Mechanical Properties

Mechanical tests of various candidate materials were designed primarily based on their functional requirements.

3.1.4.1 Adhesive

Bonding performance of adhesive candidates was measured by either component-size full-scale coupons or subscale specimens mimicking the actual magnet to magnet-can bond (Refs. 6, 8, and 9).

3.1.4.1.1 Full-Scale Bond Strength

Full-scale test specimens were designed for the actual curved magnets and to simulate either pure shear stress state or normal stress state. Figure 4 illustrates the custom-designed Flat-wise Tension (FWT) specimens and tubular shear specimen assemblies (typically six magnets per tube) for determining normal tensile and shear bond strength, respectively. Both full-scale specimens were employed mostly for the initial screening and down-selection of the candidates while the tubular specimens were also used for the functional fatigue performance testing of the down-selected candidates. Fabrication details including surface treatment of both magnet and titanium (Ti-6Al-4V grade) substrates, preparation and application of adhesives followed the standardized conditions and procedures developed by a SOA convertor manufacturer and GRC collaboration. Special fixtures were used for accurate alignment of magnets in the specimens. All test specimens were fabricated at GRC via vacuum-bagging and autoclave cure followed by the standard cure and postcure cycles without further bake-out. Most mechanical testing of the full-scale specimen in either static or fatigue mode was performed at CTL (Cincinnati, OH). Figure 5 shows

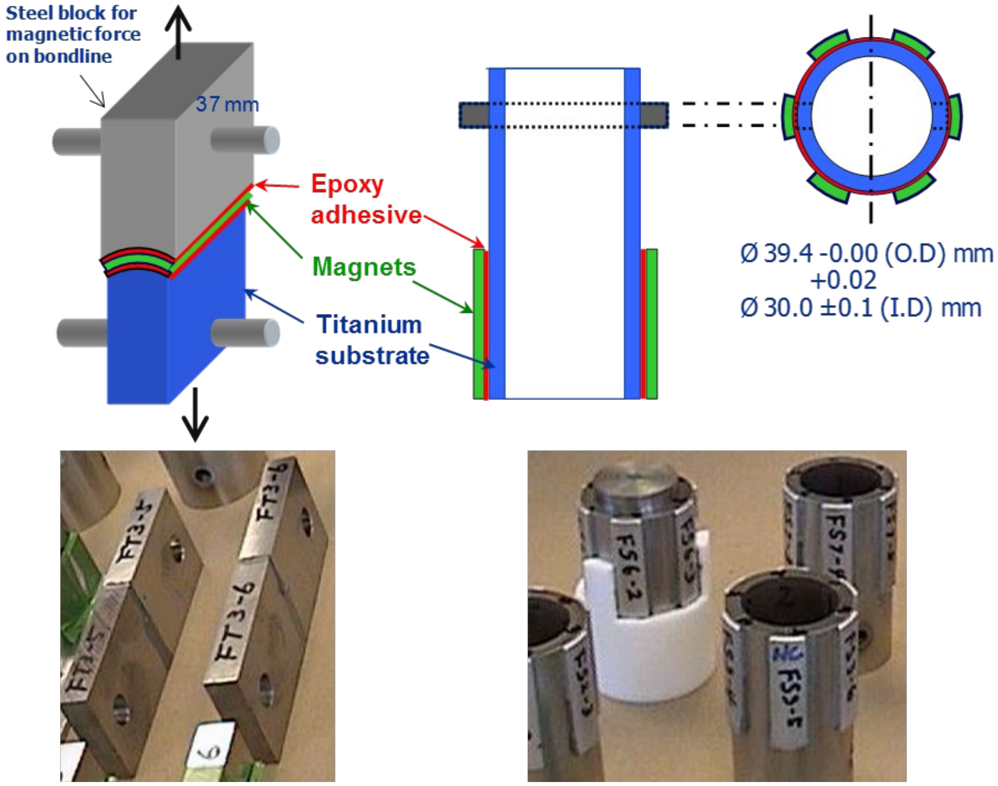

Figure 4.—Schematics and pictures of full-scale test specimens for bonding performance measurement of adhesive materials: FWT specimens on left side, Tubular shear assemblies (six test specimens per tube) on right side.

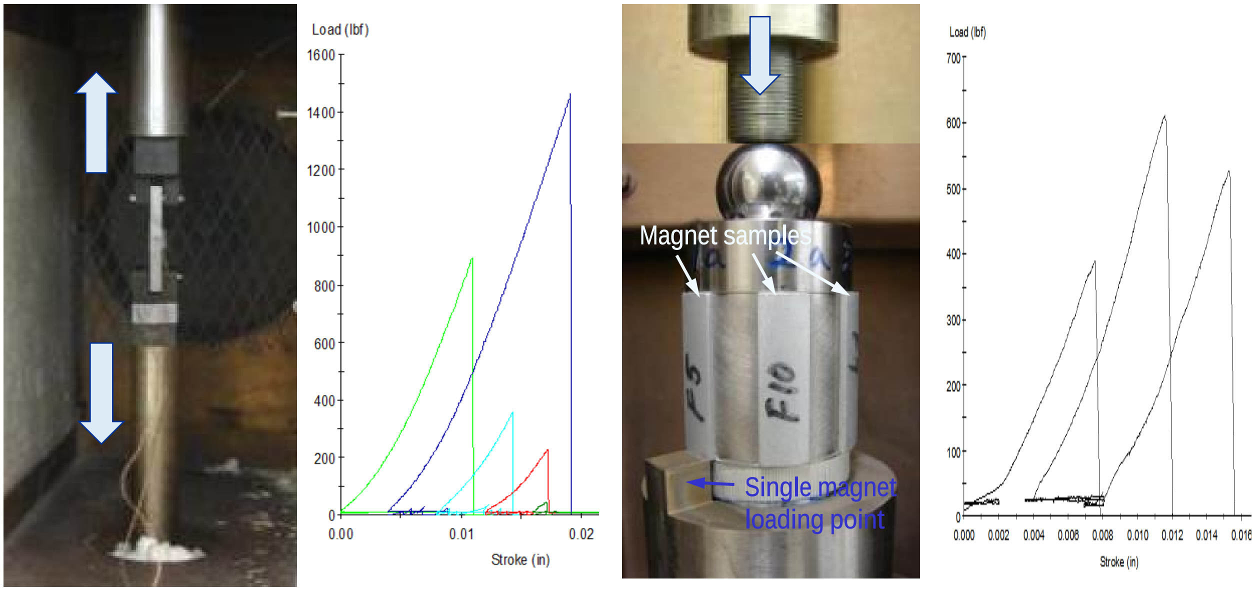

Flat-wise Tension (FWT)

Tubular Shear w/ single magnet testing

Figure 5.—Test set-up and typical load-stroke curves for FWT and tubular shear testing.

the test set-ups at CTL and typical static load-stroke curves of the FWT specimen at 176 °F with 0.02 in./min cross-head displacement (CHD) and from the tubular shear specimen at 248 °F with 0.02 in./min CHD. The tubular shear specimens were also used for fatigue testing. All fatigue tests were conducted isothermally at 180 °C using sinusoidal loading with a minimum load of 15 lbf at 20 Hz frequency. The goal of fatigue testing was to build the master SN (Stress- number of cycle at failure) curve, and about 50 to 100 million cycles was targeted for the maximum number of cycle if no failure had occurred. It should be noted that only two magnet specimens were involved per tube assembly for fatigue testing in order to avoid accumulated thermal exposure resulting in premature thermal degradation-induced failure.

3.1.4.1.2 Sub-Scale Bond Strength

In order to minimize various constraints in fabrication and testing of the full-scale specimens for a large test matrix involved in the extended property-performance evaluations of the candidates, the sub-scale test specimen was designed based on the single lap shear geometry but inserting a section of magnet material between the titanium substrates, thus introducing a sandwiched bondline between the magnet and titanium to represent the actual magnet bonding in a typical Stirling convertor, Figure 6. It is imperative to note that while its advantages involved simplistic fabrication and testing, it might not produce absolute bonding properties of the adhesives but rather comparable and statistical trends of the properties as a function of material or test variables due to the end effects of the relatively small overlap area in the subscale specimen. As also shown in the figure, custom-designed stainless steel molds were used to fabricate a large number of specimens, 44 specimens per batch per each standardized vacuum-bagging and autoclave curing process.

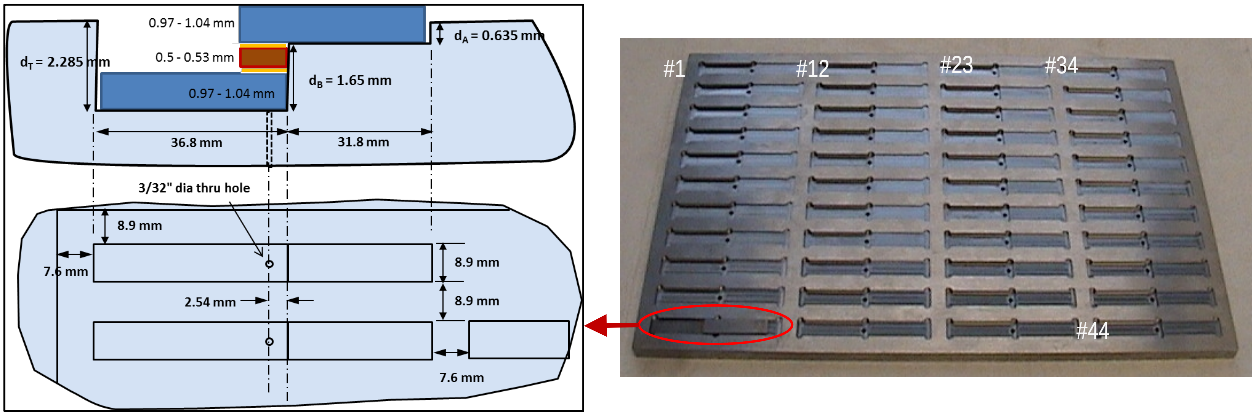

Figure 6.—Schematic diagram of subscale lap shear specimen with dimensions and picture of stainless steel molding fixture.

About 500 lap shear specimens were needed for the aging tests per candidate, i.e., total of 1,000 lap shear specimens were fabricated in 23 batches. Descriptions of the batch and specimen nomenclature are as follows: Epoxy type, i.e., ‘C’ for EA9394C-2 vs. ‘A’ for AF131-2 + ‘Batch #’ + Mold used, ‘A’ or ‘B’ + Specimen #, 1 through 44 starting from the marked left top to right bottom, e.g., C7A1 stands for Hysol, 7th batch with mold ‘A’, specimen #1, thus that fabrication history of each specimen can be tracked down if needed. Adhesives were applied on both surfaces of magnet insert and titanium substrates. Typical bondline thickness of the lap shear specimen was 0.12 ± 0.02 mm for EA9394C-2 and 0.13 ± 0.03 mm for AF131-2, averaged from 500 specimens each. It should be noted that the subscale lap shear specimens used for the 15-day short-term thermal aging experiment were fabricated in the molds made of PTFE Teflon, and their typical bondline thickness was 0.13 ± 0.01 mm for EA9394C-2 and 0.11 ± 0.02 mm for AF131-2, averaged from 156 specimens each which turned out to be slightly different than those from the stainless steel mold. The stainless steel molds were introduced since the Teflon molds were badly warped and deformed after repeated use at the cure temperature and pressure. For the stainless steel molds, it required to use a mold release, “Monocoat”.

Static lap shear testing was performed on a screw-driven Instron frame equipped with temperature chamber using an alignment fixture in an edge grip. Typical test conditions employed were 0.05 in./min CHD, ~ 30 mm grip-to-grip separation, ~ 10 min temperature stabilization if tested at elevated temperature. Six or more repeats per each aging and test conditions were tested for the average values. Bonding integrity was evaluated by both the shear bond strength and a strain term-to-failure or toughness-term which were calculated by the following formula: F/A and $\Delta l/h/t$, respectively, where F is force applied, A is overlap area, Δl is cross-head displacement, h is overlap height, and t is average bond line thickness of both sides. More accurate measurements of the overlap area of each lap shear specimen was made from imaging the fracture surface using sOM.

For the 6-month accelerated thermal aging experiment, the subscale lap shear specimens were used for both static and fatigue bond strength tests. Two table top fatigue testers (ElectroForce model 3200 from BOSE or currently TA Instruments) equipped with a hot/cold chamber were used for fatigue testing of the subscale sandwich lap shear specimens. Typically about 14 specimens were employed to build a fatigue SN curve as indicated in Table A.10 in Appendix A. The test conditions were similar to those used in the full-scale testing, but more specifically, isothermal fatigue at 175 °C, under sinusoidal loading with the minimum load of 10 N at 100 to 200 Hz frequency. The load levels for the assigned specimens were determined based on the static strength of the lap shear specimen at the test temperature

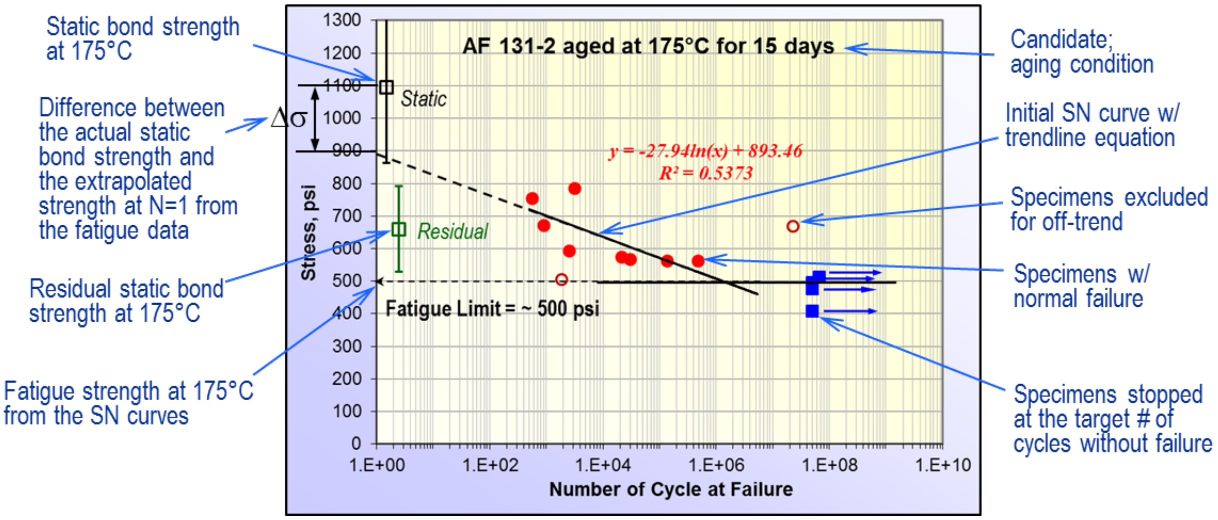

Figure 7.—Typical fatigue SN curve developed for adhesive bonding using subscale lap shear specimens and standardized interpretation of a data set.

and used consistently for various aging conditions. The target max number of cycles was again 50 to 100 million cycles. This target number was verified by a special fatigue test using the EA9394C-2 sample aged for 100 days at 225 °C at the load level near its fatigue strength determined by the target values. The validation test completed up to 250 million cycles without failure. Figure 7 shows a typical SN curve of the adhesive bonding developed by the subscale lap shear specimens with various properties and data analysis protocols. Static bond strength at 175 °C was obtained by curve fitting of the static test results. The residual static bond strength was determined from the samples that were fatigued and terminated at 175 °C to quantify the potential fatigue-induced degradation of bonding integrity.

3.1.4.2 Thread Locker

3.1.4.2.1 Torque Strength

Torque strength was the primary mechanical property monitored for evaluating thread locker candidates. Since there were many different types of joints involved in a typical Stirling convertor, efforts were made to determine torque strengths in a few representative joint systems, such as the magnet-can to piston in a blind-hole configuration, displacer spring to spring standoff in a through-hole configuration, and flex rod to displacer end or to displacer end in through-hole configuration, as a function of temperature. After torque testing, microscopic failure mode and IR microscopy chemical analyses were conducted to determine changes in the molecular structures or thermal degradation with respect to the aging time and temperature. Design of torque specimen assemblies is illustrated in Figure 8. The mating parts and washers were made of the same materials and followed the same dimensions and configurations as the actual convertor components assembled with the fasteners, Table 3. The actual fasteners fabricated for a recent SOA convertor were used in this study. The design torques listed in the table were calculated for the SOA convertor and used for this task as the actual installation torque.

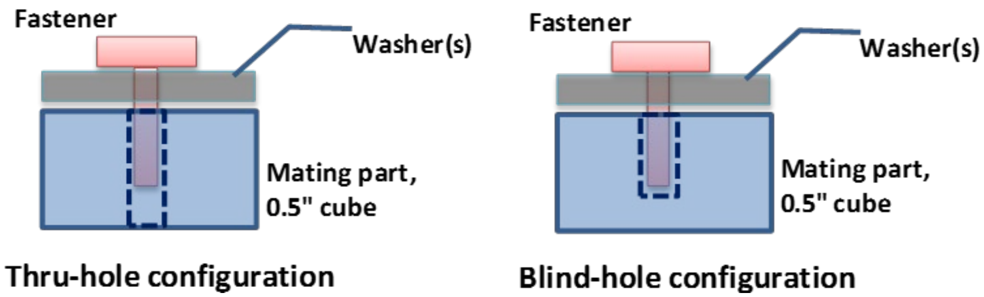

Thru-hole configuration

Blind-hole configuration

Figure 8.—Schematic diagrams of torque specimen assemblies per hole configuration

TABLE 3.—SPECIFICS OF FASTENERS, WASHERS, AND MATING PARTS USED IN TORQUE SPECIMEN ASSEMBLIES

Joint type	Fastener type			Mating part (female thread)				Hole conf.
	Where	Material	Design torque, N-cm	Material	Clearance (washer) material and thickness, mm		Contact length, mm	
#2	Magnet can to piston	SS316	36.8 ±2.2	4032-T6 AL	7075 Al (1.0) top; Ti-6Al-4V (1.5) bottom	2.50	3.50	Blind
#6	Planar displacer spring to spring standoff	SS416/C4-70	76.4 ±4.6	Ti-6Al-4V	4130 Steel (1.88) top; Ti-6AL-4V (1.9) bottom	3.78	2.22	Through
#7	Flex rod to end spring	SS416	74.5 ±4.5	SS316	4130 Steel (1.88)	1.88	7.45	Through
#8	Flex rod to displacer end	SS416	13.0 ±0.8	IN718	N/A	0.00	3.37	Through

TABLE 4.—AVERAGE AMOUNT OF THREAD LOCKER APPLIED ON VARIOUS JOINT TYPETORQUE ASSEMBLIES USED FOR 15-DAY THERMAL AGING TESTS

	Joint type	 #2	 #6	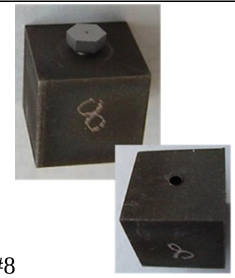 #8
Average weight of TL applied,[a] grams	Loctite 294	0.0043 ± 0.002	0.0081 ± 0.002	0.0062 ± 0.002
	Resbond 507TS	0.0073 ± 0.003	0.014 ± 0.003	0.0082 ± 0.001
	Poly-Lok PET	0.0006 ± 0.0007	0.0011 ± 0.0004	N/A

[a] The amount of threadlocker was not accurately controlled, but typically applied excessively based on manufacturer's recommendation.

Detailed step-by-step installation procedure was developed based on the standard procedure implemented by the manufacturer of the recent SOA convertor. All parts were cleaned with solvents (acetone followed by isopropyl alcohol) via sonication for 20 min each, then dried. All TL candidates used in this study were commercial batches within expiration dates. In all cases, TL was applied on both fastener and cube threads with either a plastic toothpick brush or via dipping. The installation torques were applied using calibrated torque wrenches. The assemblies were then cured at room temperature for 24 hr followed by 24 hr at 80 °C. Table 4 shows pictures of the complete torque specimen assemblies and the average amount of TL applied on each joint type per candidate prepared for the 15-day thermal aging experiment. As can be seen in the pictures of the torque assemblies, the mating cubes were engraved with two ID numbers on two consecutive side faces which indicate the joint type and sample number, respectively. Thus, their fabrication history including date of fabrication, cure status, and the amount of TL applied can be tracked down when needed.

The average TL amount applied on the torque assemblies made for the 6-month accelerated thermal aging experiment was considerably smaller but more consistent than those for the 15-day aging experiment, Table 5. However, in all cases, the amount applied for this studies was much greater than the theoretical amount calculated, typically 0.0006 grams, for the recent SOA convertor. However, it was proved in our previous investigation that the more was not necessarily bad for locking performance (Ref. 6).

Torque strength testing was conducted on the test setup built on the table-top MTS torsion test frame (Model 858, A/T #4) consisting of high resolution torque load cell (280 N-cam capacity with ±0.5 N-cm resolution), axial tension/compression load cell, custom designed sample holder fixtures for various fastener types, and custom designed air-circulated oven rated to 300 °C, Figure 9. The overall setup complied the BS EN 15865 Standard. Outputs from all transducers including torque cell, axial load cell, and RVDT or angular displacement device were digitally read and stored into the designated computer hard drive by MTS Flex Test SE controller and DAQ system.

TABLE 5.—AVERAGE AMOUNT OF THREAD LOCKER APPLIED ON VARIOUS JOINT TYPE TORQUE ASSEMBLIES USED FOR 6-MONTH ACCELERATED THERMAL AGING TESTS

	Joint type	#2	#6	#7	#8
Average weight of TL applied,[a] grams	Loctite 294	0.0026 ± 0.0006	0.0076 ± 0.0024	0.0041 ± 0.0009	N/A
	Resbond 507TS	0.0033 ± 0.0006	0.0044 ± 0.0008	0.0092 ± 0.0021	N/A
	Poly-Lok PET	0.0015 ± 0.0012	0.0010 ± 0.0004	N/A	0.0026 ± 0.0033

[a] The amount of threadlocker was not accurately controlled, but typically applied excessively based on manufacturer’s recommendation.

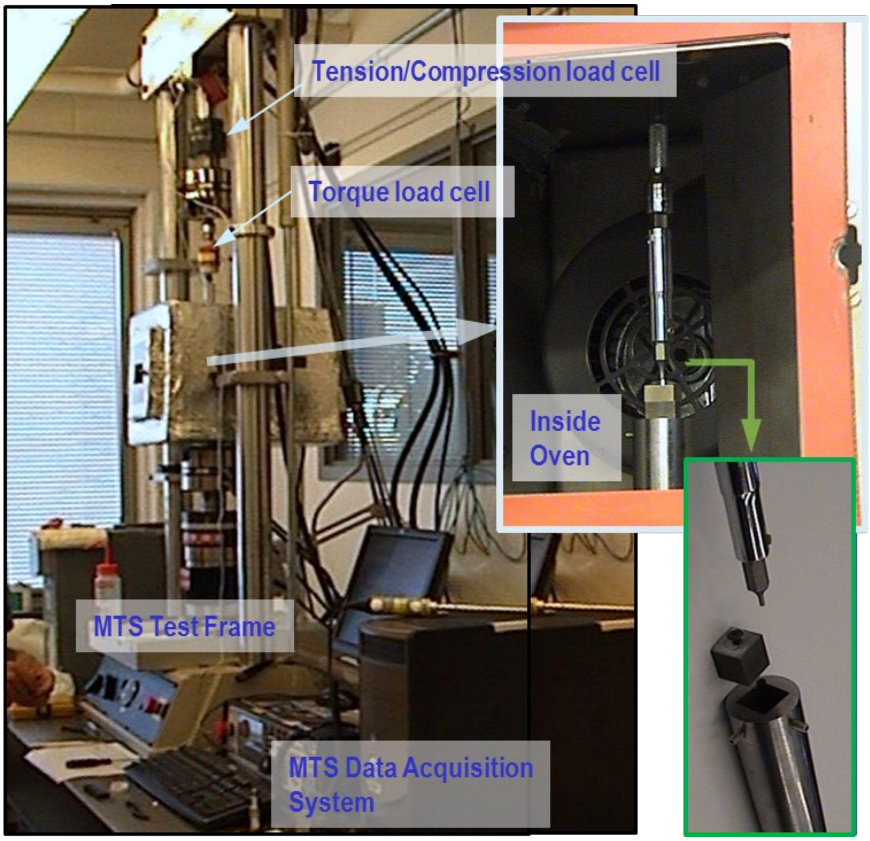

Figure 9.—Torque strength test set-up with a table-top MTS torsion test frame.

Test conditions were standardized based on the British Standard (EN 15865/ISO 10964):

- Counter-clockwise loosening for either breakaway or breakloose strength
- Rotation range from 0° to 250°
- Rotation rate of 1.9°/sec (2 rad/min)
- Data sampling rate of 50 point/sec
- Minimum 10 min equilibrium for elevated temperature testing

Data acquisition included test temperature, run time, torque, torque angle, axial force, and axial displacement. The three torque strengths calculated were defined as follows:

- Breakloose or breakaway torque: initial torque required to decrease or eliminate the axial load or to break the bond, respectively, normally from the initial peak of the torque-torque angle curve
- Prevailing torque: Torque measured after the initial breakage of the bond at 180° angle of rotation or an average of torque values within ± 50° range from the 180° or plateau region if torque-torque angle curve fluctuates more than 5%
- Maximum torque: maximum prevailing torque measured within the first 250° rotation after the initial breakage

After the torque strength testing, failure mode and verification of TL application in terms of relative amount, locations, and coverage were examined under a sOM mostly on fastener surface. Their failure mode was classified as (i) cohesive failure—TL residue covered most of the contact area, (ii) adhesive failure—less or no residue on surface, (iii) mixed failure—powdery/localized residues on surface, and (iv) thermally degraded—charred or darkened residue.

3.1.4.3 Shrink Tubing

3.1.4.3.1 Notched Tensile Properties

Mechanical performance of shrink tubing material was evaluated by tensile testing of a single edge notched strips specimens as the notch sensitivity. Shrink tube samples were sectioned into test strips using a specially designed cutting fixture, Figure 10(a), to control specimen width accurately (~ 0.12 in. or 3 mm), axially and radially, Figure 10(b). A notched was made on one edge up to ~0.04 in. (1 mm) deep using a sharp surgical blade after mounting on another fixture that could maintain the unnotched width of the strip samples constant. The notch dimensions were measured via sOM, Figure 10(c), and the sample thickness was measured using a caliper.

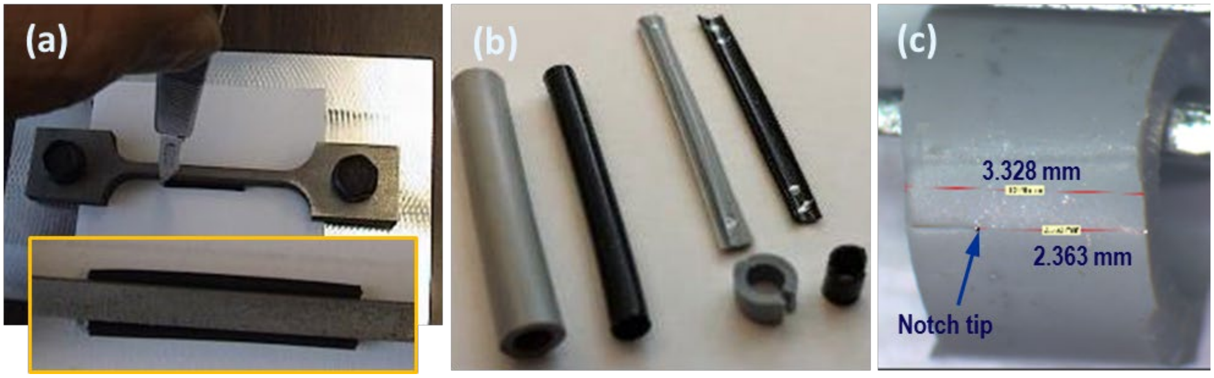

Figure 10.—Preparations of test specimens for shrink tubing candidates, (a) sectioning fixture, (b) axial and radial sections from the tubing, and (c) dimensions measured by optical microscope.

A table-top MTS load frame equipped with a custom-made air-circulated oven was used for the notched tensile testing at RT and elevated temperatures. Test conditions were standardized as follows: initial grip-to-grip distance of ~ 30 mm for the axial specimen, and ~ 10 mm for the radial specimen, CHD speed of 0.5 in./min. Typically 8 repeats were run per test condition. The properties calculated were ultimate strength via force divided by area of the uncut section and ultimate elongation via CHD at break divided by the uncut width.

3.1.4.4 O-Ring

For various mechanical property testing, o-ring thickness was measured with a Randall & Stickney thickness gage using ~4 oz weight.

3.1.4.4.1 Compression-Set Property

ASTM D395, Method B was followed. All o-ring samples were placed between polished tool steel plates at 25% compression of original o-ring thickness, Figure 11(a), and were then conditioned at 200 °C (392 °F) for 70 hr under dry N_2 gas flow in a Blue M Nitrogen oven. The property was calculated by $C_B = 100*(t_o – t_f)/(t_o – t_{\text{shim}})$, where: t_o is the original o-ring thickness, t_f for the final o-ring thickness, and t_{shim} for the shim thickness (typically $t_{\text{shim}} = 0.75\ t_o$).

3.1.4.4.2 Hardness

ASTM D2240, Shore A scale was followed using the Type M Durometer, Figure 11(b).

3.1.4.4.3 Tensile Properties

Tensile tests were conducted in a screw-driven Instron test frame using a custom-designed fixture, Figure 11(c), followed by ASTM D1414, Method B. All tests were conducted at the crosshead speed of 20 in./min. For various mechanical property testing, o-ring thickness was measured with a Randall & Stickney thickness gage using ~4 oz weight. The properties calculated were tensile strength = $F/1.57*CS^2$ and ultimate elongation, % = [(2*CHD at rupture + 3.14*0.25 – ID*3.14)/ID*3.14] *100.

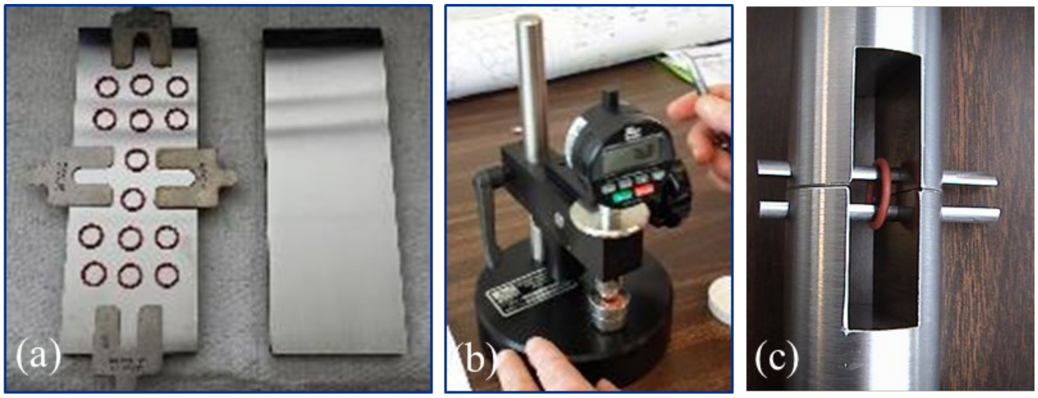

Figure 11.—(a) O-ring compression-set test setup, (b) Type M Durometer for o-ring hardness, and (c) Fixture for o-ring tensile test.

Figure 12.—Various ovens and pressure vessel systems equipped with dry nitrogen gas flow control used for thermal aging experiment.

3.2 Thermal Aging Testing

All thermal aging tests were conducted under an inert gas environment with dry shop nitrogen gas. Various ovens with either its own capability of flowing N_2 gas or employing a pressure vessel equipped with N_2 gas flow control system, Figure 12, were set up for various aging tests. Inertness of the test environment was validated experimentally via weight change monitoring of copper powder, most sensitive to oxidation, e.g., less than 0.15 wt% maximum increase in the sealed PV. In most cases, the aging temperature and N_2 gas flow rate were monitored and adjusted daily for the entire aging intervals, and documented for future reference.

All aging tests followed the standardized operating procedure:

1. Weighed all samples as a group or individually after drying at 80 °C under full vacuum for 24 hr
2. Sorted test samples by the aging temperature and interval

3. Loaded the sorted samples into pressure vessels (PVs) for each aging temperature, but the longer aging interval samples first, and sealed
4. Installed the PVs into the aging ovens including the dry N_2 gas line connection, and attached a calibrated thermocouple to the surface of PV
5. Purged PVs with dry N_2 gas for 1 to 2 hr and set the optimum flow rate, then continued purging for 24 hr at RT. The flow rate was high enough to keep positive internal pressure to move air out, but low enough not to disturb thermal equilibrium.
6. Heated the ovens to 80 °C and dwell for 24 hr under N_2 flow as a final drying step
7. Heated the ovens to the target aging temperatures
8. Monitored PV temperatures and N_2 flow rate daily
9. Cooled down the oven to room temperature while flowing dry N_2 gas, when the planned aging intervals were achieved
10. Disassembled PVs from the oven
11. Removed the assigned test sample sets from PVs and weighed them accordingly
12. Repeated the steps 4 to 8 to resume the aging tests

In the case of the short-term 15-day thermal aging tests involving more than seven or eight temperatures, the experiment was performed in two phases – the initial phase at four different temperatures, and then the second phase in which temperatures were determined based on the first test results to confirm the trends, and thus to ascertain more accurate temperature dependency. Since the maximum temperatures for the accelerated aging test identified for each organic type were fairly close, with the exception of the TL, it was decided to run the 6-month accelerated aging tests by combining those three organic candidates: adhesives, shrink tubing, and o-ring specimens to preserve resources. Sample boats made of stainless steel wire and sheet were used to organize and sort out various test specimens for three aging temperatures and four aging durations (i.e., four boats per aging temperature), Figure 13.

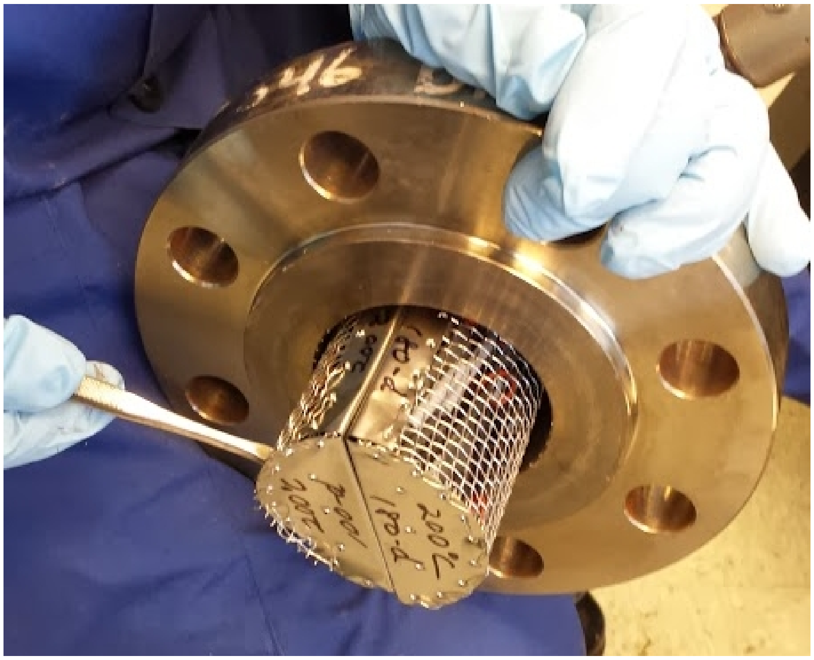

Figure 13.—The sample boats filled with various test specimens were loaded into pressure vessel, two out of four boats are seen in this picture.

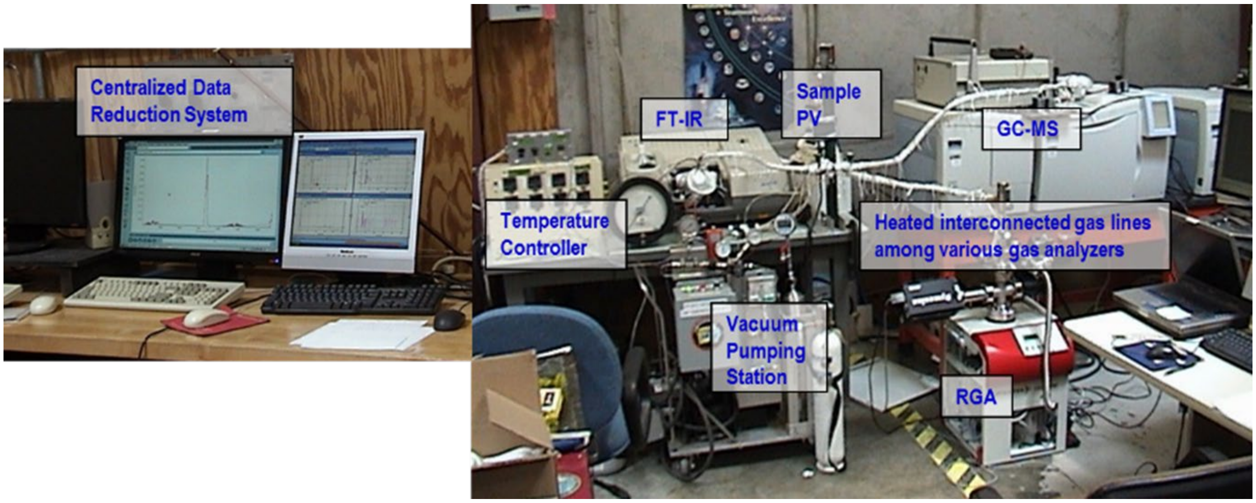

Figure 14.—Integrated in-situ outgassing test set-up combining RGA-GRC/TCD-FTIR with vacuum and temperature control system.

3.3 TCIOP Testing

Based on previous experiences with respect to the accurate and reliable gas analysis in terms of composition and concentration down to 10 ppm range, an Integrated RGA-GC/TCD-FTIR Gas Analysis System directly connected to the sample PVs was developed, Figure 14. The set-up was designed not only to combine those three analyzers into one system, but also to minimize potential sources of contamination and be capable of controlling gas temperatures. The set-up was also designed to simultaneously run two samples per experiment. In this test, various organic candidate materials were loaded into the PV and charged with the premixed gases (107 ppm H_2, 1,060 ppm O_2, 3,081 ppm N_2, 312 ppm CO_2, and the balance of UHP helium) that were representative of a typical gas sample from the SOA convertors following exposure to long-term performance simulation test runs up to several thousand hours.

For adhesive/potting materials, both epoxy-alone thick sample (~0.5-in. L by 1.0-in. W by ~ 0.06-in. t), 7 to 8 ea. per epoxy type, and subscale lap shear specimens, 7 ea. per epoxy type, were used. In the case of the TL material, only Loctite 294 and Resbond 507TS candidates were tested with modified torque specimen assemblies in the shape of a 0.18 in. inner radius, 0.5 in. high hexagonal prism instead of the regular 0.5 in. cube geometry due to the inlet size of the PV. Fifteen samples used per test for Joint type #2 and #8, in addition to a few fasteners containing thread locker residues from the 15-d thermal aging test. Then, the 0.5 in. cube adapter with center hexagonal hole was used for torque testing. For the shrink tubing material, 3/16 in. OD – 9 in. long sections were tested in as-received, expanded condition. Note that specimens used for the 6-month thermal aging experiment were pre-shrunk or fully recovered. The o-ring material was used in as-received form.

The standardized test procedures for TCIOP testing included the following: Specimens were preconditioned in a sealed PV. Each PV contained only one material type) → specimens were baked-out under vacuum at 90 °C for 24 hr → vessels were pressurized w/ the premix gas to ~ 400 psi at RT → PVs were monitored for leaks for 24 hr → initiated the TCIOP test. The following thermal exposure profiles were used: Temperature ramp from RT → 100 °C at 1 °C/min with 3 day dwell → temperature ramp to 150 °C at 1 °C/min with 2 day dwell → temperature ramp to 200 °C at 1 °C/min with 7 day dwell. A standardized outgas monitoring scheme was also developed. At $t = 0$ at RT (20 °C), RGA, GC-TCD, and FT-IR were all run as the baseline. During temperature ramps, only FT-IR spectroscopy was run, one spectrum was collected every ~ 20 min (all gas lines were vacuumed between runs). During dwell times, RGA, GC/TCD, and FT-IR tests were run daily. For FT-IR analysis, the amount of gas sample was maintained at 1 atm pressure. In all cases, the peak intensities can be quantitatively analyzed as the actual concentration of each gas species.

After the in-situ outgassing test, the systematic residual property evaluations were conducted on the TCIOP tested samples to determine outgas-induced degradation following the aforementioned specific test methods per organic material type, whenever applicable.

4.0 Results and Discussions

4.1 Initial Screening and Down-selection

Screening for two or three better candidates from the potential candidates was carried out by assessing their processability, short-term thermal stability, outgassing potentials, and required basic functional properties. The first three assessments were normally achieved by basic process analysis, various thermal property analyses using DSC/mDSC, TGA, isothermal TGA, and DMA, and FT-IR molecular structure analysis. The functional property/performance assessment involved (i) full-scale bond strength in both shear and normal mode as a function of temperature up to 200 °C for the adhesives, (ii) torque strength on M10 steel nuts and bolts at room temperature as a function of cure conditions for the TL, (iii) notched tensile properties in both axial and radial directions as a function of temperature up to 200 °C for the shrink tubing materials, and (iv) 200 °C compression-set and tensile properties as a function of temperature up to 200 °C for the o-rings.

4.1.1 Adhesive/Potting Applications

As summarized in Table 6, most candidates showed reasonably good short-term thermal stability based on their high T_d, ~ 300 °C or higher. T_g and % cure of Hysol EA9394C-2 were significantly lower than those of other candidates, but it was due to the typical formulation such as the regular Hysol EA9394, and they both increased with the extended postcure or bake-out at elevated temperature. It was proved that the formulation did not compromise bonding performance or outgassing behavior (Refs. 6 and 9). L313U and AF191K adhesives exhibited unidentified endothermic reaction at ~ 250 °C, possibly compositional phase change or decomposition. Most candidates cured by the initial process conditions showed poor outgassing characteristics compared to those acceptable ranges listed in the bottom of the table. There were, however, some evidences of improvement via extended thermal treatment or bake out, especially in the case of the Hysol EA9394C-2.

Figure 15 and Figure 16 summarize the results of full-scale bond strength of various candidates as a function of test temperature in shear and FWT mode, respectively. Wide variations in bond strengths among candidates can be easily seen. The 3M AF131-2 performed best and most thermally stable in shear mode while the Hysol EA9394C-2 showed best bonding performance in FWT mode. The effect of the structural support (scrim) on bond strength was significant in most adhesive types but the Hysol EA9394C-2 as an unsupported paste form performed exceptionally well. The cyanate ester adhesives, such as FM 2555 or RS-4A, were rated as a higher temperature system up to 232 °C/450 °F, but displayed inferior performance on such a metal-to-metal bonding.

TABLE 6.—INITIAL THERMAL PROPERTIES AND OUTGASSING CHARACTERISTICS OF ADHESIVE CANDIDATES IN TERMS OF THICKNESS

Properties / Candidate	mDSC							Standard TGA				Isothermal TGA: normalized								
	T_g, °C	T_{exo}, °C	ΔH, J/g	T_{edo}, °C	ΔH, J/g	Cure, %	T_d, °C	T_d	ΔWt% RT-100 °C	Δ%Wt 100-200 °C	ΔWt% at 700 °C	Initial Δwt%			Dwell Δwt%			Wt loss rate [(wt%/min)×1000]		
												120 °C	150 °C	200 °C	120 °C	150 °C	200 °C	120 °C	150 °C	200 °C
L-313U, thin (~0.45 mm)	223	175	1.8	256	2.1	99.3	345	380	0.492	0.916	63	1.037	1.540	2.697	0.773	1.007	0.689	0.441	1.081	0.611
	221	193	3.3	256	5.3	98.8	338	382	0.074	1.597	63									
AF131-2, thin (~0.15 mm)	218	233	11.9			96.7		402	0.716	0.304	63	2.299	2.522	2.159	0.799	0.290	0.469	0.465	0.000	0.647
	219	235	4.3			98.8		411	0.475	0.426	73									
AF131-2, thick (~1.3 mm)	253	254	7.8			97.9		410	0.212	0.597	97	0.405	0.873	0.801	0.697	0.041	1.002	0.281	0.000	0.329
	246	263	10.2			97.2		407	0.101	0.380	97									
AF191K, thin (~0.3 mm)	221	194	0.3	257	3	99.9		411	0.266	0.581	100	0.768	1.646	1.615	2.020	0.601	0.394	0.608	0.120	0.775
	226	155	6.5	258	1.8	98.1		412	0.498	0.664	100									
	224	138	4.7	258	1.6	98.6		402	0.745	0.896	95									
EA9394C-2, thin (~0.1 mm)	141	148, 245	17.4			93.1		378	0.612	1.127	60	0.900	1.220	1.430	2.497	0.480	1.043	0.089	0.054	1.238
	140	147, 248	17.3			93.1														
EA9394C-2, thick (~1.5 mm)	143	154, 238	18.6			92.6	337	373	0.225	0.449	67	0.474	0.747	1.072	0.727	0.684	1.067	0.687	0.663	1.891
	142	152, 238	18.2			92.7														
EA9394C-2, thick baked at 110 °C for 144 hr	162	168, 241	16.7			93.3	339	372	0.466	0.021	64									
Outgassing characteristics acceptable range:									< 1.0	< 0.8		< 1.0			< 1.4			< 0.4		

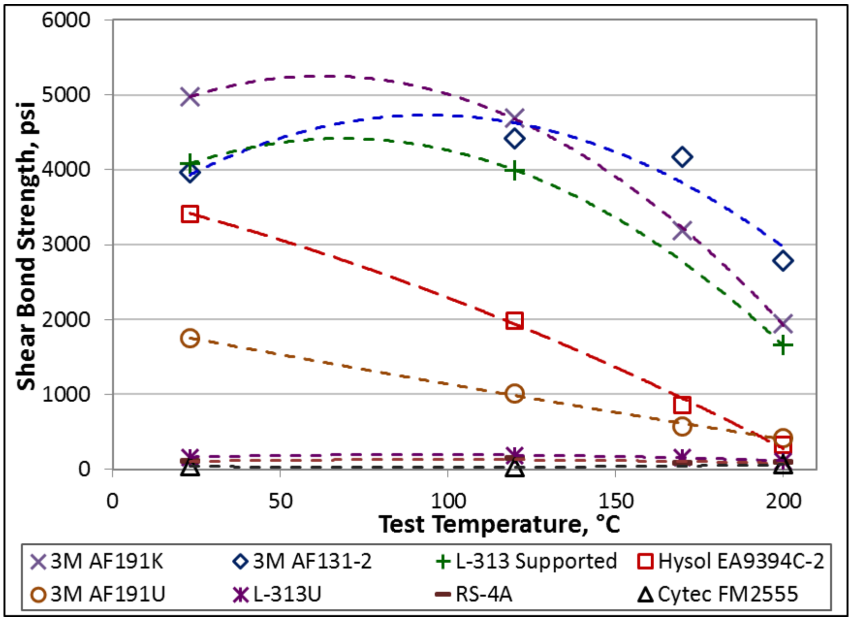

Figure 15.—Full-scale shear bond strength of various high temperature adhesive candidates.

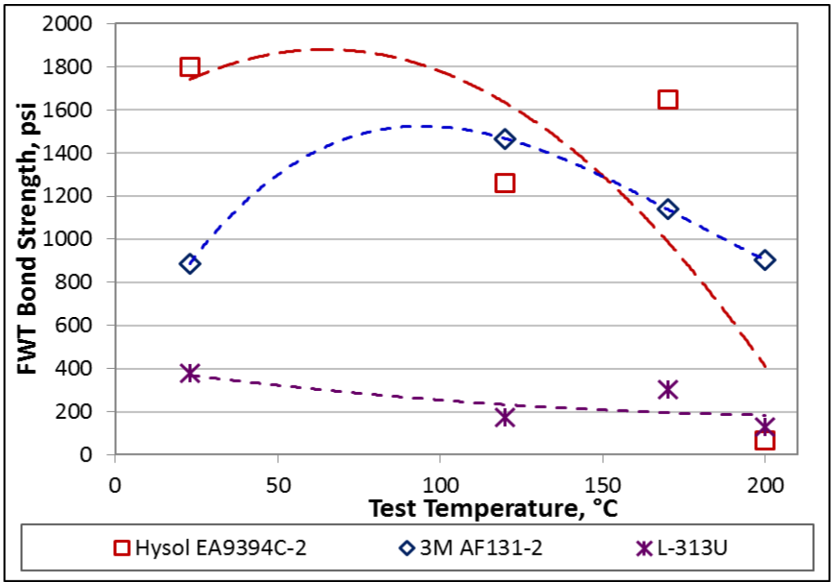

Figure 16.—Full-scale FWT bond strength of a few adhesive candidates showed high shear bond strength.

TABLE 7.—OVERALL RATINGS OF ADHESIVE/POTTING CANDIDATES FOR DOWN-SELECTION

Material type Properties	L-313	RS-4A	FM2555	AF131-2	AF191K	EA9394C-2
Cure condition	–	–	–	–	–	+
Processability/applicability	0	–	–	0	0	+
Multi-purpose application	+	–	–	–	–	+
Thermal degradation temperature/TGA	+	+	+	+	+	+
Weight loss/outgassing potential	–			+	0	0
Thermal transition/mDSC	0	0	0	0	0	0
Shear bond strength	+	–	–	+	+	+
FWT bond strength	–			+		+
Final selection				✓		✓

Note: 0, neutral or insignificant effect; +, positive performance; –, negative performance

Table 7 summarized the results of preliminary screening evaluations in terms of performance ratings on each properties. Based on that, both Hysol EA9394C-2 and AF131-2, were down-selected. Moreover, the 3M AF131-2 was credited for superior thermal performance and stability in terms of bond strength and high T_d, while the Hysol EA9394C-2 was considered for the best paste form adhesive due to its usefulness for multiple-applications, such as bonding, laminating, and potting etc. Large supportive database from the basic formulation, EA9394, evaluated and validated for lower temperature use in a SOA Stirling convertor with long positive history in terms of processability, performance, durability and reliability was another strength of the EA9394C-2 adhesive.

4.1.2 Thread Locker Application

Initial screening evaluations of thread locker candidates involved the aforementioned short-term thermal stability, outgassing characteristics, cure/processability, and locking performance by torque strength tested on M10 steel bolt and nut as summarized in Table 8.

The three cure conditions designated as T1, T2, and T3 were selected based on the manufacturer's recommendations and our previous experiences on similar thread locker materials. Figure 17 shows that

FT-IR spectra of cured thread locker material at the three different conditions were almost identical for all candidates which ascertained no thermal degradation or major molecular structural changes from the cure processes.

TABLE 8.—TEST MATRIX FOR INITIAL SCREENING EVALUATIONS OF THREAD LOCKER CANDIDATES

Properties	Cure condition	Torque Specimens with M10 (3 repeats ea.)			
		Loctite 266 (L1)	Loctite 294 (L2)	Resbond 507TS (R1)	Resbond 907TS (R2)
Torque strength at RT	T1: 4 days at RT	L1T1-1, 2, 3	L2T1-1, 2, 3	R1T1, 2, 3-1	R2T1-1, 2, 3
0° → 270° at 1.9°/sec (2 rad/min)	T2: 1 day at 40 °C	L1T2-1, 2, 3	L2T2-1, 2, 3	R1T1, 2, 3-2	R2T2-1, 2, 3
	T3: 1 day at 80 °C	L1T3-1, 2, 3	L2T3-1, 2, 3	R1T1, 2, 3-3	R2T3-1, 2, 3
Post-torque testing evaluations					
mDSC (under N_2)	T1	L1T1-1	L2T1-1	R1T1-1	R2T1-1
RT to 350 °C at 5 °C/min	T2	L1T2-1	L2T2-1	R1T1-2	R2T2-1
	T3	L1T3-1	L2T3-1	R1T1-3	R2T3-1
TGA (under N_2)	T1	L1T1- 2, 3	L2T1- 2, 3	R1T2, 3-1	R2T1- 2, 3
RT → 750 °C at 10 °C/min	T2	L1T2- 2, 3	L2T2- 2, 3	R1T2, 3-2	R2T2- 2, 3
	T3	L1T3- 2, 3	L2T3- 2, 3	R1T2, 3-3	R2T3- 2, 3
Iso-TGA (under N_2)	T1	L1T1-1, 2, 3	L2T1-1, 2, 3	R1T1, 2, 3-1	R2T1-1, 2, 3
RT to 120 °C at 10 °C/min dwell 7 hr	T2	L1T2-1, 2, 3	L2T2-1, 2, 3	R1T1, 2, 3-2	R2T2-1, 2, 3
	T3	L1T3-1, 2, 3	L2T3-1, 2, 3	R1T1, 2, 3-3	R2T3-1, 2, 3
RT to 150 °C at 10 °C/min dwell 7 hr	T1	L1T1-1, 2, 3	L2T1-1, 2, 3	R1T1, 2, 3-1	R2T1-1, 2, 3
	T2	L1T2-1, 2, 3	L2T2-1, 2, 3	R1T1, 2, 3-2	R2T2-1, 2, 3
	T3	L1T3-1, 2, 3	L2T3-1, 2, 3	R1T1, 2, 3-3	R2T3-1, 2, 3
RT to 200 °C at 10 °C/min dwell 7 hr	T1	L1T1-1, 2, 3	L2T1-1, 2, 3	R1T1, 2, 3-1	R2T1-1, 2, 3
	T2	L1T2-1, 2, 3	L2T2-1, 2, 3	R1T1, 2, 3-2	R2T2-1, 2, 3
	T3	L1T3-1, 2, 3	L2T3-1, 2, 3	R1T1, 2, 3-3	R2T3-1, 2, 3

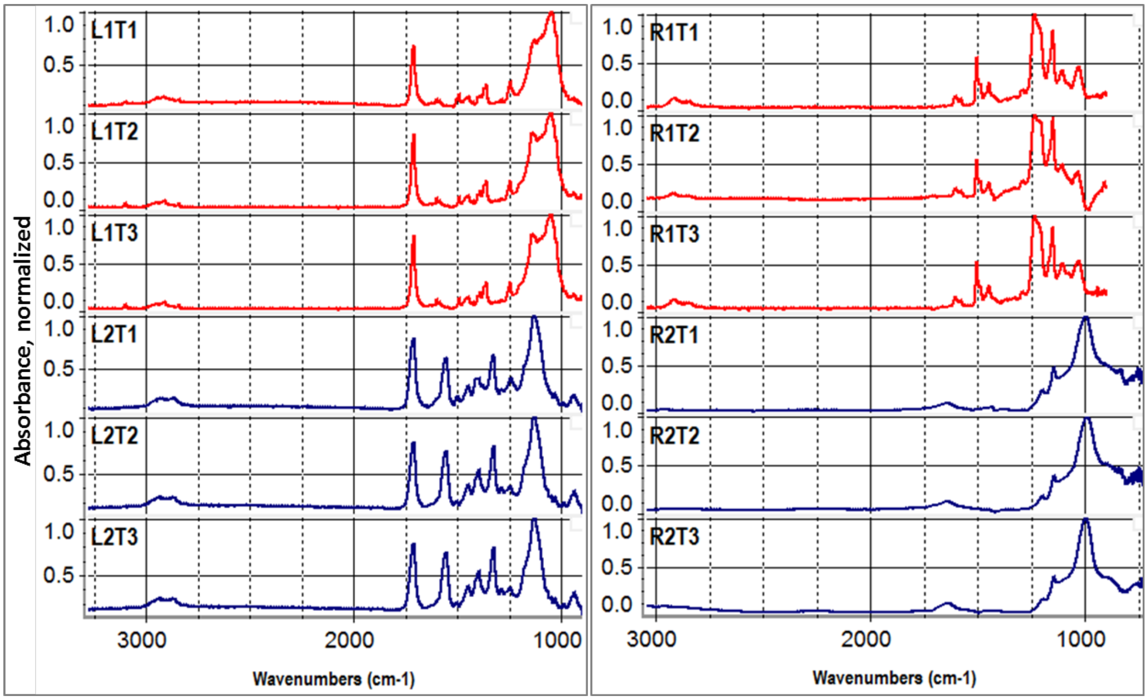

Figure 17.—FT-IR spectra of thread locker candidates at three different cure conditions.

Table 9 summarizes the results of the initial thermal and outgassing characterizations of the candidates as a function of cure condition. Note that the outgassing characteristics were compared against the acceptance guidance from the GRC database. Degree of cure (estimated by ΔH_{res} of mDSC test) of all candidates except Resbond 907 TS improved with increasing cure temperature which confirmed that the full cure state could be achieved by optimizing cure conditions and bake-out. The epoxy-based Resbond 507TS showed a clear glass transition which varied by the cure conditions. The Resbond 507 TS also showed the most acceptable outgassing characteristics based on the guideline of the GRC database, followed by the Loctite 294, but again these characteristics can be improved via cure and bake-out optimizations.

TABLE 9.—PRELIMINARY THERMAL PROPERTIES AND OUTGASSING CHARACTERISTICS OF THREAD LOCKER CANDIDATES IN TERMS OF CURE CONDITIONS

TL		mDSC								STANDARD TGA					ISOTHERMAL TGA: Normalized								
Type	Cure Cond.	T_g, °C	T_{exo}, ºC	ΔH_{res}, J/g	T_{end}, °C		ΔH_{end}, J/g		T_d, °C	T_d, °C		ΔWt% RT-100°C	Δ%Wt 100-200°C	ΔWt% at 700°C	Initial wt loss, wt%			Dwell wt loss, wt%			Wt loss rate, [(wt%/min)×1000]		
					1st	2nd	1st	2nd		1st	2nd				120 °C	150 °C	200 °C	120 °C	150 °C	200 °C	120 °C	150 °C	200 °C
L1	T1		227	26	108	191	5	6		214	350	1.5	6.2	59	1.4	2.7	5.1	3.2	4.5	13.8	3.4	2.4	2.9
	T2		205	14	108	195	2	3		211	331	1.1	5.3	56	2.3	4.0		4.1	6.1		3.0	4.6	
	T3		201	10	109	195	3	2		212	351	1.4	5.0	49	1.3	2.1	5.1	6.7	5.2	14.1	4.3	6.7	3.9
L2	T1		245	506		239		6		132	292	0.9	6.4	95	6.6	12.9	11.0	15.4	21.3	7.0	10.3	3.6	4.2
	T2		277	32						141	326	1.2	6.7	79	3.4	4.9	9.0	12.9	8.4	8.0	7.7	3.5	5.3
	T3		291	8						137	318	1.1	7.8	84	2.7	2.2	9.1	11.3	8.9	4.6	5.4	5.9	4.8
R1	T1	61	131	24					304		329	1.2	0.9	75	1.6	1.3	3.2	2.0	1.7	3.5	1.3	0.6	2.2
	T2	64	130	14					311		328	1.2	1.0	77	5.4	1.5	5.7	3.9	1.3	0.1	0.3	0.4	0.4
	T3	101	242	5					317		337	0.4	0.7	83	0.7	0.7	0.5	0.7	0.7	0.5	0.5	0.8	0.5
R2	T1				46		155				528	27.2	26.4	26	28.3	39.6	57.7	15.2	16.9	12.9	9.1	12.8	8.9
	T2	140			53	151					526	32.8	23.5	31	11.8	39.8	51.5	5.7	14.6	9.2	2.6	7.3	6.0
	T3	80			66		41				521	17.0	16.5	23	58.7	81.9	0.0	26.3	18.5	0.0	11.8	7.5	0.0
Outgassing characteristics acceptable from GRC database:												< 1.0	< 0.8		< 1.0			< 1.4			< 0.4		

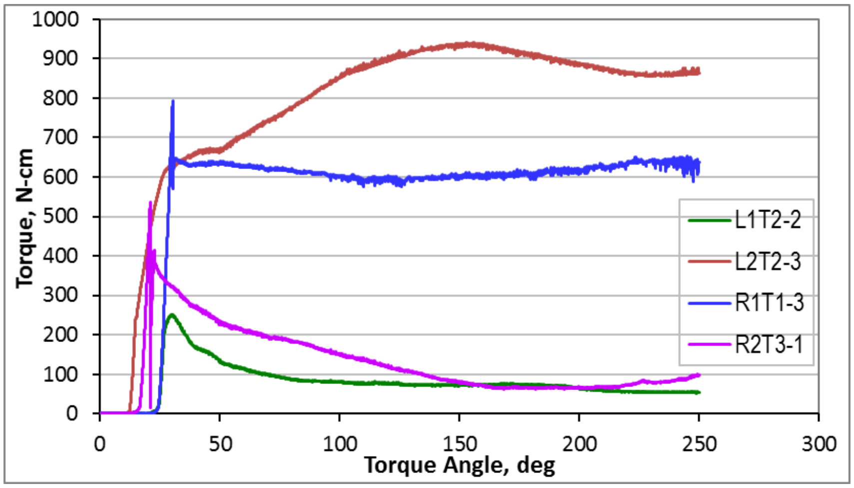

Figure 18.—Typical torque – angular displacement curves of various thread locker candidates.

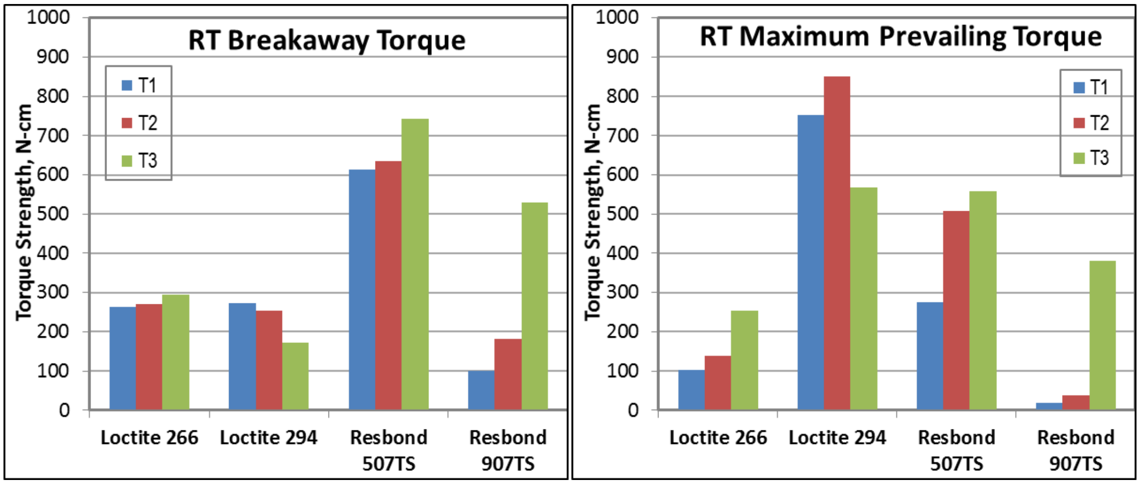

Figure 19.—Torque strengths of thread locker candidates at room temperature against cure conditions.

Figure 18 illustrations the typical torque-angular displacement curves of the four candidates at room temperature using the M10 bolts with zero installation torque (i.e., unseated) when they were optimally cure. Both Loctite 294 and Resbond 507TS showed not only high breakaway torque but also high and steady prevailing torque which are desirable as secondary locking of any fasteners in flight hardware. Torque strengths of the candidates from the unseated M10 bolts at room temperature were plotted in Figure 19 for three different cure conditions. As indicated by the torque—angular displacement curves, Loctite 294 and Resbond 507TS showed the highest torque strength, via either breakaway or prevailing, regardless of cure condition. The effects of cure temperature were more prominent in the Resbond systems, especially the ceramic based 907TS. Loctite materials being anaerobic cure system were less affected by cure temperature. The highest breakaway torque of Resbond 507TS was resulted from its strong bonding to metal surfaces while the highest prevailing torque of Loctite 294 was probably from its high toque resistance.

Table 10 summarized the results of preliminary screening evaluations in terms of performance ratings on each properties. Based on the ratings, two best high temperature candidates, Loctite 294 and Resbond 507TS, were down-selected. In addition, PET Poly-Lok thread locker was also selected as an alternative because of its unique potential as a solid patch system even though it didn’t undergo the screening evaluation process.

4.1.3 Shrink Tubing Application

A detailed test matrix for the initial screening evaluations of shrink tubing candidates is summarized in Table 11. As a part of the screening evaluations, shrinking process of each candidate was also optimization and validated. Various process parameters such as shrinking onset temperature, shrinking end temperature or full recovery temperature, % change, and shrink ratio were determined by DMA in creep mode at minimum load level of ~ 1 N. A small size dogbone specimen was designed for more accurate measurement. The dogbone specimens were cut from shrink tubing in both axial and radial directions since their shrinking behavior was supposed to be anisotropic.

TABLE 10.—OVERALL RATINGS OF THREAD LOCKER CANDIDATES FOR DOWN-SELECTION

Material type Properties	Loctite 266	Loctite 294	Resbond 507TS	Resbond 907TS
Cure Condition	+	+	+	+
Processability	0	0	0	0
FT-IR at RT	0	0	0	0
Thermal degradation temperature/TGA	+	+	+	+
Weight loss/outgassing potential/iso-TGA	0	0	+	–
Thermal transition/mDSC	0	0	0	0
Breakaway torque	0	0	+	+
Max. Prevailing torque	–	+	+	0
Final selection		✓	✓	

Note: 0, neutral or insignificant effect; +, positive performance; –, negative performance

TABLE 11.—INITIAL TEST MATRIX TO DOWN-SELECT SHRINK TUBING CANDIDATES

Material type	Viton (Alpha)			PFA			SRFR			ETFE			PEEK			PI		
Test specimen type	As-rec	Shrunk		As-rec	Shrunk		As-rec	Shrunk		As-rec	Shrunk		As-rec	Shrunk		As-rec	Shrunk	
Test conditions		(A)xial	(R)adial		A	R		A	R		A	R		A	R		A	R
Shrink process optimization	✓			✓			✓			✓			✓			✓		
FT-IR on both OD and ID	✓	✓		✓	✓		✓	✓		✓	✓		✓	✓		✓	✓	
TGA (N_2), RT to 750 °C	✓	✓		✓	✓		✓	✓		✓	✓		✓	✓		✓	✓	
Notched tensile strength 6 repeats at 25, 150, and 200 °C ea.		✓	✓		✓	✓		✓	✓		✓	✓		✓	✓		✓	✓
DMA - Tension (air) 25 to 450 °C at 5 °C/min		✓	✓		✓	✓		✓	✓		✓	✓		✓	✓		✓	✓
mDSC (N_2), –50 to 350 °C		✓			✓			✓			✓			✓			✓	
Iso-TGA (N_2) for 7 hr																		
120 °C		✓			✓			✓			✓						✓	
150 °C		✓			✓			✓			✓			✓			✓	
200 °C		✓			✓			✓			✓			✓			✓	

Figure 20 shows typical DMA-creep test results in terms of lengthwise dimensional change as a function of temperature in both axial and radial direction, as the latter being the main shrinking direction of interest. In the radial direction, ETFE showed the narrowest recovery/shrinking transition, only within 200 to 250 °C while PEEK and PI recovered throughout broad temperature ranges, from ~ 100 to above 350 °C. On the perpendicular or axial direction, PI and ETFE showed no considerable changes, but PEEK showed significant shrinking with almost same shrink ratio as the radial direction which may complicate installation processes and procedures. On the other hand, SRFR and PFA actually expanded in the axial direction. Overall, the optimum shrinking process conditions determined were as follows:

- Viton, PFA, and SRFA: 3 min at 200 °C in a preheated air circulated oven (i.e., dwell for 3 min after the oven temperature recovered to 200 °C upon placing samples)
- ETFE (RT-555): 3 min at 250 °C
- PEEK: 3 min at 345 °C
- PI: 3 min at 350 °C

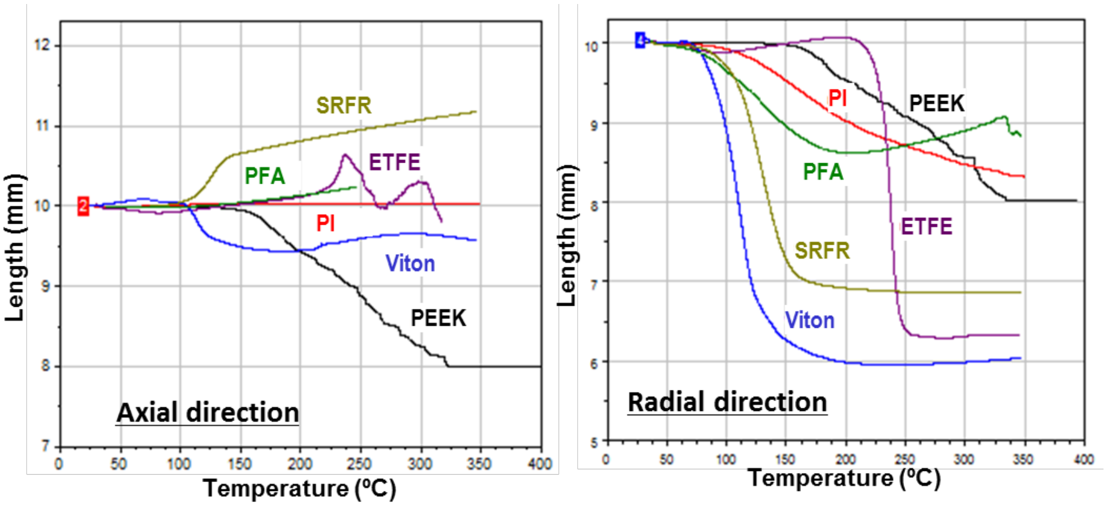

Figure 20.—Typical dimensional changes of shrink tubing candidates as a function of temperature.

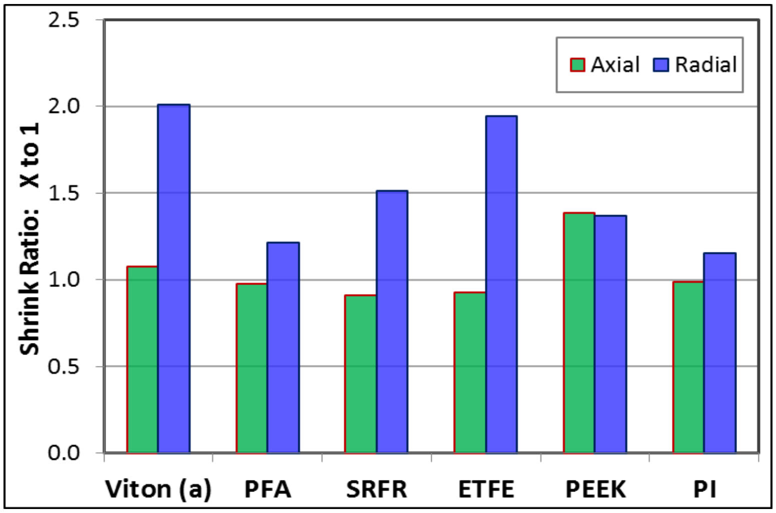

Figure 21.—Complete shrink ratio of shrink tubing candidates in both axial and radial directions.

Note that PEEK and PI required considerably higher temperature for full recovery/shrink which may limit them in this application due to possible temperature limitations of other affected components such as magnet. As shown in Figure 21, the final shrink ratio measured in radial direction were 2.01:1 or -50% for Viton, 1.94:1 or -48.4% for ETFE, 1.51:1 or -33.9% for SRFR,1.37:1 or -26.4% for PEEK, 1.22:1 or -17.7% for PFA, and 1.15:1 or-13% for PI. In axial direction, they were 1.08:1 or -6.7%, 0.93:1 or +7.9%, 0.91:1 or +10%, 1.39:1 or -26.3%, 0.98:1 or +2.6%, and 0.99:1 or +1.4%, respectively. ETFE showed the highest shrink ratio on radial direction, most comparable to that of Viton.

The optimum shrinking process conditions were also validated by ascertaining that the conditions were not causing any thermal degradation or significant molecular structural changes except the molecular rearrangement involved in the shrinking process via FT-IR analysis. Figure 22 shows typical FT-IR spectra of the candidates comparing as-received expanded vs. fully recovered shrunk state from both inner and outer surface. There were no visible changes observed in any candidate, indicating no thermal degradation or molecular structural changes.

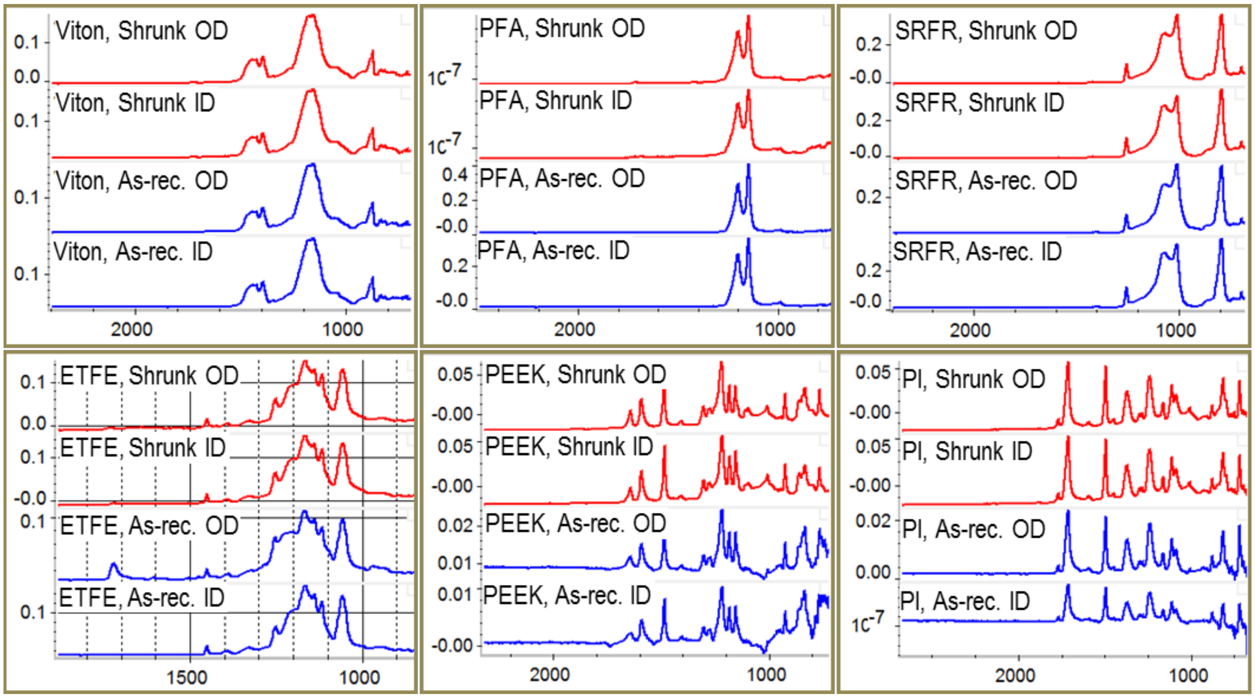

Figure 22.—FT-IR spectra of shrink tubing candidates on both ID and OD before and after their shrinking processes. Absorbance on Y-axis vs. Wavenumber (cm^{-1}) on X-axis.

The overall thermal properties and outgassing characteristics of all six candidates are summarized in Table 12, were mostly tested in the shrunken state, except TGA which included both as-received control and shrunken materials, in order to validate the shrinking conditions. With regard to the validation, there were no significant reductions in most TGA properties, particularly T_d, after shrinking process in all candidates, thus no thermal degradation. For screening evaluation, the main T_d of all candidates was above 400 °C, thus sufficient for the application. PFA, SRFR, ETFE and PEEK were semi-crystalline polymers with T_m at 308, –46, 218, and 342 °C, respectively. PI showed the highest T_g, and highest T_d, which were indications of superior thermal stability, but all candidates showed reasonably good thermal stability. PEEK and PI showed the least modulus drop at elevated temperatures, typically 150 and 200 °C, followed by SRFR and ETFE, in both axial and radial directions. In terms of outgassing potentials, PI and PEEK showed higher overall weight losses regardless of test temperature. SRFR also showed slightly higher weight losses than those acceptable values identified by the GRC database, but an optimized bake-out may reduce them down to the acceptable values. For comparison, the TML (total mass loss after 24 hr at 125 °C in vacuum) measured via ASTM E595 in the NASA database was 0.17 to 0.37 % for Viton, film, 0.7 to 1.32 % for polyimide film, 0.23 to 027 % for PEEK, and 0.22 to 0.66 % for ETFE.

The notch sensitivity of shrink tubing candidates as a function property is compared in Figure 23 and Figure 24 at various test temperatures. PEEK and PI showed superior notch strength, but were very brittle. The other candidates were considerably weaker, yet much tougher than PEEK and PI, regardless of direction.

Table 13 summarized the results of preliminary screening evaluations in terms of performance ratings on each properties. Based on that, SRFA and ETFE were down-selected as two best high temperature shrink tubing candidates. It should be noted that they were selected for least negative changes rather than more positive performance, thus the extended property-performance characterizations are more relevant.

TABLE 12.—PRELIMINARY THERMAL PROPERTIES AND OUTGASSING CHARACTERISTICS OF SHRINK TUBING CANDIDATES BASED ON TEST MATRIX

ST material Properties			Viton (α)		PFA		SRFR		ETFE		PEEK		PI	
			Avg.	SD	Avg.	SD	Avg.	SD	Avg.	SD	Avg.	SD	Avg.	SD
mDSC Shrunk	T_g, °C						131	24	-5	0.7	160	1.7	302	
	T_r, °C		84	1.4	–2	0.0								
	ΔH_r, J/g		12.0		2.6	1.0								
	T_m, °C				308	0.5	–45		218	0.7	342	1.4		
	ΔH_m, J/g				21.0	4.5	9		10.3	0.6	64.4	23.2		
TGA As-received	T_d, °C		482		538	3	406	17	487		577	19	580	16
	ΔWt%, RT-100 °C		0.052		0.018	0.006	0.023	0.022	0.009		0.049	0.051	0.858	0.097
	ΔWt%, 100-200 °C		0.098		0.023	0.007	0.093	0.030	0.144		0.179	0.033	0.483	0.554
	ΔWt% at 700 °C		87		99	0.5	18	1.5	94		44	6.4	62	25
TGA Shrunk	T_d, °C		481		534		414		485		593		596	0
	ΔWt%, RT-100 °C		0.033		0.033		0.034		0.038		0.074		0.617	0.378
	ΔWt%, 100-200 °C		0.106		0.052		0.101		0.036		0.051		0.290	0.230
	ΔWt% at 700°C		86		98		18		94		44		34	1
Isothermal TGA: Normalized, Shrunk	Initial wt loss, wt%	120 °C	0.127		0.000		0.061		0.083		0.431		4.663	
		150 °C	0.078		0.522		0.029		0.170		0.411		3.455	
		200 °C	0.139		0.013		0.000		0.126		0.976		2.818	
	Dwell wt loss, wt%	120 °C	0.546		0.000		1.313		0.341		1.634		2.185	
		150 °C	0.267		1.506		1.562		0.839		4.700		3.243	
		200 °C	0.299		0.065		0.000		0.201		0.000		2.168	
	Wt loss rate, [(wt%/min)× 1000]	120 °C	0.644		0.000		1.828		0.286		0.944		3.181	
		150 °C	0.402		0.000		1.504		0.017		3.804		6.755	
		200 °C	0.264		0.177		0.000		0.509		0.000		2.280	
DMA-Tension, Axial, Shrunk	T_t, °C		101	2.7	115	9.4	135	9.5	81	3.1	190	0.6	402	10.1
	E' at RT, ksi		3	2	75	42	3	0.5	16	11	461	0.2	192	150
	E' at 150 °C, ksi		0.1	0.00	7.6	1.7	0.6	0.1	2.4	1.0	391	21	140	140
	E' at RT/*E*' at 150 °C, %		4%	2%	12%	4%	19%	3%	22%	14%	85%	5%	60%	24%
	E' at 200 °C, ksi		0.1	0.00	4.4	2.0	0.4	0.1	1.2	0.5	124	10	176	124
	E' at RT/*E*' at 200 °C, %		3%	2%	6%	2%	13%	3%	11%	8%	27%	2%	82%	39%
DMA-Tension, Radial, Shrunk	T_t, °C		106	18.6	113		149	8.5	91		191	3.5	401	12.0
	E' at RT, ksi		2.7	1.1	47.4		1.7	0.5	21		39	11	137	267
	E' at 150 °C, ksi		0.2	0.04	5.1		0.6	0.2	4		48	14	109	212
	E' at RT/*E*' at 150 °C, %		9%	5%	11%		32%	4%	17%		99%	12%	70%	12%
	E' at 200 °C, ksi		0.2		2.6		0.3	0.1	2.5		30	6	98	191
	E' at RT/*E*' at 200 °C, %		3%	6%	6%		20%	2%	12%		82%	24%	59%	19%

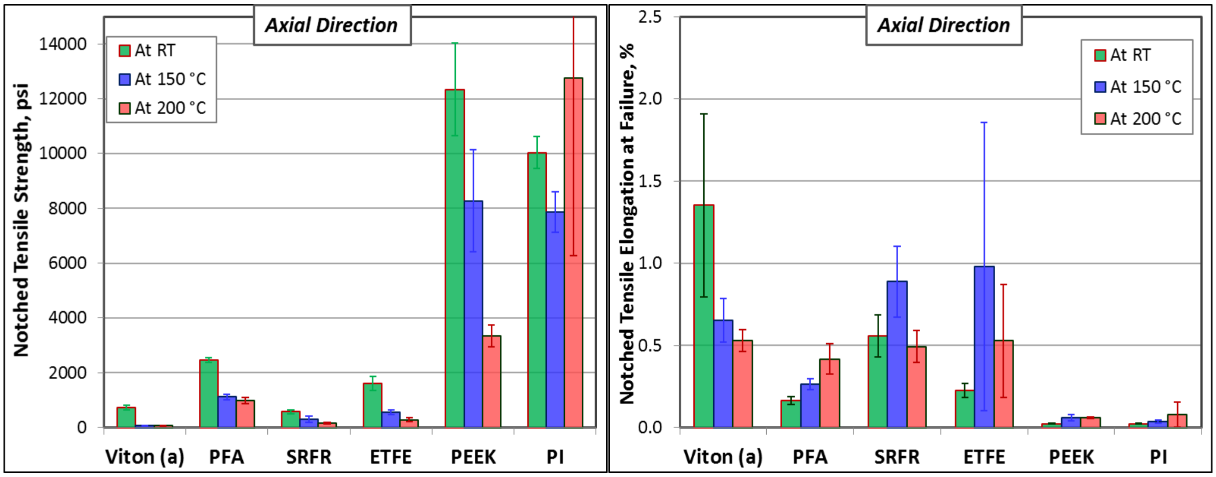

Figure 23.—Notched tensile properties in axial direction of shrink tubing candidates at various temperatures.

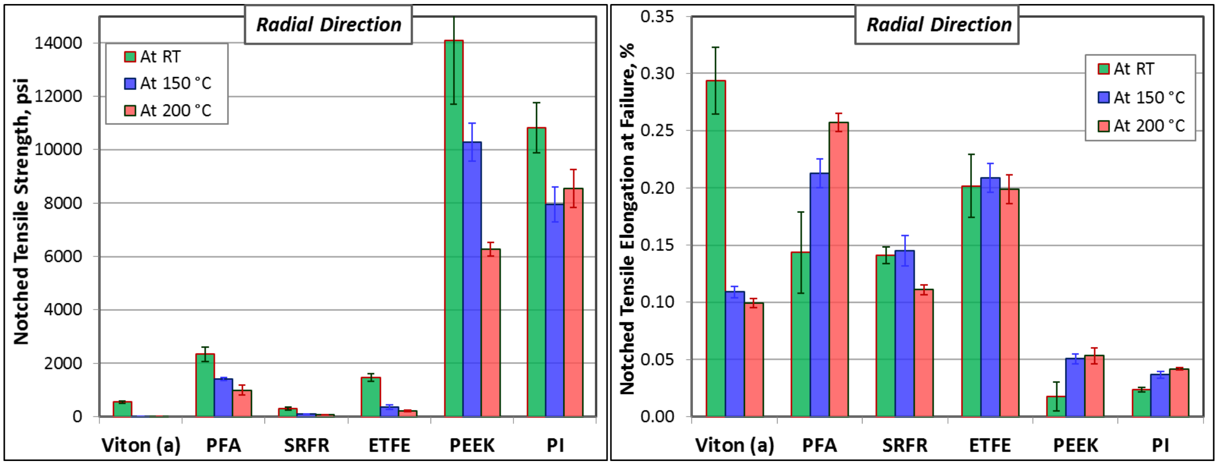

Figure 24.—Notched tensile properties in radial direction of shrink tubing candidates at various temperatures.

TABLE 13.—OVERALL RATINGS OF SHRINK TUBING CANDIDATES FOR DOWN-SELECTION

Material type Properties		Viton (α)	PFA	SRFR	ETFE	PEEK	PI
Shrinking temperature		+	+	+	+	–	–
Shrinking ratio		+	–	+	+	–	–
FT-IR at RT: on both OD and ID		0	0	0	0	0	0
Thermal Degradation Temperature/TGA		+	+	+	+	+	+
Weight loss/outgassing potential/iso-TGA		+	+	+	+	–	–
Thermal transition/mDSC		0	0	0	0	0	0
Modulus-drop ratio at temperature/DMA	Axial	–	–	0	0	+	+
	Radial	–	–	0	0	+	+
Notched tensile strength:	Axial	–	0	0	0	+	+
Notched tensile strength:	Radial	–	0	0	0	+	+
Final selection				✓	✓		

Note: 0, neutral or insignificant effect; +, positive performance; –, negative performance

4.1.4 O-Ring Application

Initial screening evaluations of o-ring candidates involved short-term thermal stability, outgassing characteristics, and mechanical performance. Mechanical performance was evaluated by compression-set at 200 °C and tensile strength at RT, 150, and 200 °C of as-received samples or samples after the compression-set at 200 °C. Other properties from manufacturer's data sheet, e.g., hardness at RT and maximum use temperature, were also considered for screening. The overall thermal properties and outgassing characteristics of all five candidates are summarized in Table 14. T_g of the fluoroelastomers were considerably higher than those of silicone materials, which can be more suitable for the high temperature applications. Both silicone materials were semi-crystalline with T_m at around –40 °C, but the high temperature T_m of Markez Z1307 came from the semi-crystalline nano-filler. T_d of all candidates, either from DSC or TGA test, was sufficiently higher than the future Stirling convertor target temperatures, i.e., satisfactory short-term thermal stability. In general, silicone materials showed greater outgassing potentials than fluoroelastomers.

Young's modulus was measured in tension mode on radial direction of o-ring while DMA storage modulus was measured in the thickness direction in compression mode and plotted in Figure 25. Temperature dependancy of both moduli was similar in most candidates except S1151. The fluoroelastomers showed much higher Young's modulus than silicones at room temperature but it ended

TABLE 14.—PRELIMINARY THERMAL PROPERTIES AND OUTGASSING CHARACTERISTICS OF O-RING CANDIDATES

	O-ring material		70SLR		S1151		Kalrez		Z 1028		Z1307	
Properties			Avg.	SD	Avg.	SD	Avg.	SD	Avg.	SD	Avg.	SD
DSC/mDSC	T_g, °C		–86	2	–91	2	–2.5	0.9	–0.5	2.5	–9.3	1.6
	T_m, °C		–42	0	–44	0					308	0
	ΔH_{mr}, J/g		6.7	3.4	7.0	1.5					5.6	0.5
	T_{exo}, °C		376	1	370	2			295	1		
	ΔH_{exo}, J/g		76.2	7.2	113.7	34.4			0.8	0.7		
	T_d, °C		452	2	449	1	439	6	442	1	435	4
TGA	T_d, °C		498	11	500	0	470	0	473	1	470	4
	ΔWt%, RT-100°C		0.337	0.14	0.478	0.00	0.039	0.01	0.031	0.02	0.018	0.01
	ΔWt%, 100-200°C		0.943	0.03	1.239	0.04	0.063	0.05	0.190	0.01	0.031	0.02
	ΔWt% at 700°C		53	0.00	55	0.07	77	0.00	88	0.00	100	0.00
Isothermal TGA: normalized	Initial wt loss, wt%	120 °C	0.832		1.000		0.204		0.036		0.019	
		150 °C	1.126		1.617		0.462		0.106		0.005	
		200 °C	1.528		2.077		0.317		0.185		0.013	
	Dwell wt loss, wt%	120 °C	1.588		1.491		0.216		0.305		0.147	
		150 °C	1.041		1.091		0.206		0.244		0.146	
		200 °C	0.766		1.063		0.214		0.064		0.032	
	Wt loss rate [(wt%/min)×1000]	120 °C	0.473		0.608		0.346		0.441		0.267	
		150 °C	0.462		0.559		0.290		0.115		0.266	
		200 °C	0.332		0.409		0.367		0.023		0.044	
DMA, compression	E' at RT, psi		225.8	59.9	609.4		445.4	0.6	293.2		543.8	
	E' at 150°C, psi		166.0	48.8	336.3		292.6	0.0	259.8		198.7	
	E' at RT/E' at 150 °C, %		73%	2%	55%		67%	14%	89%		37%	
	E' at 200 °C, psi		154.2	48.5	295.9		263.2	0.1	287.5		174.0	
	E' at RT/E' at 200 °C, %		68%	3%	49%		60%	9%	98%		32%	

up about the same at elevated temperatures in most candidates. The higher RT modulus of the fluoroelastomers could be attributed to their higher glass transition temperatures, > –9 °C, compared to ~ –90 °C for silicone materials. For both silicones and Kalrez, the increase in Young's modulus after the 200 °C compression-set testing was consistent with their higher C_B, probably due to permanent densification of the material during the compression-set testing. This densification would not be desirable as o-ring. Figure 26 shows tensile strength and elongation at failure of the candidates. Similar to modulus, the fluoroelastomers demonstrated significantly higher strength at room temperature, but their strength decreased significantly at the elevated temperatures, even lower than those of silicone materials, which was also associated with their higher glass transition temperatures. The compression-set testing at 200 °C raised the strength of most candidates at 150 °C, but lowered ultimate elongation at failure slightly for the silicone materials while no changes were observed for the fluoroelastomers regardless of changes in C_B. C_B of all high temperature candidates was lower than that of the current control o-ring, 70SLR silicone, while the Z1028 o-ring showed best performance, Figure 27. Repeat testing confirmed that the slight but continuous recovery of C_B with time was the unique behavior of the S1151. Even though no major differences were found among the candidates from the screening evaluations, but performance ratings of specific properties relative to convertor o-ring performance requirements lead to those two final selections, S1151 silicone and Markez Z1028, as summarized in Table 15.

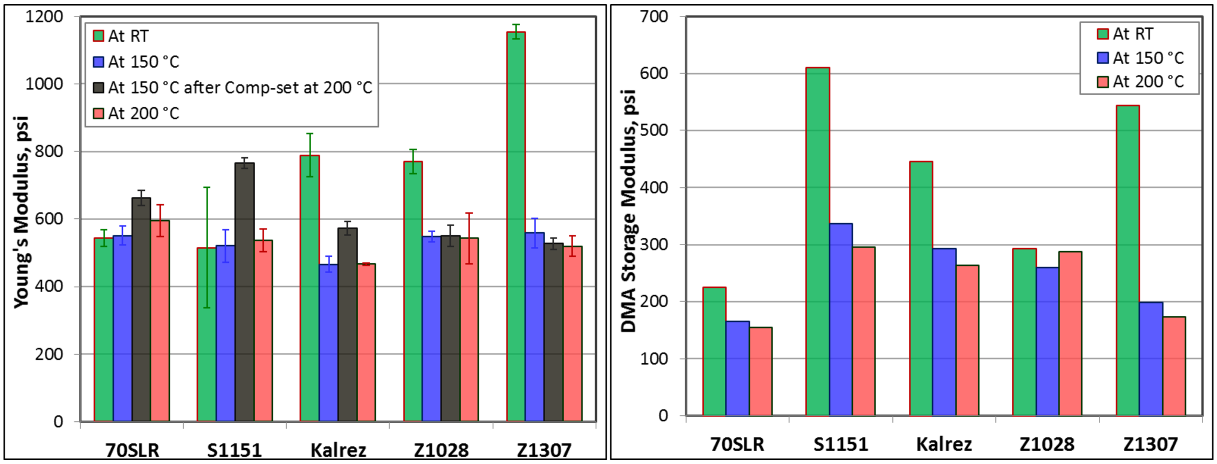

Figure 25.—Tensile Young's modulus of o-ring candidates at various temperatures compared to DMA storage modulus in compression mode.

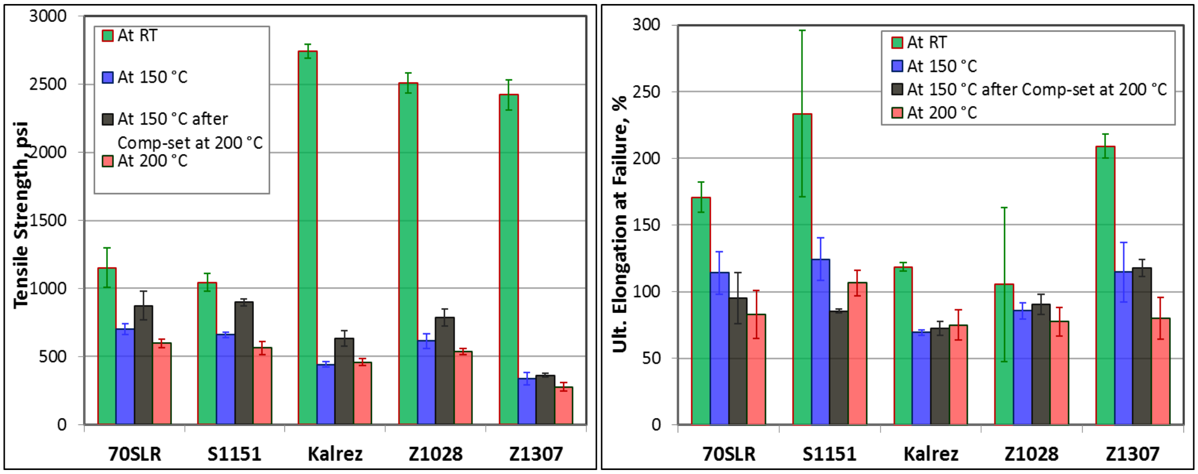

Figure 26.—Tensile strength and elongation at failure of o-ring candidates at various temperatures.

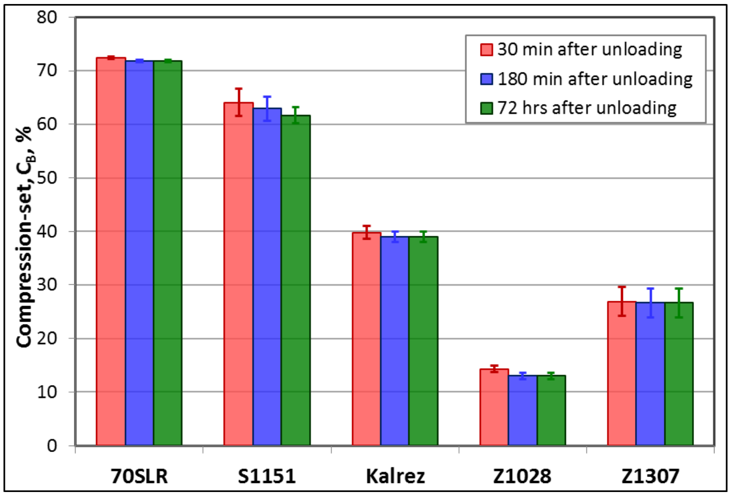

Figure 27.—Compression-set properties of o-ring candidates at various temperatures.

TABLE 15.—OVERALL RATINGS OF O-RING CANDIDATES FOR DOWN-SELECTION

O-ring type Properties	70SLR	S1151	Kalrez	Z1028	Z1307
FT-IR	0	0	0	0	0
mDSC/DSC – Thermal transitions	0	0	0	0	0
TGA – Thermal degradation onset	+	+	+	+	+
DMA – Compression Storage modulus	–	–	+	+	+
Compression-set	0	0	0	+	+
Tensile properties: Modulus	0	+	–	–	–
Tensile strength	0	0	–	+	–
Ultimate elongation	0	0	0	0	0
Max use temp by manufacturer	0	+	+	+	+
Final selection		✓		✓	

Note: 0, neutral or insignificant effect; +, positive performance; –, negative performance

4.2 Extended Property-Performance Evaluations

The down-selected candidates from the initial screening evaluations, typically 2 to 3 candidates per material type, were further evaluated more extensively and systematically for functionality performance, longer-term thermal stability, and material compatibility using various thermal or accelerated thermal aging tests for up to 6 months and TCIOP tests involving comprehensive and systematic residual property characterizations as summarized in the overall program plan, Figure 1. Based on the extensive evaluations, application limits of each candidate were identified and thus the final selection of the best candidate was recommended for the future high temperature more efficient or more reliable convertors.

4.2.1 Functional Performance

Since the adhesive material was identified as the most critical organic material for the Stirling convertor application due to its single point failure reliability assessment, e.g., magnet bonding (Refs. 6 and 9), more efforts were made especially on its functionality-related performance evaluations. It is also well known that overall performance of thermoset polymer adhesives is greatly affected by how they are cured, primarily bonding integrity, particularly under fatigue loading mode. Therefore, additional efforts were made to optimize the cure conditions of the down-selected adhesive candidates and ultimately, their fatigue performance in the full-scale component level testing.

4.2.1.1 Process Optimization

4.2.1.1.1 Cure Optimization of Adhesive/Potting Candidates

While the standard cure conditions recommended by the manufacturers were validated and used for the initial screening evaluations, additional efforts were made to fully understand their cure kinetics and to further optimize the cure conditions of the down-selected candidates because of their critical impact on properties and performance of the epoxy adhesives. Figure 28 shows the typical exothermic cure reaction behavior of the candidates as a function of temperature considered as a total cure reaction. 3M AF131-2 showed the main reaction starting at 160 °C, peaked at 201 °C, and its total heat of reaction, ΔH_T, for full cure was 376.1 J/g. Even though the total cure reaction under temperature ramp showed one main exothermic peak, the isothermally cured samples appeared to involve two exothermic peaks upon reheating, possibly related to changes in molecular diffusion process. On the other hand, EA9394C-2 underwent two-step cure process with two exothermic peaks, the first major reaction had the onset at 81 °C and peaked at 118 °C while the second peaked at 247 °C. Thus, for EA9394C-2, $\Delta H_T = 243.6 + 13.59$ J/g = 157.2 J/g. This total heat of reaction was used in calculating degree of cure (or % cure) as follow: % cure = 100 × $(\Delta H_T - \Delta H_R)/\Delta H_T$ where ΔH_R was residual heat of reaction involved in curing the uncured part of the adhesives. In general, the manufacturer’s recommended cure temperatures were consistent with their cure profiles.

Overall cure kinetics analyses are summarized in Table A.1 and Table A.2 for AF131-2 and EA9394C-2, respectively, in Appendix A. Based on extensive evaluations in terms of cure temperature-time-% cure-thermal properties relations including the results from both 15-day thermal aging and 6-month accelerated thermal aging tests, the most acceptable optimum cure-postcure conditions, typically the degree of cure higher than 99.5% were determined for both candidates. Conditions that were not acceptable due to either under-curing or potential thermal degradation were also identified. The optimum conditions typically required higher cure temperatures or much longer cure time than the manufacturer’s recommended conditions. For example, increasing the postcure temperature to 190 to 205 °C for up to 360 hr improved thermal stability of both candidates.

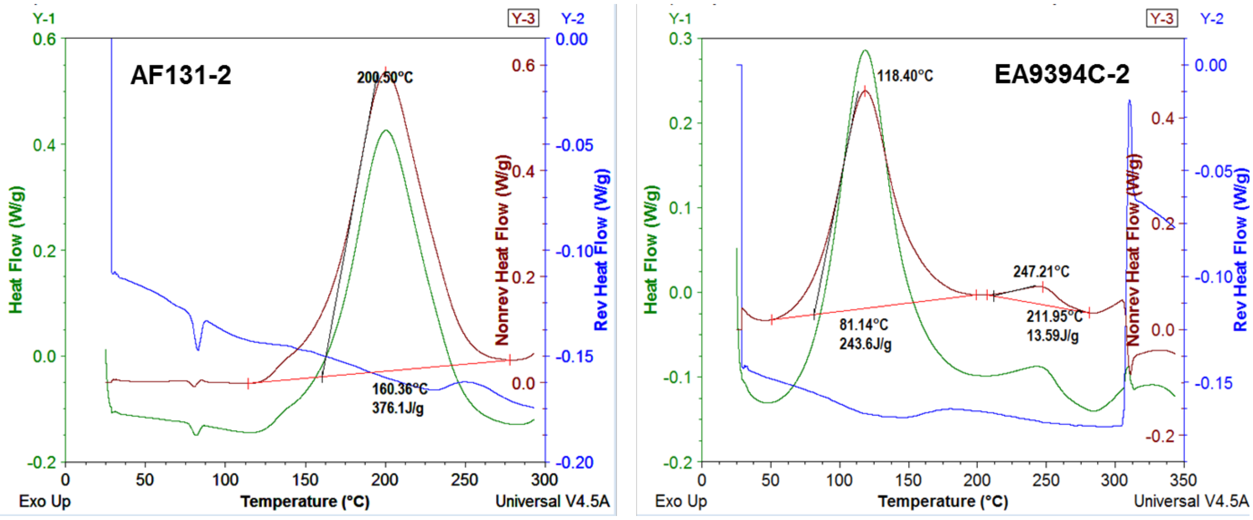

Figure 28.—Typical cure reaction behavior of the down-selected adhesive candidates via mDSC.

From the combined cure kinetics data, a distinctive % cure-T_g correlation which can be used for performance predictions was derived for both epoxy candidates regardless of specimen thickness, Figure 29. The cure-postcure conditions caused possible thermal degradation were clearly off the trends and illustrated that their T_g was significantly lower from those of the fully cured samples. As can be seen in the plot, AF131-2 reached the full-cure state faster compared to the T_g increase, while EA9394C-2 showed a nonlinear relationship with increasing degrees of cure. The highest T_g achieved was fairly close for both adhesive candidates, 260 °C for EA9394C-2 vs. 270 °C for AF131-2, even though the AF131-2 started with considerably higher T_g at the primary cure states. Similarly, a % cure-T_d correlation was also derived from the combined cure kinetics data for both epoxy candidates, Figure 30. The cure-postcure conditions caused potential thermal degradation were also clearly off the trends. The AF131-2 reached the full-cure state quicker than EA9394C-2 against the T_d increase even though the maximum T_d achieved in EA9394C-2 was slightly higher than that of AF131-2. The cure-thermal aging-% cure–thermal property relationship can be used to differentiate cure advancement from thermal degradation, thus to predict aging performance or thermal stability of the epoxy candidates. Based on various thermal properties, degrees of cure, and outgassing characteristics as a function of cure conditions, the initial standardized cure conditions determined by the manufacturer's recommendations were acceptable for both magnet bonding and stator potting and were thereby used for the extended performance evaluations for both adhesive candidates.

4.2.1.2 Fatigue Performance of Adhesive Candidates

Fatigue performance on bonding between magnets to titanium magnet-can with the down-selected adhesive candidates was assessed by full-scale component level coupon testing. Figure 31 show the master fatigue SN curves of magnet bonding at 180 °C for EA9394C-2 and AF131-2, respectively. Fatigue performance of the Hysol EA9394C-2 at 180 °C (FS = ~ 630 psi, R = 0.86) was comparable to those of the regular Hysol EA9394 tested at 115 °C (~ 800 psi, 0.74) which was evaluated extensively for the one of current SOA lower temperature Stirling convertors (Refs. 6 to 8), and exhibited potential to improve with further bonding process optimizations. Fatigue performance of the AF131-2 (FS=~3,560 psi, 0.97) was superior to EA9394C-2 epoxies. It was less reliable due to a fewer data points, but the results were verified with the sub-scale sand-witch lap-shear samples as a part of thermal stability assessment. In either case, the fatigue endurance strengths of both candidates calculated from the SN curves were much higher than the theoretical bond strength needed for this application (Refs. 6 and 9).

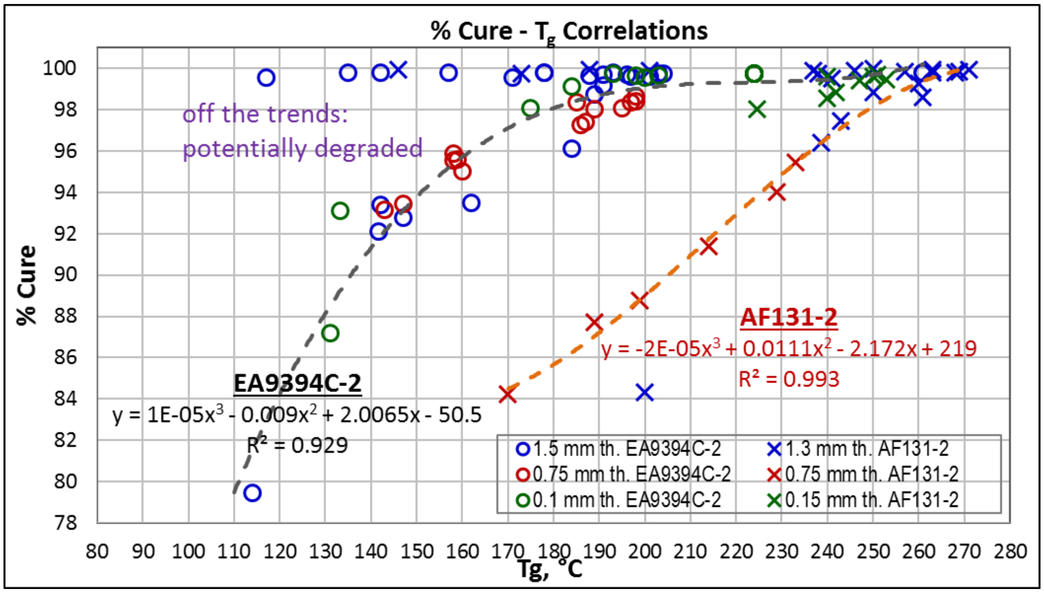

Figure 29.—Degree of cure – T_g correlations of adhesive/potting candidates.

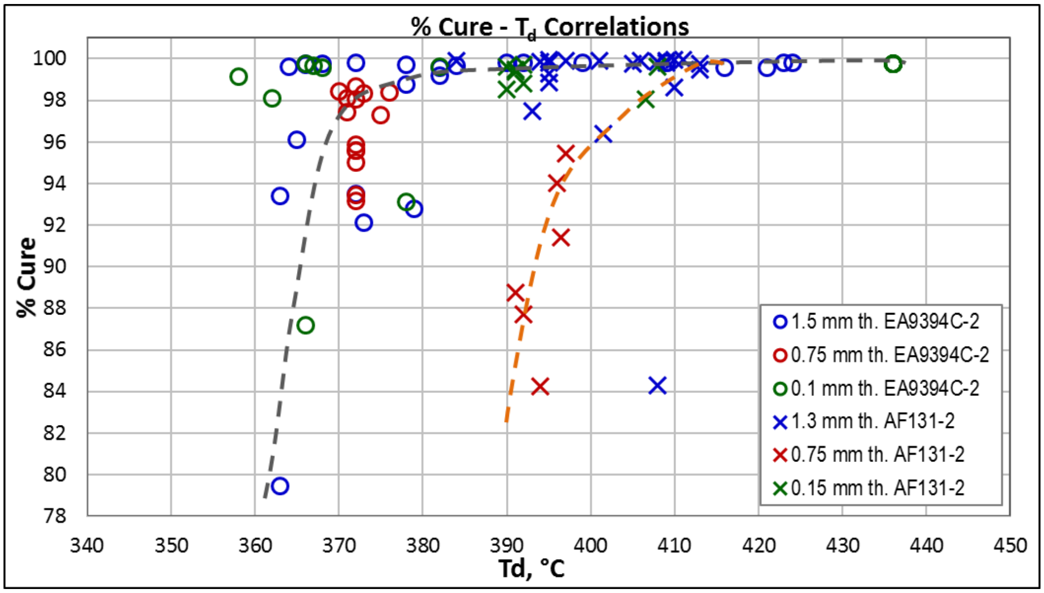

Figure 30.—Degree of cure – T_d correlations of adhesive/potting candidates.

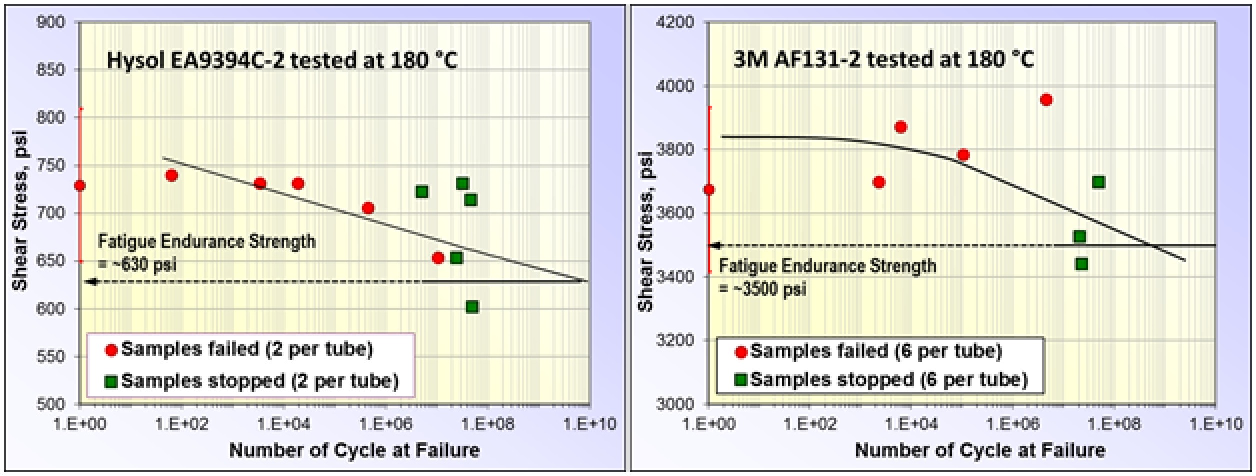

Figure 31.—Fatigue SN curve of Hysol EA9394C-2 adhesive bonding at 180 °C.

4.2.2 Long-Term Thermal Stability

The longer-term performance and thermal stability were evaluated by 15-day thermal aging tests at various temperatures up to 260 °C, followed by the 6-month accelerated thermal aging experiment. Typically, two to three temperatures were planned for the accelerated thermal aging tests in order to assess longer-term performance and life predictions. The maximum temperatures for the accelerated aging tests, which would maintain the same aging mechanisms as the target use-temperature but accelerate their aging processes, were determined from the results of the 15-day thermal aging tests.

Figure 32.—Typical color changes of the adhesive/potting candidates after 15-day thermal aging at various temperatures.

4.2.2.1 15-Day Thermal Aging Test

Specific objectives of this test were to assess more meaningful but practical short-term thermal stability of various down-selected organic candidates and to determine the aging mechanism-based maximum temperatures for the next longer-term 6-month accelerated thermal aging tests.

4.2.2.1.1 Adhesive/Potting Candidates

The overall test matrix is summarized in Table A.1 in Appendix A in terms of various assigned test specimens (their identification numbers listed), selected aging temperatures, and residual properties to be monitored. As described in the experimental section, the test matrix was completed in two test sets, the first set at four temperatures; 130, 160, 190, and 260 °C, followed by the second set at three additional temperatures at 175, 205, and 220 °C. The temperatures for the second set were decided based on the results of the first set to ascertain the trends of the systematic physical, thermal, chemical, and mechanical properties from the first set. Figure 32 shows typical changes in color and shape/physical state of the neat resin samples, both thin and thick, from the first series of 15-day thermal aging tests. It was clear that the most visible changes occurred at 260 °C where both candidates darkened significantly, and appeared to have blistered and cracked, which are signs of thermal degradation. Figure 33 illustrates that both candidates showed a dramatic change in weight loss rate around 220 to 230 °C regardless of specimen thickness, which was a strong indication of changes in aging mechanism or onset of thermal degradation. The EA9394C-2 epoxy showed slightly higher weight losses than AF131-2 epoxy in the lower aging temperature range below the transition, but considerably lower than the regular EA9394 (Refs. 6 and 9). Its transition temperature was about 30 °C higher than the regular EA9394 epoxy.

Effects of aging temperature on static bonding performance of the candidates evaluated by the sub-scale sandwich lap shear specimens at the 120, 170, and 200 °C test temperatures are summarized in Figure 34 and Table A.4 in Appendix A. Both bond strength and toughness began to decrease at aging temperatures exceeding 130 °C and continued to increase as the aging temperature increased, independently of the test temperature. The rate of decrease was considerably higher after about 220 °C for both candidates. This was another indication of changes in aging mechanism or onset of thermal degradation. Slight increases in bonding properties up to 130 °C in both candidates were probably due to cure advancement during aging. Differences in bonding properties between the two candidates were narrowed with increasing aging temperature. The EA9394C-2 showed much improved bonding properties than the regular EA9394 and increased the transition temperature by ~ 30°C.

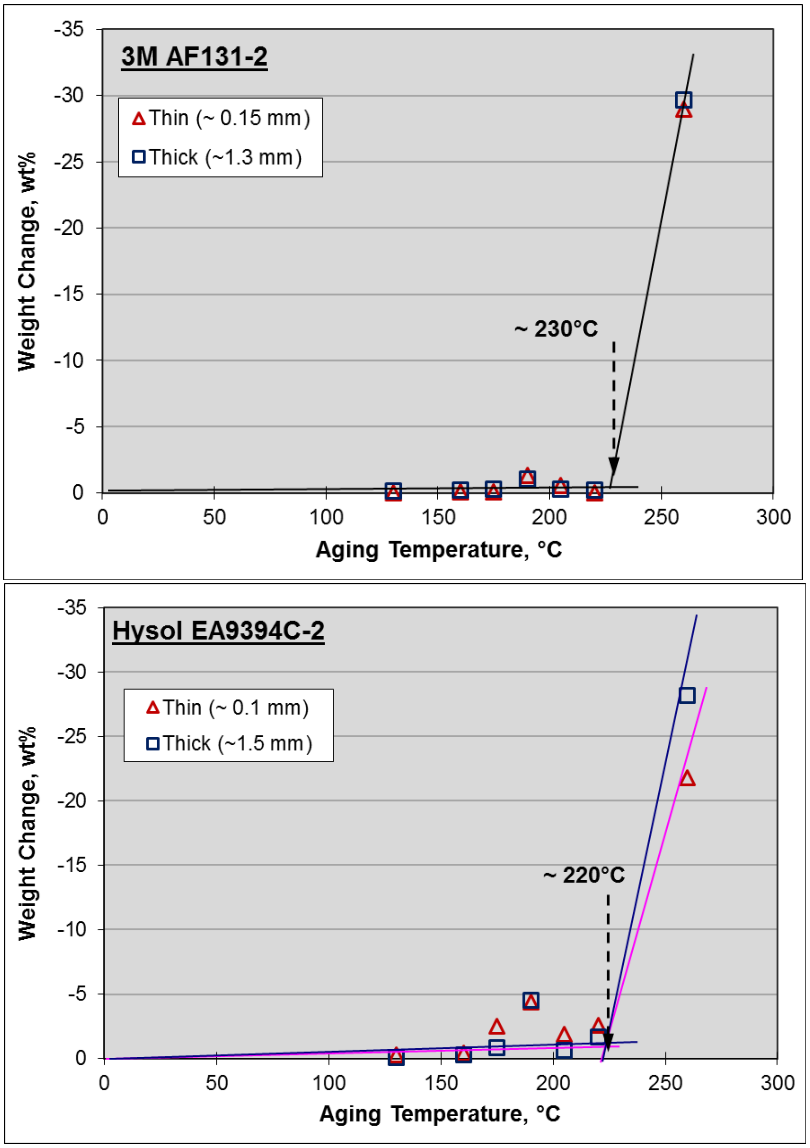

Figure 33.—Weight losses of adhesive candidates after 15-day thermal aging as a function of aging temperature.

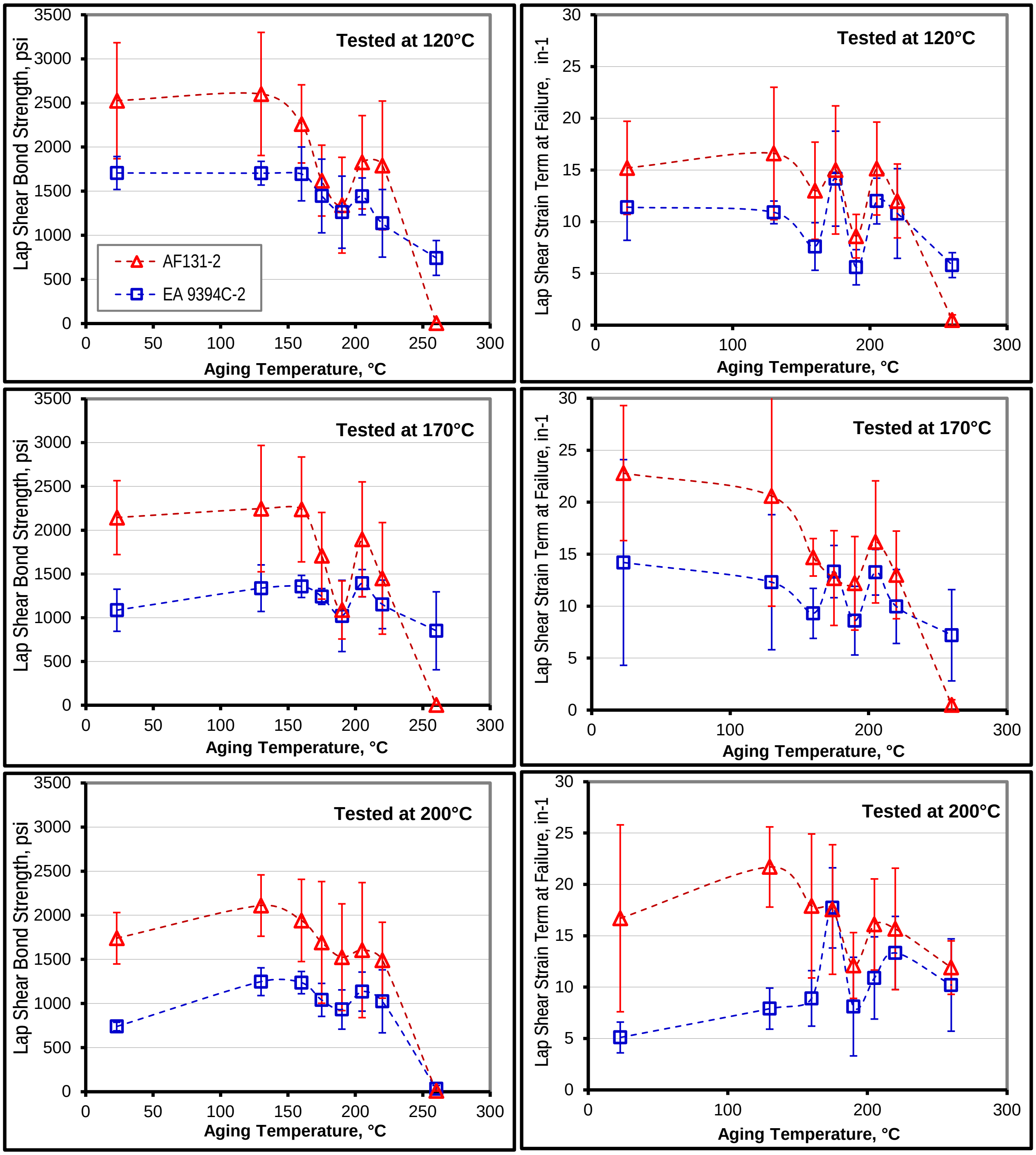

Figure 34.—Lap shear bonding properties of adhesive candidates after 15-day thermal aging as a function of aging temperature at various test temperatures.

Figure 35 shows various thermal properties of the candidates as a function of aging temperature. It was clear that major transitions in most thermal properties occurred at around 220 to 230 °C regardless of sample thickness or test method in both candidates. This was consistent with other properties in terms of changes in aging mechanism or onset T_d. Increases in T_g and/or T_d after the transition were probably due to oxidative thermal degradation or char formation which was manifested by a significant drop in ΔW% at

700 °C. Again, the transition temperature of the EA9394C-2 was about 30 °C higher than that of the regular EA9394 epoxy.

The transition behavior was also characterized by FT-IR. Figure 36 shows typical FT-IR spectra of AF131-2 from thin (left) and thick (right) sheet samples aged at various temperature. Most noticeable molecular structural changes were observed after aging at 260 °C. This was consistent with the transitional behavior of other properties. The EA9394C-2 showed the similar behavior as the AF131-2 epoxy, which was indicated by a stable molecular network structures up to 220 °C and apparent degradation-related changes in IR spectra after aging at 260 °C, Figure 37.

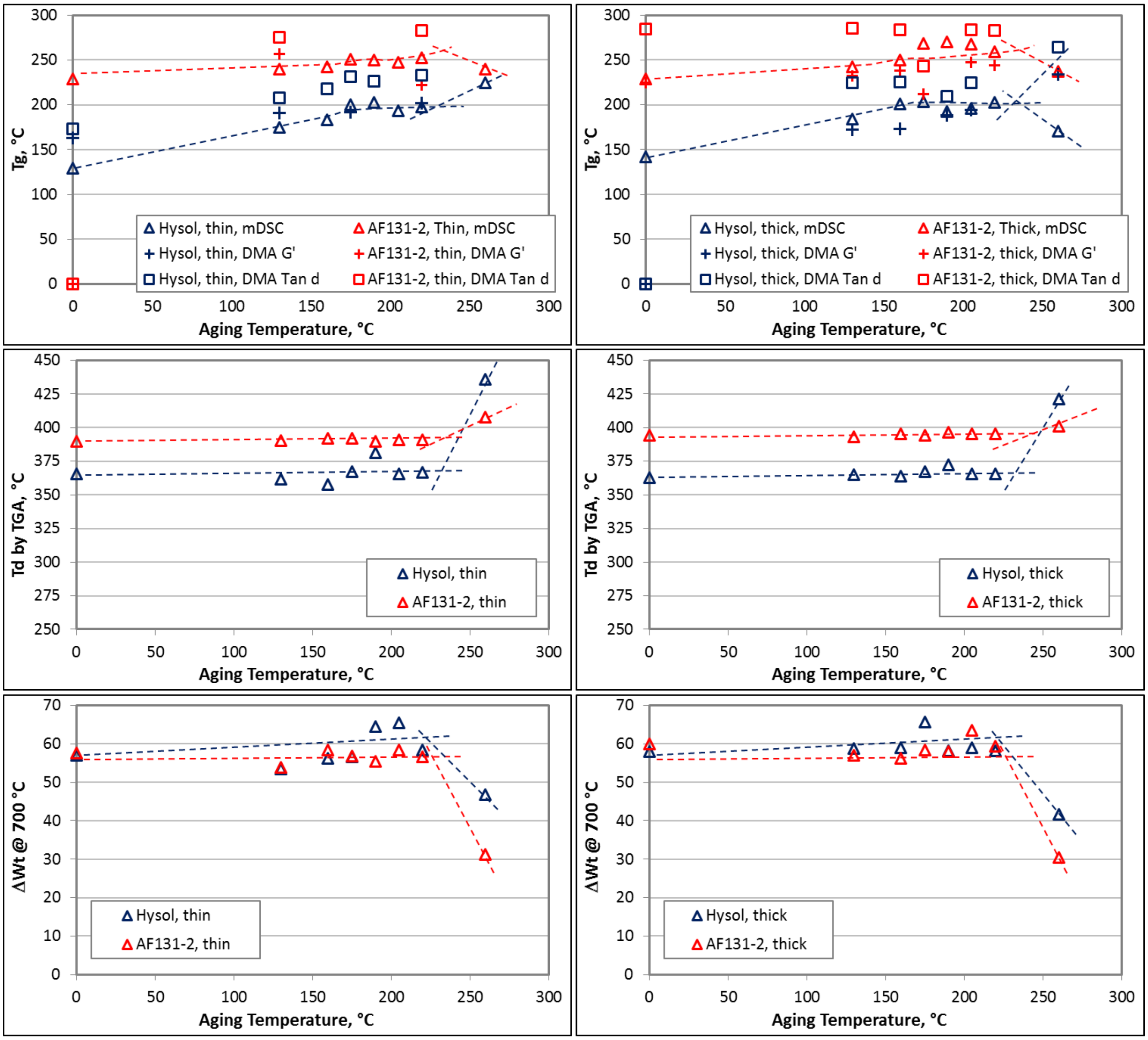

Figure 35.—Various thermal properties of adhesive candidates after 15-day thermal aging as a function of aging temperature.

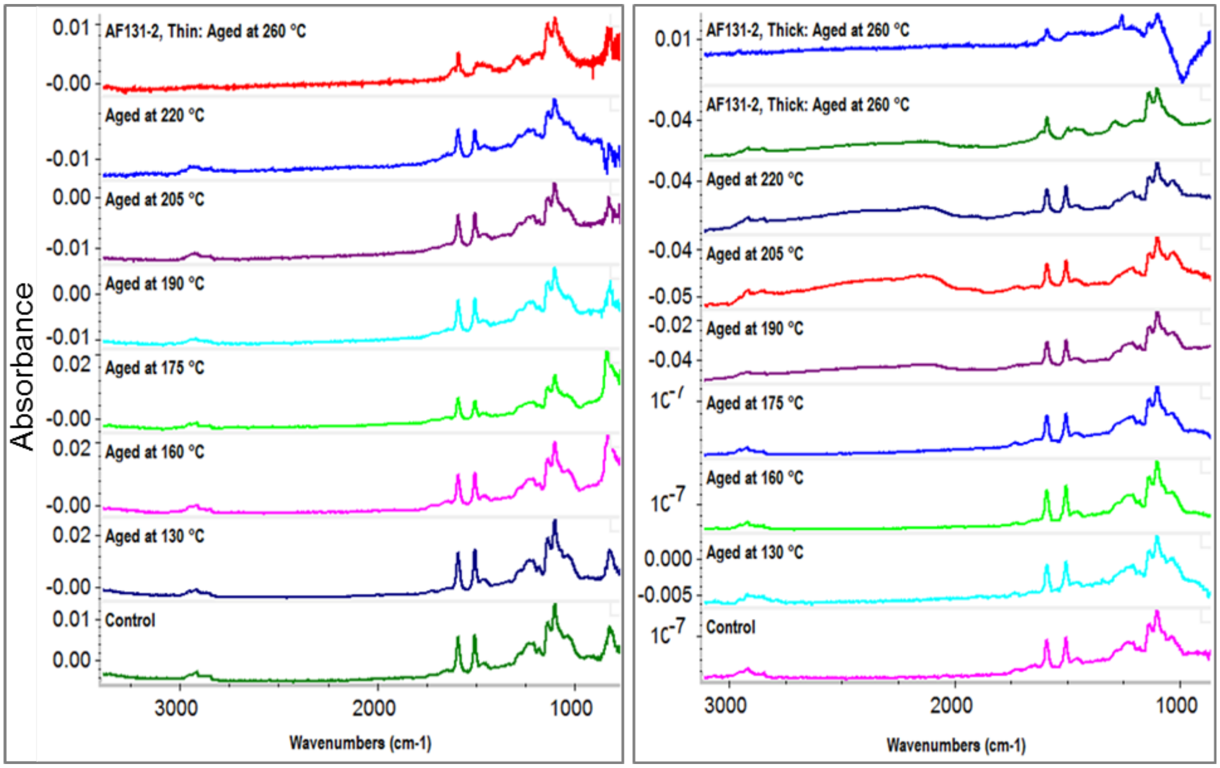

Figure 36.—Typical FT-IR spectra of AF131-2 epoxy from both thin and thick sheet samples aged at various temperatures.

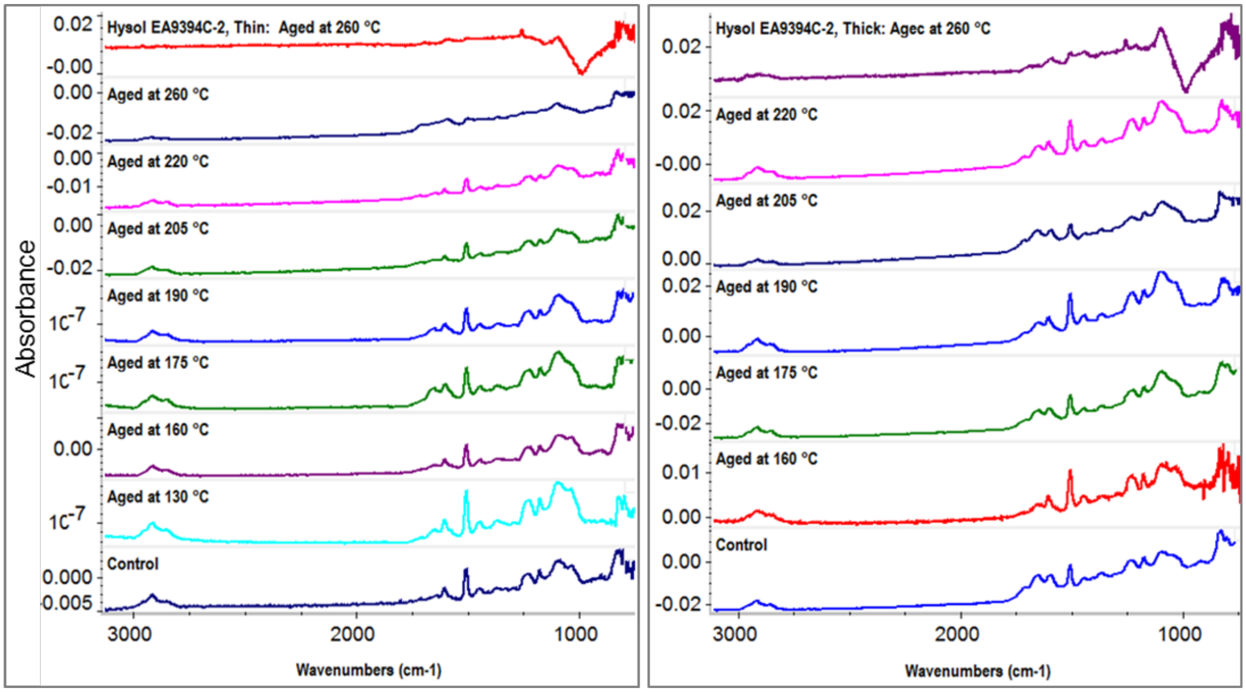

Figure 37.—Typical FT-IR spectra of EA9394C-2 epoxy from both thin and thick sheet samples aged at various temperatures.

Based on the overall test results of the 15-day thermal aging experiment, both epoxy candidates can be considered stable up to 220 to 230 °C for a short-term exposure, and involved no noticeable changes in aging mechanisms. Thus, the maximum temperature determined for the longer-term accelerated thermal aging tests was 225 °C. Consequently, the three temperatures, 175, 200, and 225 °C were selected for the accelerated aging tests for more comprehensive and systematic evaluation of the candidates. The high temperature formulation, EA9394C-2, was proven for its improved thermal stability than the original EA9394 epoxy, by about 30 °C.

4.2.2.1.2 Thread Locker Candidates

Overall test matrix was summarized in Table A.5 in Appendix A in terms of torque sample assignment for various aging temperature and post-aging torque test temperature for three down-selected candidates. The aging experiment was performed at only five temperatures, 130, 160, 190, 220, and 260 °C. All aging experiments were carried out simultaneously. For all five aging test setups, both temperature and nitrogen gas flow rate were controlled reasonably well throughout the entire 15-day aging experiment. Weight changes, mostly losses, of the candidates as a function of aging temperature are plotted in Figure 38 for all three joint types. Overall, all candidates showed similar weight loss behavior with increasing aging temperature. The trends for all samples started with slower mass loss rates at the lower aging temperatures up to ~ 220 °C, but then followed much steeper rates as the temperature increased. This suggested that above the transition temperature, ~ 220 °C, the TL materials underwent potential changes in aging mechanism or T_d. The Poly-Lok PET patch showed most data scattering since the exact amount of patch was not directly measured but calculated based on average weight of the fastener. Greater data scattering from the #2 joint samples in both Loctite 294 and Resbond 507TS was probably related to its blind-hole configuration, such as a large variation of thread locker amount in the contact area, excessive material outside of the contact area, or more under-cured material due to trapped air, etc.

Figure 39 illustrates typical torque-angular displacement curves of the down-selected candidates per joint type regardless of test temperature. Note that the shape of the curve depended more on joint type than material type.

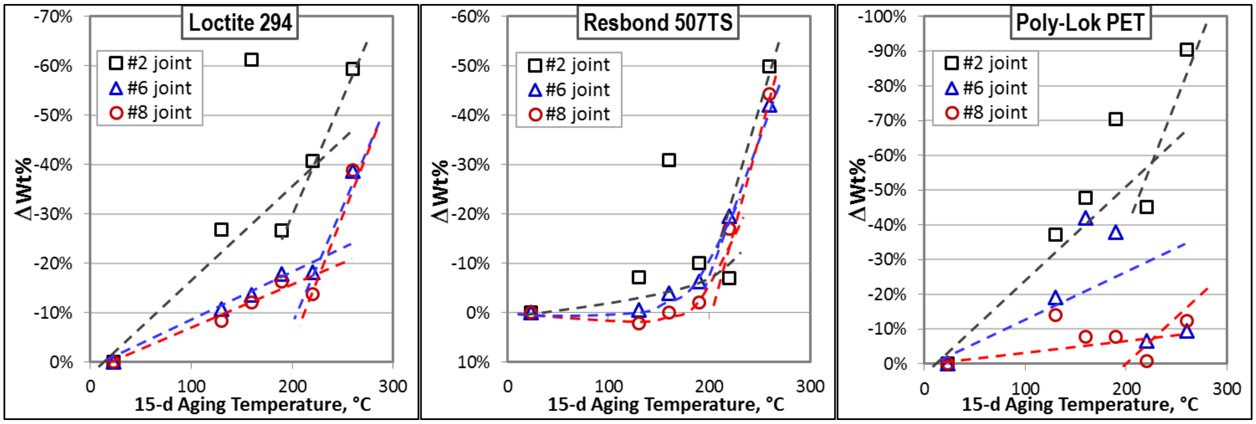

Figure 38.—Weight loss trends of thread locker candidates as a function of aging temperature.

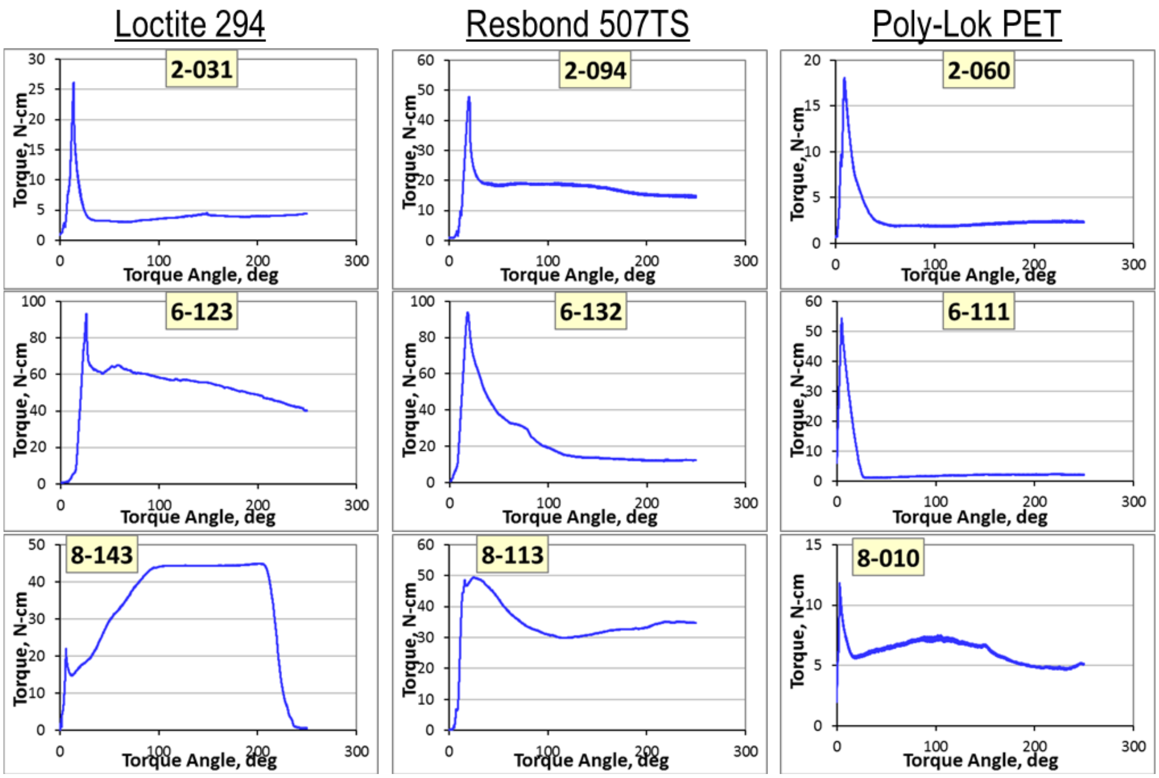

Figure 39.—Typical torque-angular displacement curves of thread locker candidates per joint type.

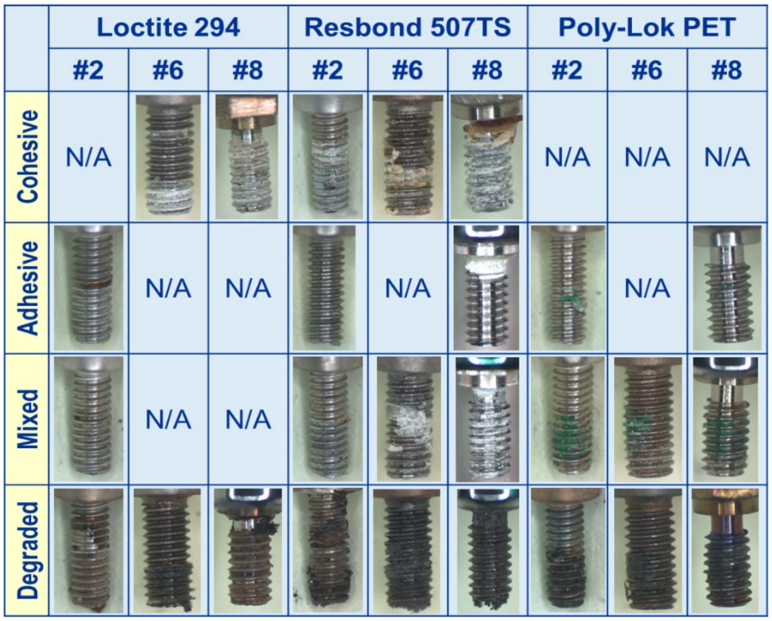

Figure 40.—Micrographs showing typical failure modes of thread locker candidates in various joint types.

Figure 40 shows failure modes of the TL candidates per Joint type. As can be easily seen in the pictures, the cohesive mode involves failure throughout TL layer indicated by more TL residues covering most fastener surfaces while the adhesive mode involves failure at the fastener surfaces which shows little or no TL residues on fastener. The mixture mode can be presented by powdery or localized TL residues on fastener. When the residues of TL was severely darkened, it was called ‘degraded’. This classification was mostly based on fastener-side observation. Degree of cure and solidification pattern of Loctite 294 or Resbond 507TS TL were considerably affected by the joint type and configuration, and ultimately the failure mode. Amount of TL residues adhered on fasteners varied considerably with the joint type. In some cases of the Poly-Lok PET, the patch location was not optimal, and symbolized lower engagement in the contact area.

For evaluating torque performance of the down-selected TL candidates, the unaged control samples were tested first as a function of test temperature as summarized in Table A.6 in Appendix A and Figure 41. The summary table presented both torque strengths and failure modes (via color code). Breakloose torque was also calculated in terms of % installation torque, defined by 100 × Breakloose torque/Installation torque. Regardless of material type, the joint #2 with blind-hole configuration always showed less favorable failure modes, either adhesive or mixed mode. Samples indicated by a red comment mark on prevailing torque values were prematurely failed as fastener head braking off. Also note that samples marked with a red comment mark on the ID were used for FT-IR microscopy analysis. In the Figure 41, numbers listed next to the breakloose torque data points are the nominal percent installation torque.

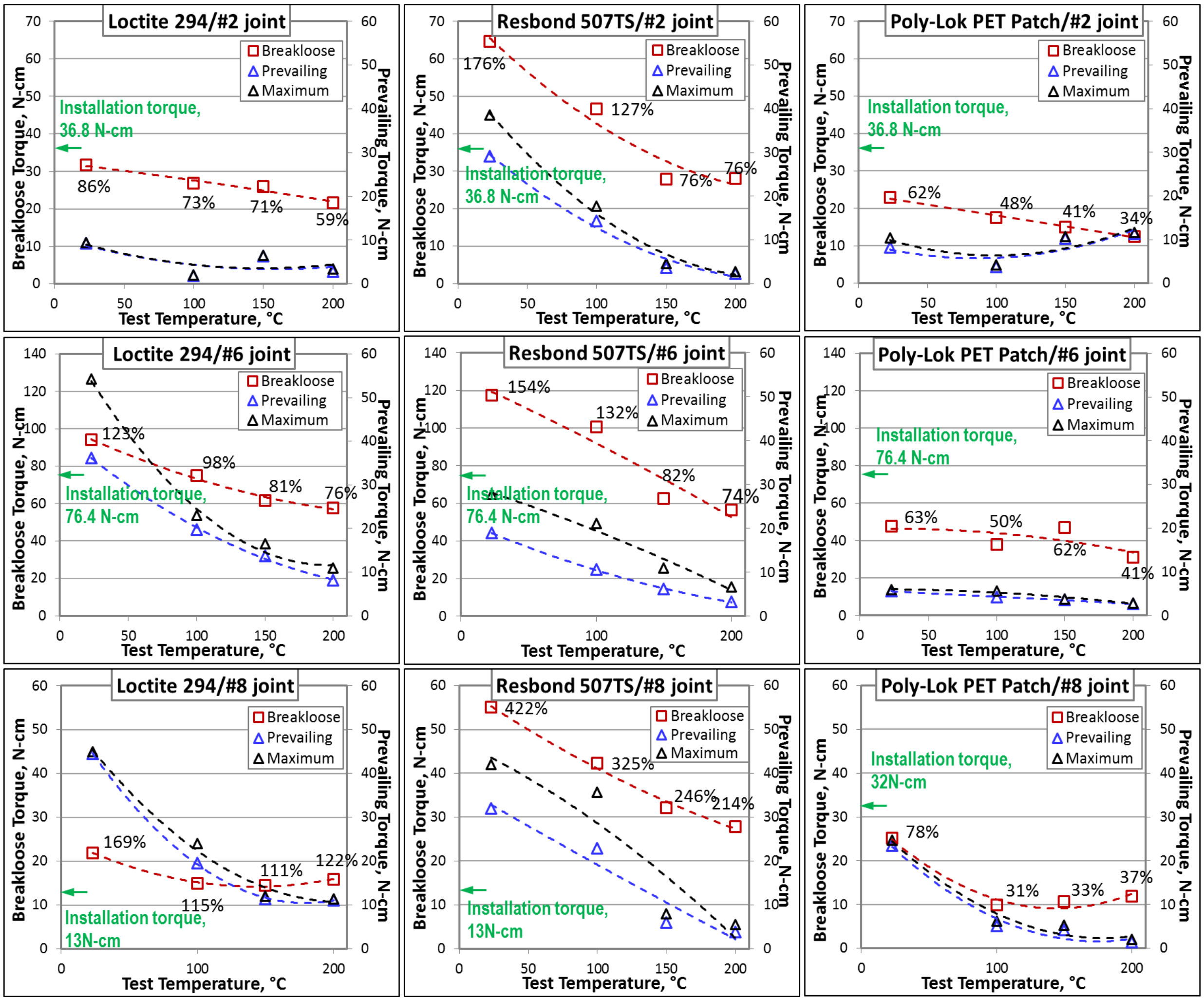

Figure 41.—Effects of test temperature on torque strengths from the unaged controls of thread locker candidates in various joint types. The figures listed next to breakloose data indicate percentage of breakloose torque to the installation torque.

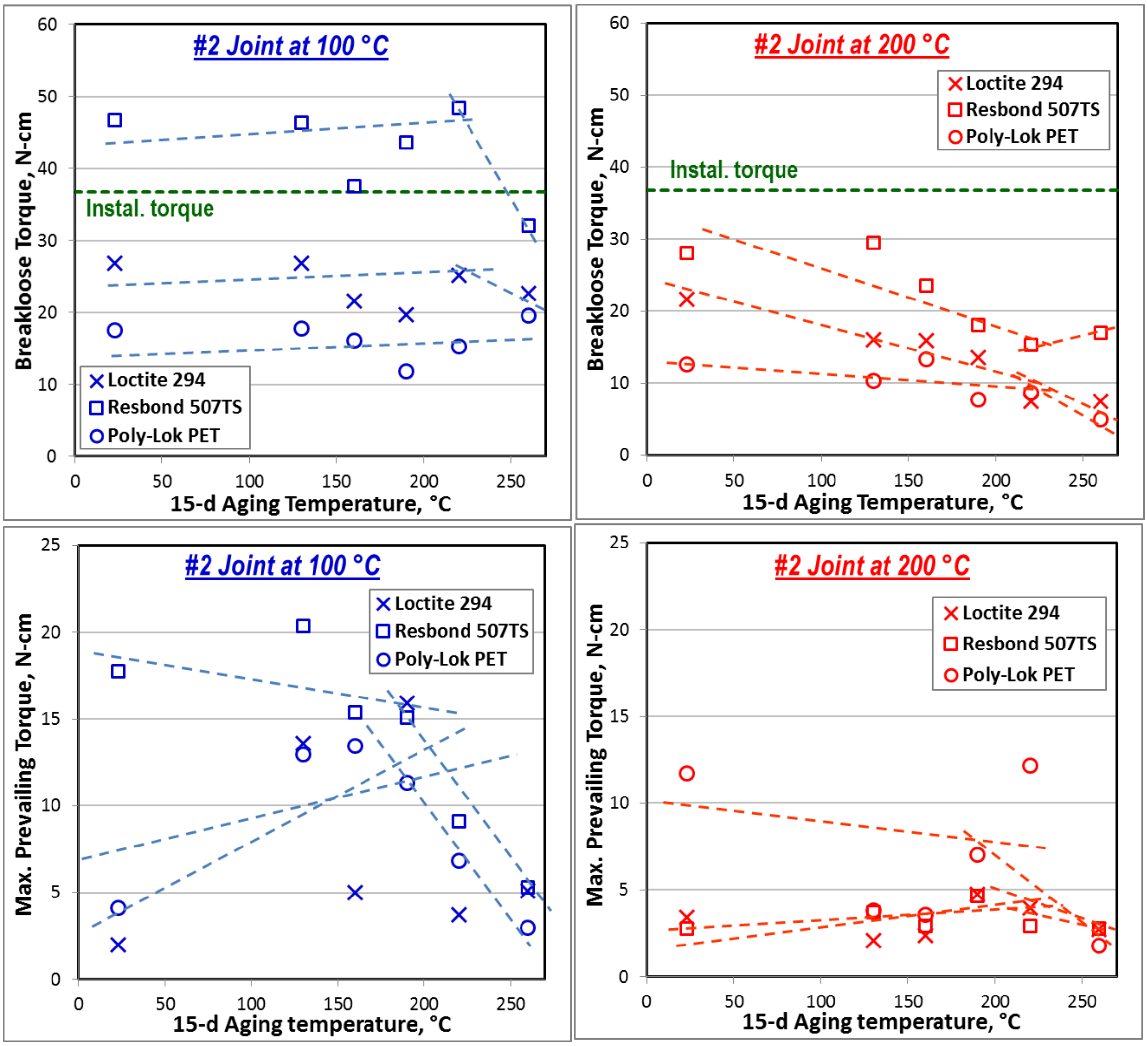

Figure 42.—Torque strengths of thread locker candidates in #2 joint tested at 100 and 200 °C as a function of aging temperature.

Effects of aging temperature on torque strengths of the candidates in joint type #2 tested at both 100 and 200 °C are illustrated in Figure 42, and also summarized in Table A.7 in Appendix A. Regardless of TL type, most samples failed by either adhesive or mixed mode. In most cases, regardless of TL type, the torque strengths remained stable or either slightly changed with temperatures up to ~ 220 °C. At 260 °C, the rate changed was more abrupt, which may have been indicative of changes in aging mechanism. Most samples aged at 260 °C showed completely blackened or charred TL residues on fasteners, which suggested thermal degradation. Resbond 507TS performed best on the blind-hole joint in the aging temperature range. The candidates also exhibited similar transition behavior in joints #6 or #8 as illustrated in Figure 43 (also summarized in Table A.8 in Appendix A) or Figure 44 (also summarized in Table A.9 in Appendix A), respectively. Resbond 507TS still performed best in most cases, but Loctite 294 showed equivalent performance, particularly in prevailing torque. It should be noted that Resbond 507TS underwent the color change at somewhat lower temperatures, at around 220 °C. Most joint #6 and #8 samples of Loctite 294 and Resbond 507TS failed by cohesive mode, while all of Poly-Lok PET failed by mixed mode. Slight increases in torque strengths with increasing temperature up to the transition point were probably related to additional cure advancement. Both Loctite 294 and Resbond 507TS maintained breakloose torque strengths much higher than the installation torque for all of aging temperatures up to 260 °C which suggested good thermal stability.

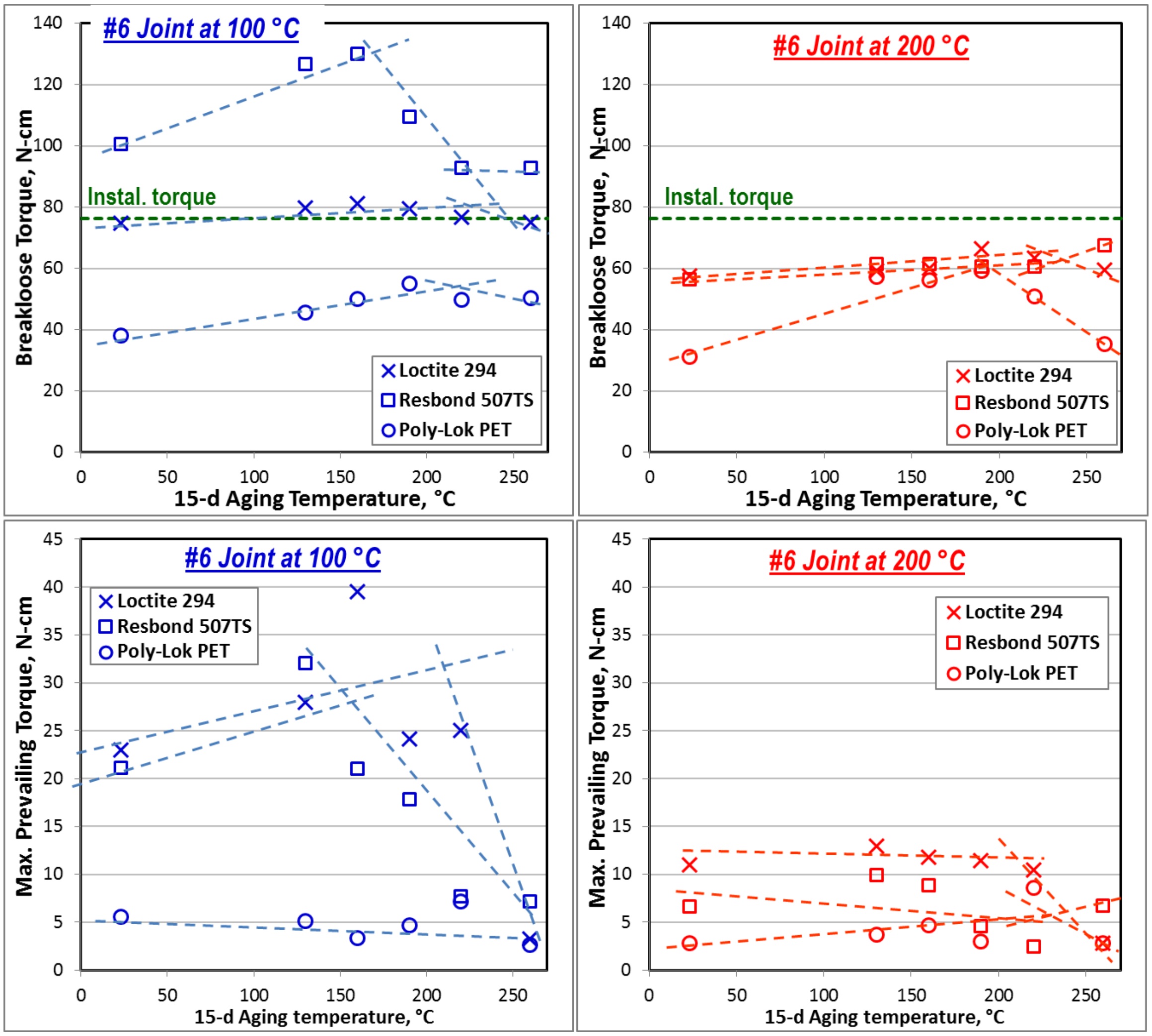

Figure 43.—Torque strengths of thread locker candidates in #6 joint tested at 100 and 200 °C as a function of aging temperature.

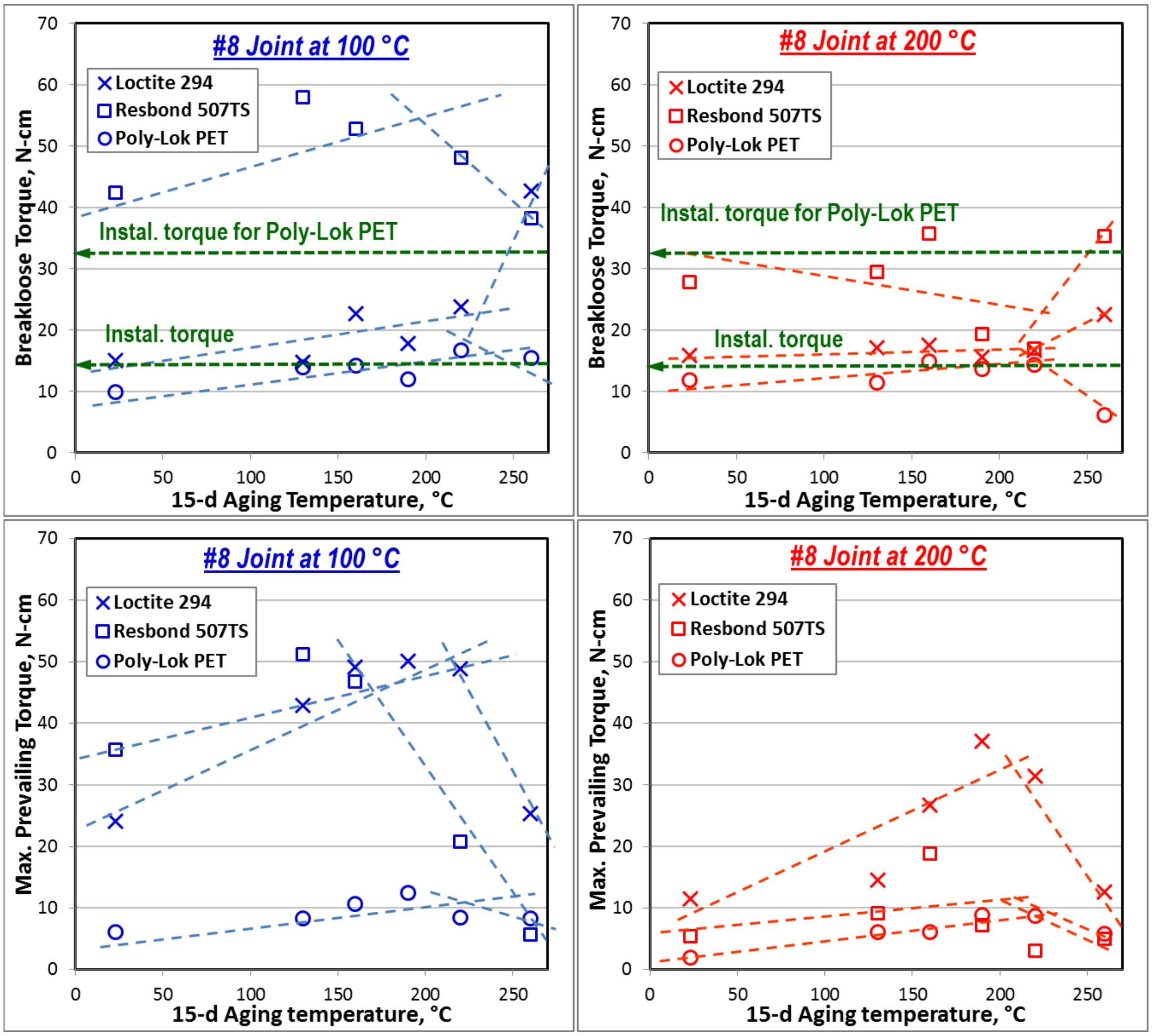

Figure 44.—Torque strengths of thread locker candidates in #8 joint tested at 100 and 200 °C as a function of aging temperature.

In addition, the systematic FT-IR analysis indicated no sign of significant thermal degradation up to 260 °C despite of the color changes in all three candidates as illustrated in Figure 45, Figure 46, and Figure 47. In the case of Loctite 294, a strong peak at 1573 cm^{-1} from the controls started to decrease with thermal aging and disappeared after aging at temperatures above 190 °C. It seemed to suggest that the change was related with cure advancement not necessarily thermal degradation since the change occurred at fairly low temperature. However, when Resbond 507TS was aged at 260 °C, it showed broadening of a few major peaks, such as 1511 and 1454 cm^{-1} peaks and also possibly 1600 cm^{-1} peak. Those changes could be sign of thermal degradation as also suggested by color changes, thus Resbond 507TS can be considered thermally stable only up to 220 °C. Based on the overall test results of the 15-day thermal aging experiment, both 190 and 220 °C were selected for the 6-month long-term accelerated aging tests.

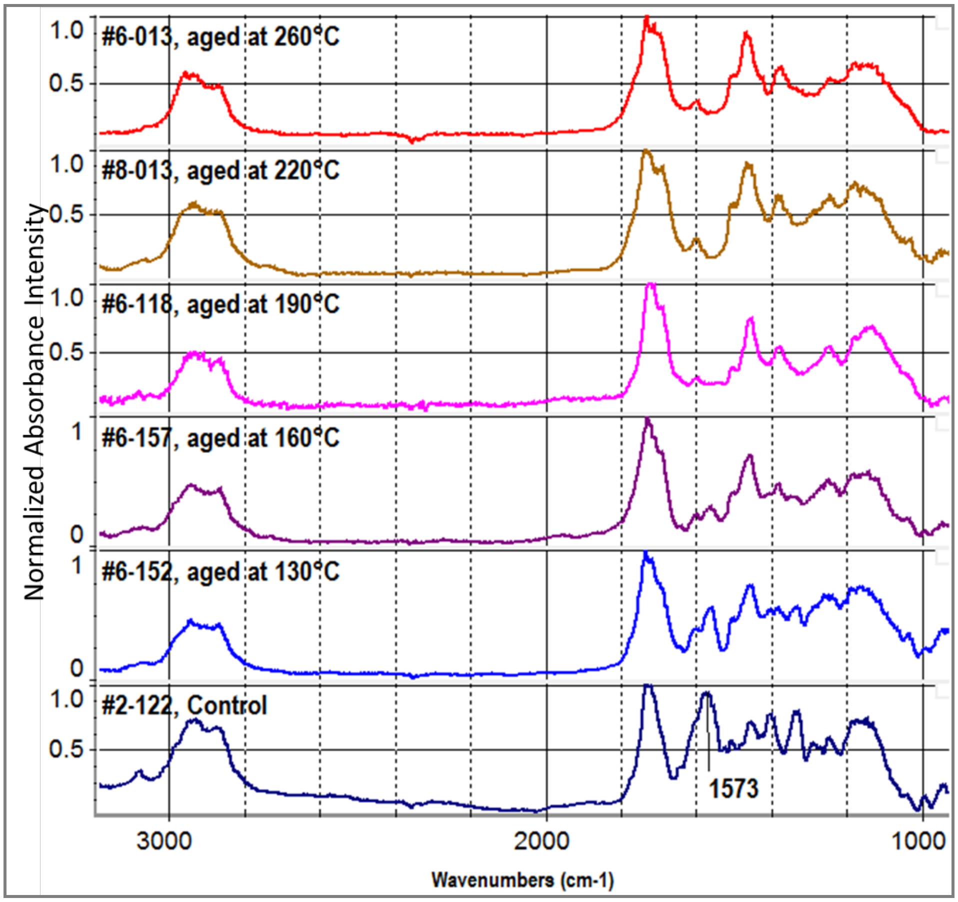

Figure 45.—Typical FT-IR spectra of Loctite 294 after 15-day thermal aging at various temperatures regardless of joint type or test temperature.

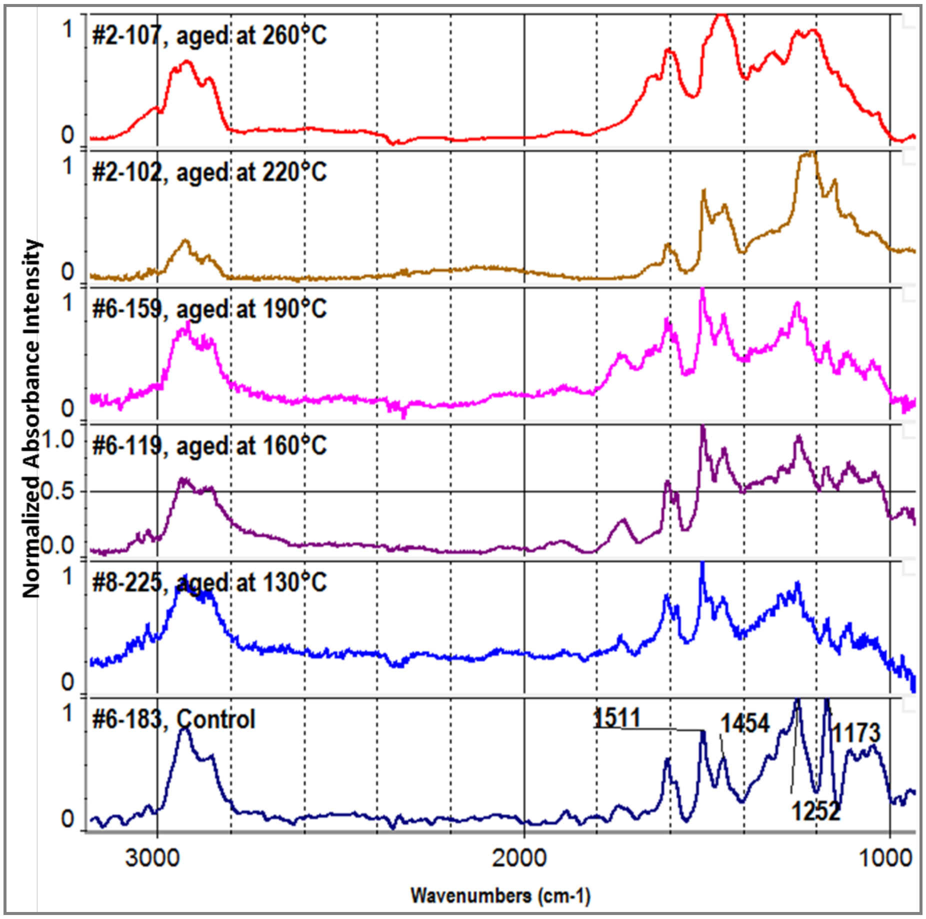

Figure 46.—Typical FT-IR spectra of Resbond 507TS after 15-day thermal aging at various temperatures regardless of joint type or test temperature.

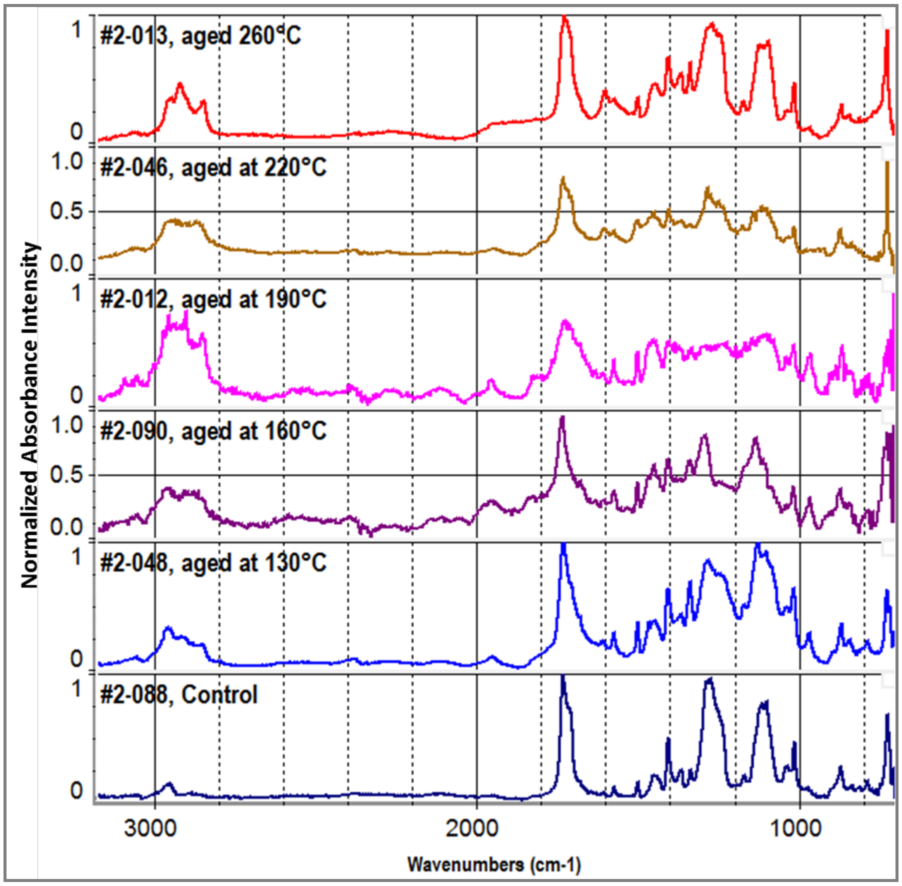

Figure 47.—Typical FT-IR spectra of Poly-Lok PET after 15-day thermal aging at various temperatures regardless of joint type or test temperature.

4.2.2.1.3 Shrink Tubing Candidates

The 15-day short-term thermal aging tests were not performed on shrink tubing candidate due to logistics issues. Based on the initial screening test results, the manufacturer’s technical data, and maximum use temperature ratings, the same temperatures selected for the adhesive/potting candidates were selected for the 6-month long-term accelerated aging tests.

4.2.2.1.4 O-Ring Candidates

The 15-day short-term thermal aging tests were not performed on o-ring candidate due to logistics issues. Based on the initial screening test results, the manufacturer’s technical data, and maximum use temperature ratings, the same temperatures selected for the adhesive/potting candidates were selected for the 6-month long-term accelerated aging tests.

4.2.2.2 6-Month Accelerated Thermal Aging Test

Specific objectives of this task were to assess longer-term thermal stability and integrity via longer-term accelerating aging experiment and to determine the application limits of the down-selected organic candidates via extended and systematic property-performance characterizations, and subsequently down-select the final candidate.

4.2.2.2.1 Adhesive/Potting Candidates

Overall test matrix for adhesive/potting candidates is summarized in Table A.10 in Appendix A in terms of various test specimens (their identification numbers listed) assigned for selected aging temperatures, aging intervals, and residual property test conditions. Figure 48 shows typical changes in color and physical appearance of thick sheet samples of AF131-2 and EA9394C-2 candidates, respectively, after various aging exposures. For both candidates, the samples aged at 225 °C (especially those aged for 100 days or longer) showed the most visible changes where the samples completely darkened, blistered, and cracked, which were all signs of thermal degradation.

Figure 49 shows weight loss behavior of both candidates in either laminated thin film or thick sheet form as a function of aging time at various aging temperatures. Overall, the EA9394C-2 samples lost more mass than AF131-2 at majority of the aging temperatures. Mass losses of the AF131-2 epoxy were well-contained up to 200 °C aging, but increased rapidly at 225 °C with increasing time due to potential

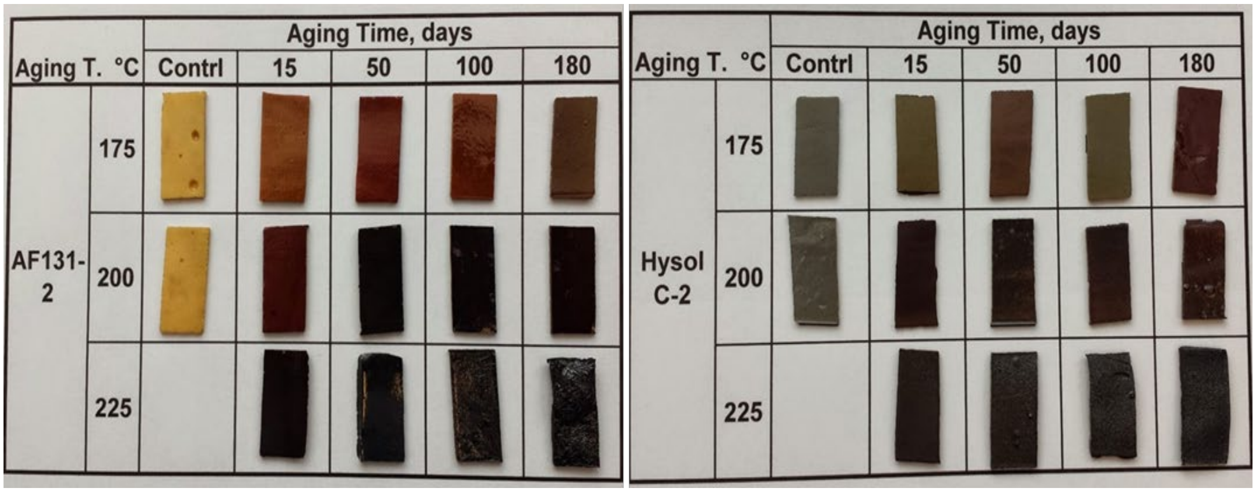

Figure 48.—Typical changes in color and physical appearance of thick sheet samples of adhesive candidates after various accelerated thermal aging exposures.

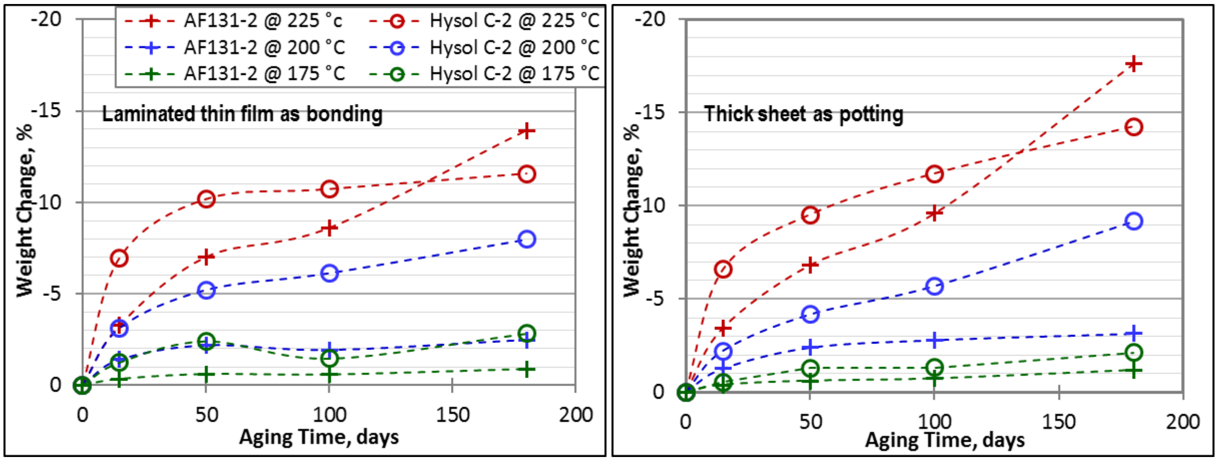

Figure 49.—Weight losses of adhesive candidates as a function of the accelerated thermal aging conditions.

thermal degradation. EA9394C-2 showed significant mass loss at aging temperatures above 200 °C, but in the case of the laminated thin film, it leveled off after 50 days. The weight loss rate of AF131-2 exceeded EA9394C-2 after about 150 days at 220 °C regardless of sample type. In general, the laminated samples mimicking the magnet bondline showed less mass losses since the only edges of the epoxy film were exposed, and thus limited diffusion paths. Overall weight loss of the EA9394C-2 was still less than that of the regular EA9394 epoxy within the aging temperature ranges studied (Refs. 6 and 9), Figure 50.

Effects of the accelerated thermal aging on static bonding properties of the candidates were evaluated with the sub-scale sandwich lap shear specimens. The overall results are summarized in Table A.11 in Appendix A in terms of average value, standard deviation, and percent change from the control values as a function of aging condition and test temperature. It was of interest to note that more accurate and consistent bonding properties were obtained with more realistic overlap dimensions of the lap shear specimens measured from their fracture surfaces using a stereo-OM and averaged over the entire specimen batches, Figure 51.

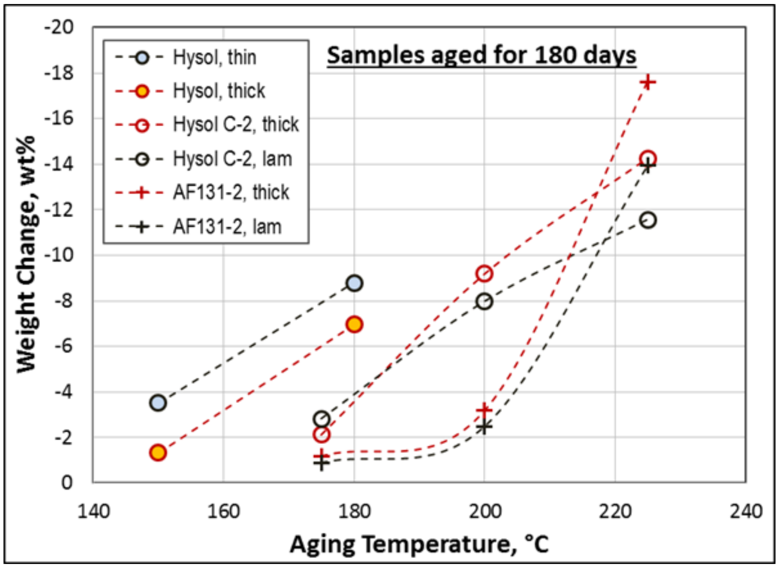

Figure 50.—Overall weight loss comparison among adhesive candidates.

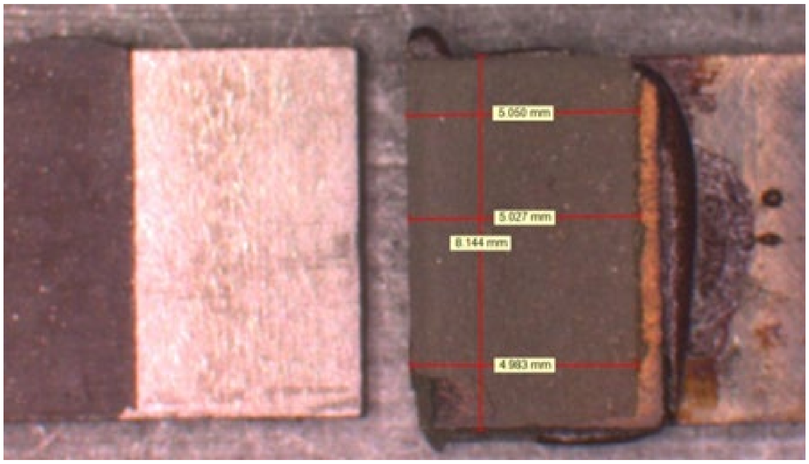

Figure 51.—Micrograph of typical facture surface of lap shear specimens showing overlap dimensions of adhesive bonding.

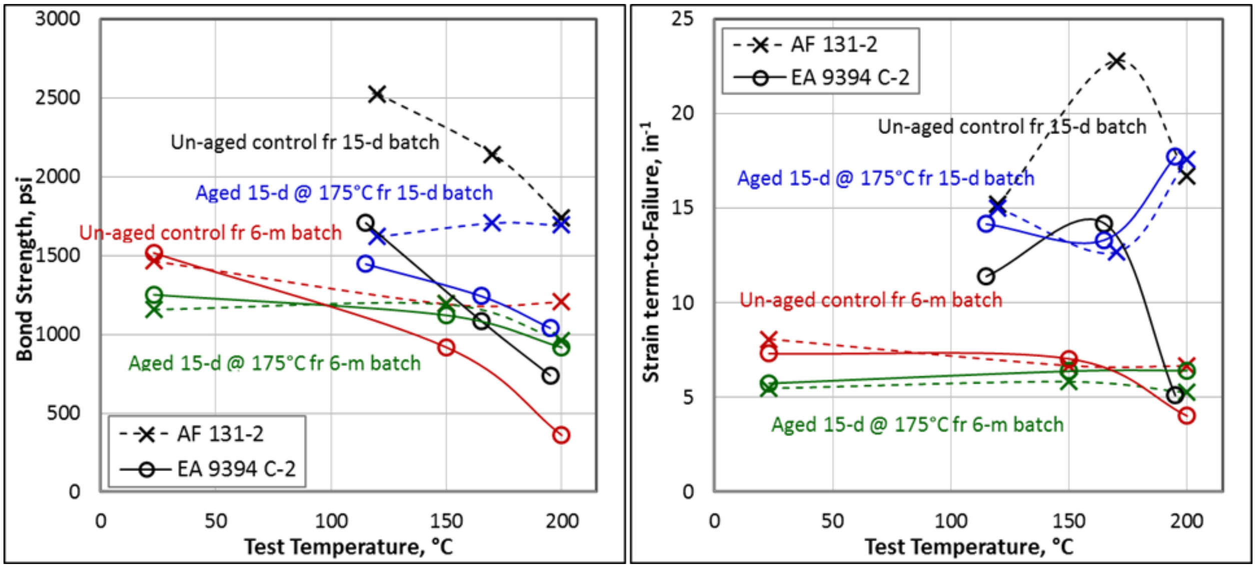

Figure 52.—Effects of specimen batch on lap shear properties of adhesive candidates.

It should be also noted that considerable differences in lap shear bonding properties were observed between the old sample batches made for the 15-day thermal aging experiment and the new batches for the 6-month accelerated aging experiment, Figure 52. The differences were attributed to changes in specimen fabrication conditions and procedures such as the following: molding fixture—Teflon for the former vs. tool-steel mold for the latter, in which led to different bondline thickness; fresh titanium substrates and magnet inserts for the former vs. recycled ones for the latter, testing fixtures (e.g., grip types), load cell calibration status, and overlap area measurement techniques (e.g., manual using a caliper externally on as-made specimen for the former vs. more accurate OM digital measurement on fracture surfaces for the latter). Specimens from the 15-day batch showed greater or more dramatic property changes with test temperature or aging condition, and greater data scattering, especially for the AF131-2 epoxy; suggesting that more variables were involved in sample fabrication or testing. However, regardless of all the changes, their cure states should be the same since both batches were exposed to the same cure cycles and procedures. Furthermore, the properties from the 6-month batches were more consistent in most cases. Thus, the extended property-performance evaluations for assessing long-term thermal stability in newer batches should be valid and effective since its potential effects were carefully gauged in every data analyses and interpretations.

From the static bonding properties of the candidates via the sub-scale sandwich lap shear specimens plotted as a function of aging time and temperature, Figure 53, EA9394C-2 was more stable at all aging times and temperatures up to 225 °C regardless of test temperature. The AF131-2 appeared to suffer significant property degradation when aged above 200 °C due to thermal degradation. However, the property decrease leveled off with increasing aging time for both candidates which suggested no more or less thermal degradation. Initial increases in bonding properties of the EA9394C-2, particularly at the elevated temperatures, were probably due to cure advancement. By plotting the lap shear properties against test temperature, Figure 54, it can be easily seen that both candidates suffered significant strength drop at 200 °C, especially EA9394C-2 regardless of aging temperature. However, the drop was associated with its intrinsic temperature capabilities of the material based on its relatively lower T_g, and adhesion mechanisms, and did not necessarily involve thermal degradation. These plots confirmed again that bonding properties of the EA9394C-2 epoxy were not significantly affected by aging time for all aging temperatures up to 225 °C. Nevertheless, both candidates showed considerably higher bond strengths than the required strength for the magnet bonding regardless of the aging conditions or test temperature.

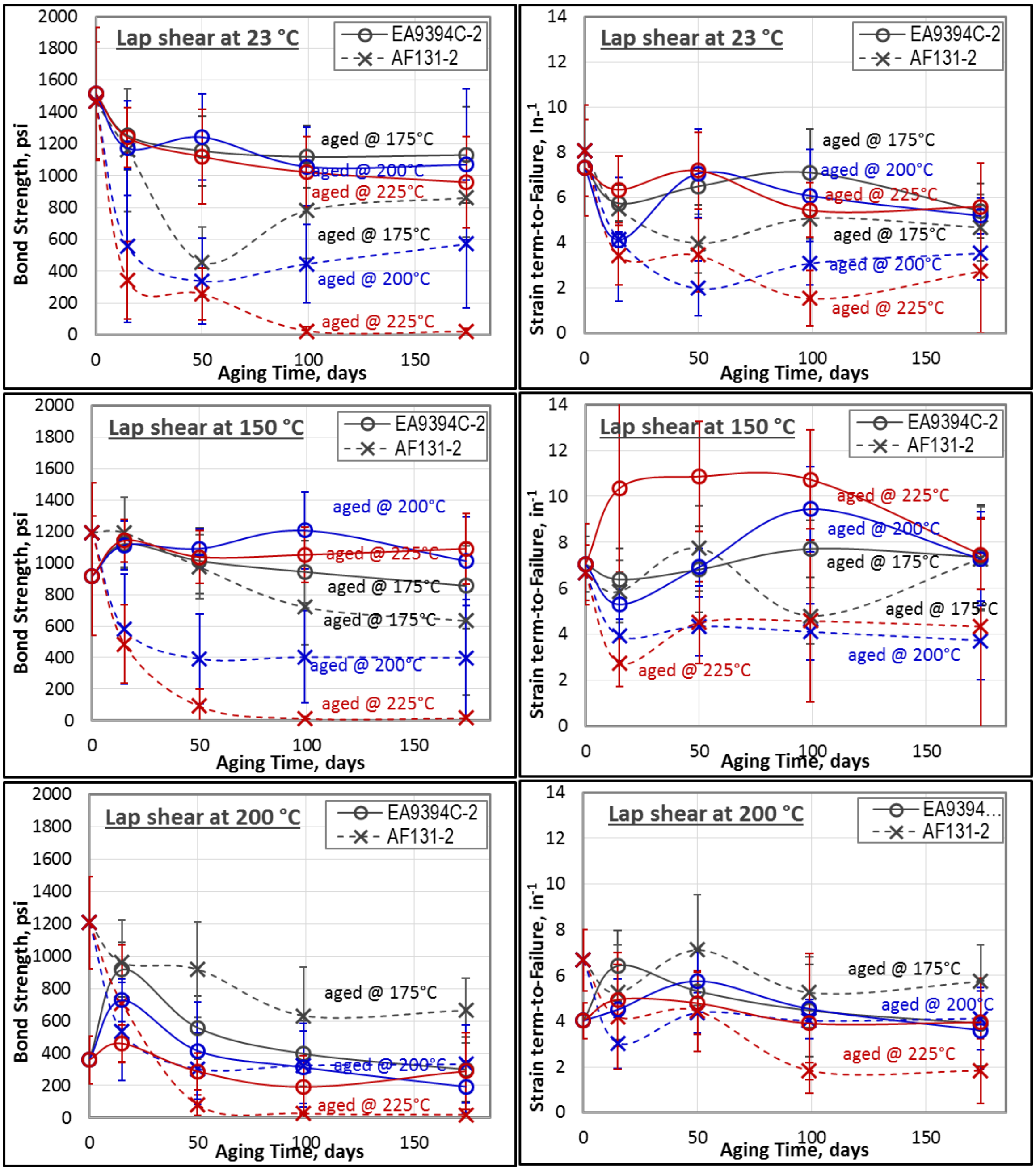

Figure 53.—Lap shear bonding properties of adhesive candidates after accelerated thermal aging tests plotted against aging time.

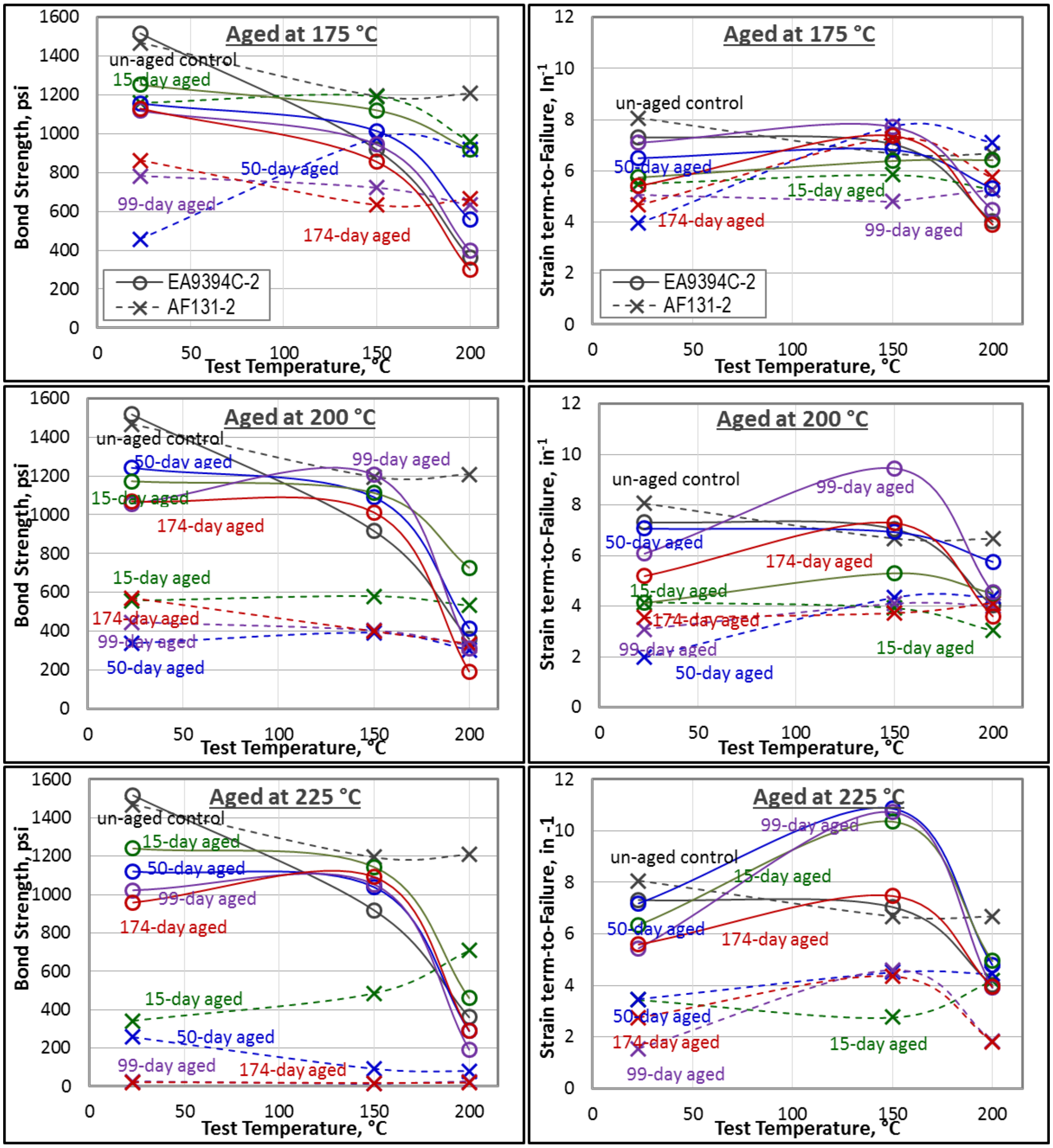

Figure 54.—Lap shear bonding properties of adhesive candidates after accelerated thermal aging tests plotted against test temperature.

Fatigue performance was characterized via various parameters determined from the master SN curve, which included FS or Endurance limit, the ratios of the fatigue to static strength, the residual strength to static strength, the residual strength to fatigue strength, and the residual strain-term to static strain-term as summarized in Table A.12 in Appendix A. The shape and trend of the SN curves were also characterized with the initial slope indicating load sensitivity and Δσ, a possible indication of any molecular structural changes due to the combined exposure of temperature and fatigue loading. In theory, Δσ can be small or near zero if no changes, positive for destructive changes, such as micro-cracking, localized debond, or negative for constructive changes in terms of adhesion. In overall fatigue performance, EA9394C-2 outperformed AF131-2 epoxy regardless of the aging conditions. As shown in Figure 55, fatigue strength of EA9394C-2 was more stable and consistent against the aging conditions, and was thereby considered more thermally stable than AF131-2, as was also in the case of the static bonding properties. The AF131-2 also showed reasonable fatigue performance and thermal stability, but only up to 200 °C aging, thus it is recommended that its maximum operation temperature be limited to 200 °C. As shown in Figure 56, for both candidates, the initial slope of the SN curve generally decreased initially and leveled off with

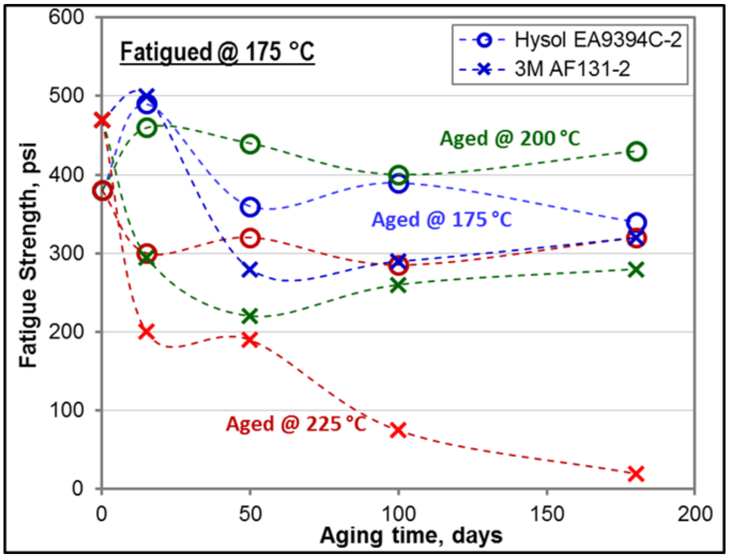

Figure 55.—Fatigue strength/endurance limit at 175 °C of adhesive candidates at various accelerated thermal aging conditions

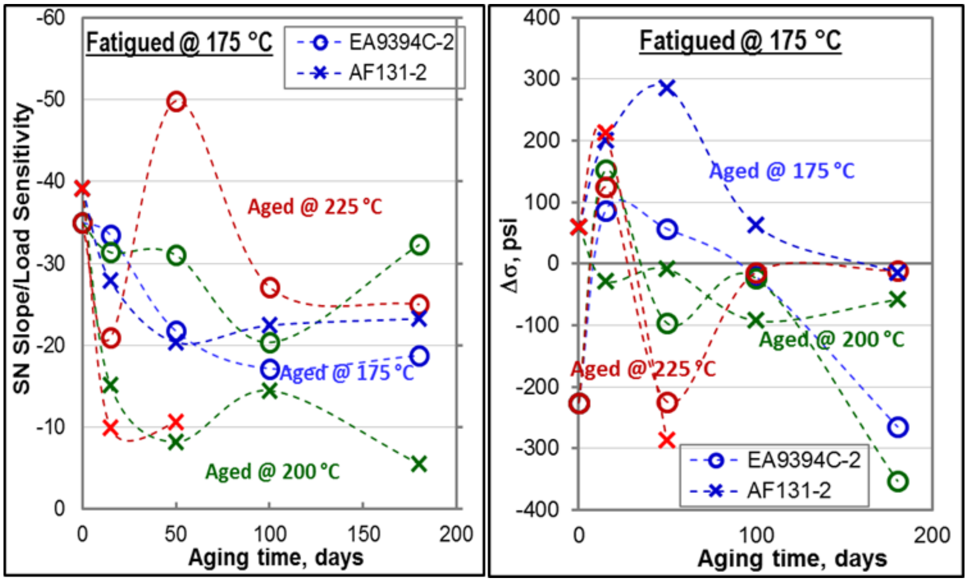

Figure 56.—Slope of SN curve and Δσ at 175 °C of adhesive candidates after the various accelerated thermal aging exposures.

increasing aging time for most aging temperatures, which indicated that their fatigue behavior became less sensitive to the applied load and may have also related to their cure state. The Δσ increased initially, but then it returned to a neutral or negative position. This was especially the case for the EA9394C-2 epoxy, where the trend increased with aging time, which was indicative of no major structural changes by fatigue loading in both candidates. Various other fatigue performance parameters, Figure 57 suggested that both candidates performed better under fatigue loading than static loading, especially with increasing aging time in most aging temperatures. No sign of fatigue-induced bonding integrity degradation in both candidates regardless of the aging conditions, rather, in most cases, the residual to static strength ratio was even higher than 1.0, i.e., improved bonding integrity with fatigue testing. AF131-2 aged at 225°C showed the biggest increase until it completely degraded after aging for longer than 100 days. In general, the EA9394C-2 was more stable and consistent in fatigue performance.

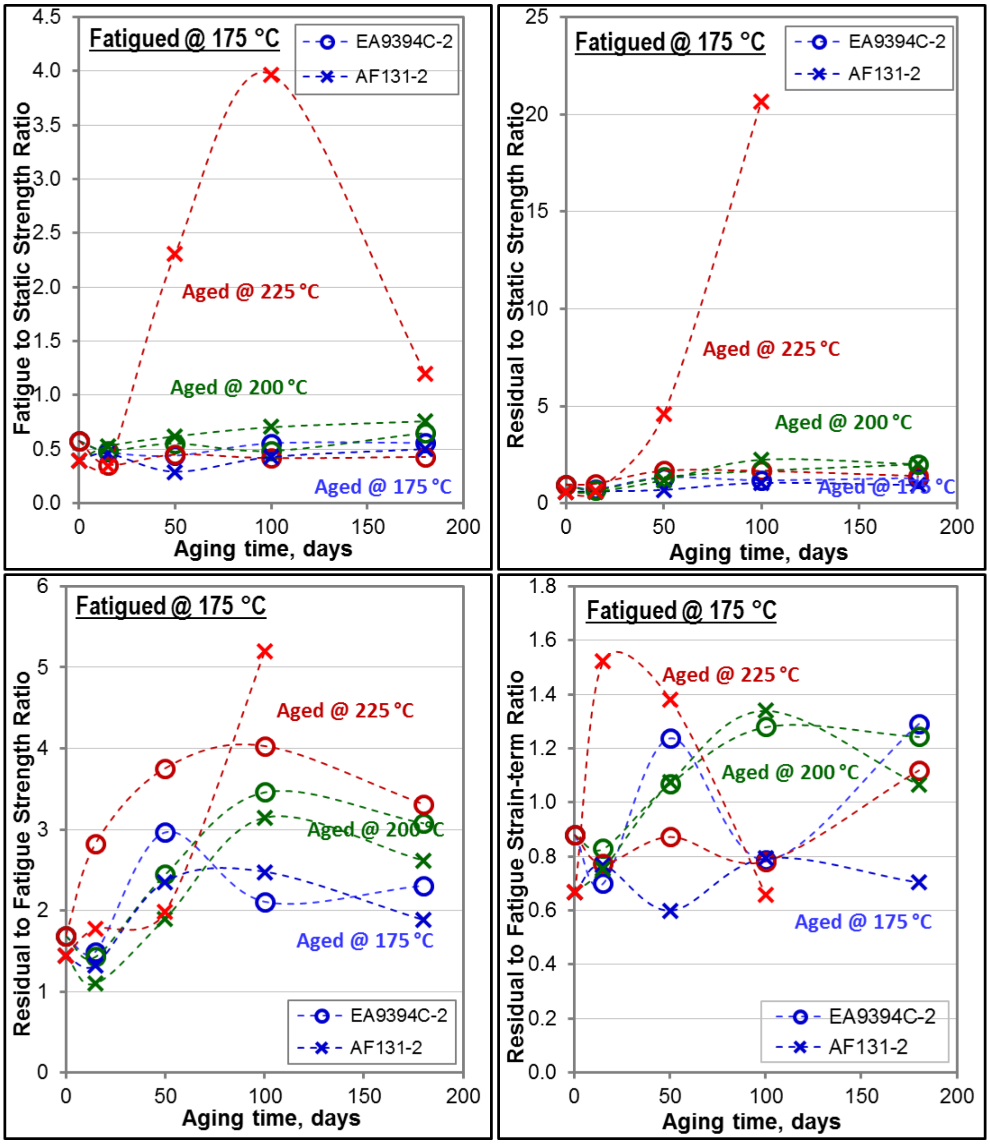

Figure 57.—Other fatigue properties at 175 °C of adhesive candidates after the various accelerated thermal aging exposures.

Various thermal properties and outgassing characteristics of the candidates from the accelerated thermal aging experiment were summarized in Table A.13 in Appendix A and plotted in the following several figures. T_g was measured by various techniques including DMA, TMA, and mDSC for the thick sheet samples, but only by mDSC for the laminated thin film. Overall, the results were consistent as shown in Figure 58. For both candidates, T_g increased initially at the early aging stage mostly due to cure advancement. The trend then either leveled off or continued to increase with increasing aging time, and then decreased significantly when aged at 225 °C due to thermal degradation, particularly for the AF131-2. The overall trends were in good agreement with the results of their bonding properties. Potential mechanisms for thermal property changes from thermal aging in typical epoxy adhesives include:

- Cure advancement via additional cross-linking
- Molecular rearrangements in main backbone or in side chains
- Physical aging, relaxation of molecular network
- Outgassing or de-volatilization
- Depletion of thermal stabilizers
- Thermal decomposition
- Thermal reaction of separated molecules, oxidation, char formation

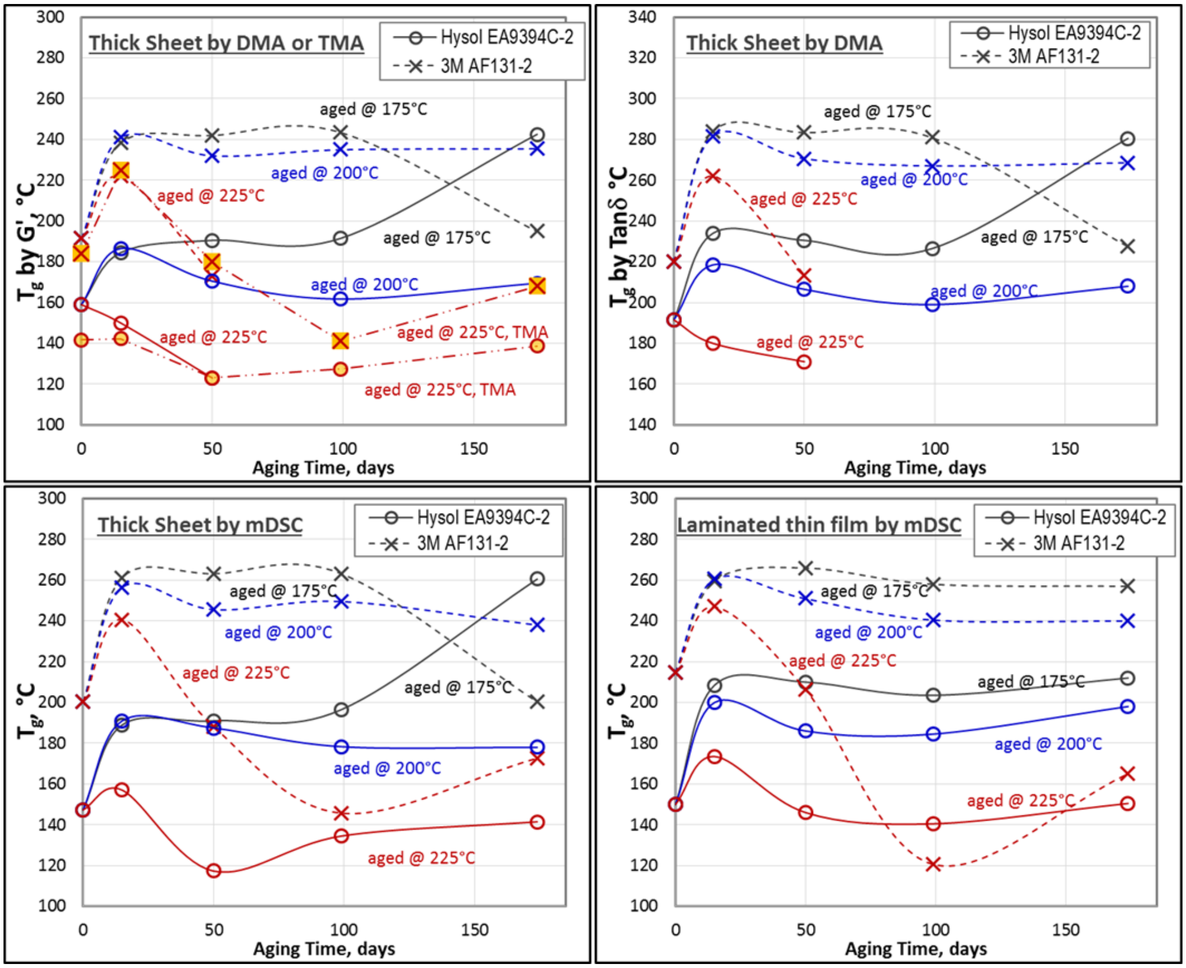

Figure 58.—T_g of various adhesive samples as functions of the accelerated thermal aging conditions measured by various techniques.

T_d of both thick and laminated film followed similar trends even though the latter involved greater changes, Figure 59. Both candidates suffered most significant T_d changes when they were aged at 225 °C due to various competing mechanisms discussed above. Up to 200 °C thermal aging, the materials seemed to be stable because they underwent more gradual changes with time, thus suggesting again their max use temperature should be lower than 225 °C.

Similarly, both candidates maintained good rigidity ratio at 200 °C up to 200 °C aging but suffered significant drops after 225 °C aging, Figure 60. A gradual but considerable decrease in ΔWt% at 700 °C occurred after 225 °C aging regardless of specimen type for both candidates, Figure 61, which was consistent with other thermal properties and weight loss data. This suggested that during the aging at 225 °C, the epoxies had already lost more substances than just typical volatiles or unreacted small molecules, possibly due to more substantial thermal degradation or decomposition.

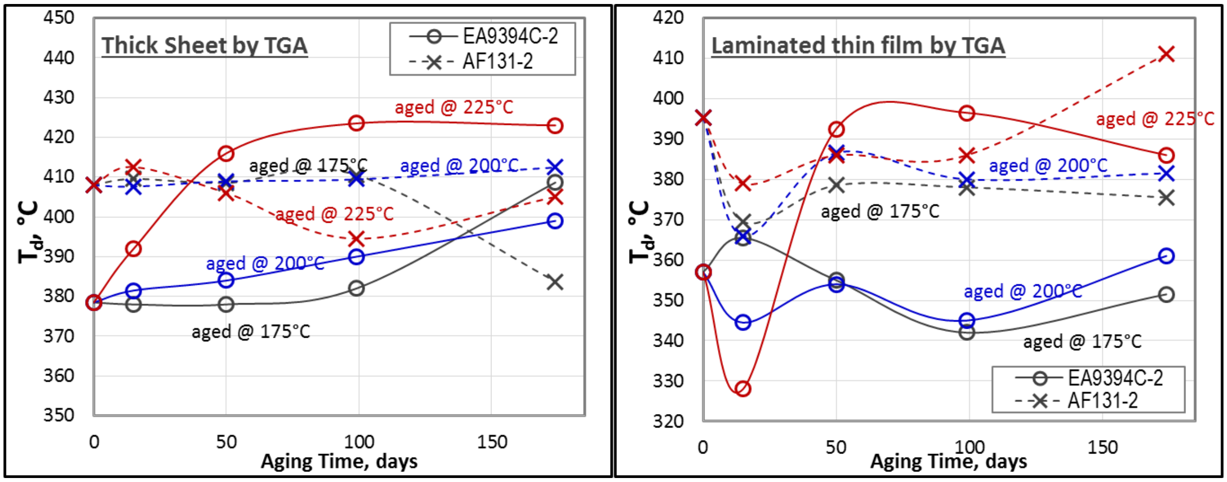

Figure 59.—T_d of various adhesive samples as functions of the accelerated thermal aging conditions.

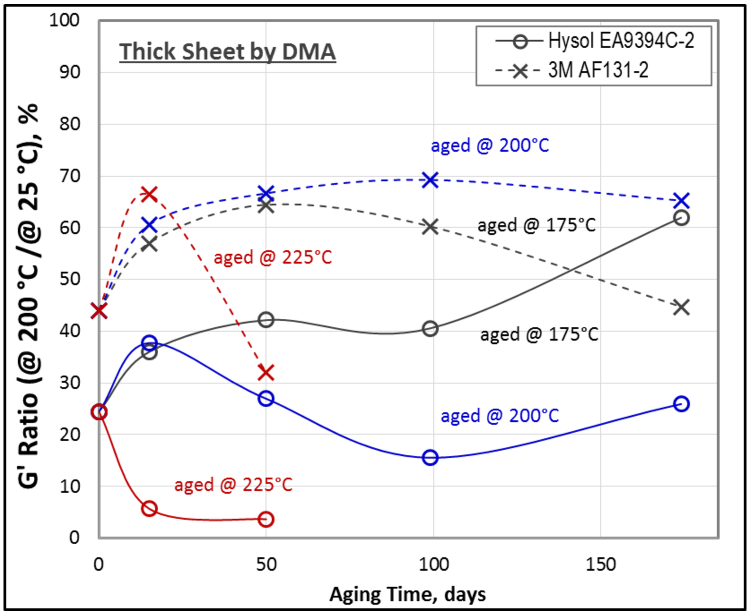

Figure 60.—Ratio of storage modulus at 200 °C and RT of adhesive candidates after the accelerated thermal aging exposures.

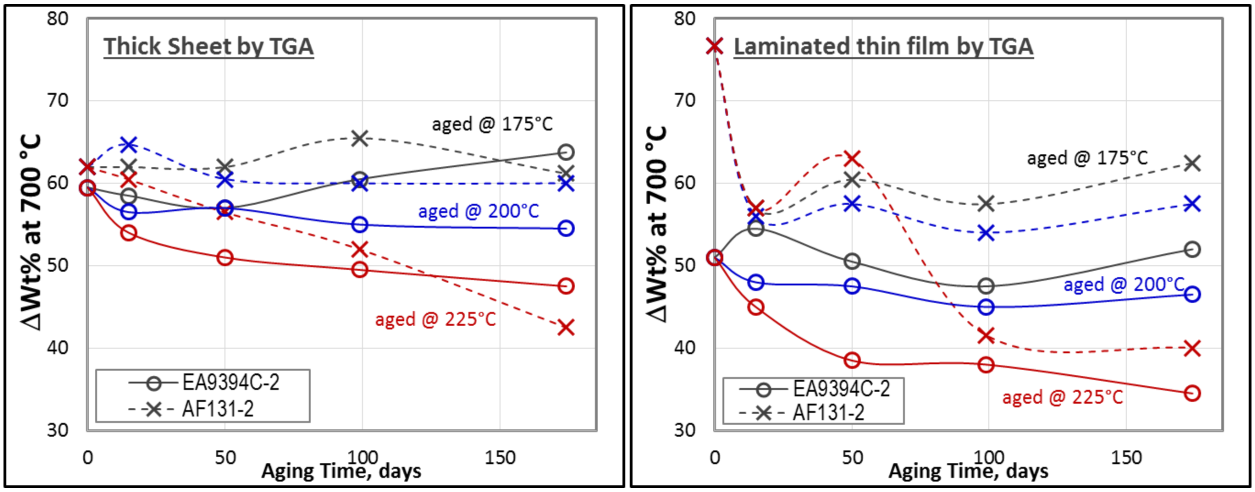

Figure 61.—Total weight loss of adhesive candidates at 700 °C as functions of the accelerated thermal aging conditions.

Figure 62 shows typical FT-IR spectra of AF131-2 from either thick sheet or thin laminated specimen indicating possible changes in its molecular network structures from the accelerated thermal aging test. Most visible changes in FT-IR spectra occurred when the epoxy samples were aged at 225 °C regardless of specimen format, but up to 200 °C aging there were no visible changes or only benign nondestructive changes, especially from the thick sheet samples. Appearance of a broad peak at ~1720 cm^{-1} could be associated with additional cross-linking, but disappearing of the shoulder, and broadening of ~1513 cm^{-1} and ~1296 cm^{-1} peaks might be due to breaking of certain molecular bonds as a part of thermal degradation or decomposition. Similar to the AF131-2 epoxy, the EA9394C-2 showed the most evident spectral changes when the epoxy samples were aged at 225 °C in either thick sheet or laminated thin samples, Figure 63. However, in addition to the benign changes at the lower aging temperatures, some visible changes also occurred from 200 °C aging, especially from the thick sheet sample. Appearance of a broad peak at ~1720 cm^{-1} was associated with additional cross-linking, but disappearance of the peaks at ~1720, ~1513, ~1241, or ~1180, and ~1042 cm^{-1} might be due to breaking of certain molecular bonds or chain scissions upon thermal degradation. However, the laminated thin film sample representing magnet bonding did not show any changes when aged at 200 °C, which suggested that this particular sample was more thermally stable.

In most residual property characterizations, changes in properties seemed to level-off or stabilize after 180-day aging at all aging temperatures studied, and thus the 180-day properties can be considered as representative values per each aging temperature for longer-term predictions. Therefore, all of the residual properties at the end of 180 day aging experiment were plotted together as a function of aging temperature for more direct and practical comparison in terms of percent change from the respective baseline control property, Figure 64. As can be easily seen in the plot, AF131-2 suffered greater reductions in most properties than EA9394C-2, with sharper, more distinctive transitions in the reduction rates at 175 to 200 °C, the temperature that may be used as the upper limit for long-term applications. On the other hand, EA9394C-2 adhesive showed better thermal stability without significant property reductions up to 225 °C, but low bond strengths at 200 °C have to be counted for when determining its upper limit. It should be also noted that the larger changes either, up or down, indicate the greater effects of the thermal aging, but whether the changes is positive or negative have to be determined by more extensive evaluation.

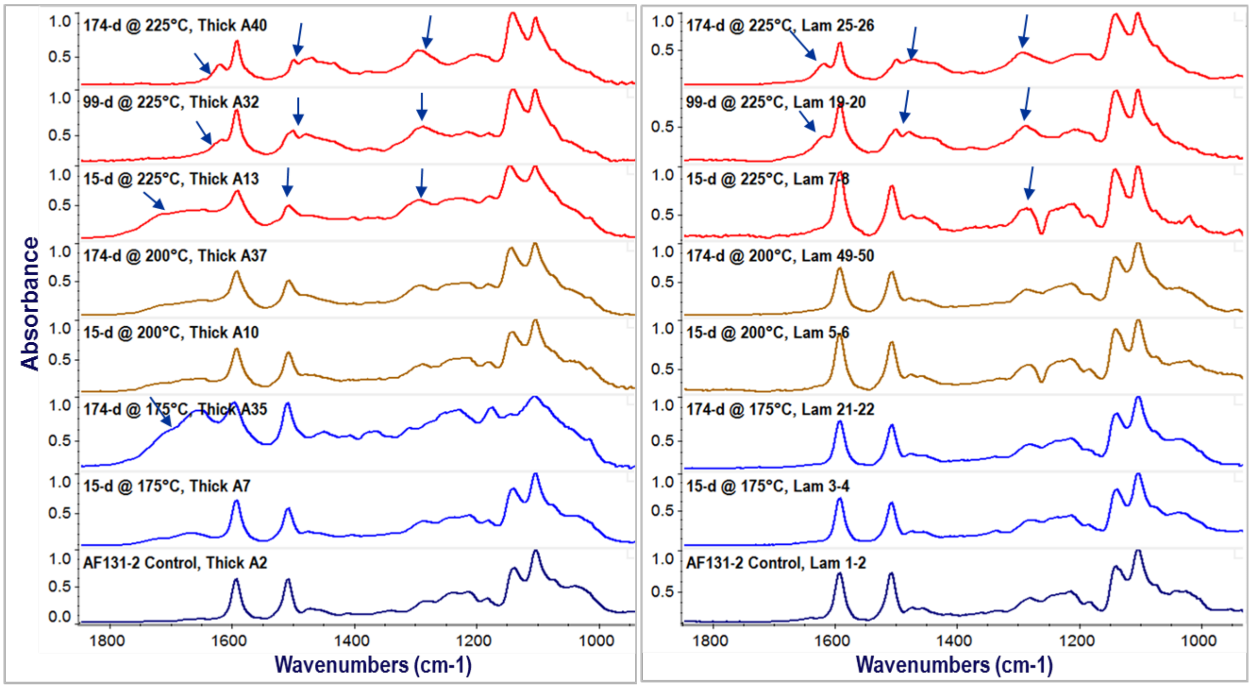

Figure 62.—Typical FT-IR spectra of AF131-2 epoxy from both thick sheet (left side) and thin laminated (right side) samples after the various accelerated thermal aging exposures.

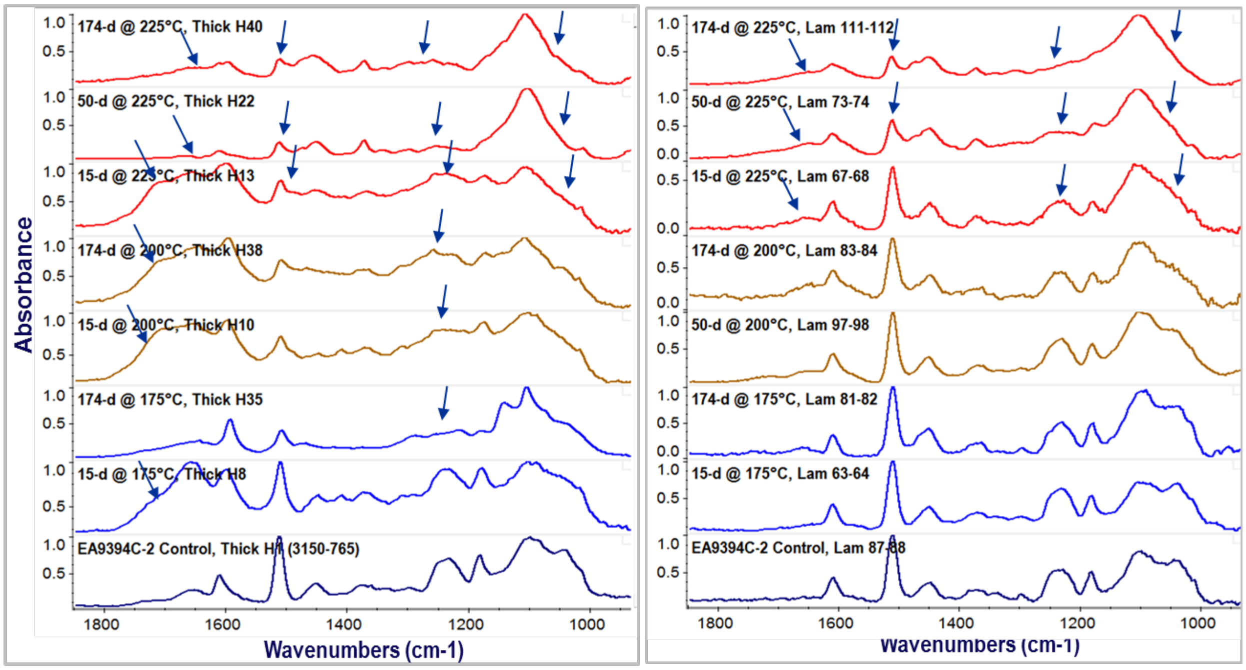

Figure 63.—Typical FT-IR spectra of EA9394C-2 epoxy from both thick sheet (left side) and thin laminated (right side) samples after the various accelerated thermal aging exposures.

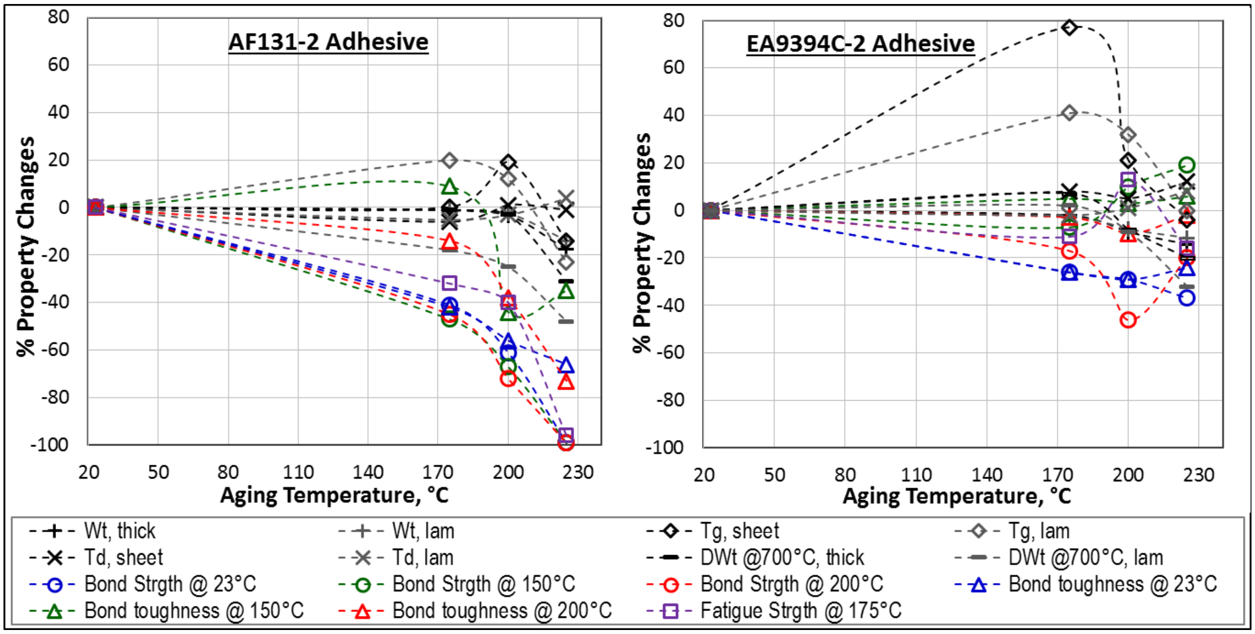

Figure 64.—Overall percent changes in various properties of adhesive candidates after 180-day aging as a function of the accelerated thermal aging temperature.

In summary,

- Both candidates suffered significant weight losses when aged above 200 °C, but the laminated samples mimicking magnet bondline showed less because of limited diffusion paths. Overall weight loss of the EA9394C-2 was considerably less than that of the regular EA9394 epoxy.
- EA9394C-2 showed much more stable bonding properties at all aging conditions up to 225 °C than the AF131-2 which suffered significant property reductions when aged above 200 °C due to apparent thermal degradation. However, the property drop was leveled off with increasing aging time for both candidates, (no or less further thermal degradation).
- Both candidates suffered significant strength drop at 200 °C, especially EA9394C-2, but it might be only associated with intrinsic temperature capability of the material and not necessarily due to thermal degradation. Both candidates still showed considerably higher bond strength than the required strength for the magnet bonding.
- EA9394C-2 outperformed the AF131-2 epoxy in fatigue performance regardless of the aging conditions and showed stable and consistent fatigue properties for all aging conditions up to 225 °C. The AF131-2 also showed reasonable fatigue performance but only up to 200 °C aging.
- No fatigue-induced bonding integrity degradation was observed in both candidates regardless of the aging conditions. Various fatigue performance characteristics suggested that they performed better under fatigue loading than static loading.
- For both candidates, T_g increased initially due to cure advancement, leveled off or continued to increase with time similar to their bonding properties, but when aged at 225 °C, decreased significantly due to potential thermal degradation, particularly for the AF131-2. Other thermal properties including T_d, G', and ΔWt% at 700 °C as well as the FT-IR molecular network structural changes showed similar behavior. More dramatic changes were observed, but only after 225 °C aging regardless of sample configuration, either in thick sheet or laminated thin film form. In most cases, the changes were greater for the AF131-2.

- From the overall % changes of various properties as a function of aging temperature, AF131-2 suffered greater reductions in most properties than EA9394C-2, and sharper, more distinctive transitions in the reduction rates at 180 to 200 °C, which could be considered as the upper limit for longer-term applications. On the other hand, EA9394C-2 adhesive showed better thermal stability in most properties with lesser reductions and didn't involve clear transitions up to 225 °C.

4.2.2.2.2 Thread Locker Candidates

The overall test matrix was presented in Table A.14 in Appendix A by detailing torque sample assignment in terms of two aging temperatures and four aging intervals including the unaged controls as well as two post-aging torque test temperatures for the three down-selected candidates. Total weight losses of the thread locker candidates from the accelerated thermal aging were rather significant, ~ 15 wt% up to 40 wt% or higher, compared to other Stirling organic materials studied, Figure 65. The mass losses depended not only on aging temperature and time, but also on joint type. For both Loctite 294 and PET, the #2 joint with blind-hole configuration resulted in the highest weight loss regardless of aging temperature. The mass loss of Resbond 507TS was more dependent upon aging temperature regardless of joint type. In most cases, the rate of mass loss either decreased or leveled off with increasing aging time for both aging temperatures. Greater data scattering of PET patch came from the fact that the mass of the patch was roughly calculated by subtracting the average weight of the fastener from the weight of the patched fastener since the patch was applied without measuring weight of the fastener. Whether the weight losses were due to thermal degradation, chemical reactivity, or just benign outgassing will be further assessed along with other residual property evaluations and TCIOP in-situ outgassing analyses.

The complete torque test results of the aged samples are summarized in Table A.15, Table A.16, and Table A.17 in Appendix A for the joint type #2, #6, and #7 or #8, respectively, in terms of torque strength and failure mode per aging condition or test temperature. Breakloose torque was also calculated in terms of the % installation torque. Samples marked by the small red triangular comment indicator on the right corner of their ID boxes were selected for FT-IR analysis. Those typical torque-angular displacement curves identified earlier per candidate or joint type, Figure 39, were closely followed for the most aged samples. Most of the aged samples also followed the typical failure modes per candidate or joint type presented in Figure 40.

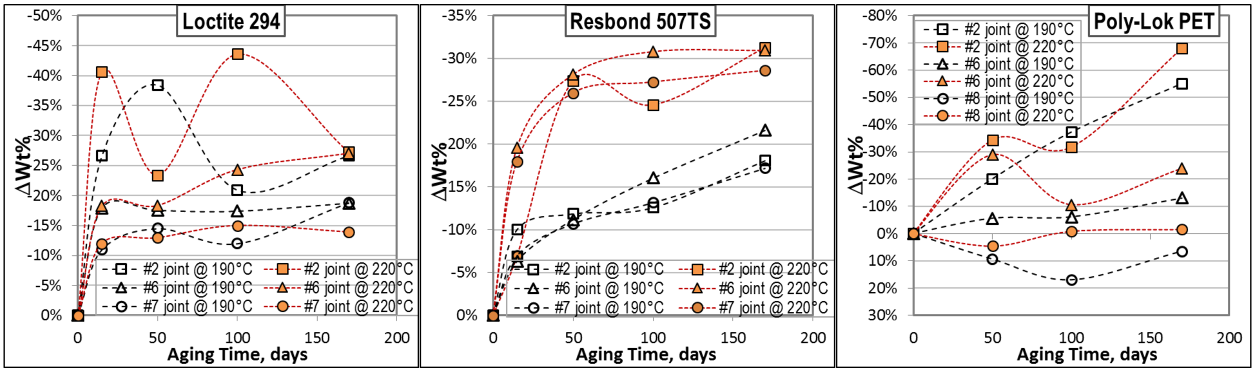

Figure 65.—Overall weight losses of thread locker candidates against the accelerated aging conditions.

As listed in the test matrix, two different sets of the unaged control samples were prepared and tested; one for the 15-day thermal aging and the other for the 6-month accelerated thermal aging experiment. Torque strengths of both control sets were analyzed and compared in this report (the control data from the 15-day testing were listed first in the summary tables). It should be also noted that the torque strength and FT-IR data from the 15-day thermal aging experiment were used for the 15 day aging interval for the 6-month accelerated aging experiment for both aging temperatures, 190 and 220 °C in most analyses. The 15-day aging interval was skipped in the 6-month accelerated aging experiment to reduce the scope of test matrix. Regardless of TL type, the joint #2 with blind-hole configuration always showed less favorable failure modes, either adhesive or mixed mode. Loctite 294 and Resbond 507 TS in the join type #7 showed more favorable cohesive failure modes, but the latter seemed to be more prone to thermal degradation. In many cases of the Resbond 507 TS with the joint type #7, their prevailing or maximum torque strength was greater than torque strength of the fastener itself, and they failed at the fastener head during torque testing. Thus, their prevailing torques and failure modes were not available. Figure 66 shows torque strengths of the three candidates with #2 Joint Type at 100 and 200 °C against accelerated aging conditions. For the breakloose torque at 100 °C in the blind-hole configuration, Resbond 507TS performed best regardless of aging temperature. Resbond was the only candidate generating 100 °C

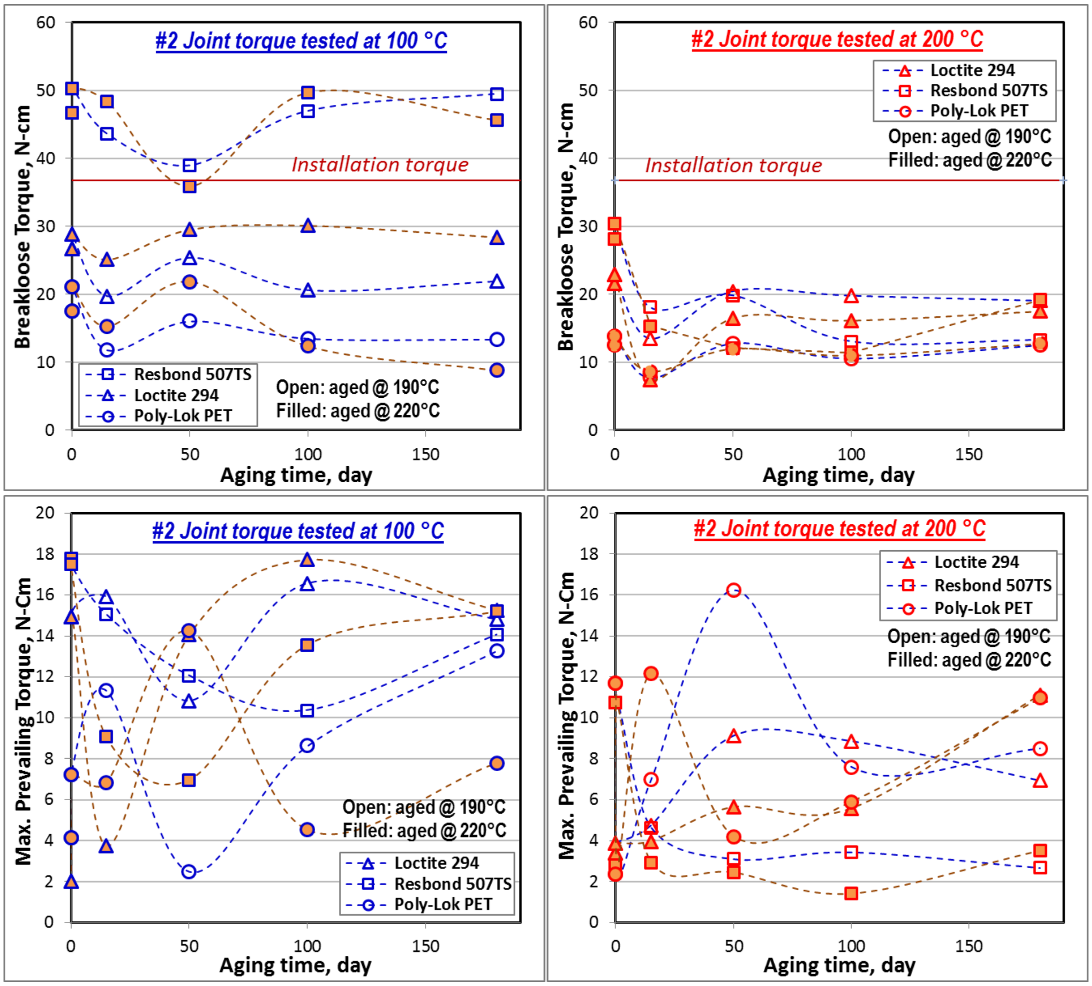

Figure 66.—Torque strengths at 100 and 200 °C of thread locker candidates in #2 joint as a function of the accelerated thermal aging conditions.

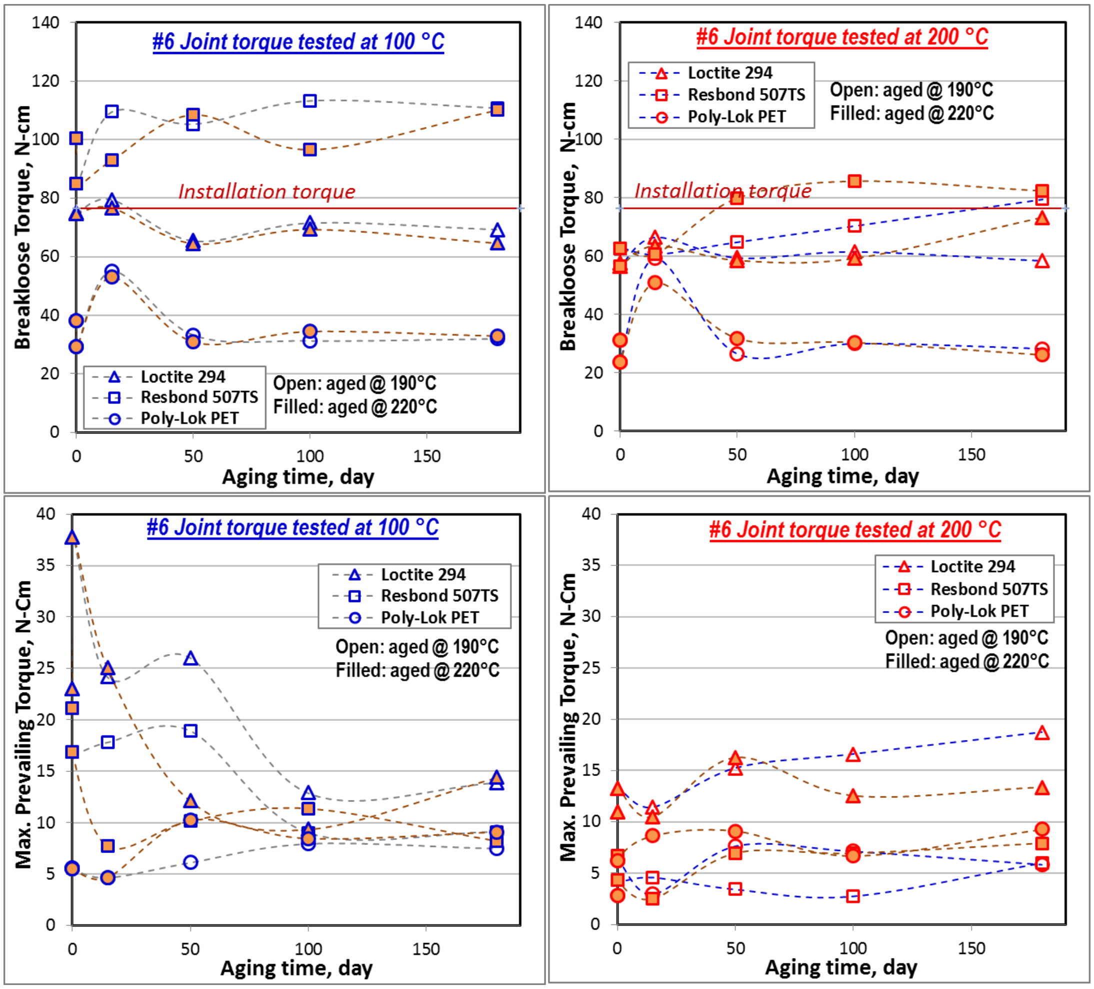

Figure 67.—Torque strengths at 100 and 200 °C of thread locker candidates in #6 joint as a function of the accelerated thermal aging conditions.

breakloose torques greater than the installation torques for all aging conditions. Other candidates showed low torque strengths far below the installation torque, but for all three candidates, they were not significantly affected by the accelerated aging. At 200 °C, Resbond 507 TS suffered the most loss of breakloose torque among all candidates. Overall, their values were significantly lower than the installation torque. After the initial drop, however, they leveled off with increasing aging time, and showed no visible effects of aging temperature. For all candidates, their prevailing torques fluctuated a lot with the aging temperature and time, and were considerably lower than the installation torque. They also decreased at higher test temperature of 200 °C, especially for Resbond 507TS. The effects of accelerated thermal aging on torque strengths of the candidates in #6 Joint are summarized in Figure 67. Behavior of the breakloose torque of the three TL candidates at 100 °C in the joint type #6, a through-hole configuration, was very similar to that of the joint type #2 in that Resbond performed best regardless of aging temperature with torque strengths much greater than the installation torque. Loctite also showed reasonably good torque performance. Overall, torque strength of all three candidates was not significantly impacted by the accelerated aging. At 200 °C, all three candidates maintained their breakloose torque reasonably high unlike the joint type #2 even though Resbond lost more torque strength than other candidates. All showed no visible effects of aging temperatures or time. Unlike the joint type #2, the max prevailing torque behavior of all candidates was steadier with the aging temperature and time. The 100 °C max prevailing torque strength of Loctite and Resbond seemed to decrease with aging time initially, but at 200 °C they showed either no change or slight increase with aging time, especially for Loctite.

Figure 68 shows the test results for the #7 or #8 Joint Type. The joint type #7 or #8 with the through-hole configuration produced the highest breakloose torque among all joint types, especially in terms of the percent installation torque for all TL candidates regardless of test temperature. The Resbond still performed best regardless of aging temperature or time, but the Loctite also showed improved torque strength. In general, torque strength of all three candidates increased considerably with aging, especially at the early stage up to 50-day aging, then leveled off with further increasing aging time for both aging temperatures. Even at 200 °C, all three candidates maintained their breakloose torque considerably high unlike the other joint types. However, Resbond lost more torque strength than other candidates except the samples aged at 220 °C, which showed significant increase with aging time. In joint #7 or #8, the max prevailing torques of the candidates were also significantly higher, particularly Loctite and Resbond. In many cases of the Resbond 507 TS in #7 joint, their max prevailing torque strength was greater than torque strength of the fastener itself, which lead to failure at the fastener head during torque testing. Strengths of Loctite at both 100 and 200 °C increased significantly with aging time, especially those aged at 190 °C.

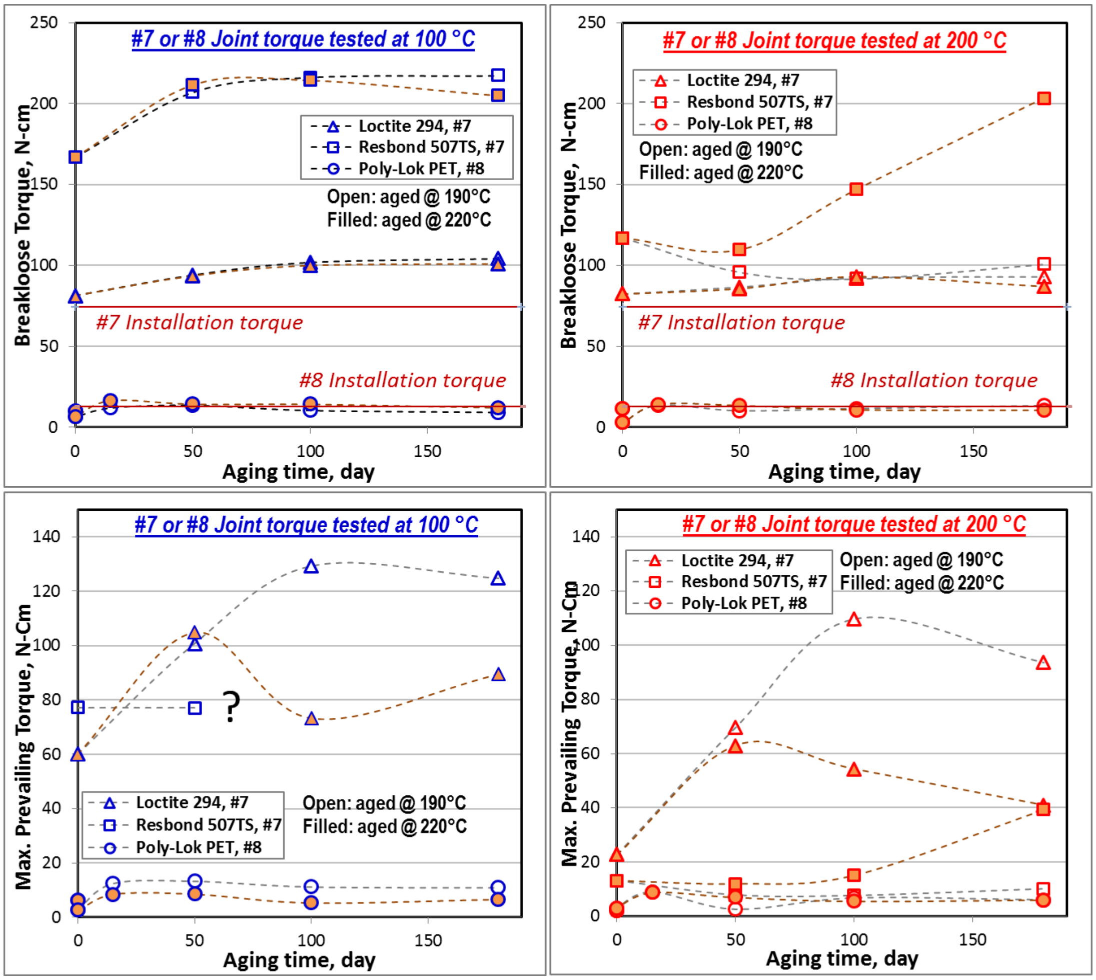

Figure 68.—Torque strengths at 100 and 200 °C of thread locker candidates in #7 or #8 joint as a function of the accelerated thermal aging conditions.

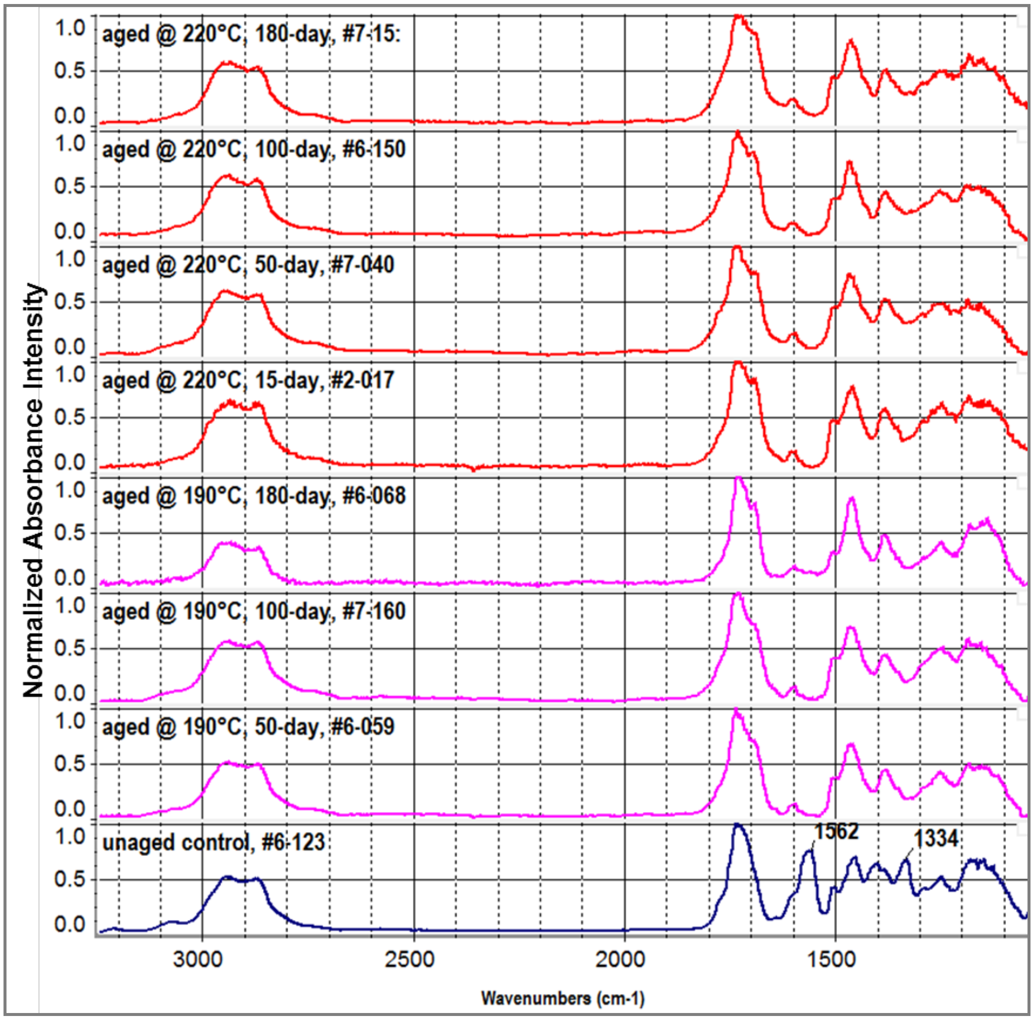

Figure 69.—Typical FT-IR spectra of Loctite 294 at various accelerated thermal aging conditions regardless of joint type or test temperature.

Changes in molecular chemical structures or potential thermal degradation of the thread locker candidates were assessed with FT-IR microscopy analysis on the thread locker residues on the fasteners removed after the torque strength testing. For all candidates, IR spectra was not affected by joint type or test temperature, but only by aging temperature and time, thus the best representative spectra was selected from each accelerated thermal aging condition regardless of joint type or test temperature for more practical comparison. In general, no significant change was observed from the Loctite 294 regardless of aging temperature and time, Figure 69. This suggested no or minor thermal degradation up to 220 °C aging even though sometimes OM failure mode analysis indicated considerable color changes in some samples aged for 180 days at either aging temperature. A strong peak at 1562 cm^{-1} appeared in the unaged controls but disappeared in all aged samples was not always observed from other control samples, thus it was assumed that the peak was from other contaminant since some of the fasteners used in this study were recycled. Overall, there were no noticeable changes in IR spectra regardless of aging conditions, thus no significant thermal degradation in the Loctite 294 from the accelerated thermal aging exposures up to 220 °C for 180 days. In the case of Resbond 507TS, there were consistent changes in IR spectra against the accelerated thermal aging exposure, for example, decrease in intensity of ~1173 cm^{-1} peak and broadening of a few peaks, e.g., ~1252, ~ 1454, and ~1600 cm^{-1} with increasing aging temperature or time, especially at 220 °C, Figure 70. This suggested that the Resbond underwent potential molecular changes in agreement with thermal degradation, especially when aged at 220 °C or at longer aging times, regardless of joint type. These observations were somewhat consistent with the results of OM failure mode analysis. Both Loctite and PET were thermally stable up to 220 °C aging for the entire aging time. Results of IR microscope analysis of Poly-Lok PET are shown in Figure 71. IR spectra of Poly-Lok PET was less accurate in general due to fluorescence interference. The overall trend seemed to show that changes in IR spectra were not consistent or pronounced, and no sign of significant thermal degradation. OM failure analysis also indicated no thermal degradation regardless of aging conditions or torque test temperature. However, due to poor IR resolution, no solid conclusions could be drawn.

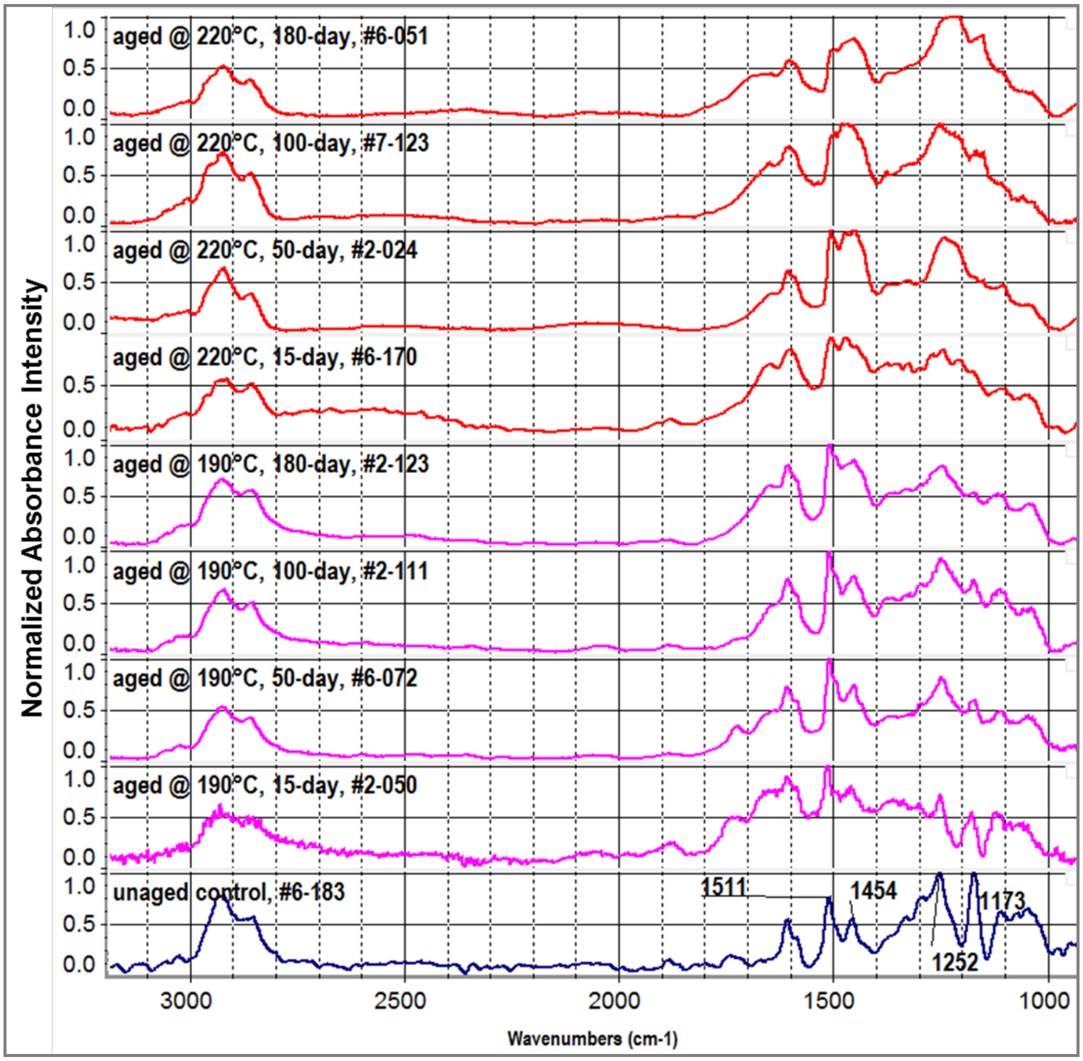

Figure 70.—Typical FT-IR spectra of Resbond 507TS at various accelerated thermal aging conditions regardless of joint type or test temperature.

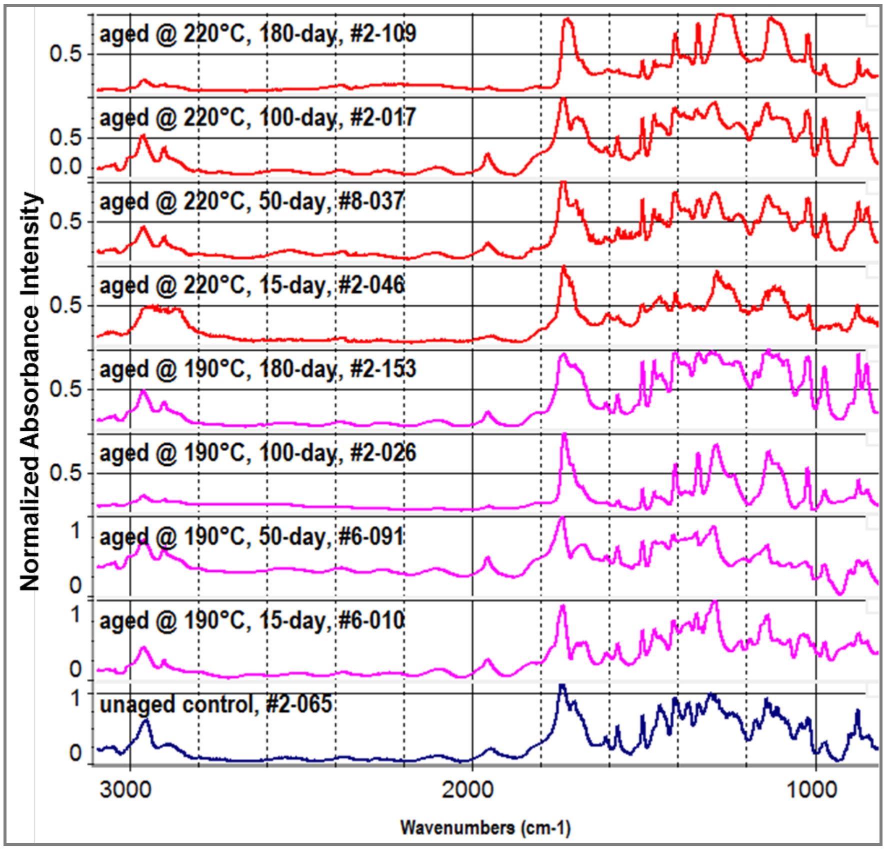

Figure 71.—Typical FT-IR spectra of Poly-Lok PET at various accelerated thermal aging conditions regardless of joint type or test temperature.

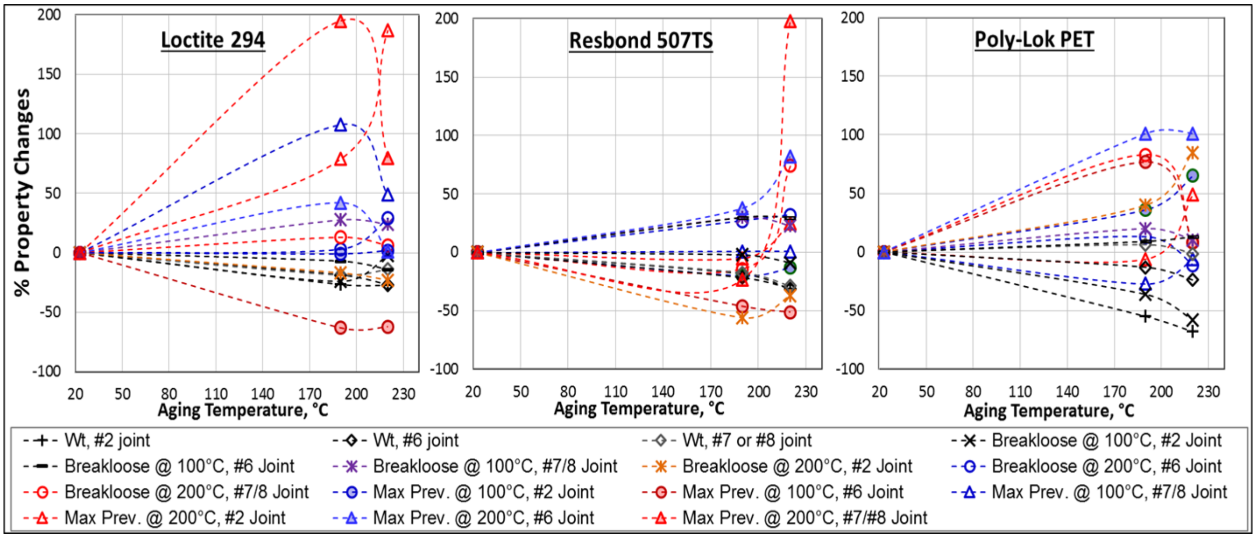

Figure 72.—Overall percent changes in various properties of TL candidates after 180-day aging as a function of the accelerated thermal aging temperature.

Finally, Figure 72 summarizes all of residual properties at the end of 180 day aging in percent change from those of the controls as a function of aging temperature for more direct and practical comparison. Even though there were more positive changes in Loctite 294 and Poly-Lok PET, the Resbond 507TS showed less changes in most properties, which could be interpreted as better thermal stability.

In summary,

- Overall weight losses of the TL candidates from the accelerated thermal aging were rather significant compared to other organic materials studied, which showed approx.15 to 40 wt% in Loctite, 20 to 30 wt% in Resbond, and up to 50 to 70 wt% in PET at the end of the aging, and depended on not only aging temperature and time, but also joint type. The #2 joint, blind-hole configuration, resulted in the highest weight loss regardless of aging temperature for both Loctite and PET, but weight loss of Resbond was solely aging temperature-dependent regardless of joint type. However, whether the weight losses were due to thermal degradation or chemical reactions or just benign outgassing should be further assessed with other residual property evaluations.
- Failure mode analysis showed that the joint #2 with blind-hole configuration mostly failed in less favorable mode, either adhesive or mixed mode, regardless of TL type. In other joint types, Loctite and Resbond showed more favorable cohesive failure mode in most cases, but PET mostly failed by adhesive or mixed mode.
- For the overall torque strengths, Resbond 507TS performed best regardless of aging conditions or joint type, especially at 100 °C. Resbond was the only candidate generating 100 °C breakloose torques greater than the installation torques in all three joint types. Loctite was the next best candidate but with considerably lower breakloose torques.
- In general, torque strength of all three candidates increased considerably with aging, especially at the early stage up to 50 day aging, except in joint #2, then leveled off with further increasing aging time at both aging temperatures. Overall, torque strengths of all three candidates were not significantly affected by the aging temperature up to 220 °C.
- At 200 °C, Resbond 507 TS suffered most loss of breakloose torque among all candidates even though its strength was still higher than other candidates, especially in joint #7. Overall, their values were considerably lower than the installation torque. After the initial changes, they were leveled off with aging time, and showed no visible effects of aging temperatures up to 220 °C.
- For all candidates, their prevailing torques were much lower than their breakloose torques or installation torque except Loctite in joint #7, but less affected by the higher test temperature of 200 °C than breakloose torques. In joint #7 or #8, prevailing torques of the candidates were significantly higher, particularly Loctite and Resbond.
- Systematic changes according to IR spectroscopy analysis of TL candidates after torque testing, indicated that Resbond suffered potential molecular structural changes or thermal degradation, especially at 220 °C or longer aging times regardless of joint type, somewhat consistent with the results of OM failure mode analysis. Both Loctite and PET seemed to be thermally stable up to 220 °C aging for the aging time up to 180 days.

4.2.2.2.3 Shrink Tubing Candidates

Overall test matrix for the accelerated thermal aging test of the shrink tubing candidates is summarized in Table A.18 in Appendix A. In this case, assignment of test specimen for various aging conditions was made with a group of tube specimens (also listed the number of tube specimens in the group) instead of an individual specimen since all test specimens were cut from the tube specimens after the aging. Figure 73 shows physical and color changes of the candidates after various aging exposures. In general, SRFR was slightly discolored, especially when aged at 225 °C, but no visible physical changes were observed. The ETFE material seemed to become less elastic, and sometimes adhered together or with the Z1028 o-ring with increasing aging time or temperature.

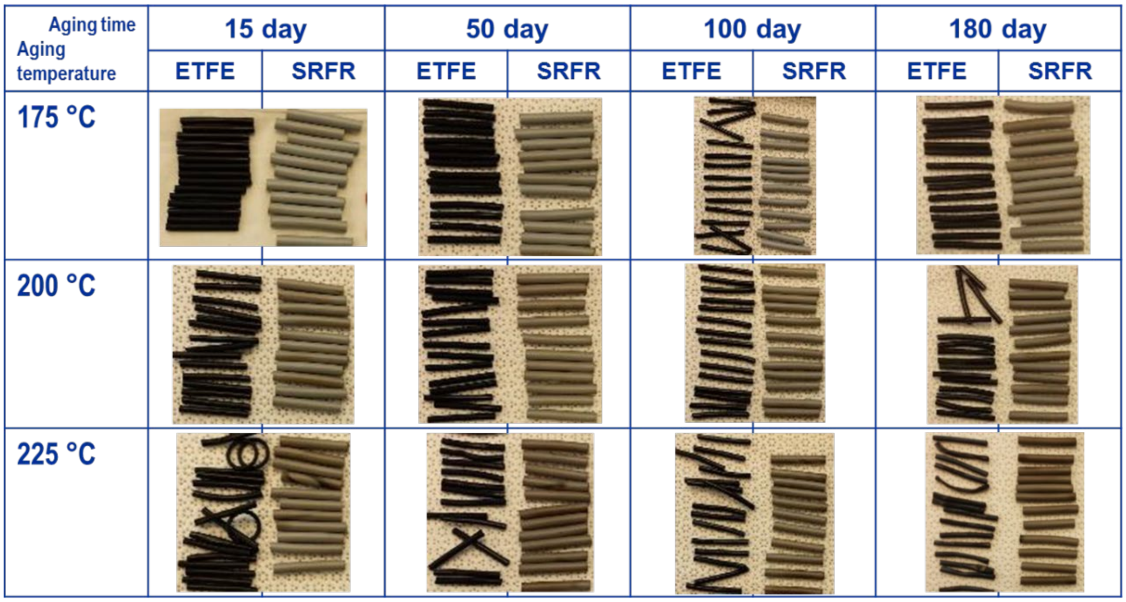

Figure 73.—Physical and color changes in shrink tubing candidate samples as a function of the accelerated aging conditions.

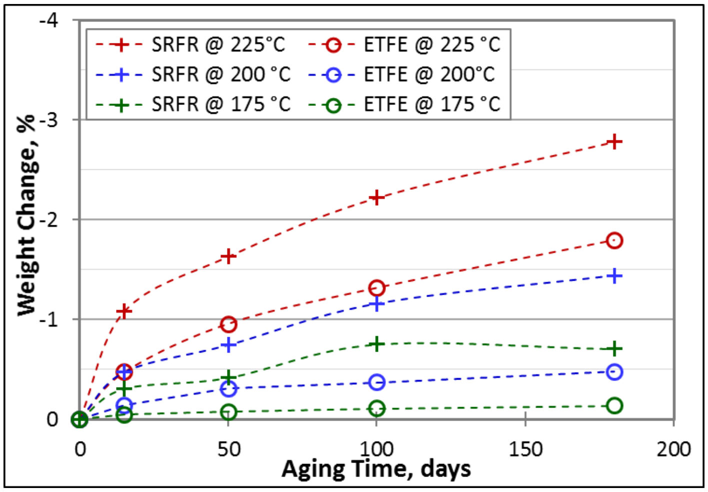

Figure 74.—Overall weight losses of shrink tubing candidates as a function of the accelerated aging conditions.

Weight losses of the shrink tubing candidates were reasonably contained up to 200 °C aging for ETFE or 175 °C aging for SRFR, but at higher aging temperatures, their rates increased steadily with increasing time, Figure 74. The weight losses can be attributed to either outgassing of trapped volatiles or low molecular weight species, or potential thermal decomposition, particularly at higher aging temperature of 225 °C. Exact mechanisms of the weight loss shall be identified, so that the annealing/bake-out conditions can be optimized in order to minimize the outgassing during operation.

Various thermal properties of both shrink tubing candidates against the accelerated thermal aging exposures are summarized in Table A.19 and Table A.20 in Appendix A. In general, changes in T_g or T_m with the aging exposures were insignificant for both candidates, Figure 75.

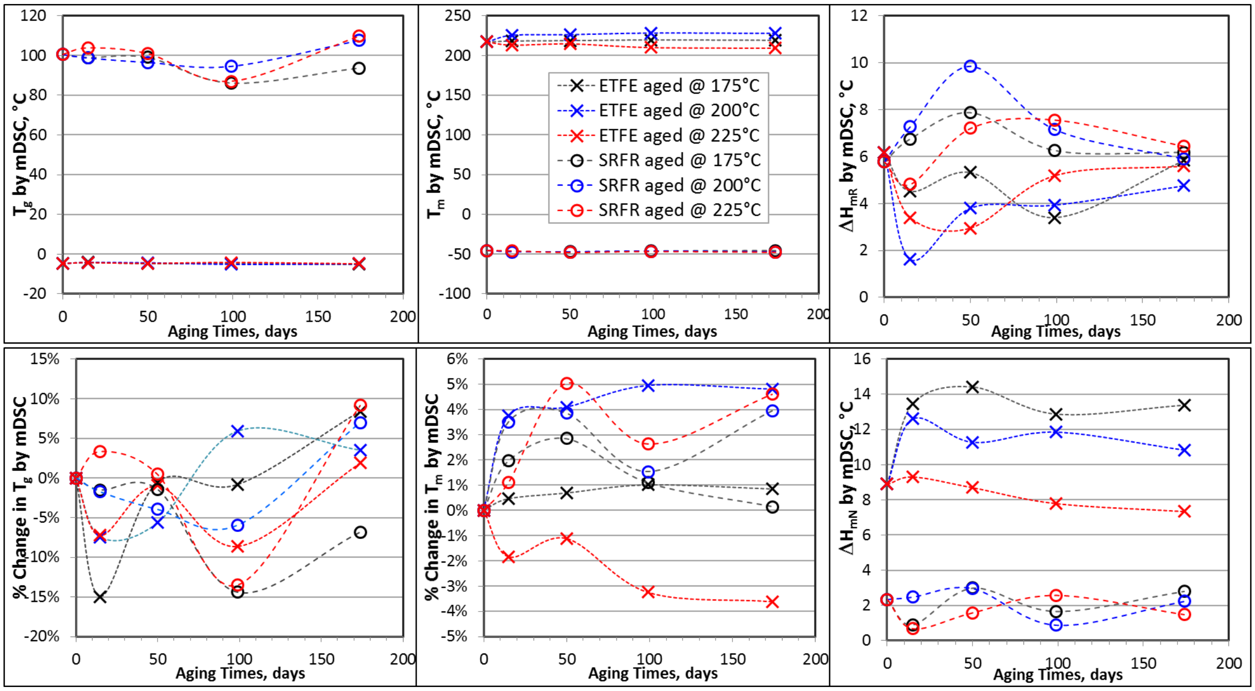

Figure 75.—Thermal properties by mDSC/DSC of shrink tubing candidates as a function of the accelerated thermal aging conditions.

Results of DMA testing in axial direction under tension mode are summarized in Figure 76. ETFE showed two transition peaks, T_{t1} and T_{t2}, from tan δ curve which were associated with molecular rearrangement or relaxation triggered by molecular memory effects between the original expanded versus the recovered/shrunk configuration. On the other hand, only one transition was observed from the SRFR. The first transition temperature increased with increasing aging time for both candidates, but more significantly in SRFR. The transition temperature of SRFR also increased with increasing aging temperature, up to 17% after 180 days at 225 °C. This suggested significant molecular structural changes of SRFR occurred during the thermal aging. The changes during the second transition temperature of ETFE were somewhat more sensitive to aging temperature in that it increased with aging time at lower aging temperatures below 200 °C, but decreased at 225 °C. While the cause of the opposing changes was not clearly identified, it may not be desirable since it suggests a possible change in aging mechanism. The changes in E' ratios at 150 °C to E' at 23°C or E' at 200 °C to E' at23 °C, indicated that SRFR was more negatively affected by the accelerated thermal aging since its molecular structure was more susceptible to thermal aging. The ratios of SRFR decreased considerably with aging time or temperature and indicated material softening, while those of ETFE remained either unchanged or slightly hardened. Figure 77 summarizes the results of DMA testing in radial direction under tension mode. T_{t1} in radial direction of both candidates followed the similar pattern as the axial direction, but with slightly smaller changes. Changes in T_{t2} of ETFE in radial direction were also similar to those of axial direction, which was consistent indication of possible changes in aging mechanism. The changes of E' ratios in radial direction were somewhat opposite of those in axial direction probably due to directional difference in their recovery behavior, such as shrinking ratio. In this case, ETFE was more negatively impacted by thermal aging exposure, but the overall changes were rather trivial.

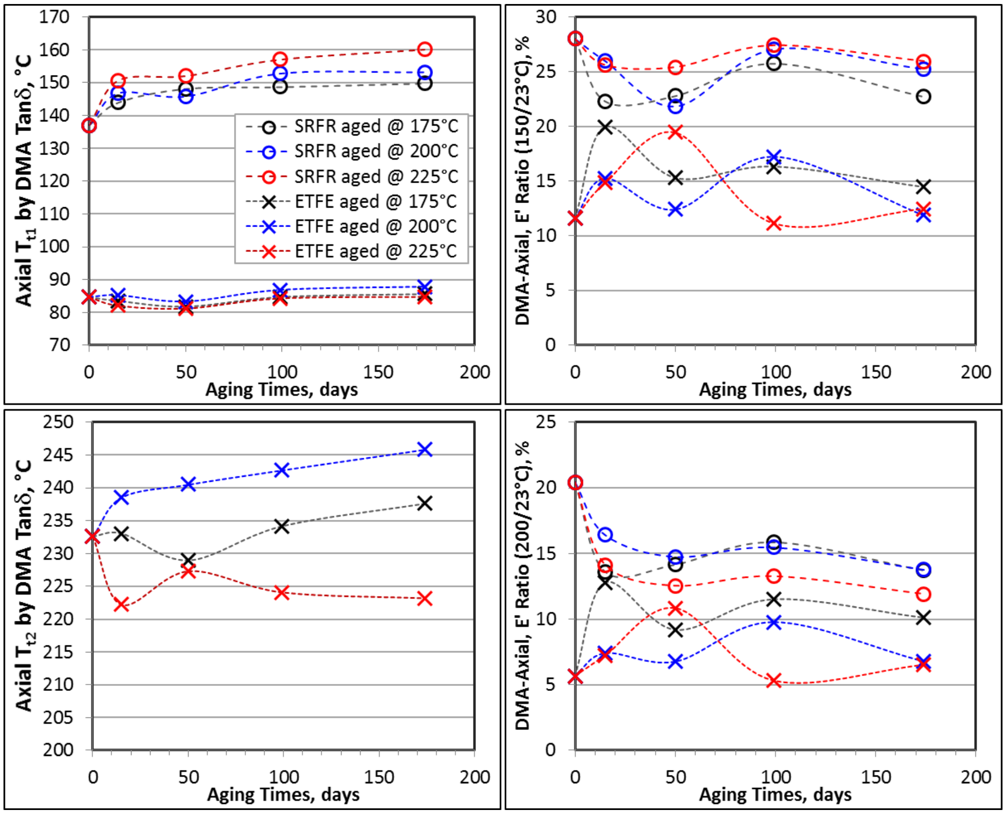

Figure 76.—Axial thermal properties by DMA of shrink tubing candidates as a function of the accelerated thermal aging conditions.

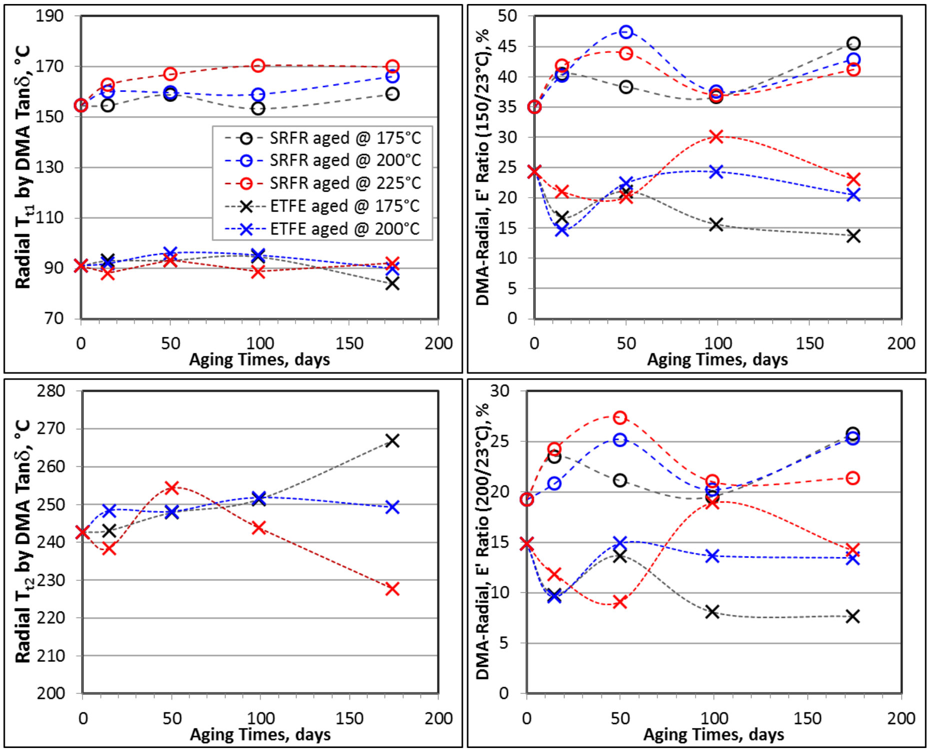

Figure 77.—Radial thermal properties by DMA of shrink tubing candidates as a function of the accelerated thermal aging conditions.

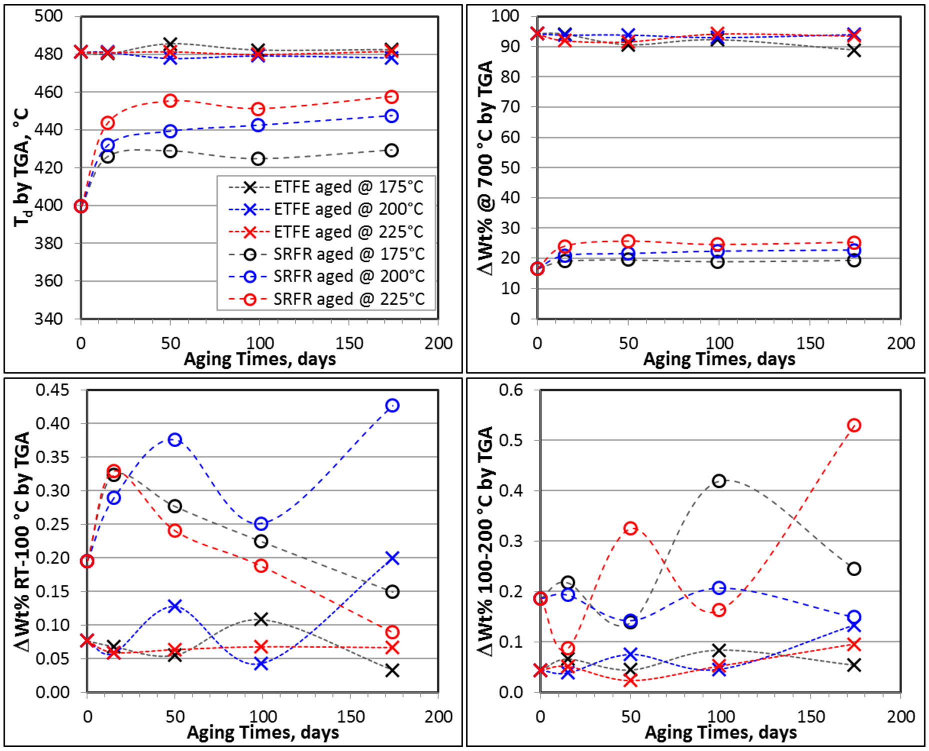

Figure 78.—Thermal properties by TGA of shrink tubing candidates as a function of the accelerated thermal aging conditions.

Other thermal properties and outgassing characteristics by TGA are summarized in Figure 78. T_d of both candidates was sufficiently higher than the target use temperature regardless of the accelerated thermal aging exposures. While ETFE showed no changes with thermal aging, the T_d of SRFR increased significantly with increasing aging temperature even though it leveled off with increasing time. This change can be minimized if the samples were baked with an optimized condition at higher temperatures. Overall, outgassing potentials of SRFR were greater and more affected by thermal aging compared to ETFE. The ΔWt% at 700 °C for ETFE was not significantly affected by the thermal aging regardless of temperature or time, however, SRFR showed considerable increase, especially when aged at 225 °C, from ~17 to ~ 25 wt%.

In general, iso-TGA outgassing characteristics against the accelerated thermal aging exposures were similar to TGA outgassing characteristics for both candidates in that the outgassing potentials of SRFR were greater than ETFE in most cases, but decreased significantly with aging, Figure 79. This suggested that outgassing potentials of SRFR can be reduced by preconditioning assuming that the outgassing was primarily caused by trapped volatiles or low molecular weight species and not by thermal decomposition.

Changes in molecular chemical structure of the shrink tubing candidates were assessed by FT-IR analysis, but from both the inner surface and the outer surface since they might experience different thermal exposure effects. The typical FT-IR spectra of both shrink tubing candidates with major peak wavenumbers identified are shown in Figure 80 using those from the fully aged at 225 °C for up to 180 days. It was observed that there were no changes in the peaks of interest during aging test.

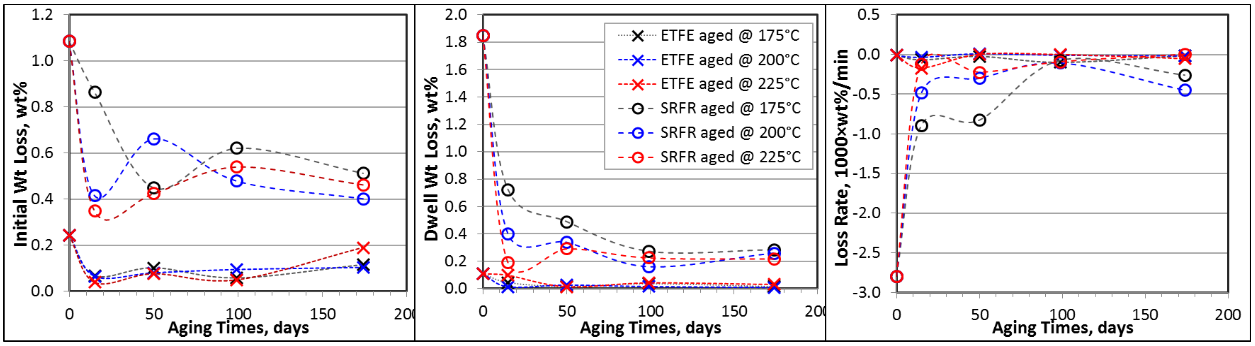

Figure 79.—Thermal properties by 200 °C iso-TGA of shrink tubing candidates as a function of the accelerated thermal aging conditions.

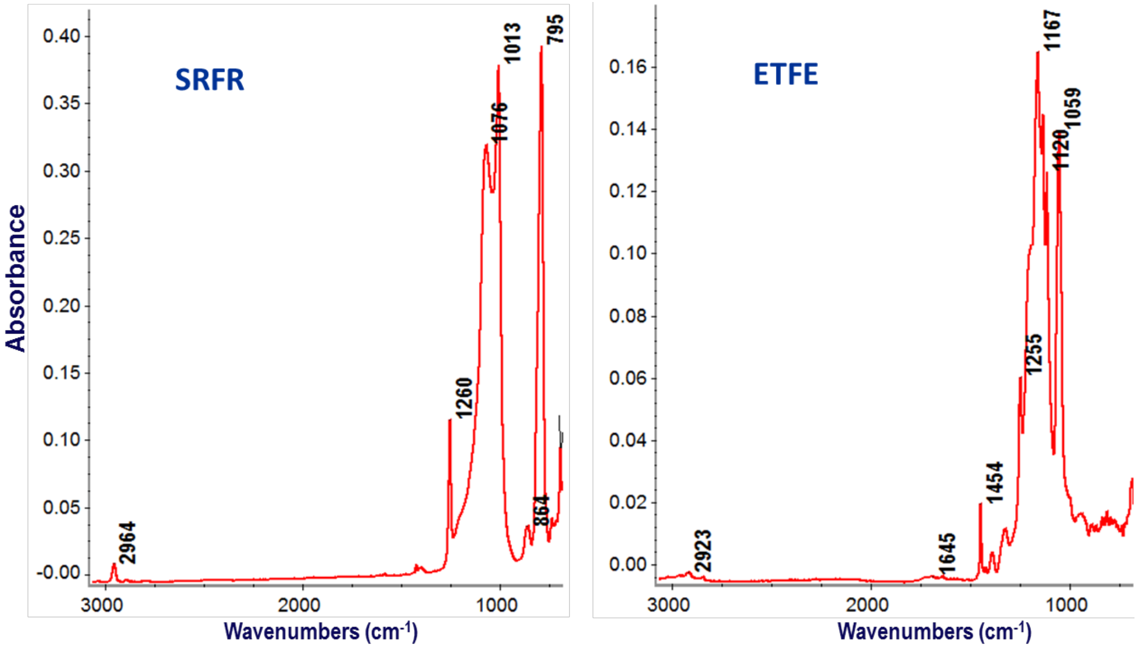

Figure 80.—Typical FT-IR spectra of the fully aged shrink tubing candidates with major peaks identified for quantitative analysis against accelerated thermal aging conditions.

Since thickness of all shrink tubing specimens was supposed to be same, the peaks in the IR spectra peak were quantitatively analyzed and directly compared to other aged samples for ascertaining any evidence of potential degradation or chemical structural changes against the aging conditions. For SRFR, intensities of several peaks, such as those located at 1260 cm^{-1} (Si-CH$_3$), 1075 cm^{-1} (Si-O-Si), 1014 cm^{-1} (Si-O-Si), and 796 cm^{-1} (Si-C) decreased consistently and considerably with aging time when aged at 225 °C, regardless of surface side, Figure 81. The decrease in peak intensities might result from thermally-induced chain scissions. In the case of ETFE, a couple of small peaks at 1645 cm^{-1} (C=O) and 1454 cm^{-1} (-CH3) increased with aging time when aged at 225°C, mostly from OD side, but the changes were considered to be surface artifact or not necessarily bulk material behavior, Figure 82. Overall, no consistent or significant changes in peak intensities were observed in ETFE, regardless of aging temperature or time. Thus, molecular chemical structures of ETFE should be considered thermally stable up to 225 °C exposure.

Effects of the accelerated thermal aging on mechanical properties of the shrink tubing candidates were evaluated by notched tensile strength in both axial and radial direction because of their anisotropy. The overall test results of the notched tensile properties are summarized in Table A.21 in Appendix A based off the average value of eight specimens, standard deviation, and percent changes from their controls.

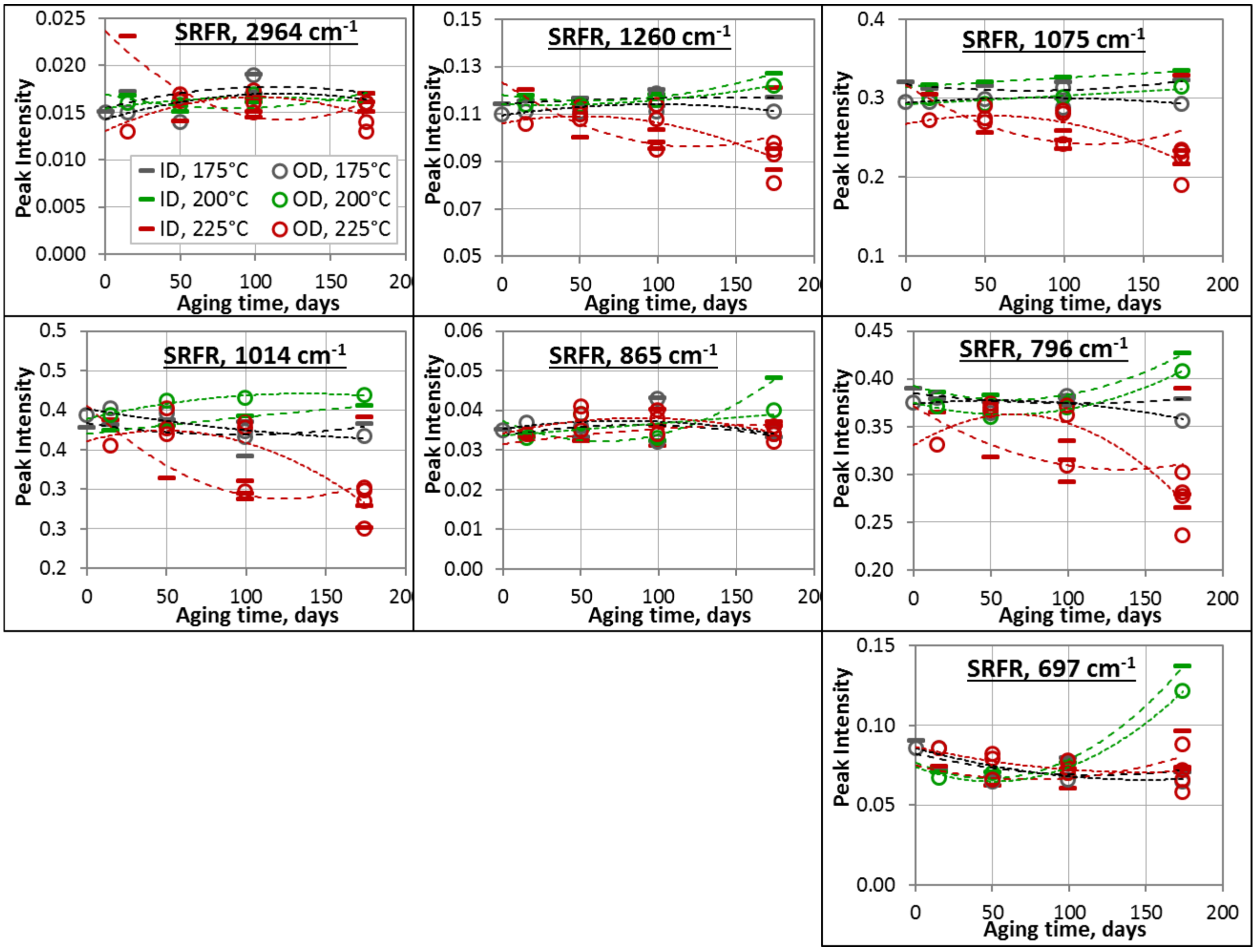

Figure 81.—Changes in IR peak intensities of SRFR shrink tubing from both ID and OD as a function of the accelerated thermal aging conditions.

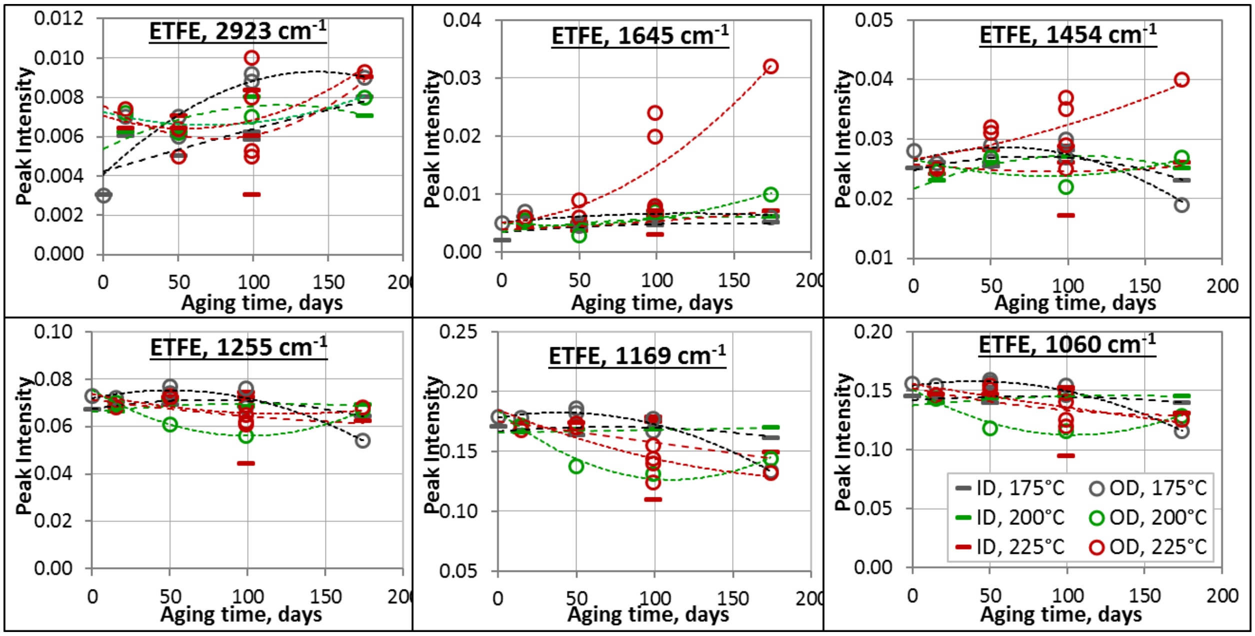

Figure 82.—Changes in IR peak intensities of ETFE shrink tubing from both ID and OD as a function of the accelerated thermal aging conditions.

In both axial and radial direction, ETFE displayed significantly higher notched strength or resistance to notch propagation than SRFR regardless of aging conditions or test temperature while their ultimate elongation was similar in most cases, Figure 83 and Figure 84. For both candidates whether tested axially or radially, the 25 °C strength was not significantly affected by the aging temperature, but showed opposite effects with aging time, where the strength increased in ETFE but decreased in SRFR with aging time. The 200 °C strengths showed similar aging behavior except that the strength of ETFE, particularly in axial direction, decreased considerably when aged at 225 °C. Ultimate elongation of both candidates, especially SRFR, suffered significant reductions with thermal aging, typically right after the initial 15-day exposure regardless of test temperature. Ultimate elongations in the radial direction were more consistent, but generally lower than those in the axial direction for both candidates at all aging temperatures. For more direct comparison, the notched tensile properties, both ultimate strength and elongation, were plotted together in terms of percent changes from their respective properties of the unaged controls at various aging conditions, Figure 85. In the axial direction with a radially introduced notch, ETFE performed better overall and was generally more thermally stable than SRFR, but the changes seemed to level off with increasing aging time in both candidates. The percent changes in the radial direction with axially introduced notch followed similar trends as the axial direction in both candidates, but property reductions were slightly lower in most cases. SRFR showed significant property decreases in all cases while ETFE only suffered in ultimate elongation at 200 °C.

Similar to the other material's evaluation, all of the residual properties at the end of 180 day aging in percent change from the respective baseline control properties were plotted together as a function of aging temperature, Figure 86. Overall, SRFR suffered more undesirable reductions in more properties with increasing aging temperature than ETFE. On the other hand, ETFE shrink tubing showed better thermal stability or positive changes in more properties, even though the low ultimate elongation at 200 °C have to be considered when determining its upper limit.

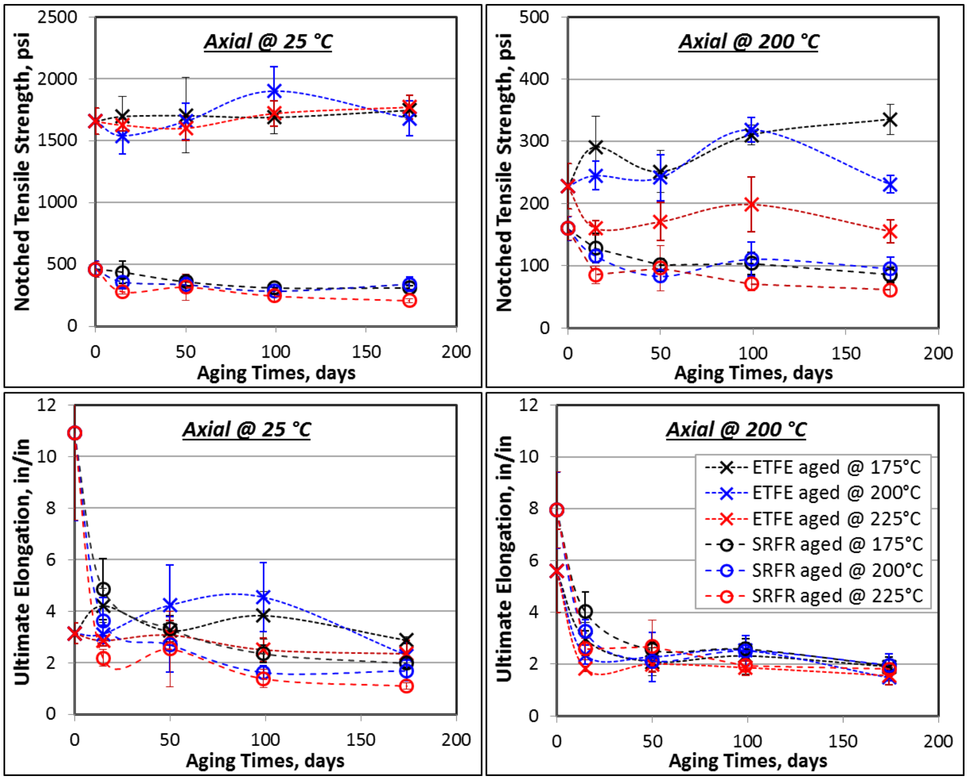

Figure 83.—Notched tensile properties in axial direction of shrink tubing candidate as a function of the accelerated thermal aging condition.

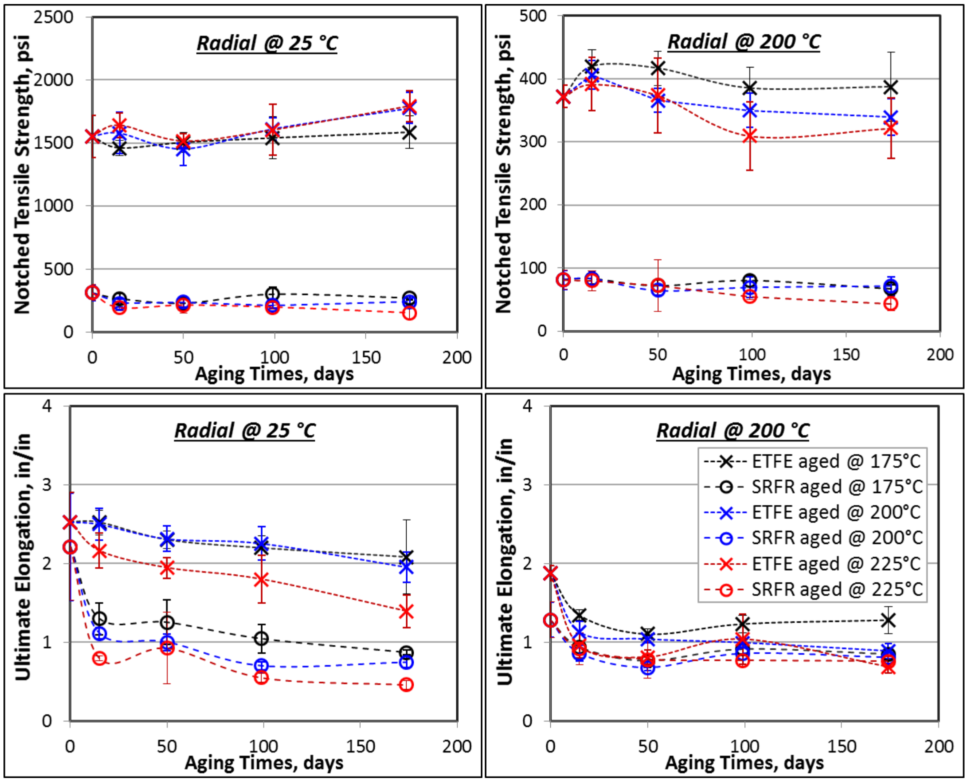

Figure 84.—Notched tensile properties in radial direction of shrink tubing candidate as a function of the accelerated thermal aging condition.

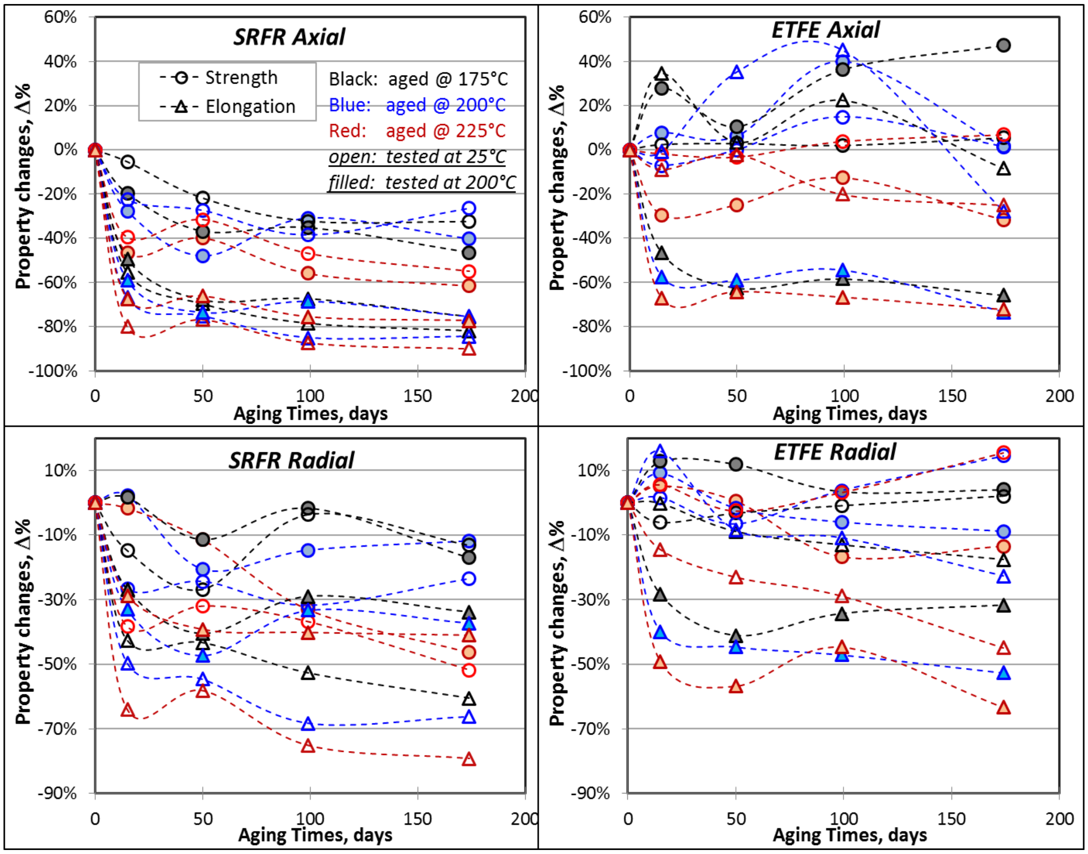

Figure 85.—Overall percent changes in notched tensile properties of shrink tubing candidates from both axial and radial direction as a function of the accelerated thermal aging conditions.

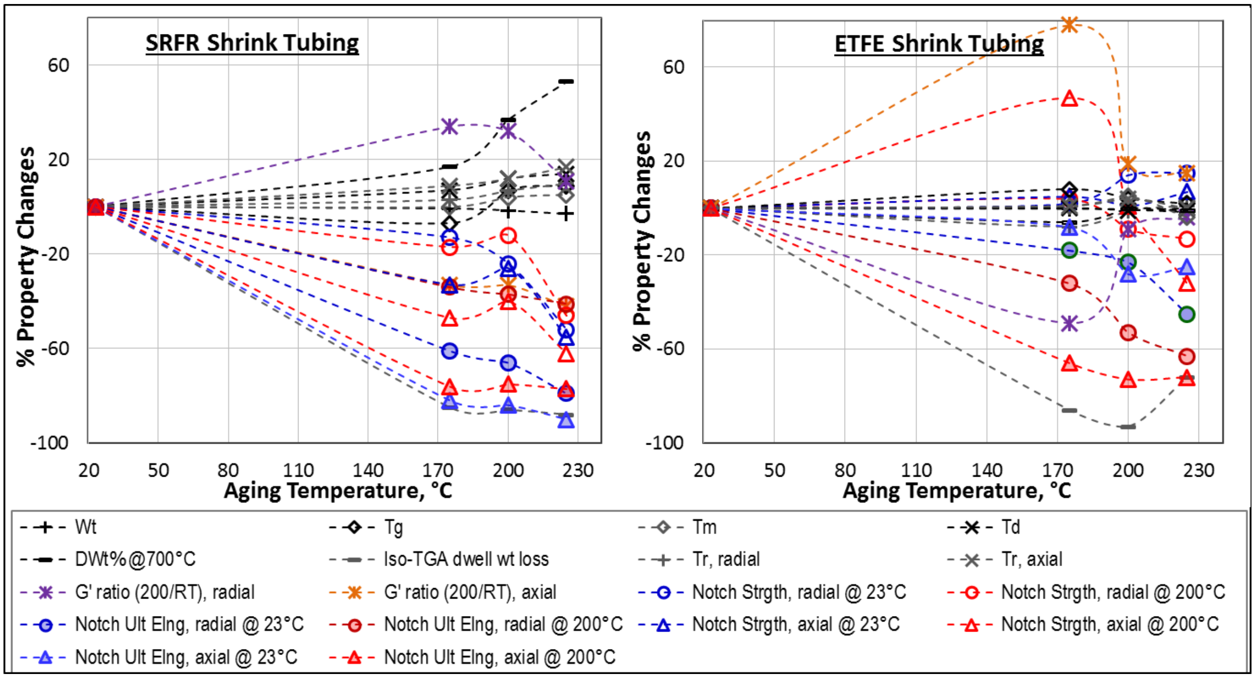

Figure 86.—Overall percent changes in various properties of shrink tubing candidates after 180-day aging as a function of the accelerated thermal aging temperature.

In summary,

- Similar to o-ring, aging caused slight discoloration of SRFR shrink tubing, especially after 100 days at 225 °C, whereas the ETFE shrink tubing was less elastic and stickier with increasing aging time or temperature.
- The weight loss of ETFE with aging was less than 0.5 wt% up to 200 °C at 180 days, and then increased gradually with increasing aging time at 225 °C up to 1.8 wt% after 180 days. In the case of SRFR, the mass loss gradually increased starting at approximately 200 °C and increased to 1.44 wt% at 180 days, reaching ~ 2.8 wt% at 225 °C by 180 days. Its rate further increased with increasing aging time.
- For both candidates, T_g or T_m was not significantly affected by aging regardless of temperature and time, but T_t and E' ratios by DMA varied considerably with aging in both sample directions, especially for SRFR. In the case of T_d, SRFR showed substantial changes, mostly at the beginning of aging for all three aging temperatures, and then leveled off with increasing time while ETFE showed no significant changes regardless of aging time and temperature.
- From both TGA and iso-TGA characterizations, the outgassing potentials of SRFR were greater than ETFE and more affected by thermal aging. The char yield at 700 °C of ETFE, ~ 6 wt%, was little affected by the thermal aging regardless of temperature or time. SRFR showed considerable decrease, especially at 225 °C, from ~83 to ~ 75%.
- The systematic and quantitative FT-IR analysis indicated that SRFR suffered possible chain scissions upon thermal degradation when aged at 225 °C, especially with increasing aging time. The molecular network structure of ETFE was considered to be thermally stable up to 225 °C aging.
- Based on the extensive mechanical performance evaluation via notched tensile properties, ETFE performed better and more thermally stable than SRFR regardless of sample direction (either axial or radial) and test temperature (25 or 200 °C). Generally, the thermal aging caused considerable deterioration of the properties, but the changes mostly occurred at the early stage of aging and seemed to level off with increasing aging time for all three aging temperatures. SRFR suffered greater deterioration in both ultimate strength and elongation than ETFE in most cases. The rate of deterioration in strength in SRFR continued to increase instead of leveling-off when aged at 225 °C, while strength of ETFE either increased or remained unchanged. In general, the notch strength of ETFE was about three to four times higher in both directions than SRFR regardless of aging conditions or test temperature. In contrast, the ultimate elongation properties of both materials were similar in most cases.

4.2.2.2.4 O-ring Candidates

Overall test matrix for the accelerated thermal aging test of the o-ring candidates is also summarized in Table A.18 in Appendix A. Again, assignment of test specimen for various aging conditions was made as a group of o-ring specimens (also listed the number of specimens in the group) instead of an individual specimen.

Typical changes in physical appearance or color of the candidate samples against the accelerated thermal aging exposures are shown in Figure 87. The S1151 o-ring was slightly discolored, especially after 100 days at 225 °C, but no visible physical changes were observed. On the other hand, the Z1028 o-ring appeared to become less elastic, and sometimes sticking together, especially with increasing aging time or temperature similar to ETFE shrink tubing, which was typical same family of fluoropolymers.

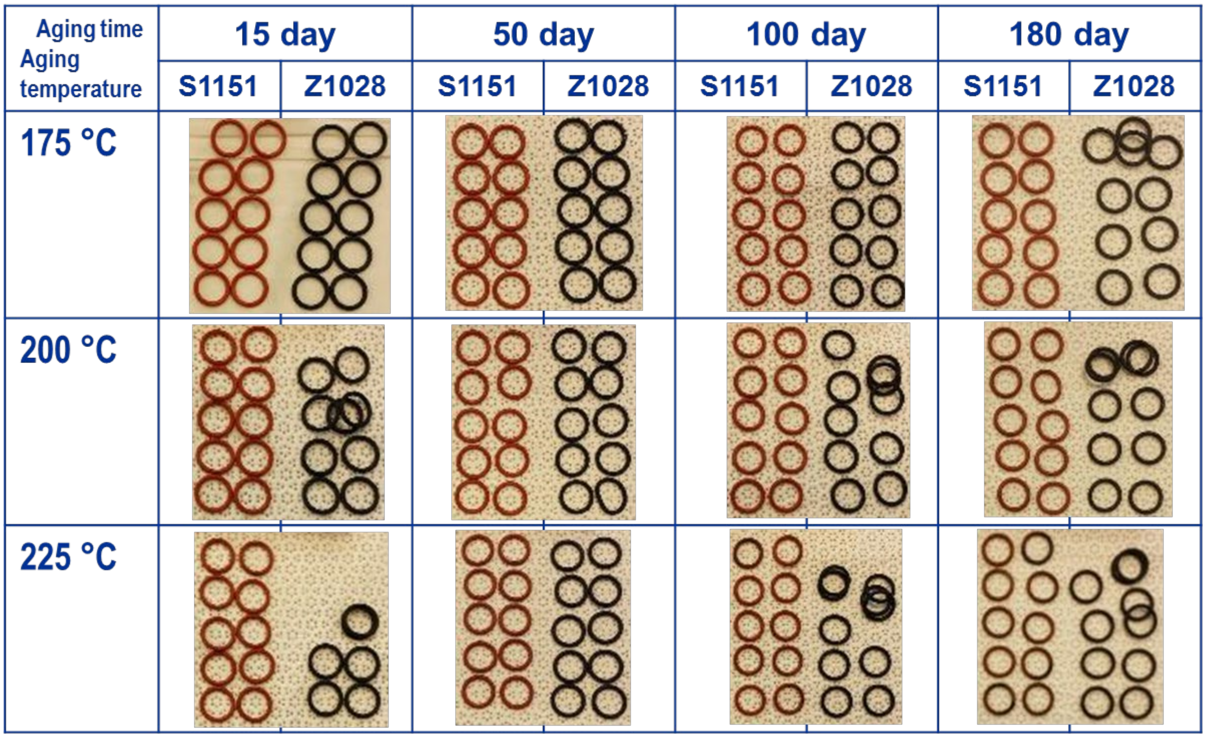

Figure 87.—Physical and color changes in o-ring candidate samples as a function of the accelerated aging conditions.

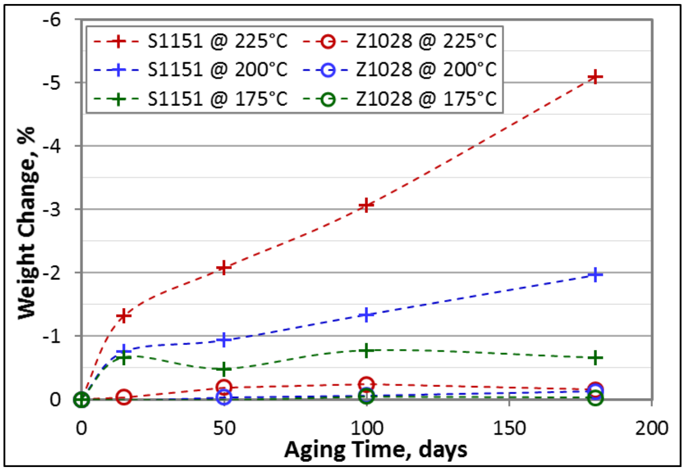

Figure 88.—Overall weight losses of o-ring candidates as a function of the accelerated aging conditions.

Figure 88 shows overall weight changes of the candidates, mostly losses with the accelerated thermal aging. The weight loss of Z1028 with aging was negligible regardless of aging time and temperature, while the S1151 lost about 2 wt% at 200 °C and more than 5 wt% at 225 °C, respectively, at the end of 180-day aging experiment. At 175 °C, the weight loss of S1151 leveled off at ~ 0.7 wt%. Weight losses of the S1151 o-ring were reasonably contained up to 200 °C aging, but increased rapidly at 225 °C with increasing time, suggesting extensive outgassing or possible thermal degradation at exposure temperatures above 200 °C.

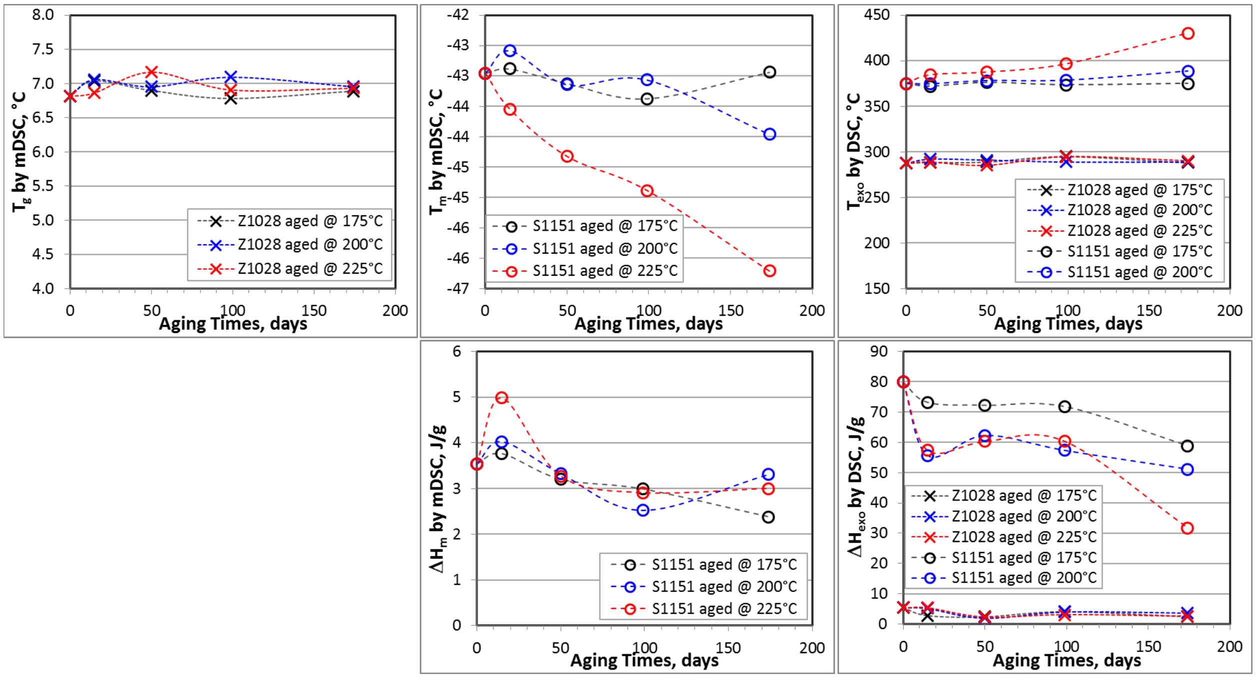

Figure 89.—mDSC/DSC thermal properties of o-ring candidates as a function of the accelerated aging conditions.

All residual thermal properties are summarized in Table A.22 in Appendix A with a similar format used for other materials. Various thermal properties determined by mDSC/DSC are plotted in Figure 89. The most significant changes came from S1151 o-ring when aged at 225 °C, especially in T_m and T_{exo}. Decrease in T_m and ΔH_m suggested that their crystalline structure became less ordered and/or crystallinity was lowered, thus low temperature o-ring performance could be impaired. Increase in T_{exo} might suggest significant additional cross-linking during aging, thus deterioration of o-ring performance. Most DSC thermal properties of Z1028 o-ring were stable regardless of aging time and temperature. As shown in Figure 90, T_d of both o-ring candidates was sufficiently higher than the target use temperature, but S1151 o-ring showed slightly higher reduction with aging, especially at 225 °C. Thermal exposure above 200 °C seemed to make the silicone molecular structure more susceptible to thermal degradation. From the TGA outgassing characteristics, outgassing potentials of S1151 o-ring were greater than Z1028 o-ring, which showed negligible changes regardless of aging time and temperature. For both o-ring materials, Δwt% at 700 °C, ~ 90% for Z1028 and ~55% for S1151 due to higher inorganic filler content, was not significantly affected by the thermal aging regardless of temperature or time. Figure 91 shows the outgassing characteristics by iso-TGA. Similar to TGA outgassing characteristics, outgassing potentials of S1151 o-ring were greater than Z1208 o-ring in most cases, but decreased significantly with aging.

Potential changes in molecular chemical structures of the shrink tubing candidates were assessed by FT-IR. Figure 92 illustrates the typical FT-IR spectra for both o-ring candidates with identified wavenumbers of major peaks using those from the fully aged samples for 180 days at 225 °C. Similar to shrink tubing materials, there was no significant changes observed in the peaks of interest during the aging test, regardless of aging temperature. Since thickness of all o-ring specimens was supposed to be same, the changes in IR spectra peak was quantitatively analyzed and directly compared among various aged samples for ascertaining any evidences of potential degradation or chemical structural changes against the aging conditions. Figure 93 and Figure 94 summarize changes in intensity of all identified peaks for S1151 and Z1028, respectively, as a function of aging time and temperature. From the S1151 o-ring, intensities of several peaks, 2963 cm^{-1} (-CH$_3$), 1259 cm^{-1} (Si-CH$_3$), 863 cm^{-1} (Si-O), and 794 cm^{-1}

(Si-C) appeared to decrease consistently and considerably with aging time, especially at aging temperatures higher than 200 °C. The decreases may be due to breaking of certain molecular bonds or chain scissions upon thermal degradation. On the other hand, Z1028 o-ring showed no significant or consistent changes in peak intensities, regardless of aging temperature and time. Molecular structure of Z1028 seemed to be more thermally stable up to 225 °C exposure.

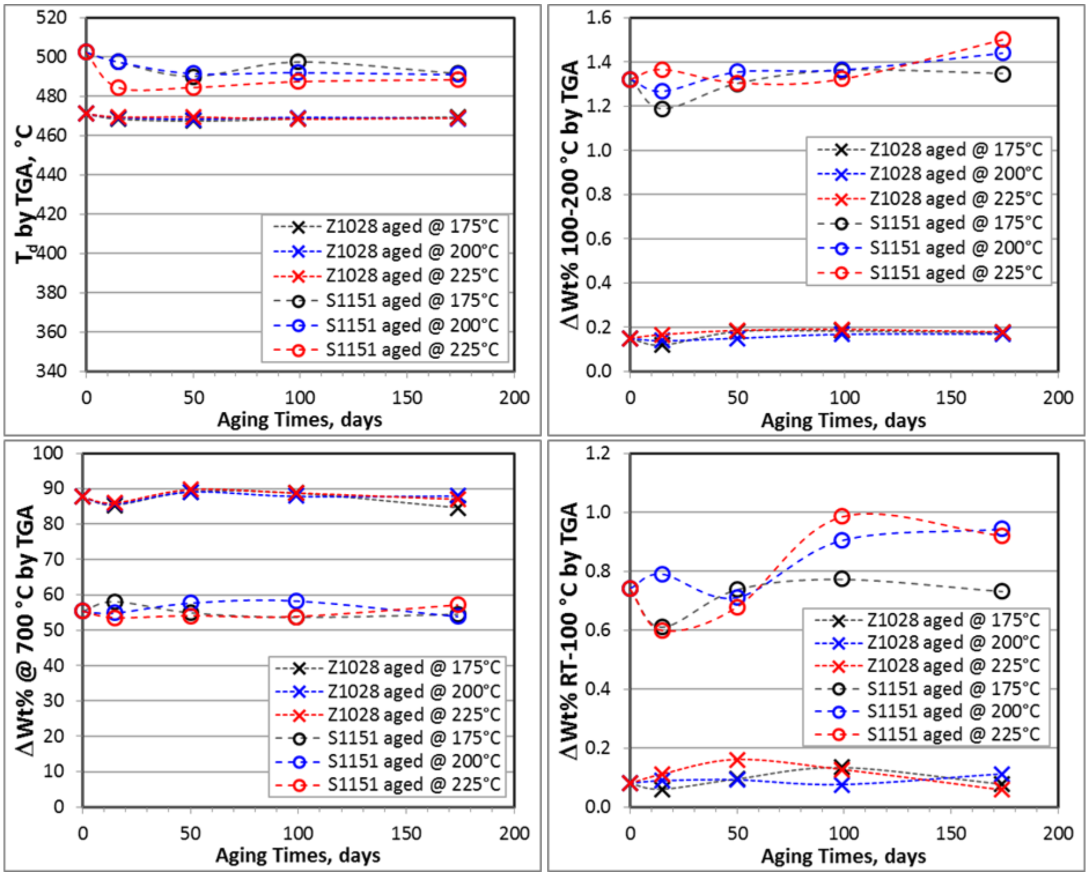

Figure 90.—TGA thermal properties of o-ring candidates as a function of the accelerated aging conditions.

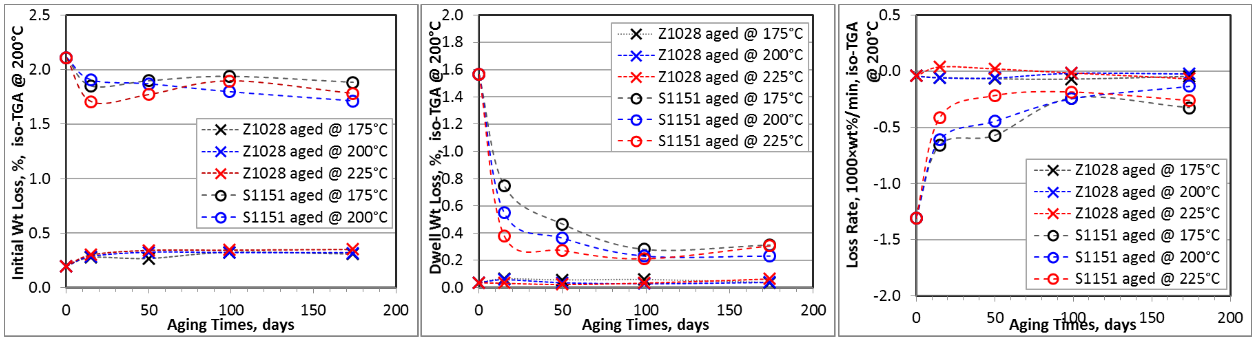

Figure 91.—Outgassing potentials of o-ring candidates as a function of the accelerated aging conditions.

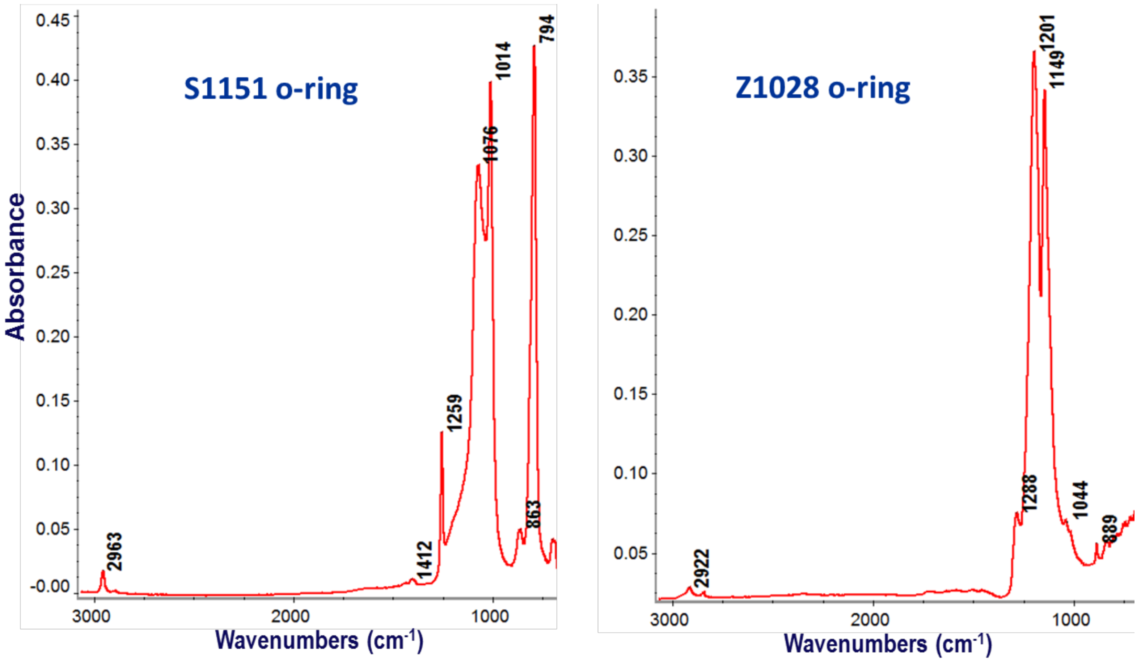

Figure 92.—Typical FT-IR spectra of o-ring candidates with major peaks identified for quantitative analysis against accelerated thermal aging conditions.

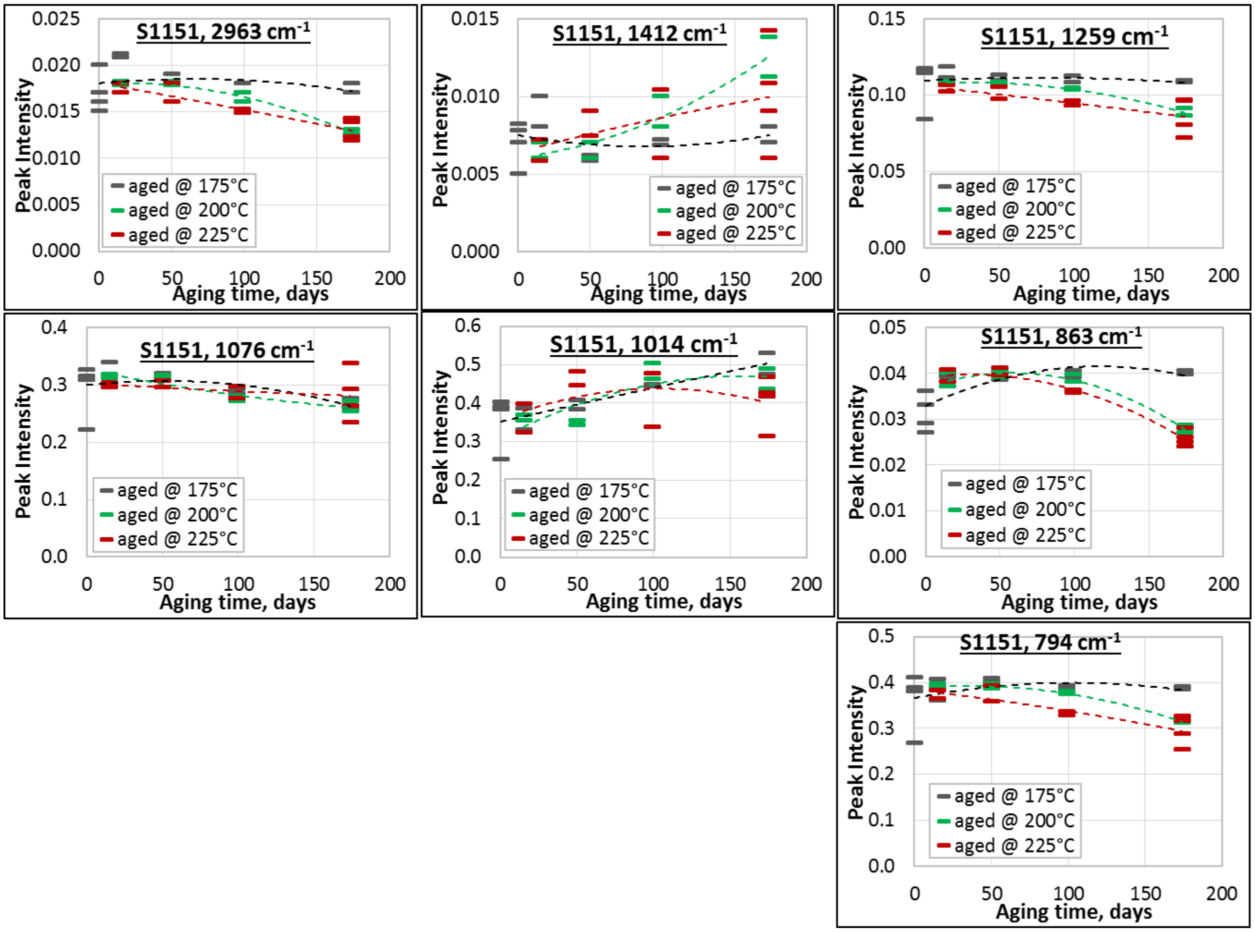

Figure 93.—Changes in IR peak intensities of S1151 o-ring as a function of the accelerated thermal aging conditions.

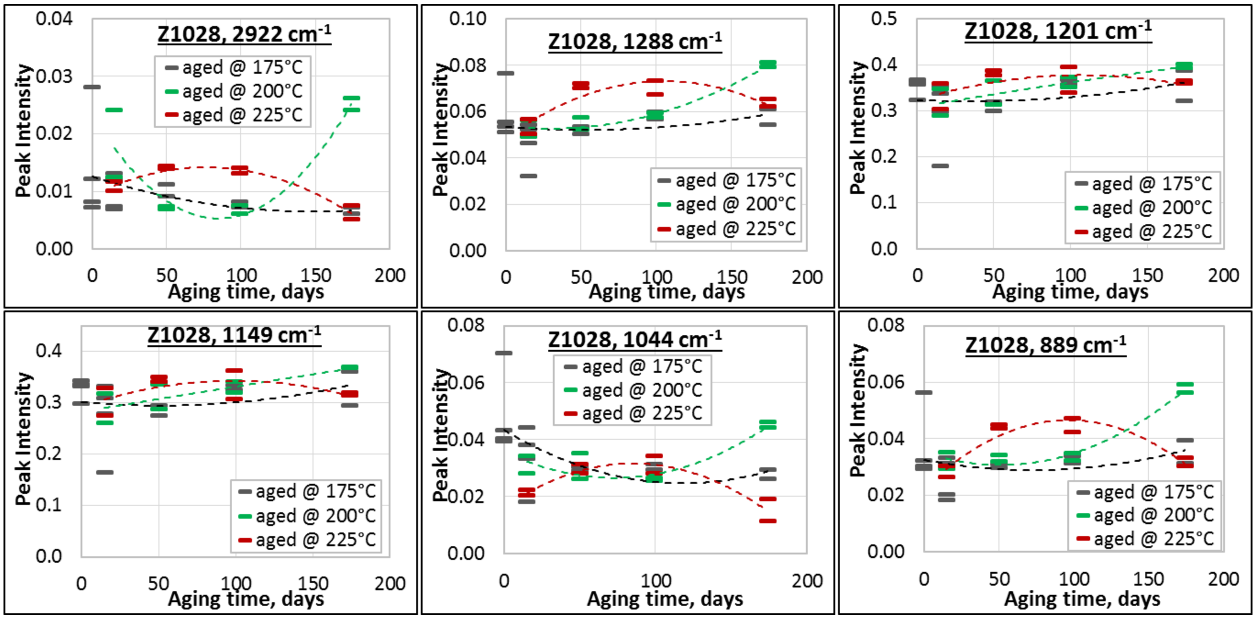

Figure 94.—Changes in IR peak intensities of Z1028 o-ring as a function of the accelerated thermal aging conditions.

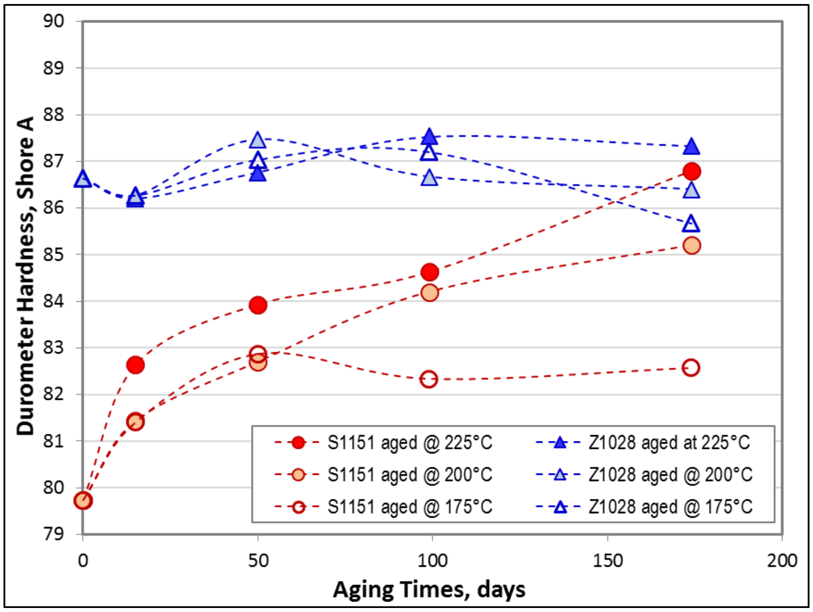

Figure 95.—Hardness changes of o-ring candidates against the accelerated thermal aging conditions.

Mechanical properties of o-ring candidates were evaluated by hardness, compression-set, and tensile properties. The overall hardness data is summarized in Table A.23 in Appendix A and plotted in Figure 95. Hardness of S1151 o-ring increased with the thermal exposures, more significantly with higher aging temperatures (i.e., ~ 4% at 175 °C vs. ~ 7 % at 200 °C or ~9 % at 225 °C at the end of 180-day aging). On the other hand, Z1028 o-ring showed no significant changes in hardness regardless of aging temperature and time, less than ±1 %.

The compression-set properties measured at three different time intervals after unloading are plotted in Figure 96. For both o-ring materials, thermal aging exposure lowered compression-set significantly, where the material more than likely became more elastic due to the additional chemical cross-linking during aging, and ultimately improved the compression-set. At the same time, thermal aging might decrease physical cross-link density, due to the formation of crystallites or densely packed blocks. In general, an appropriate range of cross-link density is needed for the optimum compression-set performance. Overall, the Z1028 o-ring performed better than S1151 regardless of aging temperature and time. Increase of C_B at 100-day, especially when aged at 225 °C, was not explainable but observed from both o-ring materials.

Overall tensile properties are summarized in Table A.24 for S1151 and Table A.25 for Z1028 in Appendix A. Figure 97 compares various tensile properties of the as-received unaged control samples of the two candidates as a function of test temperature. In most cases, room temperature tensile properties of the Z1028 were superior to those of S1151. At elevated temperatures, 150 and 200 °C, the S1151 exhibited slightly better than or equal properties to the Z1028. Note that samples tested at 200 °C were previously tested for the compression-set properties. That is, they underwent additional thermal exposure at 200 °C for 70 hr under compression in addition to the aging exposures. The compression-set exposure must have caused the higher moduli and strength by comparing to those at 150 °C whose samples only exposed to the thermal aging. With the behavior of the control properties, the effects of the accelerated thermal aging on tensile properties are only viewed in terms of a percent change of the properties from their respective control properties as a function of the aging conditions.

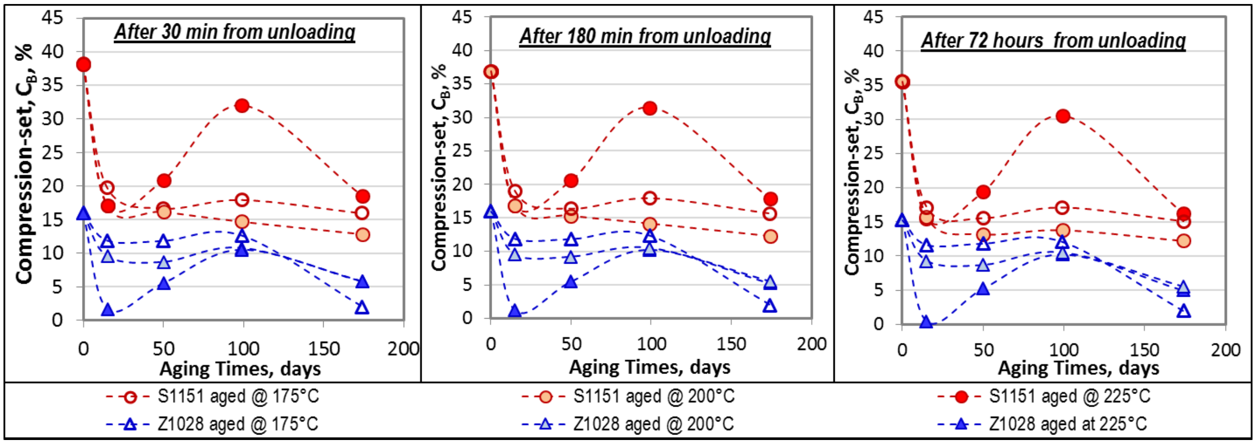

Figure 96.—Changes in compression-set property of o-ring candidates at various hold times from unloading as a function of the accelerated thermal aging conditions.

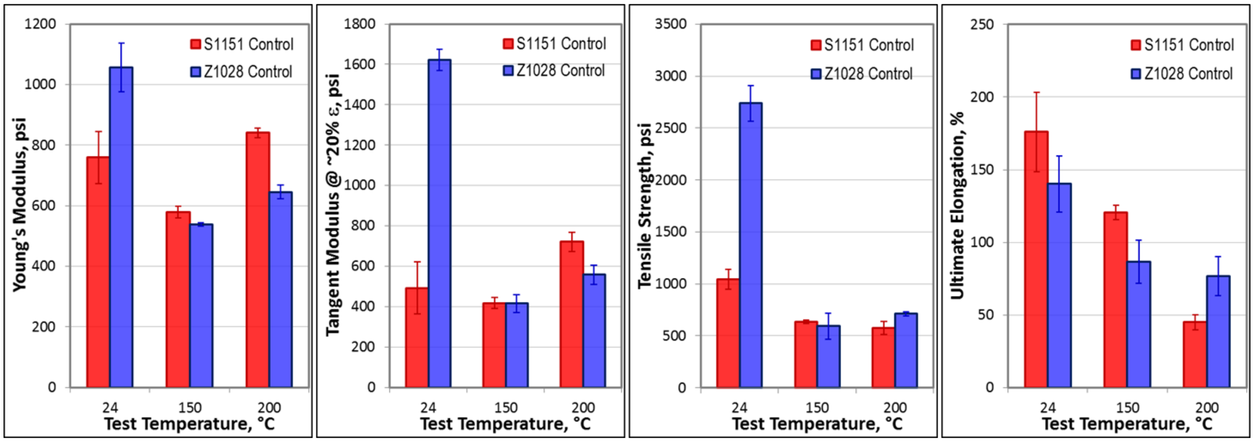

Figure 97.—Typical tensile properties of as-received control samples of o-ring candidates at various test temperatures.

Figure 98 shows the aging-induced changes in moduli of the candidates. Similar to hardness, changes in Young's modulus were much less in Z1028 o-ring regardless of aging conditions or test temperature. Significant increase in Young's modulus of S1151 consisted with changes in other properties, such as compression-set, and hardness, are indicative of poor thermal stability. Tangent modulus of both o-ring materials showed the same trends as their Young's modulus. Regardless of test temperatures, S1151 o-ring suffered a major strength drop in ultimate strength or elongation-to-failure when aged at 225 °C, Figure 99. Strength of Z1028 o-ring at test temperatures up to 150 °C was mostly unchanged regardless of aging temperature and time. Changes in tensile strength at 200 °C altered with aging time in both o-ring materials, where an initial decrease was observed followed by an increase in strength with increasing aging time for all three aging temperatures. In both o-ring materials, the ultimate elongation regardless of test temperature was reduced initially with aging but then stabilized with increasing aging time for all three aging temperatures, Figure 100. In most cases, S1151 o-ring suffered greater loss of ultimate elongation, especially when aged at higher temperatures above 200 °C. The changes in ultimate elongation of Z1028 o-ring was little affected by either the test temperature or the aging temperature, which suggested good thermal stability.

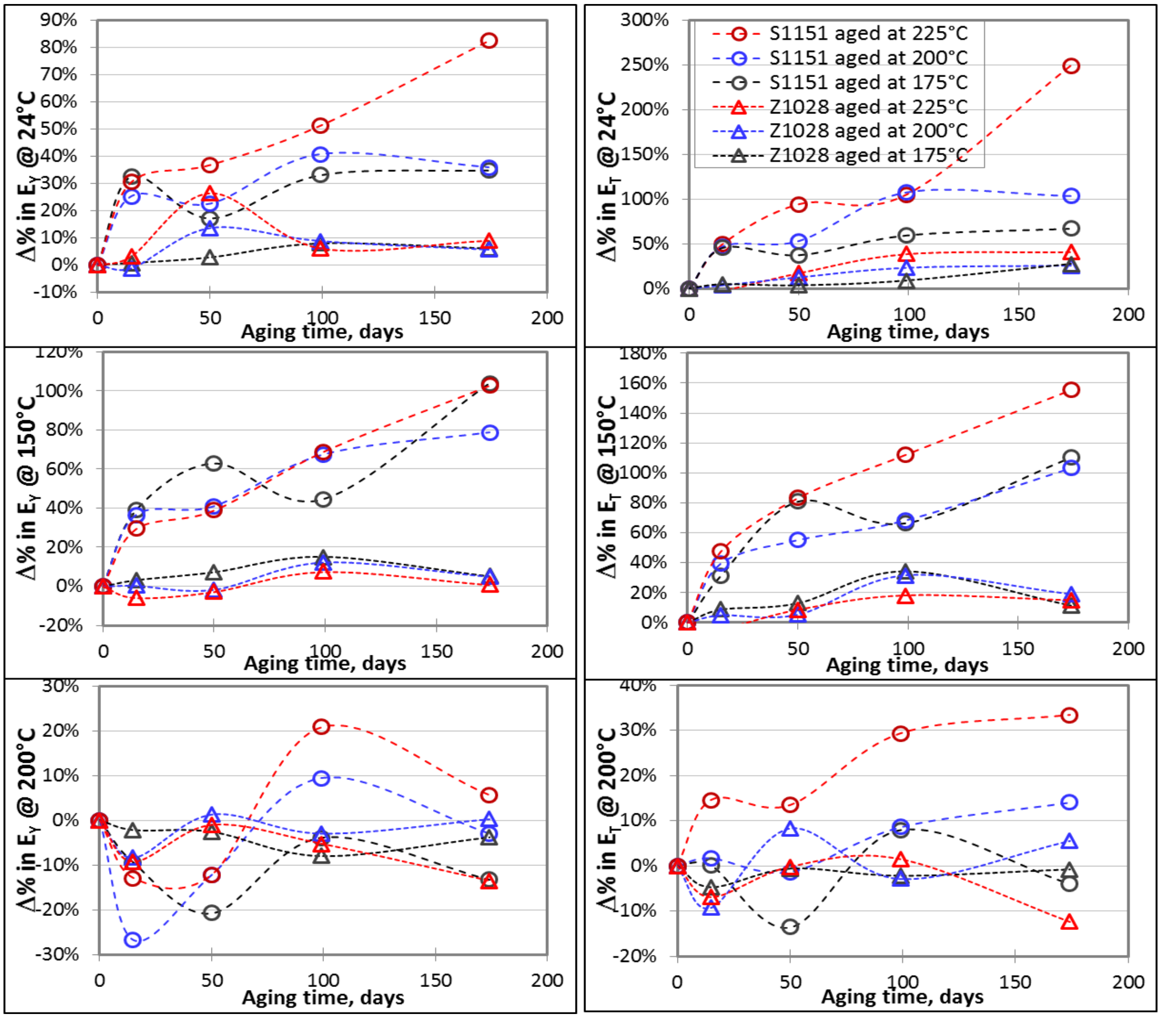

Figure 98.—Percent changes in Young's and tangent (at ε=~20%) moduli of o-ring candidates at various test temperatures as a function of the accelerated thermal aging conditions.

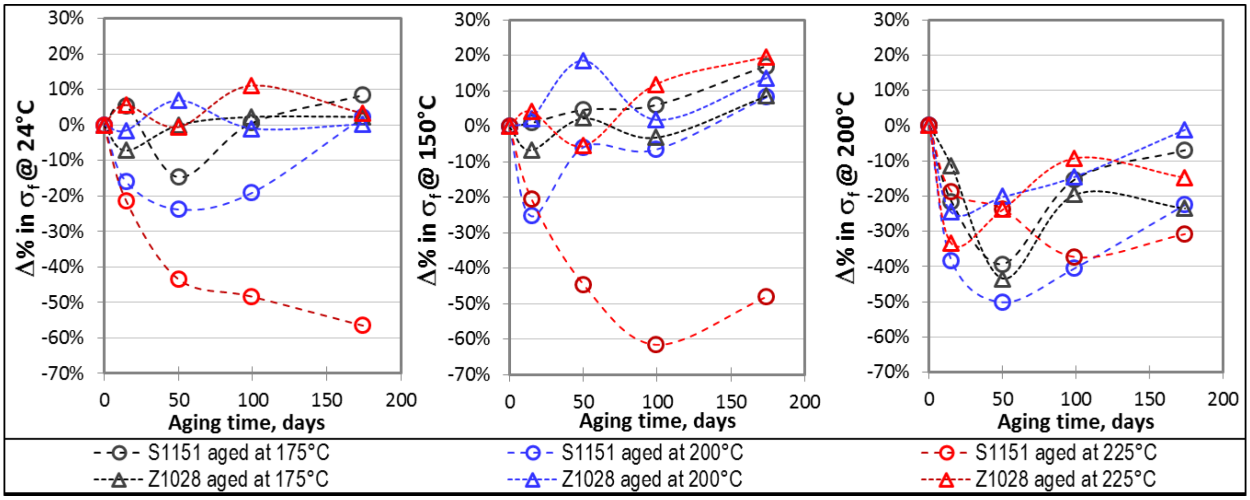

Figure 99.—Percent changes in ultimate tensile strength of o-ring candidates at various test temperatures as a function of the accelerated thermal aging conditions.

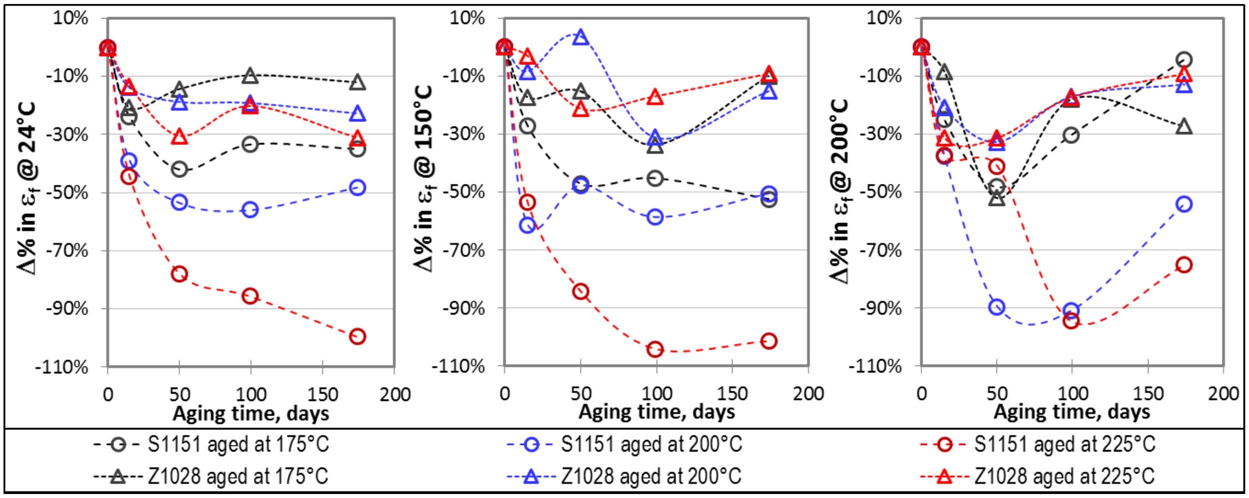

Figure 100.—Percent changes in ultimate elongation of o-ring candidates at various test temperatures as a function of the accelerated thermal aging conditions.

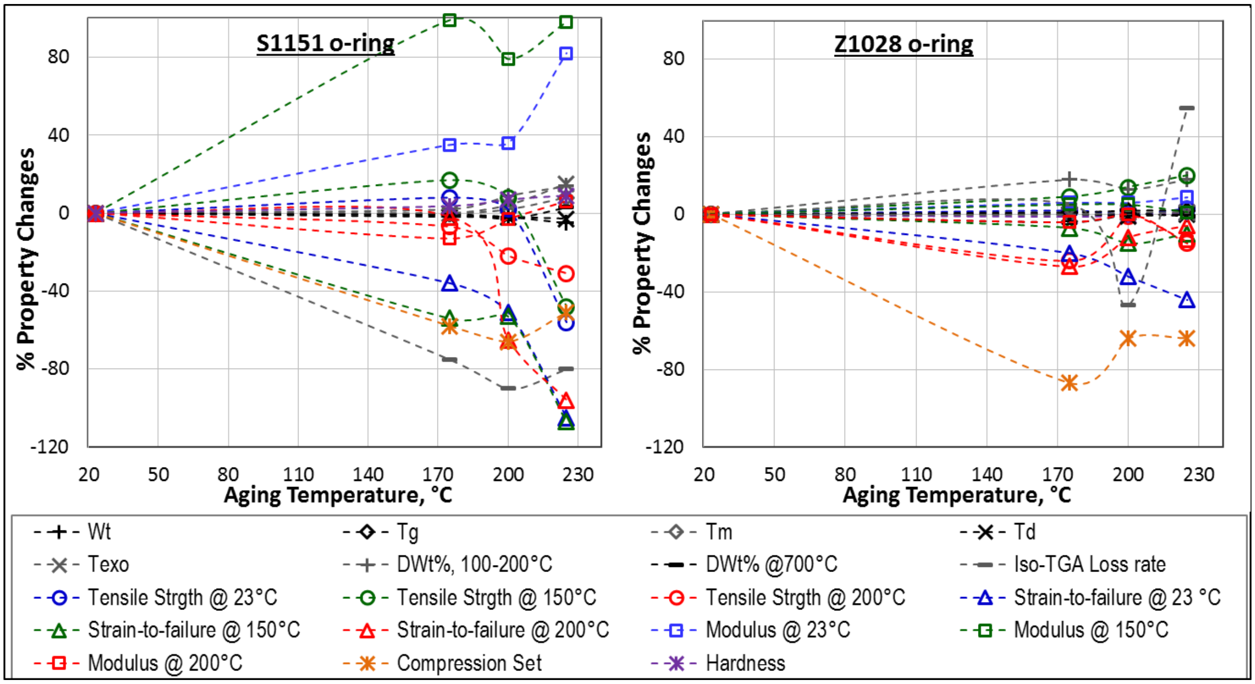

Figure 101.—Overall percent changes in various properties of o-ring candidates after 180-day aging as a function of accelerated thermal aging temperature.

Finally, all of the 180-day properties of the candidates were plotted together in terms of percent changes from their respective controls as a function of aging temperature in Figure 101. It is evident that properties of Z1028 o-ring were considerably more thermally stable than S1151 in most cases.

In summary,

- Similar to shrink tubing, aging caused slight discoloration in S1151 o-rings, especially after 100 days at 225 °C. Z1028 o-rings were less elastic and stickier with increasing aging time or temperature.
- Weight loss of Z1028 with aging was negligible regardless of aging time and temperature, but S1151 lost about 2 wt% at 200 °C or more than 5 wt% at 225 °C, respectively, at the end of 180-day aging. At 175 °C, the weight loss of S1151 was leveled off at ~ 0.7 wt%.
- For most of thermal properties including T_g, T_m, T_{exo}, T_d, and ΔH, S1151 showed considerable changes with aging, especially at 225 °C, while Z1028 showed no significant changes regardless of aging time and temperature.
- From both TGA and iso-TGA characterizations, the outgassing potentials of S1151 were greater than Z1028, which showed negligible changes up to 225 °C. However, for both candidates, their char yield at 700 °C did not show main compositional changes following to thermal aging exposure.
- Detailed FT-IR molecular network structure analysis indicated that S1151 suffered possible chain scissions upon thermal degradation when aged at temperatures above 200 °C, especially with increasing aging time, while Z1028 showed thermally stable molecular networks up to 225 °C aging.

- Based on the extensive mechanical performance evaluation via hardness, compression-set (C_B), and tensile properties, Z1028 o-ring outperformed S1151 in most cases, especially in terms of thermal stability. Z1028 was thermally stable up to 225 °C aging, while the thermal stability of S1151 considerably deteriorated at the aging temperature above 200 °C.

4.2.3 TCIOP Material Compatibility

Specific objectives of this task were to determine outgassing behavior of the down-selected candidates under the typical Stirling convertor premix gas environment and the effects of outgas on their properties and performance to assess material compatibility for the Stirling application. This TCIOP material compatibility assessment consisted of in-situ outgas analyses and residual property characterizations, consistently and systematically for all material types. The in-situ outgas analyses combined three different gas analysis techniques, RGA, GC/TCD, and FT-IR, thus the results were compared and validated.

4.2.3.1 Adhesive/Potting Candidates

4.2.3.1.1 In-Situ Outgas Analyses

Typical RGA peaks from outgas samples during TCIOP testing of the EA9394C-2 epoxy at various temperature-time exposures are shown in Figure 102 including the summary table of the identified outgases in the inset. They typically consisted of the premixed Stirling convertor gases (H_2, O_2, N_2, CO_2, He), possible residual air contamination (CH_4, H_2O, Ar, CO, Ne), and some higher molecular weight species suspected of pump oil.

AF13102 epoxy also showed identical RGA peaks and outgas compositions. Concentrations of each gas species at various temperature and time exposure conditions were calculated from their relative peak intensities against He peak based on the RGA formula, and then factored to match the initial concentrations at t=0 with those from the Stirling premix gas. Figure 103 summarizes the overall changes in concentration of various gas species registered during the TCIOP exposures. Both adhesives showed comparable level of gas concentrations, but different outgassing behavior in that the EA9394C-2 epoxy increased concentrations of CH_4, H_2O, and CO_2 with increasing exposure temperature and time while the AF131-2 epoxy caused no significant changes. Most increases occurred at the 200 °C exposure and seemed to be accompanied by decreases in H_2 and O_2, and possibly linked to its cure advancement. This result agreed with the higher weight loss of the EA9394C-2 at 200 °C from the 6-month accelerated thermal aging experiment. It should be noted that the concentrations of the gas species in the premix gas alone without any Stirling organic samples were not affected by the TCIOP exposure conditions. This was validated by various outgas analysis techniques from other TL, shrink tubing, or o-ring organics. For the GC/TCD analysis, the only registered gas species were He, O_2, and N_2 from the Channel A, and CH_4, H_2O, and CO_2 from the Channel B. Figure 104 illustrates typical GC/TCD spectra obtained in-situ during the TCIOP experiment. Even though it was limited to a few gas species, concentration calculation was more straightforward and accurate. Concentrations of various gas species were plotted as a function of TCIOP exposure conditions in Figure 105. Except H_2O, GC/TCD results were in good agreement with those of RGA. H_2O peak was rather small and broad, or less sensitive to TCD, thus subjected to greater data scattering.

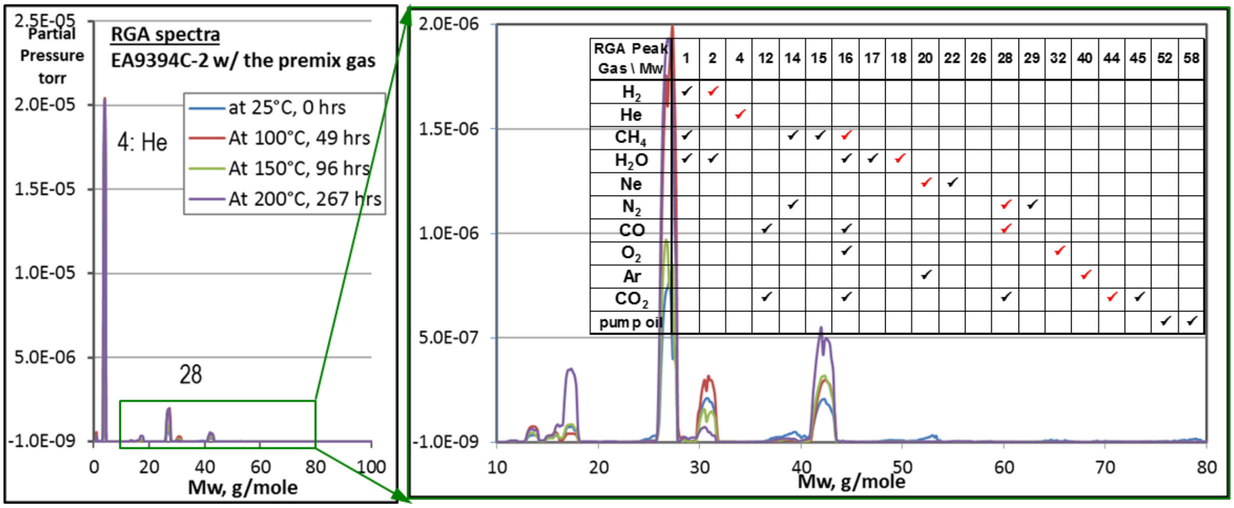

RGA Peak Gas \ Mw	1	2	4	12	14	15	16	17	18	20	22	26	28	29	32	40	44	45	52	58
H_2	✓	✓																		
He			✓																	
CH_4	✓				✓	✓	✓													
H_2O	✓	✓					✓	✓	✓											
Ne										✓	✓									
N_2					✓								✓	✓						
CO				✓			✓						✓							
O_2							✓								✓					
Ar										✓						✓				
CO_2				✓			✓						✓				✓	✓		
pum p oil																			✓	✓

Figure 102.—Typical RGA spectra from outgas samples during TCIOP testing of EA9394C-2 epoxy at various exposure conditions and identification of gas species in the table in the inset.

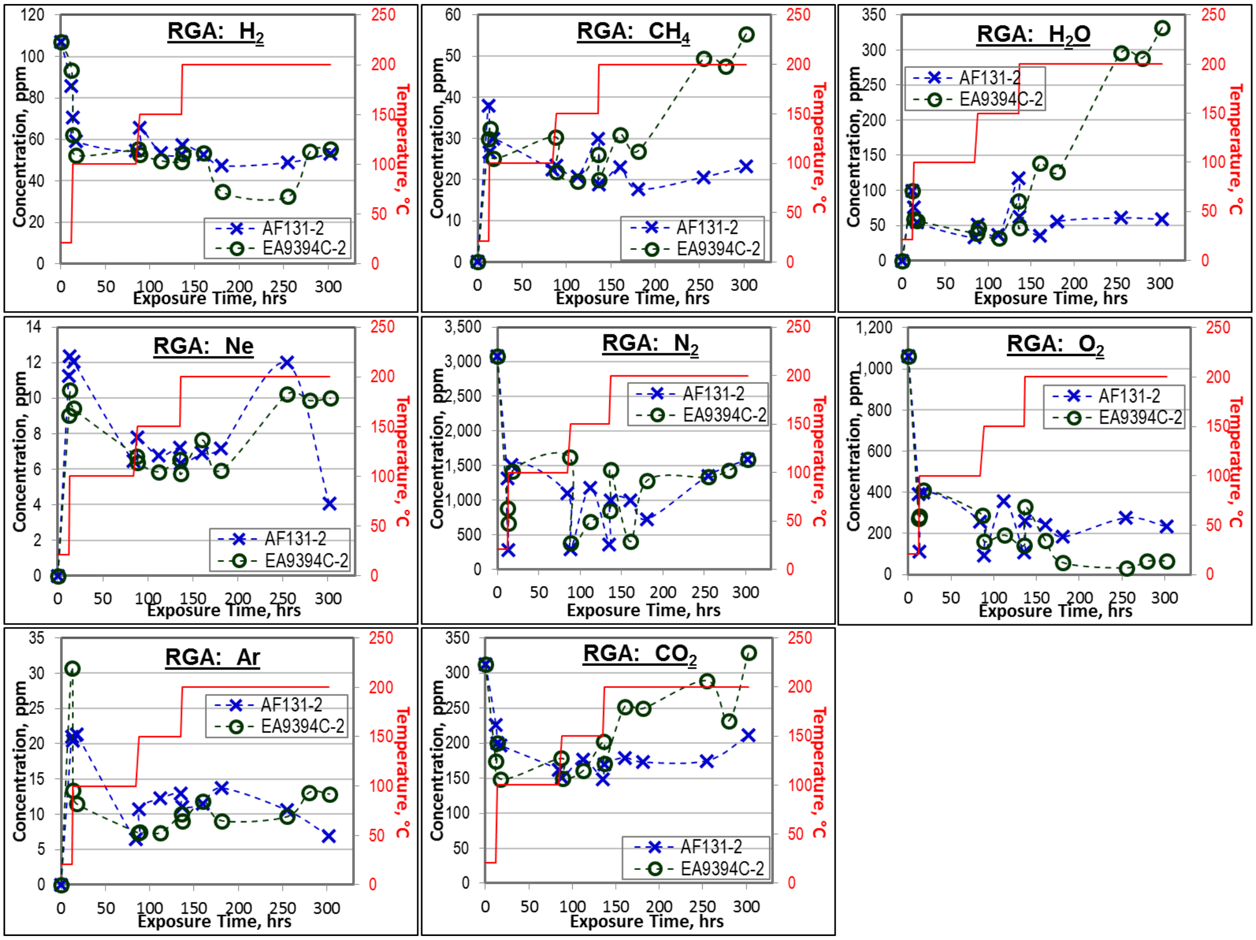

Figure 103.—Overall changes in concentrations of various outgas species by RGA during TCIOP exposures of adhesive candidates.

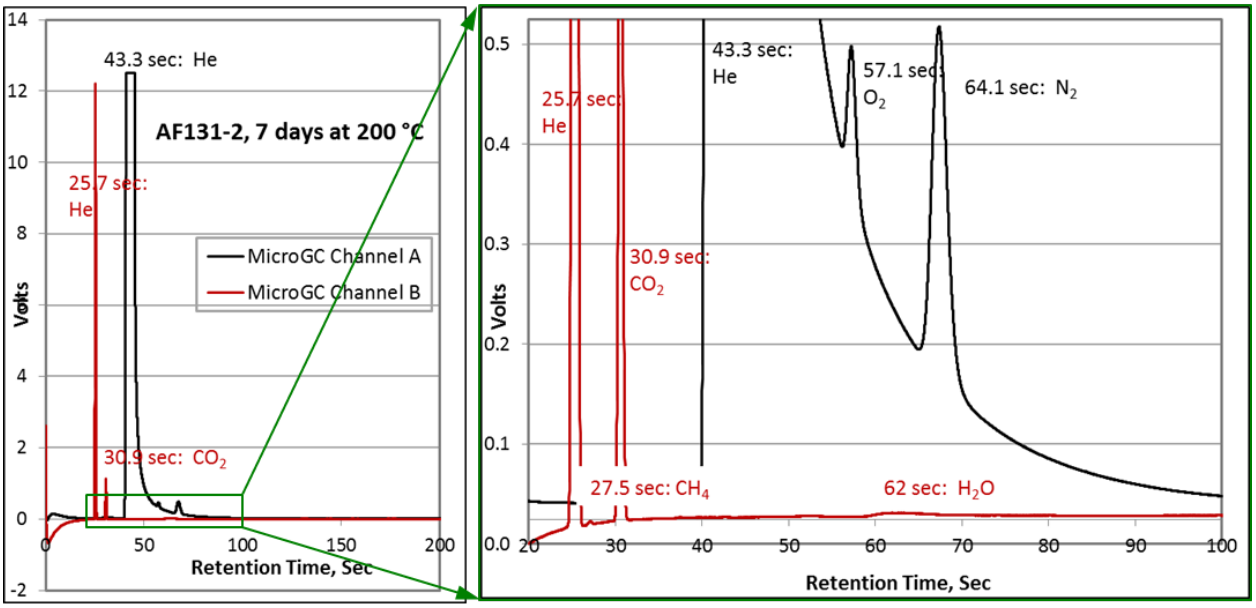

Figure 104.—Typical GC/TCD spectra showing various outgas peaks as a function of retention time during TCIOP testing of AF131-2 adhesive.

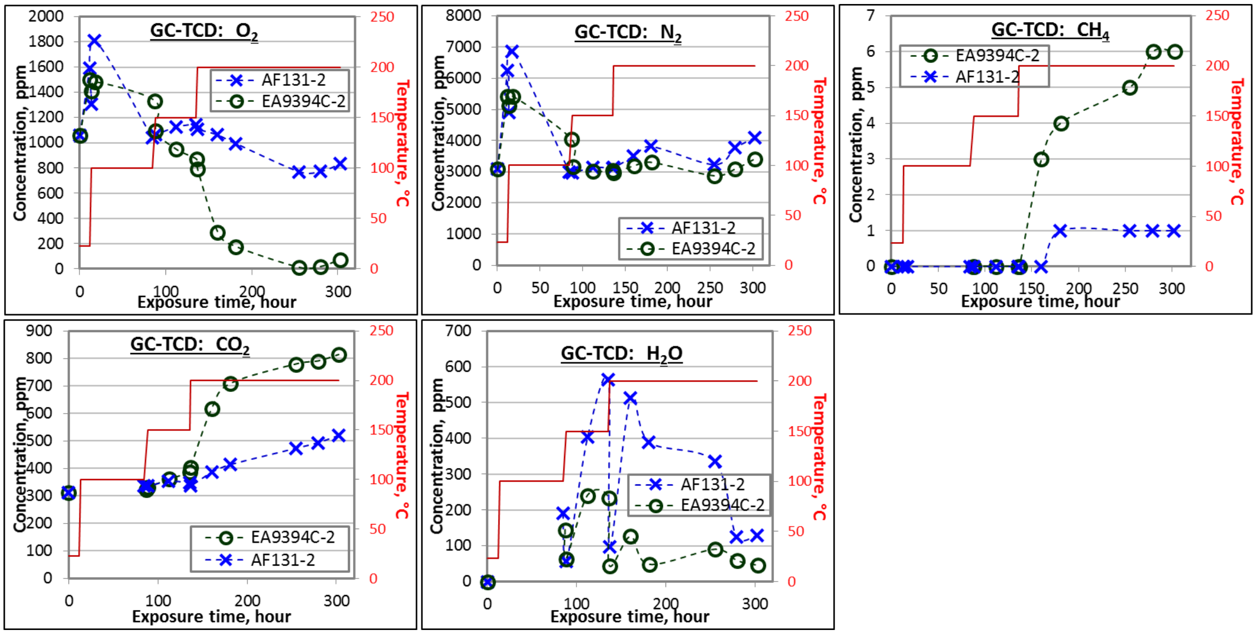

Figure 105.—Overall changes in concentrations of various outgas species by GC/TCD during TCIOP testing of adhesive candidates.

The identified gas species by FT-IR were illustrated in Figure 106 involving the NIST database for the typical IR spectra of both candidates at the end of TCIOP exposures, which was after 290 hr at 200 °C. With exception of atomic gases, such as H_2, O_2, N_2, most of the compound molecular gas species in the outgas samples were clearly identified. For both adhesive candidates, outgas samples contained H_2O, CO_2, and CO. Note that CO was indistinguishable from N_2 in either RGA or GC/TCD analyses. A peak at 1033 cm^{-1} from the outgas of the EA9394C-2 epoxy was unidentifiable by the NIST database, but appeared clearly in several IR spectra, particularly at higher temperatures above 150 °C. In Figure 107, changes in FT-IR spectra of outgas samples at various TCIOP exposure conditions were compared with those of the solid epoxy samples, red spectra at the bottom, to ascertain whether those gases resulted from possible thermal breakdown of the epoxy material. The analysis focused especially on lower wavelength region less than 1200 to 1500 cm^{-1} where the most new peaks appeared. For both adhesives, no matched peaks between the outgas samples and the solid samples were observed, which suggested no major material breakdown. However, the EA9394C-2 produced additional outgases at temperatures above 150 °C indicated by a few new peaks at ~1033, 966, 931, or 816 cm^{-1}. On the other hand, outgas samples from the AF131-2 showed no new peaks or visible changes for the entire exposure steps. The new peaks were suspected to be from the fillers or unsaturated alcohols, CH-O-H, which might result from either molecular rearrangements, possible outgas-epoxy interactions, or onset of thermal degradation. However, their actual concentration and impact on material compatibility or durability could not be assessed with the data available to date. Since the volume of each gas sample was fixed at 1 atm, the heights/intensities of unnormalized absorption peaks should represent their concentrations. Thus, all spectral peaks were identified and analyzed according to changes in peak height and intensity as a function of exposure condition as shown in Figure 108. Concentrations of both H_2O and CO_2 increased with the exposure time and temperature especially at 200 °C for the EA9394C-2 epoxy and were thus confirmed the RGA results.

Concentration of CO increased slightly in both epoxies, but seemed to be transitional due to its high reactivity. Since H_2O was not included in the premix gas, the small amount observed at $t = 0$ could be from the residual air contaminant, but its increase with increasing exposure temperature and time could be attributed to the release of trapped moisture in the sample or by-products of additional cure reactions.

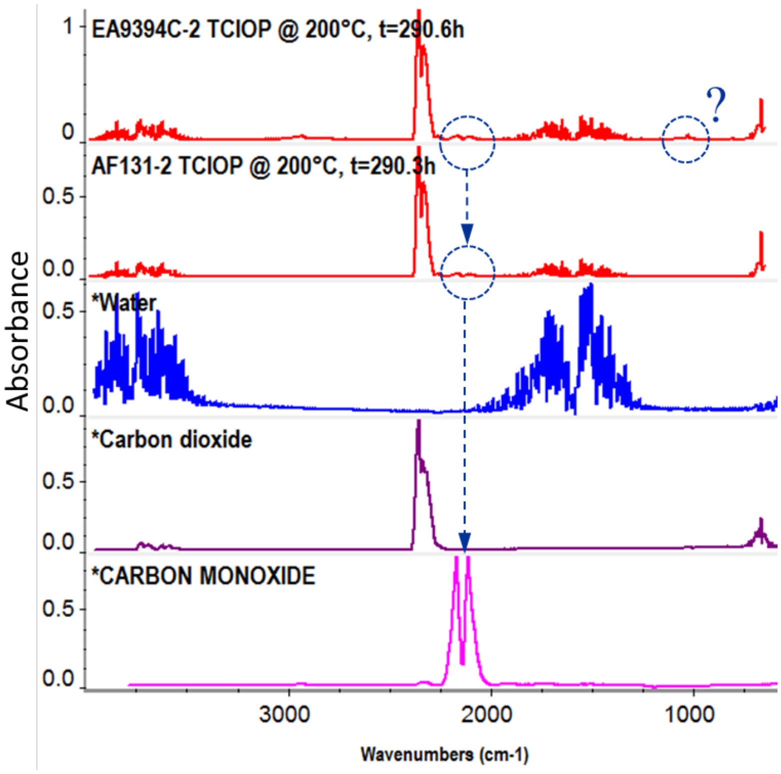

Figure 106.—Typical FT-IR spectra of outgas during TCIOP testing of adhesive candidates and peak identifications based on NIST database.

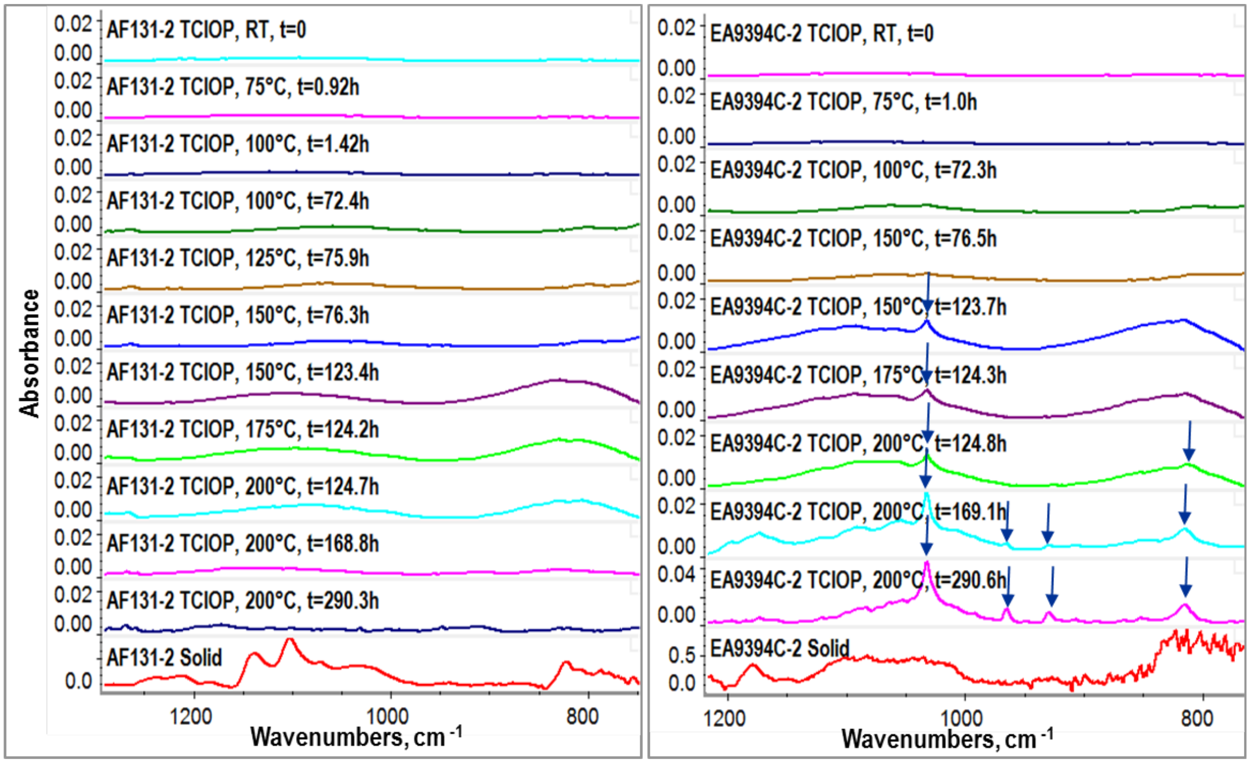

Figure 107.—Expanded section of FT-IR spectra for both adhesive candidates showing appearance of new peaks during TCIOP testing at exposure temperatures above 150 °C from EA9394C-2 system.

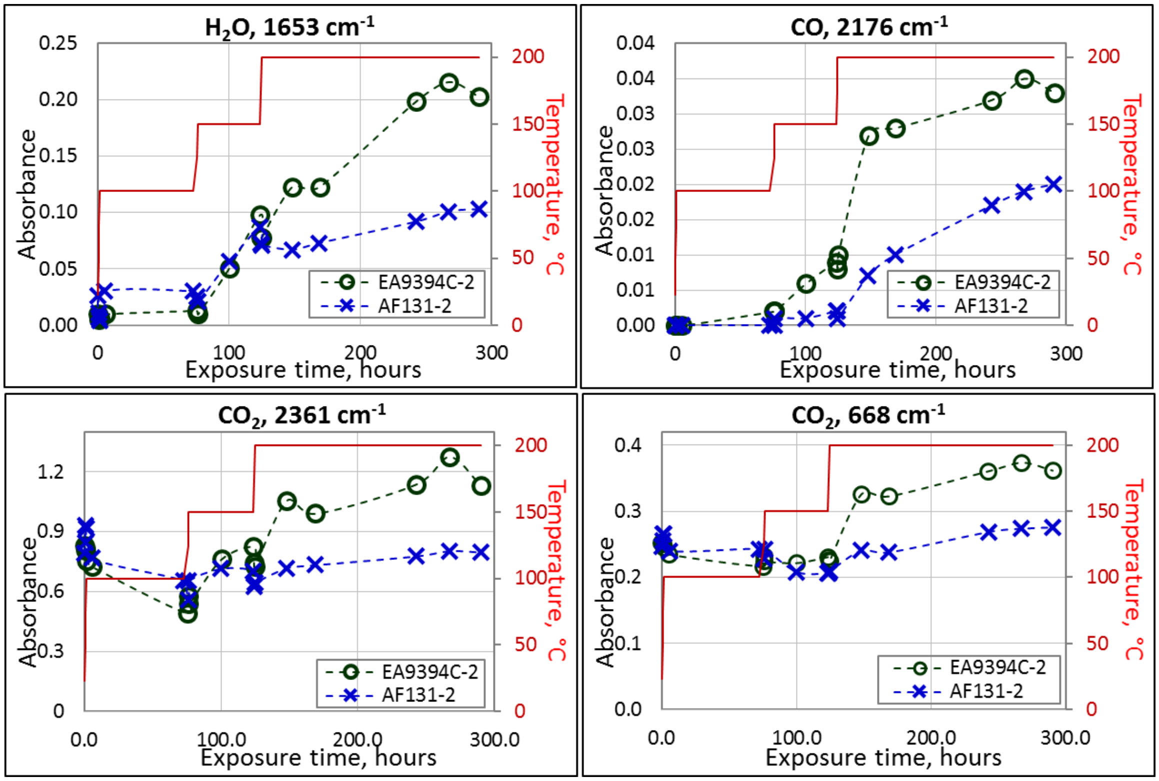

Figure 108.—Absorbance peak intensity or concentration changes of outgas species by FT-IR during TCIOP testing of adhesive candidates.

4.2.3.1.2 Residual Property Characterizations

Since the same thick sheet samples fabricated for the 6-month accelerated aging tests were used for this TCIOP tests, most residual property changes after the TCIOP test were directly compared with those from the 6-month aging test or so-called inert gas thermal aging exposure, at the same aging temperature of 200 °C, thus to determine the effects of the Stirling convertor gas environment on material properties more effectively and subsequently to assess the material compatibility. As shown in Figure 109, the weight loss of the EA9394C-2 epoxy after TCIOP was slightly higher than that observed under the inert gas thermal aging test while the AF131-2 showed slightly lower weight loss. Even though the differences were less significant in comparison with the overall weight loss trends as functions of aging temperature and time, the EA9394C-2 epoxy seemed to be adversely affected by the premix gas on weight loss. It can be speculated that certain chemical interactions between the outgases and EA9394C-2 could drive more outgassing.

The residual bonding integrity of both adhesive candidates after TCIOP testing was also compared to the results of the 6-month accelerated inert gas thermal aging tests, Figure 110. The sub-scale lap shear properties of the TCIOP tested EA9394C-2 were slightly lower than those of the inert gas thermal aged samples, while the AF131-2 showed comparable properties regardless of the exposure conditions. The additional bonding property degradation in the EA9394C-2 was consistent with its weight loss behavior. Overall, the EA9394C-2 epoxy was more susceptible to the outgas environment than the AF131-2, especially when exposed to 200 °C. However, the differences were rather small, and further analyses with more focused evaluations may be needed.

The impact of the gas environment on various thermal properties is shown in Figure 111 as comparing to those from the 6-month accelerated thermal aging experiment. In both epoxies, the T_g, % cure, and G' ratio or rigidity at 200 °C of the TCIOP-exposed samples were consistently higher than those of the inert gas thermal aging tested samples at the comparable exposure condition. This might suggest that the gas environment accelerated cure advancement of the epoxies, resulting in additional cross-linking reaction and/or possible oxidation. The T_d of the TCIOP-exposed samples were slightly lower for the AF131-2, but slightly higher for the EA9394C-2 than that of the inert gas thermally aged samples, Figure 112. Weight loss between 100 to 200 °C was higher, especially for the AF131-2 epoxy, with TCIOP exposure, that is, possibly more outgassing from TCIOP than the inert gas thermal aging. But, no significant changes in the total weight losses at 700 °C were observed from either epoxy candidate.

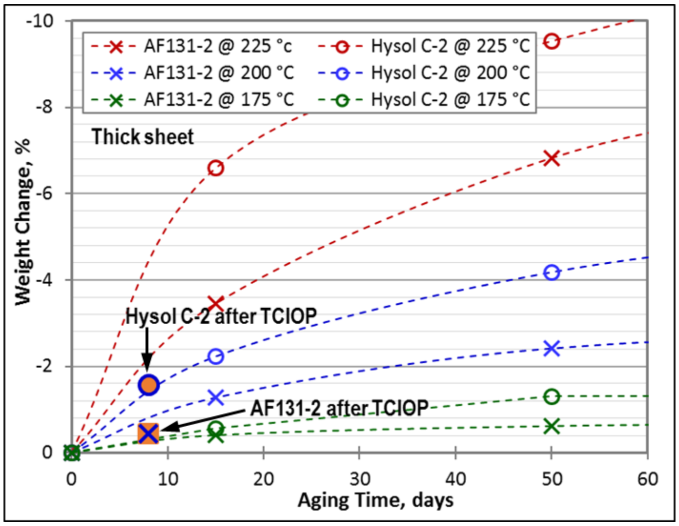

Figure 109.—Post TCIOP Weight losses of adhesive candidates compared to those after the inert gas thermal aging exposures.

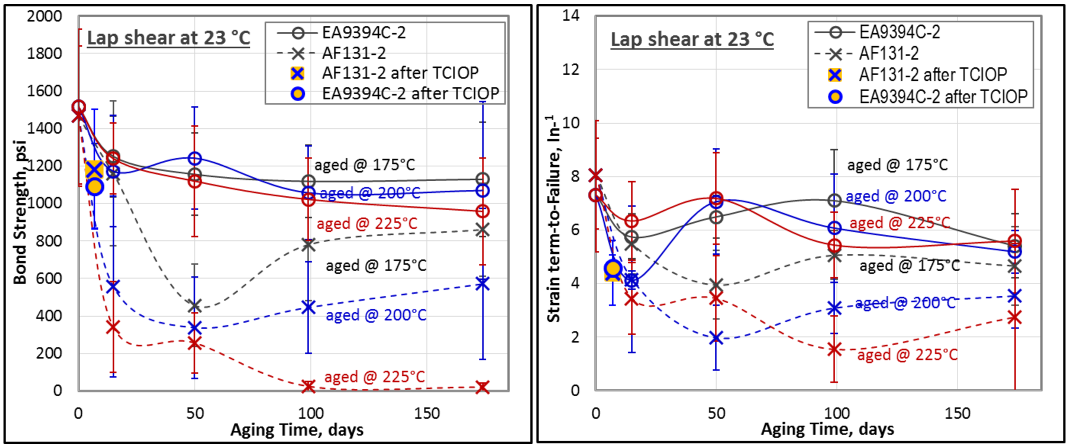

Figure 110.—Post TCIOP lap shear bonding properties of adhesive candidates compared to those after the inert gas thermal aging exposures.

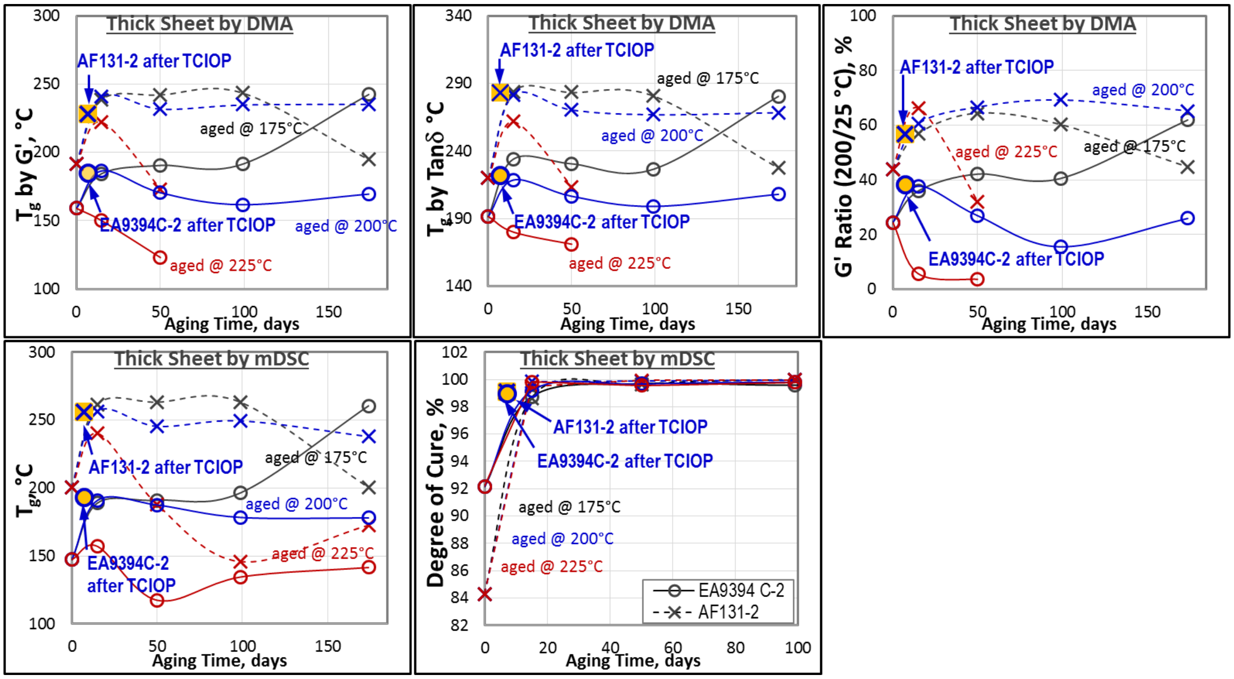

Figure 111.—Post TCIOP DMA and mDSC thermal properties of adhesive candidates compared to those after the inert gas thermal aging exposures.

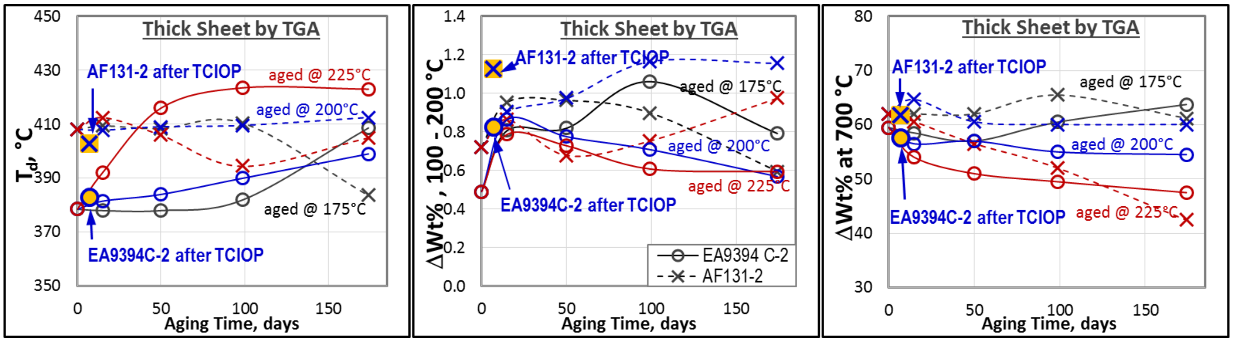

Figure 112.—Post TCIOP TGA thermal properties of adhesive candidates compared to those after the inert gas thermal aging exposures.

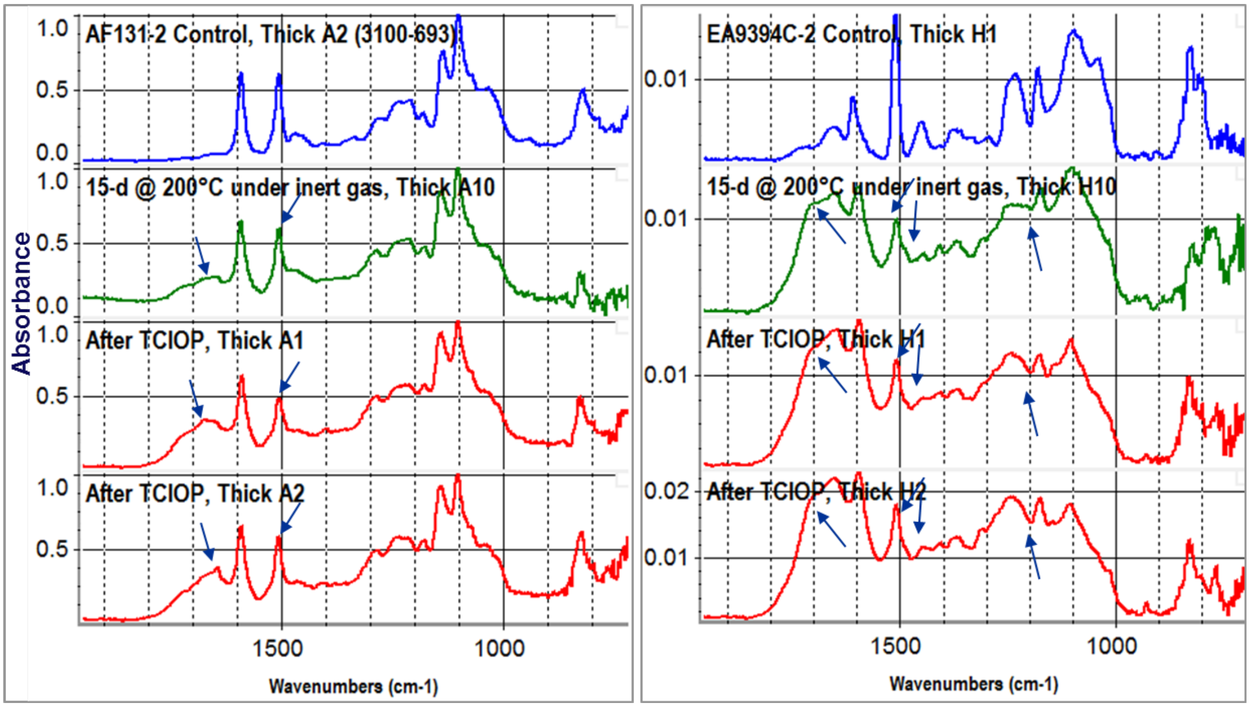

Figure 113.—FT-IR spectra of adhesive candidates after TCIOP testing compared to those after the inert gas thermal aging tests.

Figure 113 compares IR spectra of various sample conditions including the unaged control, the 6-month accelerated thermal aged as the thermally aged under inert gas, and TCIOP exposed samples, to determine the effects of the gas environment on molecular chemical structure. In both candidates, the most noticeable changes in FT-IR spectra were the appearance of a shoulder at ~1650 cm^{-1} and a peak that decreased at ~1510 cm^{-1} with thermal exposures, regardless of gas environment. The changes probably resulted from additional cross-linking, but note that the changes were more prominent with TCIOP exposure than the inert gas thermal aging which was consistent with other residual property data, especially thermal properties. EA9394C-2 showed additional changes, such as disappearance or decrease in peaks at ~1450, 1234, or 1180 cm^{-1} but no significant differences were observed between the inert gas thermal aging and the TCIOP exposure.

In summary,

- Both adhesive candidates showed similar outgas compositions during the TCIOP exposure which consisted of the premixed convertor gases (H_2, O_2, N_2, CO_2, He), and residual air contaminants (CH_4, H_2O, Ar, CO, Ne).
- Concentrations in most gas species were comparable between the two candidates, but the EA9394C-2 increased concentrations of CH_4, H_2O, CO, and CO_2 with increasing exposure temperature and time while the AF131-2 caused no significant changes. Most increases occurred at the 200 °C exposure and were accompanied by decreases in H_2 and O_2, which were possibly linked to its cure advancement.
- Based on FT-IR gas analysis, EA9394C-2 also produced additional outgases at temperatures above 150 °C, possibly from the fillers or unsaturated alcohols.

- Based on the systematic residual property characterizations of the TCIOP tested samples, the EA9394C-2 epoxy was more affected by the Stirling gas environment than the AF131-2 epoxy in terms of slightly higher weight loss, lower bonding properties, and more FT-IR molecular network structural changes.
- Most residual thermal properties indicated that the premix gas accelerated cure advancement of the epoxies through additional cross-linking reaction and/or possible oxidation in terms of considering the slightly higher T_g, % cure, and rigidity at 200 °C. However, T_d of the EA9394C-2 was not negatively affected by the TCIOP exposure.

4.2.3.2 Thread Locker Candidates

4.2.3.2.1 In-Situ Outgas Analyses

Typical RGA peaks, similar to Figure 102, showed that the outgases from the Loctite 294 samples were composed of the premixed gases (H_2, O_2, N_2, CO_2, He), possible residual air contamination (CH_4, H_2O, Ar, Ne), and some higher molecular weight species suspected of pump oil regardless of TCIOP temperature-time exposure conditions. Outgases from the Resbond 507 TS samples also showed similar RGA peaks and outgas compositions regardless of the exposure conditions. Figure 114 shows changes in concentration of various gas species as a function of TCIOP exposure conditions for both candidates. Note that outgassing behavior of the candidates was directly compared to that of the premix gas alone without involving any organic materials as a baseline control gas which confirmed no significant changes

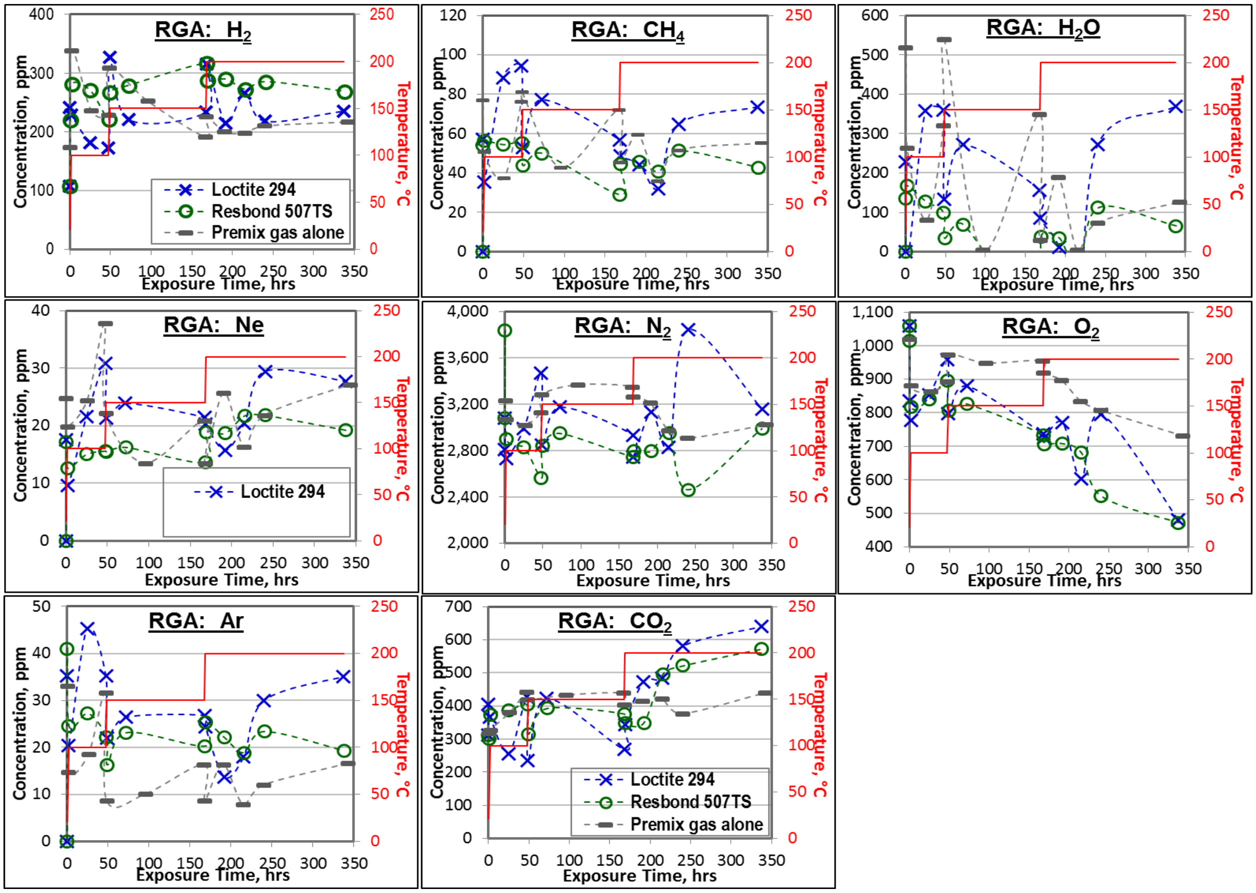

Figure 114.—Overall changes in concentrations of various outgas species by RGA during TCIOP testing of thread locker candidates directly compared to those from the convertor premix gas alone test.

in inter-gas interactions, regardless of the exposure conditions were observed. The most noticeable changes among the main gas species were gradual increases of CO_2 at the expense of O_2, mostly during 200 °C exposure for both candidates. The changes seemed to suggest that additional C was produced by the TL materials. Increase in H_2O was also observed at the 200 °C exposure, especially for Loctite 294. Changes in other species were mostly negligible or inconsistent. As shown in Figure 115, GC/TCD results were in good agreement with RGA data with greater consistency. A gradual increase of CO_2 with decreasing O_2 was observed in addition to an increase of H_2O, mostly during 200 °C exposure in both candidates.

Figure 116 shows typical FT-IR spectra of outgases from the TL candidates in the Stirling premix gas at the end of TCIOP experiment with all registered peaks clearly identified. As described earlier, those peaks were then qualitatively analyzed in terms of peak intensity as concentration at various exposure conditions, Figure 117. The results of FT-IR analysis agreed well with those of RGA and GC/TCD analyses for the increase of CO_2 and H_2O concentrations, especially at the 200 °C exposure in both candidates. It was apparent that the increases resulted from additional outgassing from the TL materials, but it was unclear whether the outgassing was due to thermal degradation or degassing of volatiles or by-products of additional cure.

FT-IR analysis uniquely showed new formation of CO and $-CH_3/-CH_2-$ compounds at 200 °C exposure and increase in concentration with increasing exposure time in both candidates. However, their formation seemed to be transitional due to their high reactivity, especially since they were not registered by RGA or GC/TCD.

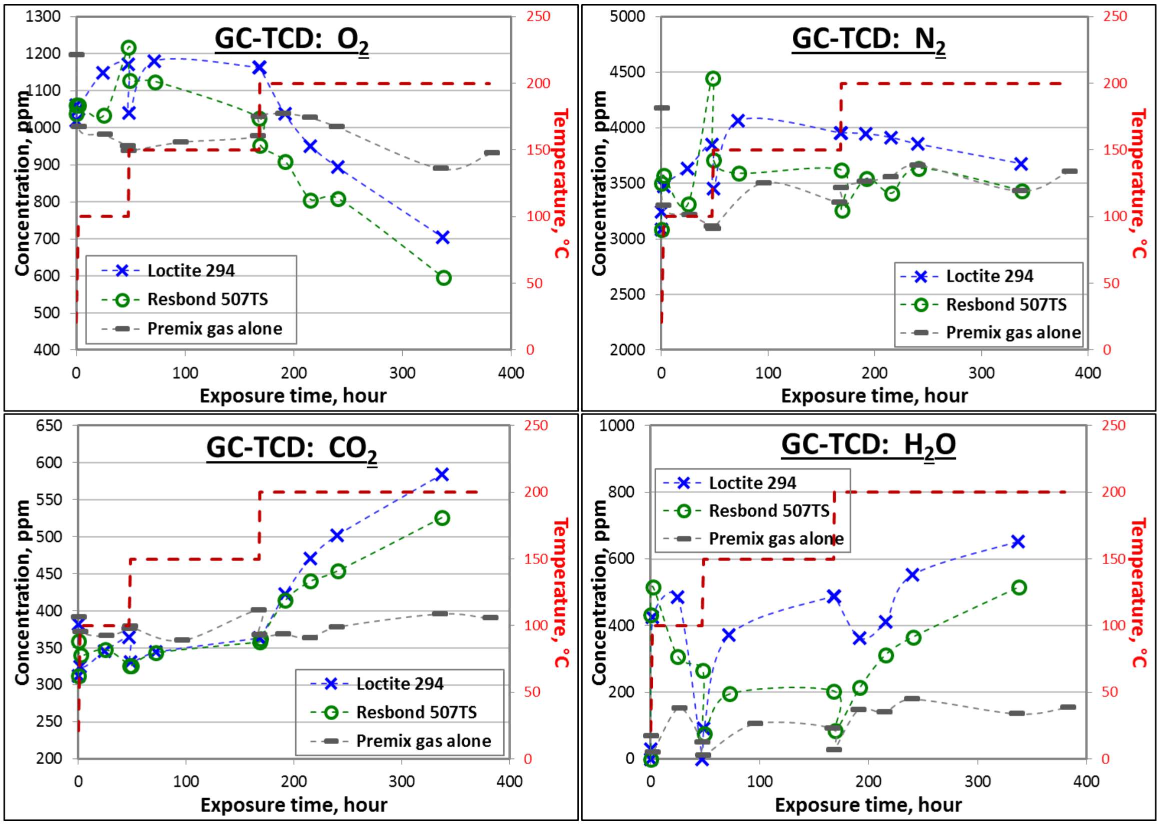

Figure 115.—Overall changes in concentrations of various outgas species by GC/TCD during TCIOP testing of thread locker candidates.

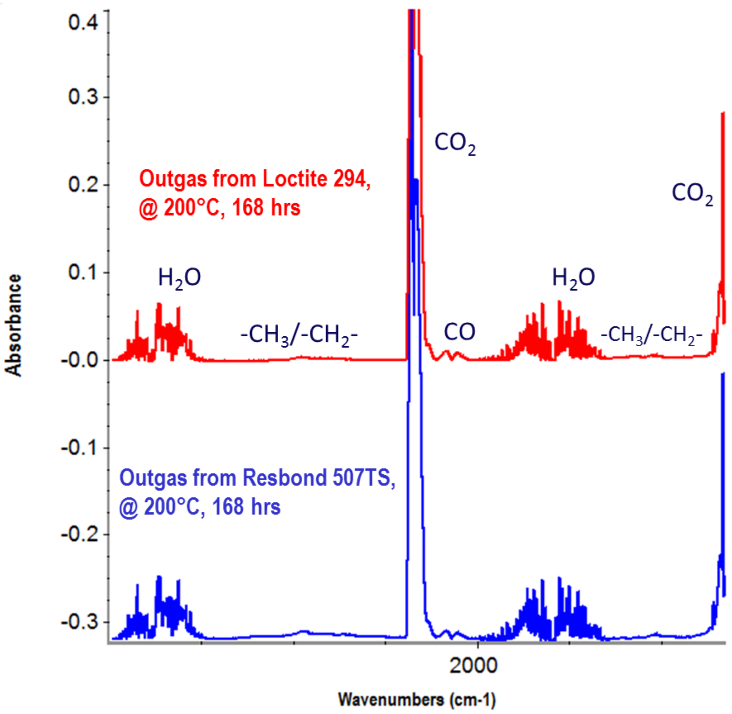

Figure 116.—Typical FT-IR spectra of outgas during TCIOP testing of thread locker candidates and peak identifications based on NIST database.

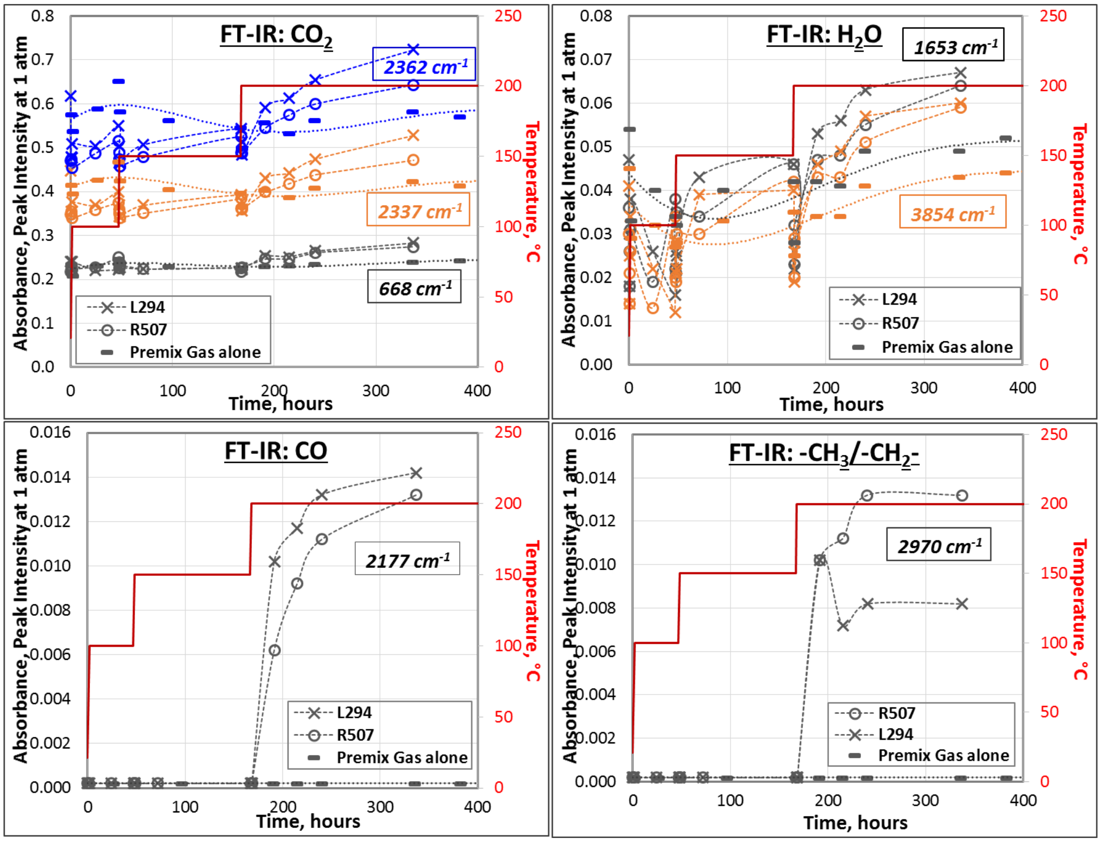

Figure 117.—Absorbance peak intensity or concentration changes of outgas species by FT-IR during TCIOP testing of thread locker candidates.

4.2.3.2.2 Residual Property Characterizations

In order to assess the effects of the outgas environment on the thermal aging behavior of TL candidates, changes in weight and torque strengths after the TCIOP tests were directly compared with those after the inert gas thermal aging exposure, more specifically: (i) 15-day thermal aging at 200 °C even though the total exposure time during TCIOP test was only 7 days or (ii) 15 days at 190 and 220 °C from the 6-month accelerated thermal aging tests. As plotted in Figure 118, weight losses of both candidates in the joint #2 blind-hole configuration after TCIOP exposures were in good agreement with those after the inert gas thermal exposure. There was no additional outgas-induced weight losses in both candidates in joint #2. This was somewhat expected since TL material was less exposed to atmosphere in such a blind-hole configuration, thereby, having less interactions with the gases. In the case of joint #8, a through-hole configuration not involving a washer, weight losses of both candidates after TCIOP exposures were slightly higher than the trends of samples after the inert gas thermal exposures, especially since duration of TCIOP exposure at 200 °C was only 7 days while all the inert gas thermal aging exposure was for 15 days. It may be speculated that TL materials were more susceptible to thermochemical degradation under exposure to the premix gas. For both cases; however, the differences were rather small to draw any meaningful conclusion.

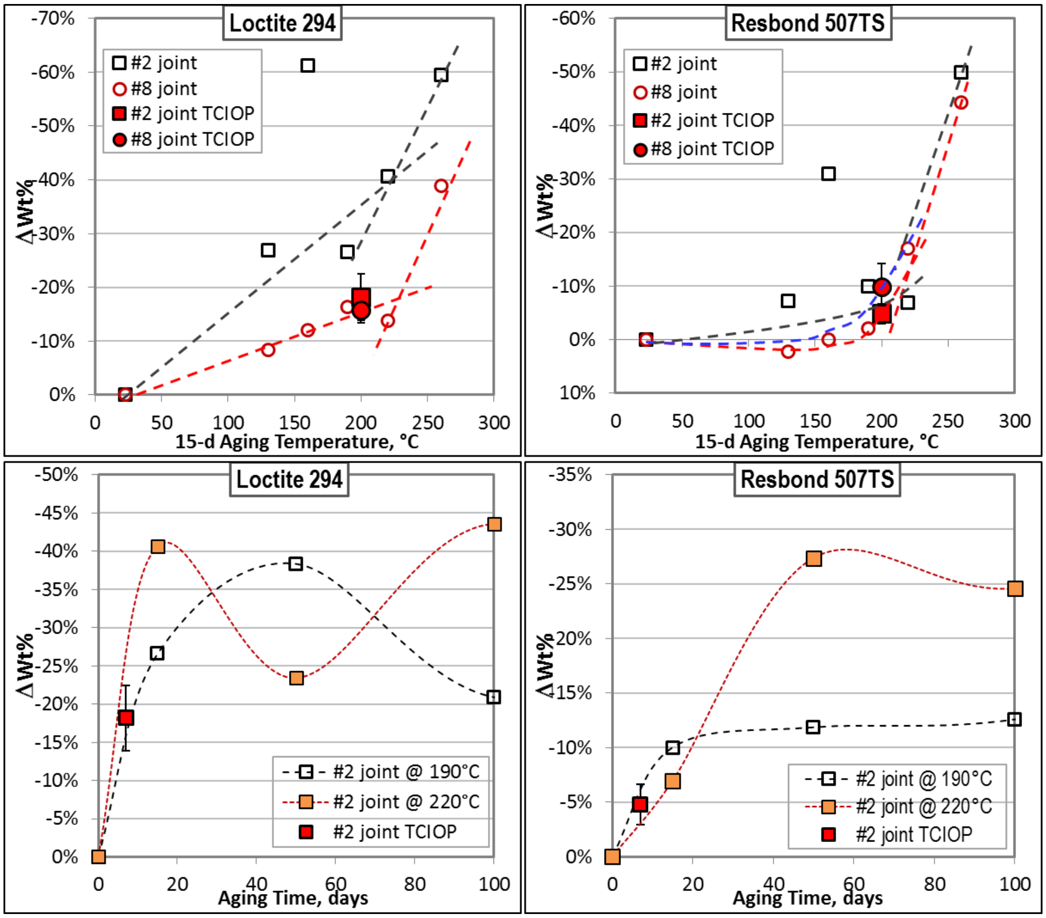

Figure 118.—Overall weight losses of thread locker candidates after TCIOP testing compared to those after inert gas aging tests, either the 15-day aging at various temperatures or the 6-month accelerated aging.

Figure 119 and Figure 120 summarize the effects of the outgas environment on torque strengths of thread locker candidates in joint type #2 and #8, respectively. Torque testing of the TCIOP exposed Loctite 294 assemblies was only conducted at 100 °C by error while Resbond 507TS assemblies were tested at both 100 °C and 200 °C. For both candidates, failure mode of the TCIOP exposed assemblies was consistent with those of the inert gas thermal aged assemblies for all joint types in that the mode was more dependent on joint type than candidate material type. Both candidates failed mostly by the mixed mode in #2 joint but by the cohesive mode in the #8 joint. In joint #2, both candidates gained mostly higher torque strengths after TCIOP exposures compared to those only exposed to the inert gas thermal aging at the same temperature. Note that torque strength was not significantly affected by aging time from the 6-month accelerated aging tests, thus it could be assumed that the difference in the exposure time between TCIOP (7 days) and the inert gas thermal aging (15 days) would not be a factor for this comparison. Torque strengths of the TCIOP exposed candidates in joint #8 did not deteriorate either, so it can be concluded that there was no negative impact of the outgas environment on TL performance.

FT-IR spectra of the TCIOP exposed Loctite 294 and Resbond 507TS in either joint #2 or #8 assemblies were compared to those of the unaged control samples and the inert gas thermal aged samples at either 190 or 220 °C for 15 days, Figure 121. Even though the resolution of IR microscopy was poor, it was evident enough that there were no major or consistent changes in IR spectra among different exposure conditions in both candidates. This suggested that whether the joint was blind-hole or through-hole configuration, exposure to the outgas environment during TCIOP test did not cause any excessive degradation or chemical structural changes of the TL materials.

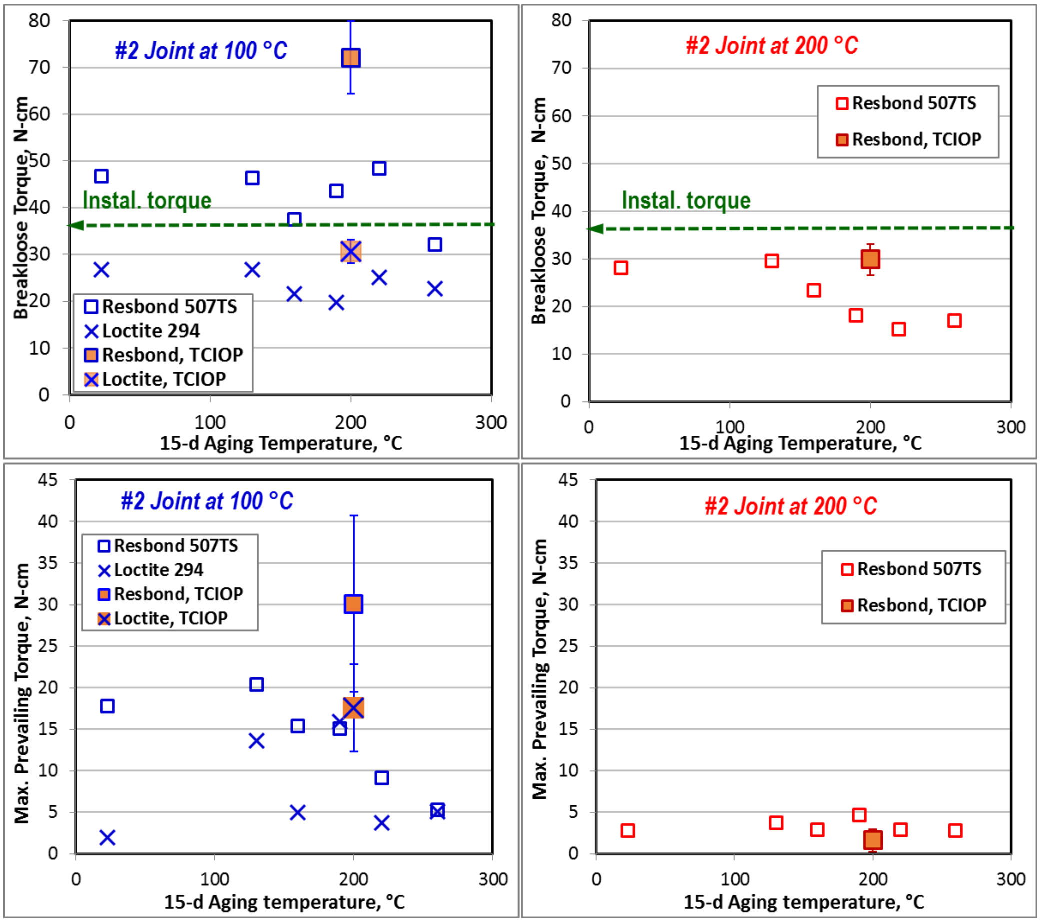

Figure 119.—Torque strengths of thread locker candidates in #2 joint after TCIOP testing compared to those after inert gas aging tests.

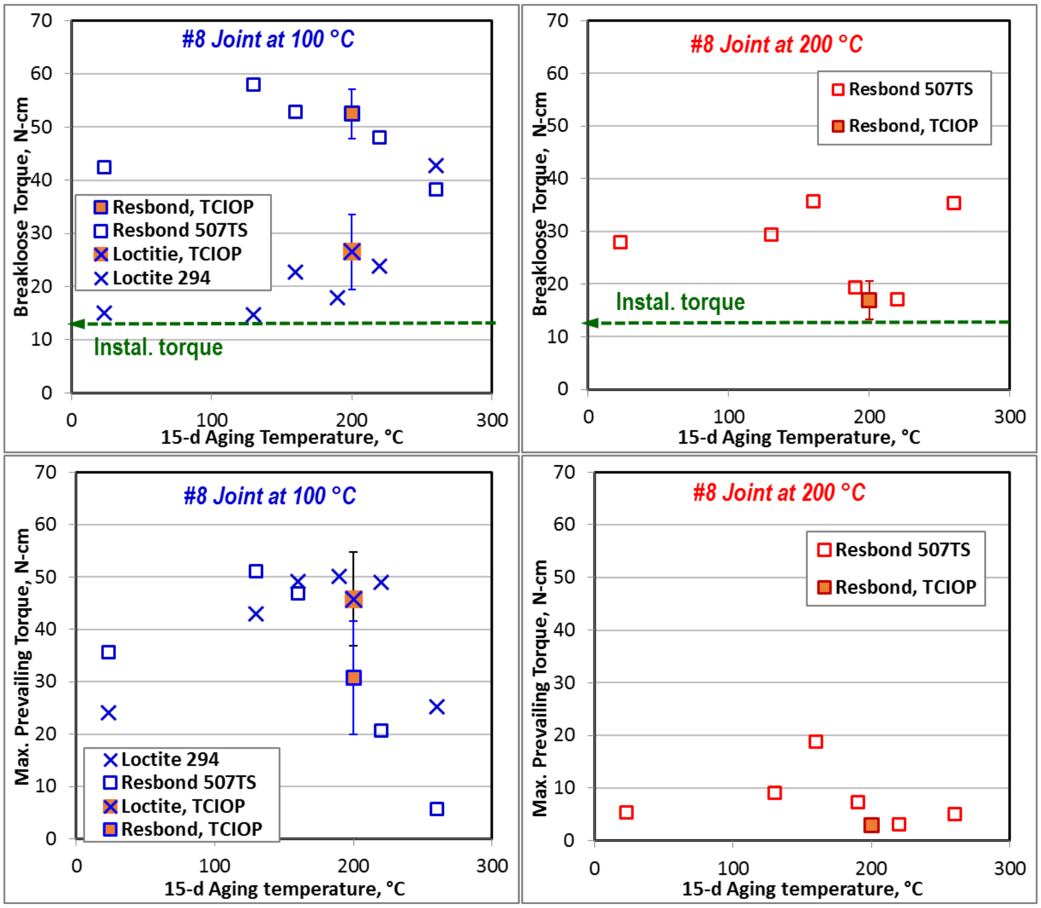

Figure 120.—Torque strengths of thread locker candidates in #8 joint after TCIOP testing compared to those after inert gas aging tests.

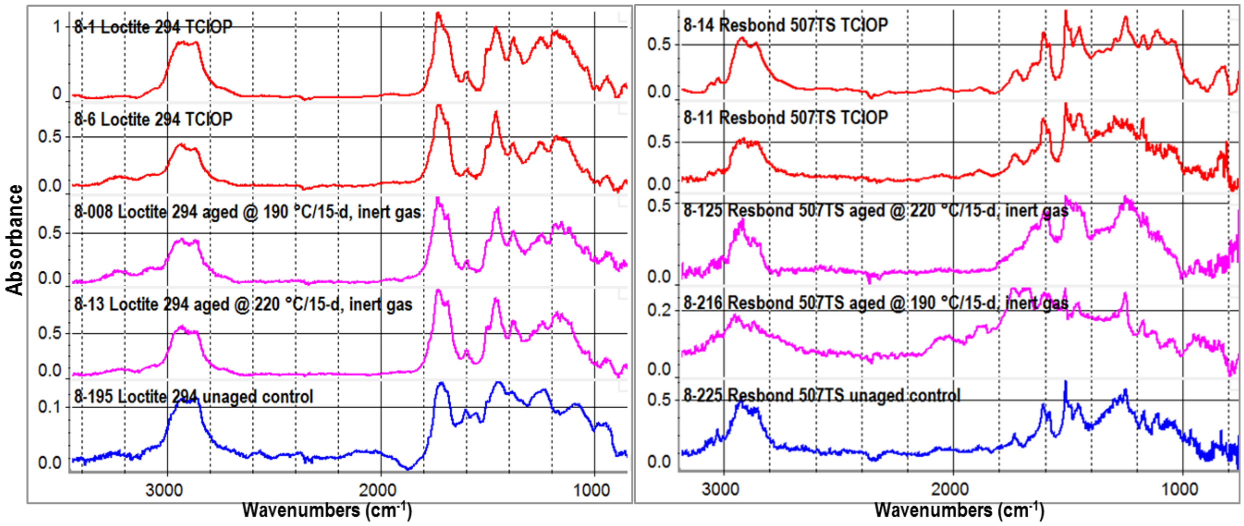

Figure 121.—Typical IR spectra of TCIOP tested samples of thread locker candidates compared to those after inert gas thermal aging tests and unaged controls.

In summary,

- Typical outgas compositions in both Loctite 294 and Resbond 507TS consisted of the premixed gases (H_2, O_2, N_2, CO_2, He) and possible residual air contaminants (CH_4, H_2O, Ar, Ne) regardless of TCIOP exposure conditions.
- Based on consistent results of RGA, GC/TCD, and FT-IR analyses, both candidates increased CO_2 concentration gradually at the expense of O_2, mostly during 200 °C exposure. Increase in H_2O was also observed at the 200 °C exposure in both candidates, especially for Loctite 294.
- FT-IR analysis uniquely showed new formation of CO and -CH_3/-CH_2- compounds at 200 °C exposure and increases in their concentrations with increasing exposure time in both candidates.
- There were no additional outgas-induced weight losses in both candidates in joint #2 with the blind-hole configuration, but slightly higher weight losses of Resbond 507TS after TCIOP exposures in joint #8 with through-hole configuration, suggested possible thermochemical degradation.
- Torque strengths, failure mode, and FT-IR molecular network structure were not negatively affected by TCIOP exposure in both candidates. This suggested that whether the joint was blind-hole or through-hole configuration, exposure to the outgas environment during TCIOP test did not cause any excess degradation or chemical structural changes of the TL materials.

4.2.3.3 Shrink Tubing Candidates

4.2.3.3.1 In-Situ Outgas Analyses

Typical composition of outgases from the shrink tubing materials at various TCIOP exposure conditions by RGA was similar to those of the adhesive or TL materials. Following the same quantitative analysis used previously, concentrations of each gas species are plotted for various temperature and time exposure conditions in Figure 122 for both candidates and the baseline control gas. ETFE showed no significant changes in most outgas species during the entire TCIOP exposure up to 200 °C. On the other hand, SRFR caused an increase of CO_2 at the loss of O_2 from the major gas species, and also increases in CH_4 and H_2O. Most changes occurred at 200 °C exposure, and seemed to suggest outgassing of C and H_2 from the silicone material.

Similarly, typical GC/TCD analysis of outgases from the shrink tubing candidates identified those key gas species including He, O_2, N_2, CH_4, H_2O, and CO_2. Their concentrations were calculated for various TCIOP exposure conditions including those of the baseline control gas, Figure 123. The results were in good agreement with those of RGA for both candidates in that ETFE caused no changes in outgas concentrations, while SRFR increased CO_2 and CH_4 concentrations, but decreased O_2 concentration.

Typical FT-IR spectra of outgas samples from the shrink tubing candidates in the premix gas at the end of the TCIOP experiment are shown in Figure 124, including peak identifications of key gas species, such as H_2O, CO_2, CH_4, and strong silicone vapor from SRFR or H_2O, CO_2, –CH_2-, CO, and weak C-F from ETFE.

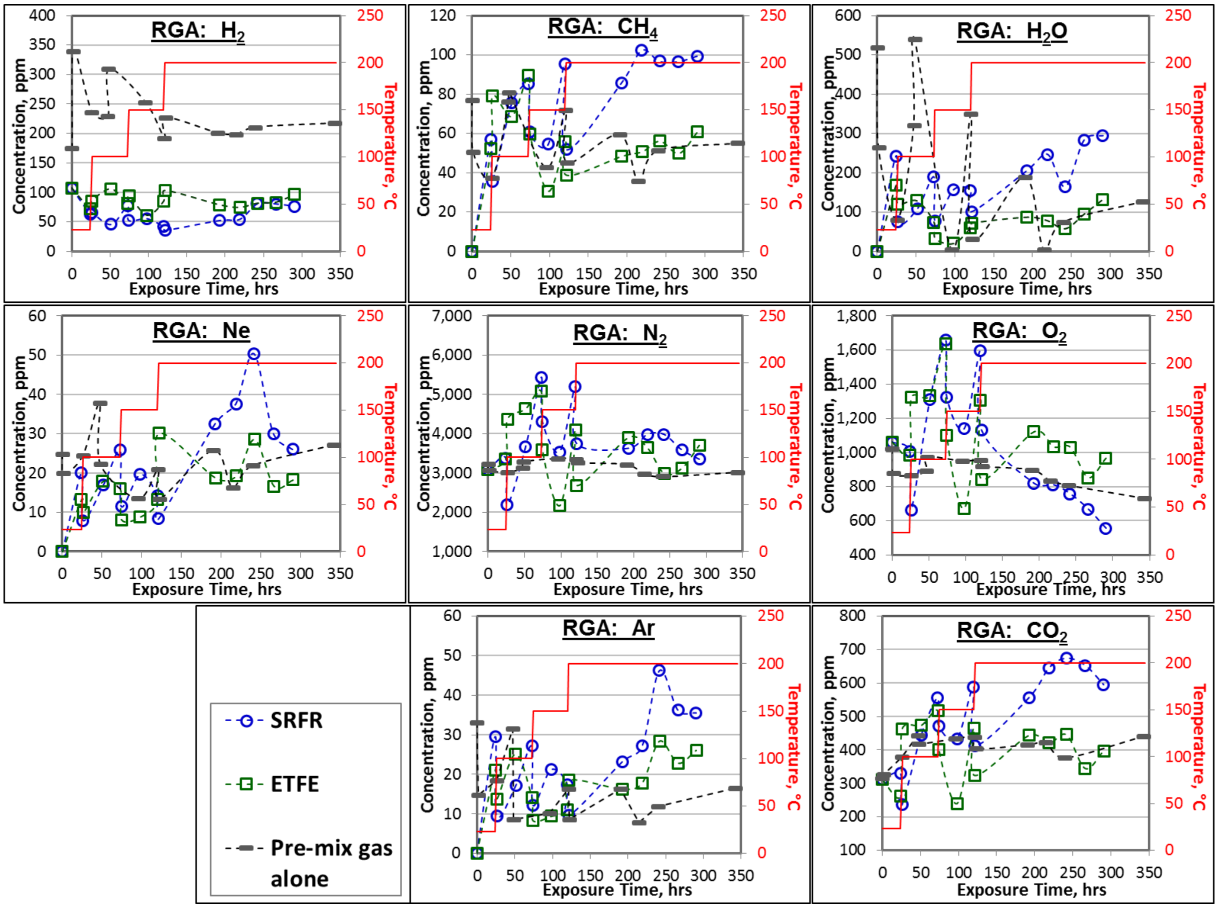

Figure 122.—Overall changes in concentrations of various outgas species by RGA during TCIOP exposures of shrink tubing candidates compared to those from the premix gas alone.

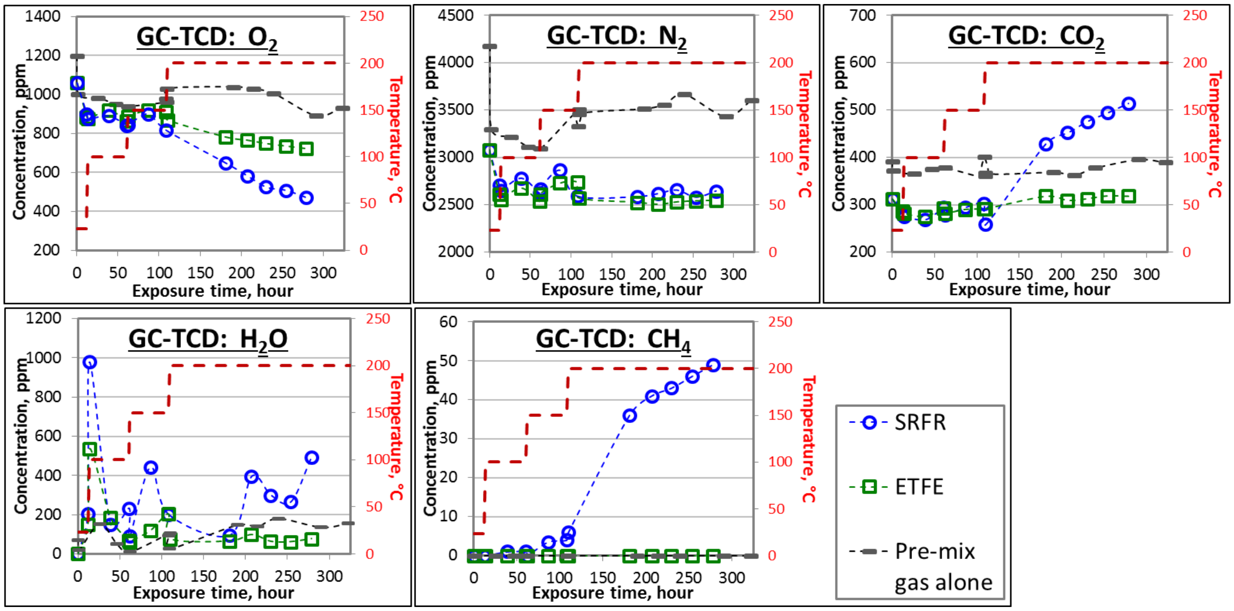

Figure 123.—Overall changes in concentrations of various outgas species by GC/TCD during TCIOP testing of shrink tubing candidates.

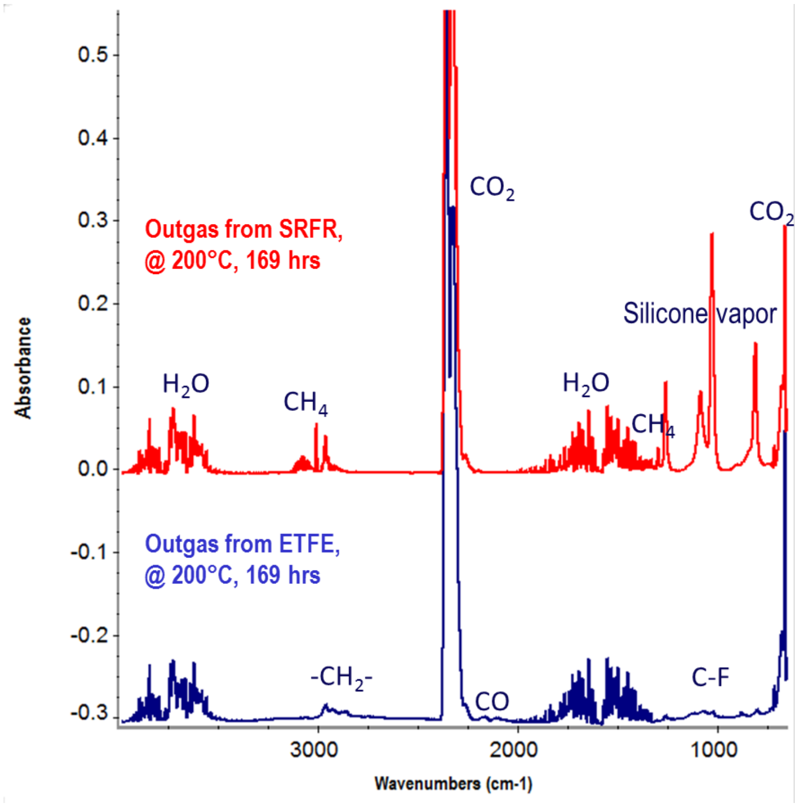

Figure 124.—Typical FT-IR spectra of outgas during TCIOP testing of shrink tubing candidates and peak identifications based on NIST database.

Figure 125 summarizes the overall changes in concentrations of various gas species as a function of TCIOP exposure conditions for both candidates and the baseline control gas. In the outgases from SRFR samples, concentrations of CO_2, H_2O, and CH_4, increased with time, especially at 200 °C, but more interestingly a couple of new gas species, such as $-CH_3/-CH_2-$ and silicone vapor, started to appear at 200 °C exposure and continued to increase significantly with increasing exposure time. These were consistent with RGA and GC/TCD results, and in combination with the silicon vapor appearance, it can be concluded that SRFR suffered thermal degradation and material incompatibility when exposed at 200 °C. In the case of ETFE, no significant changes in concentration of major gas species occurred during the entire TCIOP testing. However, even though it showed better thermal stability and material compatibility, there were signs of possible thermal degradation. A few new gas species, such as CO, $-CH_3/-CH_2-$, and C-F appeared at 200 °C exposure and their concentrations increased with increasing exposure time. But note that their peak intensities were rather small compared to other peaks.

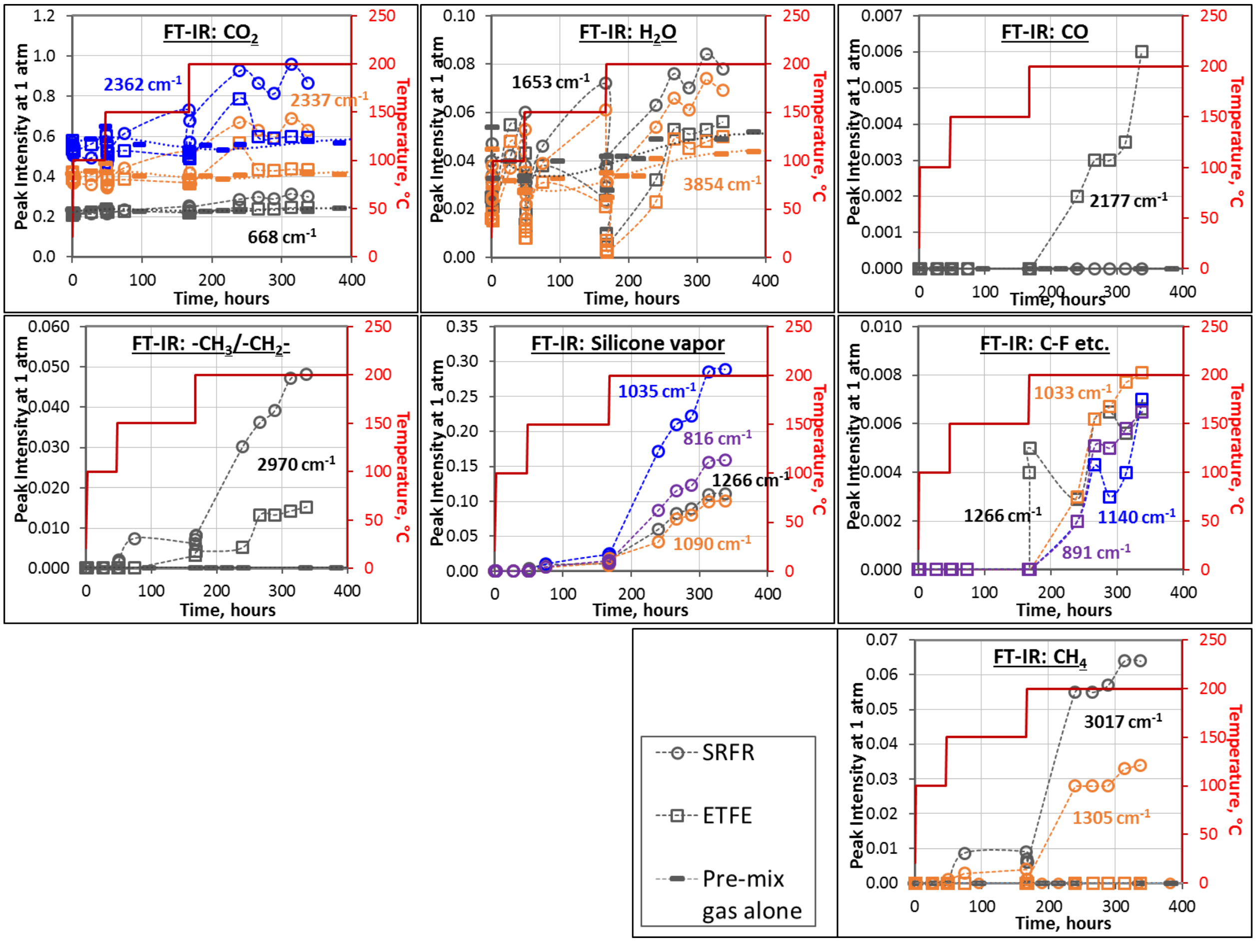

Figure 125.—Overall changes in absorbance peak intensity or concentration of outgas species by FT-IR during TCIOP testing of shrink tubing candidates.

4.2.3.3.2 Residual Property Characterizations

Residual thermal properties and outgassing characteristics of the TCIOP exposed samples were directly compared with those of the unaged control samples in Table 16. Note that the control was unmodified sample in the as-expanded condition. In general, SRFR showed more changes in most thermal properties after the TCIOP exposures, especially decrease in T_d and ΔWt% at 700 °C, increase in T_{trans} while the changes from ETFE were often less or positive, thus it was confirmed that ETFE was more thermally stable and compatible than SRFR. Outgassing potentials by TGA and Iso-TGA were slightly but consistently reduced or insignificantly affected by the TCIOP exposures in both candidates. Overall, ETFE showed much lower potentials than SRFR in most characterization areas. Residual mechanical properties via the notched tensile test in both axial and radial direction of the TCIOP tested samples were compared to those of the control samples at various test temperatures, Figure 126. Note that the control properties used in the plot were from the pre-shrunk/recovered specimens for more valid comparison. In all cases, SRFR shrink tubing suffered significant deterioration of its notched tensile properties after the TCIOP exposures which was indicative of apparent material degradation due to both temperature and outgas exposures. In the case of ETFE, notched strengths were not negatively affected by the TCIOP exposure in both axial and radial direction, but the elongation at failure decreased considerably after the TCIOP exposure. Overall, ETFE performed better than SRFR, and was determined to be more compatible.

TABLE 16.—SUMMARY OF THERMAL PROPERTIES OF SHRINK TUBING CANDIDATES AFTER TCIOP EXPERIMENT COMPARED TO THOSE OF UNAGED CONTROL SAMPLES

Properties / Material			mDSC/DSC				TGA				ISO-TGA at 200 °C, 7 hr			DMA-Tension, Axial			DMA-Tension, Radial		
			T_g, °C	T_m, °C	ΔH_m, J/g	T_d, °C	T_d, °C	ΔWt%, RT-100 °C	ΔWt%, 100-200 °C	ΔWt%, at 700 °C	Initial wt loss, wt%	Dwell wt loss, wt%	Loss rate [(wt%/t) ×103]	T_{trans} tan δ, °C	*E* ', 150 °C	*E* ', 200 °C	T_{trans} tan δ, °C	*E* ', 150 °C	*E* ', 200 °C
															% of *E* ', RT			% of *E* ', RT	
SRFR	Virgin	Avg.	131	–45	9	409	422	0.291	0.512	18	0.817	3.028	2.286	142	19%	5%	149	56%	36%
		SD	24	2	2	4	5	0.159	0.101	1	0.090	0.912	0.947	4.9		5%	3.5		
	TCIOP tested	Avg.		–46	10.0		413	0.282	0.801	16	0.778	2.580	0.233	143	21%	14%	157	34%	20%
		SD		0.7	0.0		10.6	0.1	0.4	2.6	0.2	1.3	0.2	5.0					
		%Δ		–1.1	14		–2.2	–3.0	56	–11	–4.8	–15	–90	1.1	12	186	6	–40	–44
ETFE	Virgin	Avg.	–4	218	11.2		502	0.088	0.050	88	0.318	1.941	0.975	77	41%	30%	77	19%	8%
		SD	1											3.6			8.6		
	TCIOP tested	Avg.	–4	217	14.9	430	510	0.073	0.134	93	0.103	0.137	0.200	77	22%	12%	77	46%	55%
		SD	1	1	0.5	1	1	0.015	0.094	0				2.5					
		%Δ	0.0	–0.5	33		1.5	–17	169	5.7	–68	–93	–80	0.6	–47	–60	0.0	139	579

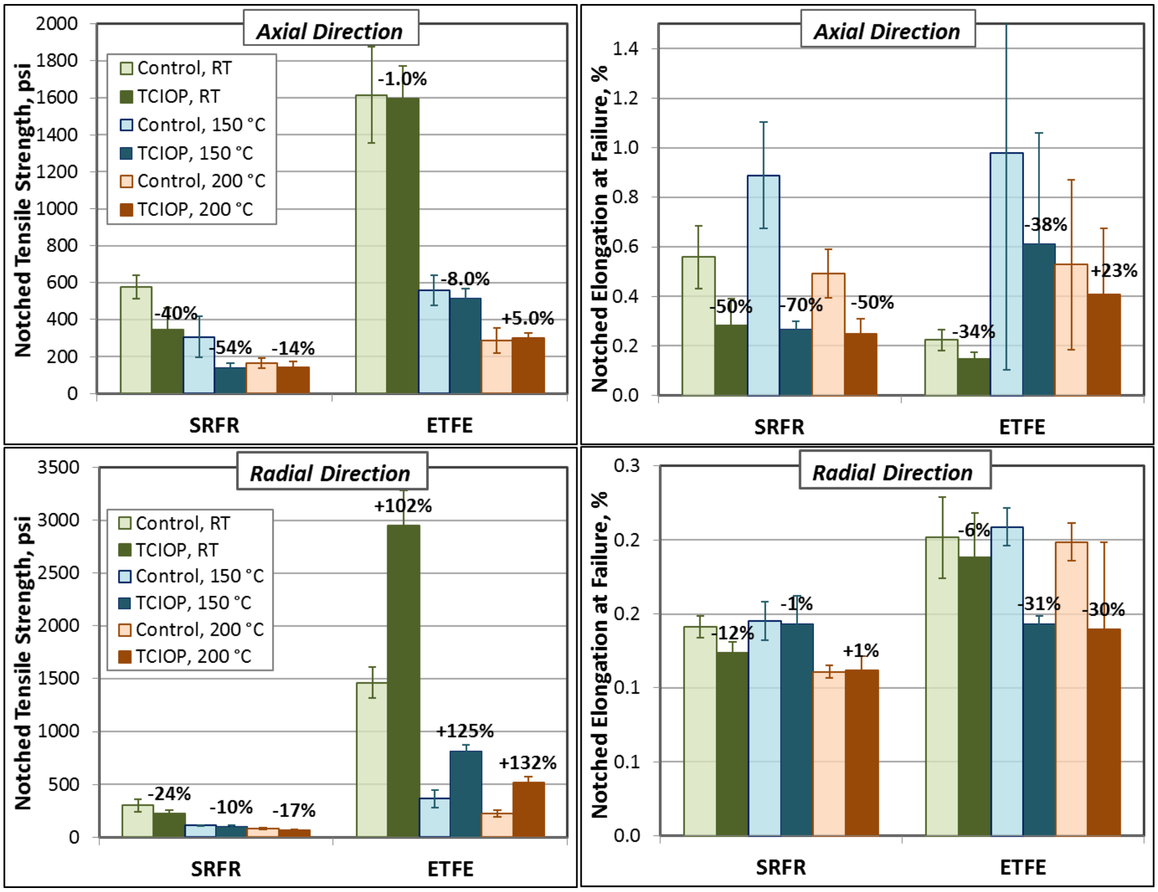

Figure 126.—Changes in notched tensile properties of shrink tubing candidates in both axial and radial directions at various temperatures after the TCIOP exposure.

In Figure 127, changes in FT-IR spectra of SRFR before and after TCIOP exposures are illustrated. It was evident that TCIOP exposure led to an increase in intensity of peaks at ~1080 cm^{-1} and ~795 cm^{-1}, which suggested oxidation and possible side-chain rearrangement, respectively. FT-IR spectra for the ETFE showed no significant changes in molecular structure following TCIOP exposure. This was consistent with other residual properties discussed earlier.

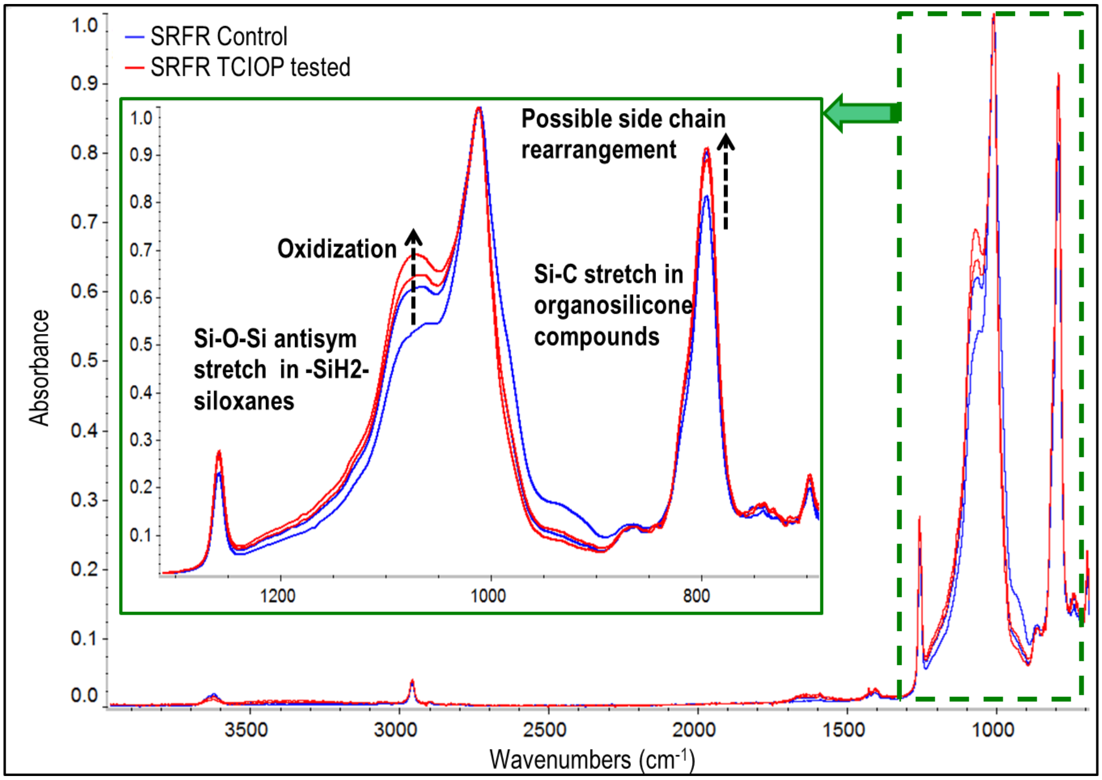

Figure 127.—Increases in certain peak intensities of SRFR shrink tubing after TCIOP exposures indicating possible changes in its molecular network structures.

In summary,

- Typical outgas compositions in both SRFR and ETFE consisted of the premixed gases and possible residual air contaminants.
- ETFE caused no significant changes in outgassing with the TCIOP exposures up to 200 °C while SRFR caused a steady increase of CO_2 at the loss of O_2, and also an increase in CH_4 and H_2O, mostly at the 200 °C exposure.
- From FT-IR analysis, SRFR formed new outgases such as -CH_3/-CH_2- and more prominently silicone vapor, especially at 200 °C, in which concentrations increased rapidly with increasing exposure time and served as a clear indication of thermal degradation. ETFE also caused formation of new outgas species, CO, -CH_3/-CH_2-, and C-F at 200 °C whose concentrations increased with exposure time, but their intensities were rather small.
- Changes in most thermal properties and outgassing potentials after the TCIOP exposures were rather insignificant in both candidates, but greater in SRFR.
- SRFR suffered significant deterioration of its notched tensile properties after the TCIOP exposures which was indicative of material degradation. Notched strengths of ETFE were not negatively affected by the TCIOP exposure, but the elongation at failure decreased considerably after the TCIOP exposures.
- FT-IR analyses of the molecular network structure of the TCIOP exposed SRFR indicated oxidation and possible side-chain rearrangement while ETFE remained relatively unchanged.

4.2.3.4 O-Ring Candidates

4.2.3.4.1 In-Situ Outgas Analyses

Typical composition of outgases from the o-ring materials at various TCIOP exposure conditions by RGA was similar to those of other organic materials listed earlier. Following the standardized analysis procedure, concentrations of each gas species were monitored as a function of TCIOP exposure conditions for both candidates and the premix gas alone baseline control, Figure 128. For both candidates, there were no significant or consistent changes in concentration of major gas species, such as CO_2 or O_2 during the entire TCIOP testing unlike shrink tubing candidates even though candidates of both material types were from the similar polymer families. In general, concentrations of some gas species by RGA fluctuated considerably, especially at 200 °C, thus, the changes were inconsistent.

Following the standardized GC/TCD analysis, changes in concentrations of a few key gas species were determined as a function of TCIOP exposure conditions for both candidates and the premix gas alone baseline control, Figure 129. The GC/TCD results were much more consistent and verified the results of RGA. For both candidates, concentrations of outgases were virtually unchanged with the TCIOP exposure conditions as those in the premix gas alone baseline control.

Similarly, Figure 130 show typical FT-IR spectra of outgases from the o-ring candidates in the premix gas during the TCIOP experiment. Note that spectra of silicon vapor was identical to that of the silicone o-ring. Changes in peak intensities or concentrations were calculated against the TCIOP exposure conditions, Figure 131. Similar to RGA and GC/TCD results, the concentration of CO_2 remained same regardless of exposure condition for both candidates, but concentration of H_2O increased slightly at

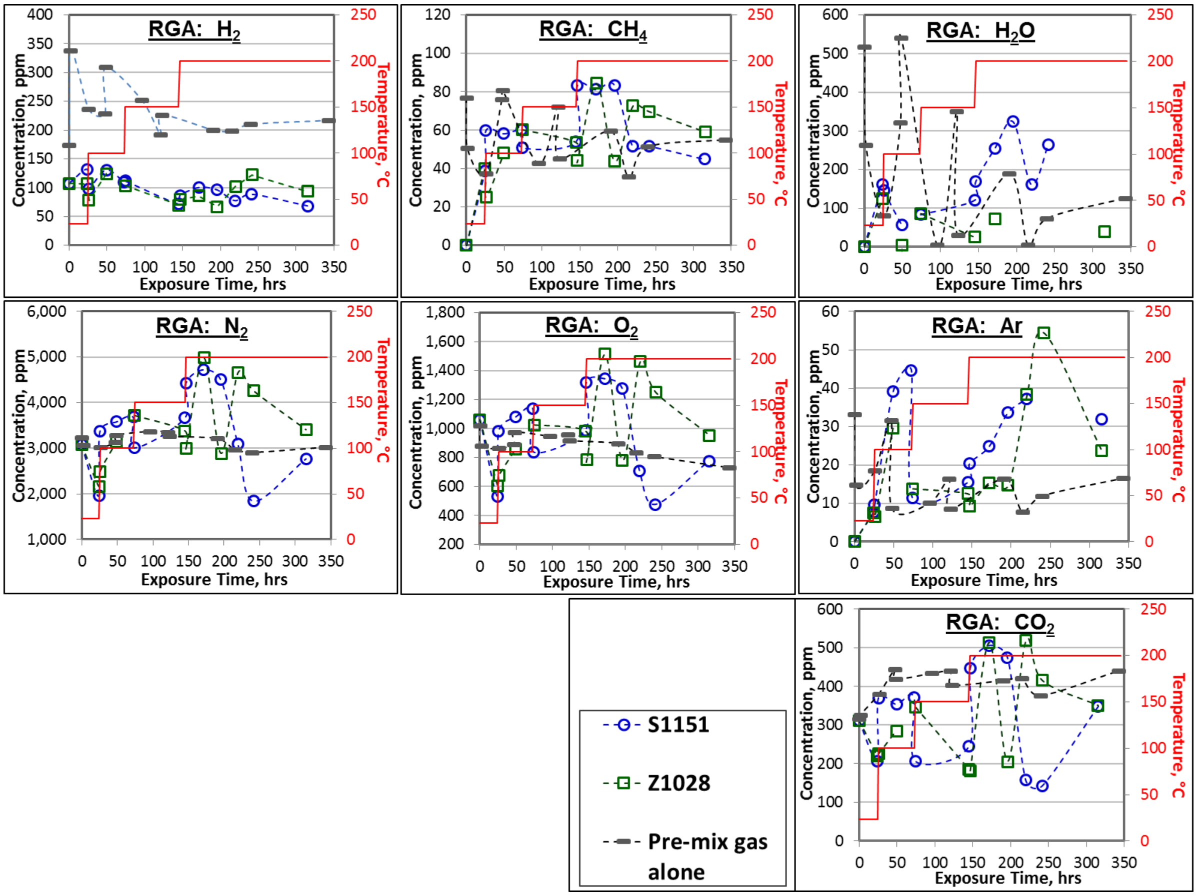

Figure 128.—Overall changes in concentrations of various outgas species by RGA during TCIOP exposures of o-ring candidates compared to those from the premix gas alone.

200 °C, especially for the S1151 o-ring, which may have been indicative of the release of trapped moisture in the sample. FT-IR analysis also indicated signs of thermal degradation of S1151 o-ring, especially at 200 °C exposure, such as formation and increases in concentrations of CO, -CH_3/-CH_2-, and more prominently silicone vapor.

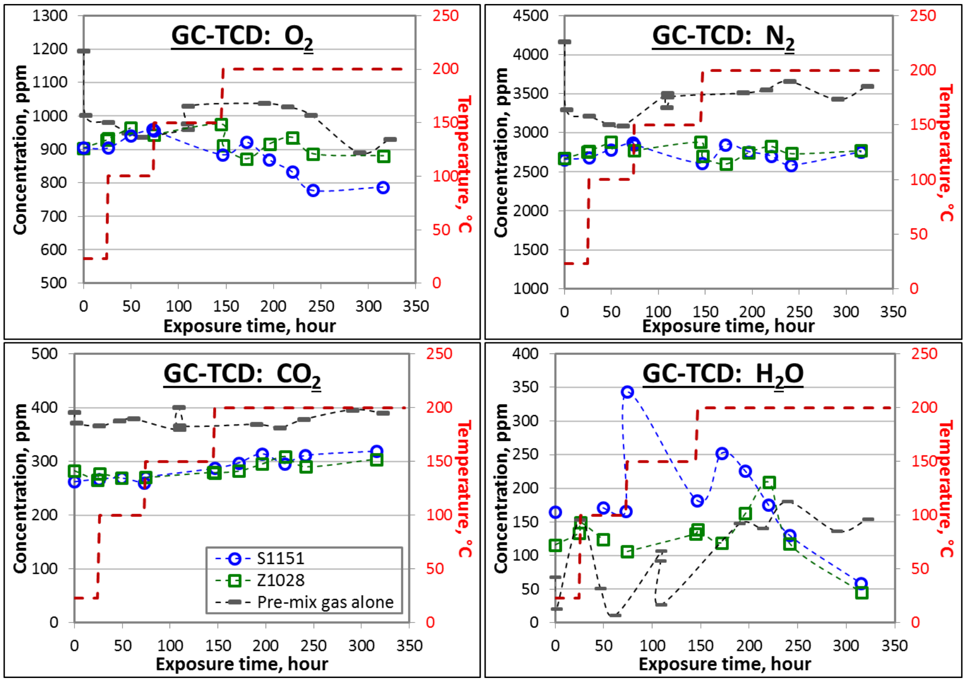

Figure 129.—Overall changes in concentrations of various outgas species by GC/TCD during TCIOP testing of o-ring candidates.

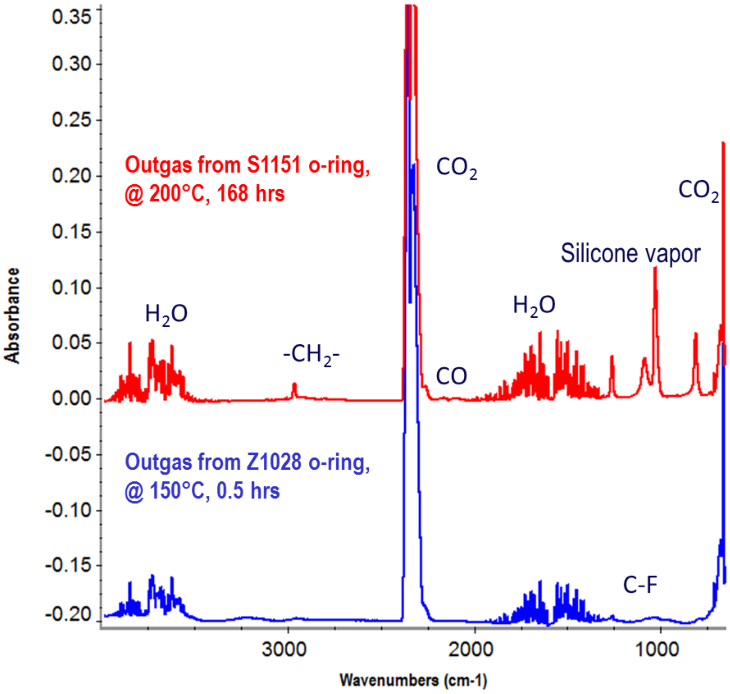

Figure 130.—Typical FT-IR spectra of outgas during TCIOP testing of o-ring candidates and peak identifications based on NIST database.

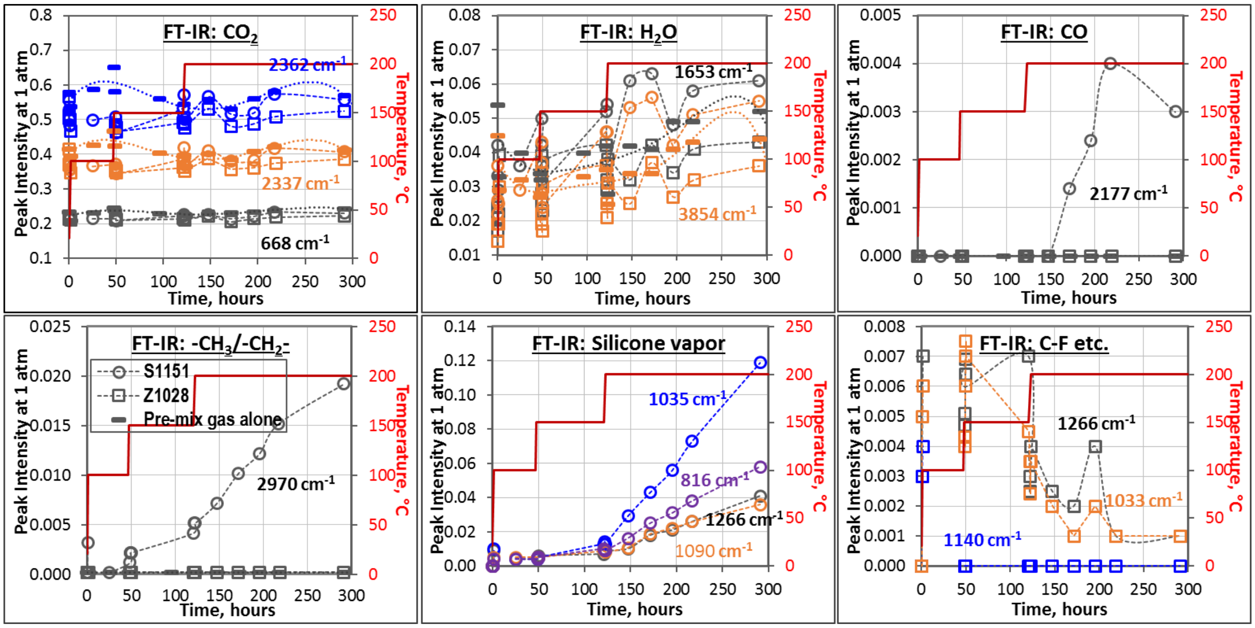

Figure 131.—Overall changes in absorbance peak intensity or concentration of outgas species by FT-IR during TCIOP testing of o-ring candidates.

TABLE 17.—SUMMARY OF THERMAL PROPERTIES OF O-RING CANDIDATES AFTER TCIOP EXPERIMENT COMPARED TO THOSE OF VIRGIN SAMPLES

Properties / O-ring material			DSC/mDSC							TGA				Iso-TGA at 200 °C, 7 hr		
			T_{g1}, °C	T_{g2}, °C	T_m, °C	ΔH_{mr}, J/g	T_{exo}, °C	Δh_{exo}, J/g	T_d, °C	T_d, °C	ΔWt% RT-100 °C	ΔWt% 100-200 °C	ΔWt% at 700 °C	Initial wt loss, wt%	Dwell Wt loss, wt%	Wt loss rate, [(wt%/t) ×1000]
S1151	Virgin	Avg.	–91		–43.7	7.3	369	91.2	449	501	0.466	1.298	55	2.093	1.053	0.301
		SD	2		0.4	1.5	2	34.4	1	1	0.021	0.106	0			
	TCIOP tested	Avg.	–87		–43.4	9.3	366	95.7	429	496	0.542	1.294	49	1.867	0.678	0.276
		SD	9.9		0.4	3.1	2	24.5	1	1	0.012	0.055	8			
		% Δ	4.4		0.7	27.2	–0.9	4.9	–4.5	–0.9	16.3	–0.3	–10.1	–10.8	–35.6	–8.3
Z1028	Virgin	Avg.	–85	–0.1			294	0.6	438	472	0.027	0.219	87	0.261	0.090	0.035
		SD		2.5			1	0.7	7	1	0.019	0.052	2			
	TCIOP tested	Avg.	–84	0.2			288	1.3	436	471	0.022	0.250	86	0.334	0.227	0.000
		SD	2	0.0			8	1.6	1	2	0.026	0.007	2			
		% Δ	1.8				–2.2	117	–0.4	–0.2	–16.7	14.0	–0.8	28.1	152.0	–100.0

4.2.3.4.2 Residual Property Characterizations

Table 17 summarizes various residual thermal properties and outgassing characteristics of the TCIOP exposed o-ring samples compared to those of the virgin samples. In general, changes in most thermal properties after the TCIOP exposures were rather insignificant in both candidates, but greater in S1151, especially for T_g, T_d, and ΔWt% at 700 °C. Outgassing potentials by TGA and Iso-TGA were slightly but consistently reduced or insignificantly affected by the TCIOP exposures in both candidates. Z1028 generally showed lower potentials than S1151.

As expected from the 6-month accelerated thermal aging experiment, TCIOP exposure lowered the compression-set of both o-ring candidates. Greater changes were observed in S1151 (–38%) than Z1028

(–9%) according to Figure 132. Note that the as-received control samples for the TCIOP experiment were not treated with any pre-conditioning processes while those tested for the 6-month thermal aging experiment had been dry-preconditioned at 80 °C for 24 hr. Overall, Z1028 maintained better compression-set property, which were less affected by TCIOP exposure.

In general, changes in tensile properties due to the TCIOP exposure were greater in S1151 than Z1028, Figure 133. Note that two different control properties were from two different batches of the o-ring samples purchased from the same vendor as a batch variation. TCIOP exposure made the S1151 harder and more brittle, which was undesirable for an o-ring. On the other hand, tensile properties of Z1028 were not significantly affected by the TCIOP exposure.

FT-IR spectra of the S1151 in Figure 134 show an increase in peak intensities at ~1080 cm^{-1} and ~795 cm^{-1} after TCIOP exposure, which was indicative of oxidation and possible side-chain rearrangement. FT-IR spectra of the Z1028 showed no significant changes in molecular structure due to TCIOP exposure, which was consistent with the results of other residual property characterizations.

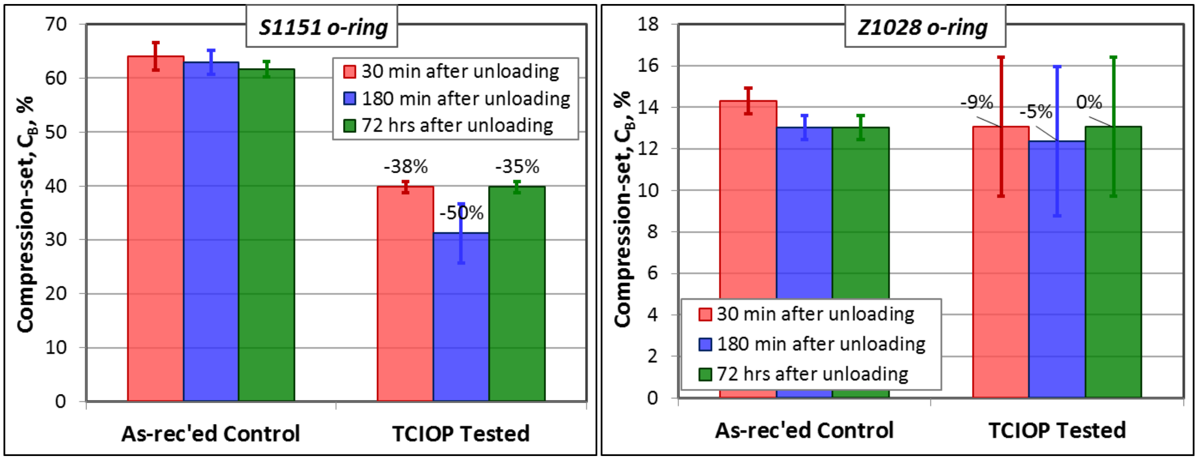

Figure 132.—Compression-set property of o-ring candidates before and after TCIOP test.

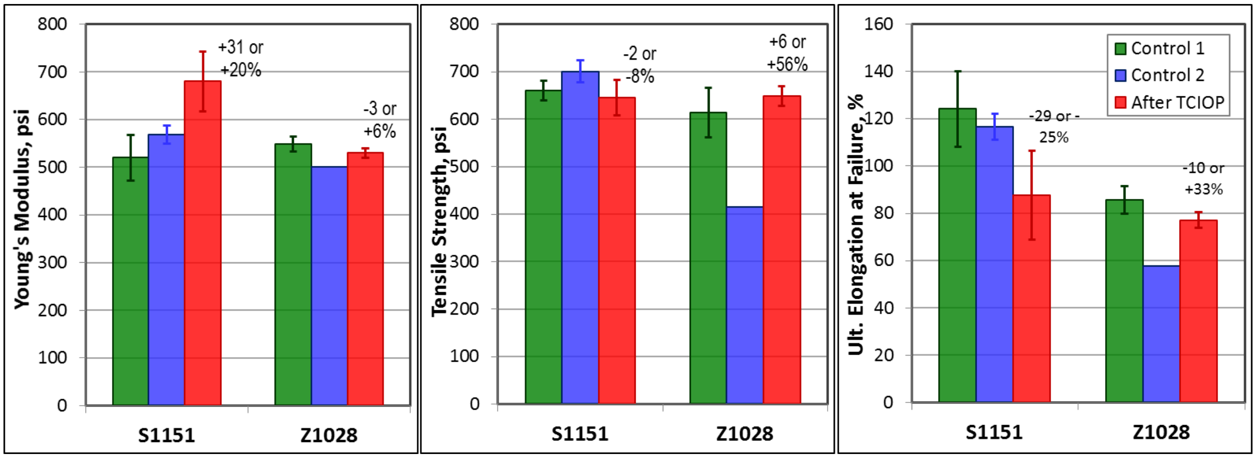

Figure 133.—Tensile properties of o-ring candidates before and after TCIOP test.

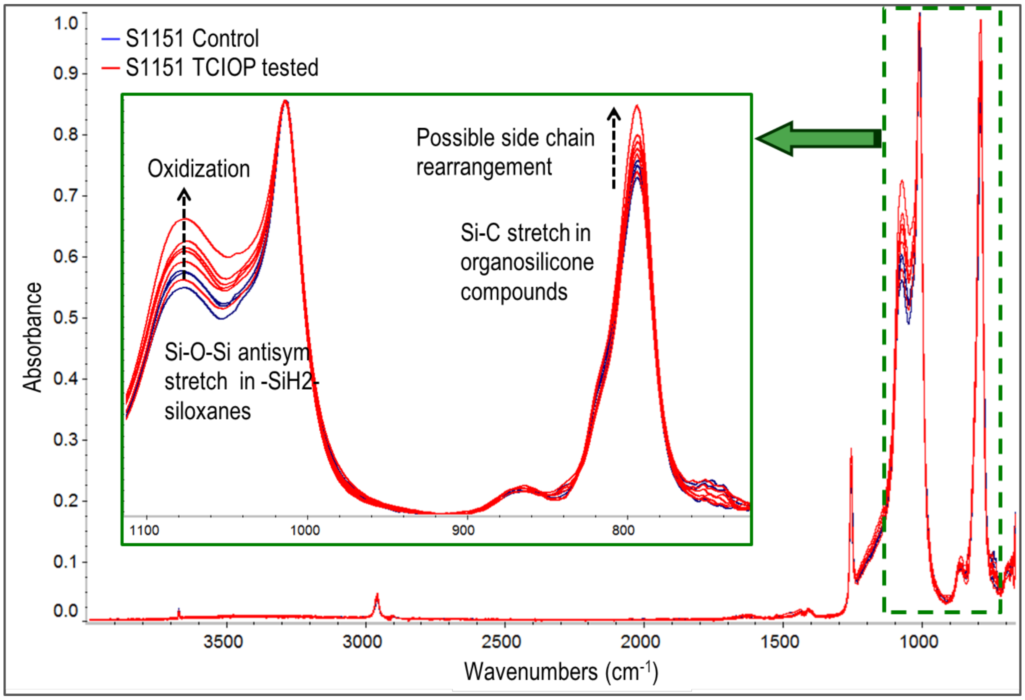

Figure 134.—Increases in certain peak intensities of S1151 o-ring after TCIOP exposures indicating possible changes in its molecular network structures.

In summary,

- There were no significant changes in concentrations of major gas species during the entire TCIOP testing for both candidates unlike shrink tubing candidates even though they both were from the similar polymer families.
- Based on FT-IR analysis, S1151, like SRFR, caused new outgases and their concentrations rapidly increased with increasing exposure time, which was an indication of thermal degradation. Z1028 samples caused no visible changes in outgas composition.
- Changes in most thermal properties and outgassing potentials from those of the baseline controls were rather insignificant in both candidates, but greater in S1151.
- TCIOP exposure lowered compression-set properties of both o-ring candidates, but greater changes were observed in S1151 than Z1028. Overall, Z1028 maintained better compression-set property.
- In general, changes in tensile properties due to the TCIOP exposure were greater in S1151 than Z1028. TCIOP exposure made the S1151 material harder and more brittle, which was undesirable for an o-ring.
- FT-IR analysis of the TCIOP exposed S1151 indicated oxidation and possible side-chain rearrangement, while Z1028 showed little to no change.

As an overall summary of the complete TCIOP tests, both outgassing and post TCIOP residual property behavior of the down-selected organic candidates are succinctly illustrated in Table 18 and Table 19.

TABLE 18.—SUMMARY OF OUTGASSING BEHAVIOR OF THE DOWN-SELECTED ORGANIC CANDIDATES DURING TCIOP EXPOSURES

	Exposure temperature, °C	100		150		200	
	Exposure time, day	1	3	1	2	1	7
Adhesive/potting	EA9394C-2			CH-O-H↑		H_2↓; O_2↓; CH_4↑; H_2O↑; CO↑; CO_2↑	
	AF131-2	No significant changes					
Thread locker	Loctite 294					O_2↓; H_2O↑; CO↑; CO_2↑; -CH_3/-CH_2-↑	
	Resbond 507					O_2↓; H_2O↑; CO↑; CO_2↑; -CH_3/-CH_2-↑	
Shrink tubing	ETFE					CO↑; -CH3/-CH_2-↑; C-F↑	
	SRFR					O_2↓; CH_4↑; H_2O↑; CO_2↑; -CH_3/-CH_2-↑; Silicon vapor↑	
O-ring	S1151					CO↑; -CH_3/-CH_2-↑; Silicon vapor↑	
	Z1028	No significant changes					

TABLE 19.—SUMMARY OF POST TCIOP RESIDUAL PROPERTY CHARACTERIZATIONS OF THE DOWN-SELECTED ORGANIC CANDIDATES

Changes in properties		Physical	Chemical	Thermal	Mechanical
Adhesive/potting	EA9394C-2	ΔWt%↑	-	T_g↑; % cure↑; G'↑; T_d↑	Bond strength↓
	AF131-2	ΔWt%↓	-	T_g↑; % cure↑; G'↑; T_d↓	Bond strength↑
Thread locker	Loctite 294	ΔWt%, joint #8↑	-	N/A	Torque strength↑
	Resbond 507TS	ΔWt%, joint #8↑	-	N/A	Torque strength↑
Shrink tubing	ETFE	N/A	-	T_d↑	Notch strength↑
	SRFR	N/A	Δ↑, oxidation, side-chain	T_m↓; T_d↓; T_t↑	Notch strength↓
O-ring	S1151	N/A	Δ↑, oxidation, side-chain	T_{exo}↓; T_d↓; T_t↑	C_B↓; E_γ↑; σ_f↓; ε_f↓
	Z1028	N/A	-	T_{exo}↓	C_B↓; ε_f↓

5.0 Summary and Conclusions

Multi-step evaluation processes were successfully conducted to screen and down-select the most capable high temperature candidates for various organic materials for use in future high performance, high temperature Stirling convertors, particularly in adhesive/potting, TL, shrink tubing, and o-ring applications. As a part of the evaluation, processing and installation conditions of the candidates have been optimized for their applications. The application limits of all material candidates were also identified based off the extensive property and performance data.

For the adhesive/potting application, the EA9394C-2 showed better thermal stability than the AF131-2, while the latter had slightly better material compatibility. The upper application limit based on the thermal stability was 180 to 200 °C for the AF131-2 and ~ 225 °C for the EA9394C-2. However, for both adhesive candidates, the low static bond strengths at 200 °C have to be accounted for when determining more practical upper limits. Neither epoxy shall be recommended for the use temperatures higher than 225 °C. Based on the thermal stability, overall bonding performance, handleability, processability and multi-functionality, and material availability, the EA9394C-2 epoxy was recommended as the final candidate for the future high temperature convertors. Presently, the highest service temperature of the EA9394C-2 can be 200 to 225 °C, but this temperature range shall be further validated by the synergistic durability life testing (SDLT).

For the TL application, all three TL candidates showed reasonably good thermal stability and material compatibility, but the Resbond 507TS was recommended as the final candidate for the future high temperature convertors based on overall locking performance. The upper application temperature based on the extensive evaluations should be ~ 200 °C for Resbond 507TS, or ~ 225 °C for both Loctite 294 and PET. The highest service temperatures recommended for those candidates in this report shall be further validated by synergistic durability life testing (SDLT) in future.

For the shrink tubing application, ETFE shrink tubing showed better thermal stability and material compatibility than SRFR shrink tubing, thus ETFE was recommended as the final candidate for the future high temperature convertors. The upper application temperature based on the extensive evaluations should be considerably lower than 200 °C for SRFR shrink tubing, or ~ 200 °C for ETFE shrink tubing.

For the o-ring application, the Z1028 o-ring showed better thermal stability and material compatibility than the S1151 o-ring, thus Z1028 was recommended as the final candidate for the future high temperature convertors. The upper application temperature based on the extensive evaluations should be considerably lower than 200 °C for the S1151 o-ring, or ~ 225 °C for Z1028 o-ring. The highest service temperatures recommended for those candidates in this report shall be further validated by the synergistic durability life testing (SDLT) in future.

6.0 Future Studies

Selection of the best candidates thus far was primarily based on the extended thermal aging experiments and was performed under an inert gas environment, even though TCIOP tests were conducted under the Stirling convertor simulated gas environment for a short duration. As illustrated in the overall program plan in Figure 1, the final candidates will be further evaluated and validated via SDLT after combining all organic materials involved in a typical Stirling convertor in a tightly sealed high pressure aging system capable of ~ 1000 psi up to 300 °C to simulate the actual Stirling service environment more closely. The tests will consist of gamma and neutron radiation exposures, and subsequent thermal aging for up to 3 years at three temperatures that have to be determined. Three aging intervals, for example 4 month, 1 year, and 3 years, are planned for outgas analyses and the extensive residual property characterizations. Once they are validated, the final process and installation optimization, and implementation optimizations will be also followed.

Appendix A

TABLE A.1.—SUMMARY OF THERMAL PROPERTIES OF AF131-2 EPOXY AS A FUNCTION OF CURE CONDITION FOR CURE PROCESS OPTIMIZATION

Adhesive type	Thick-ness, mm	Cure Condition				mDSC				STANDARD TGA				DMA, single cantilever			
		Cure T, °C	Cure t, hr	Post-cure T, °C	Post-cure t, hr	T_g, °C	ExoPeak, T, °C	Residual ΔH, J/g	% Cure, %	T_d, °C	ΔWt%, RT-100 °C	Δ%Wt, 100-200 °C	ΔWt%, at 700°C	T_g, °C G'	T_{g1}, °C tan δ	T_{g2}, °C tan δ	T_β, °C G''
3M AF131-2	0.15	177	1.5	N/A		225	234; 298	7.4	98.0	407	0.587	0.369	68				
				130	360	240	240; 298	5.5	98.5	390	3.160	4.440	54				
				160	360	242	245; 300	4.4	98.8	392	2.240	3.300	58				
				175	360	251	248; 297	1.1	99.7	392	2.870	5.200	57				
				190	360	250	297	1.5	99.6	390	2.312	2.513	55				
				205	360	247	241; 305	2.3	99.4	391	3.698	16.810	58				
				220	360	253	257; 298	2.0	99.5	391	2.807	3.544	57				
				260	360	240	296	1.5	99.6	408	4.454	15.773	31				
	1.3	177	1.5	N/A		239	255; 324	13.6	96.4	402	0.600	1.393	85	225	285		119
						200	213	59.0	84.3	408	0.220	0.720	62	192	220		109
				130	360	243	249; 320	9.5	97.5	393	1.681	3.212	57	232	285		114
				160	360	250	257; 322	4.3	98.9	395	1.460	3.170	56	238	283		119
				175	360	269	277; 320	0.6	99.8	394	1.416	2.534	58	212	243		116
					360	261	250	5.2	98.6	410	0.280	0.950	62	239	284		115
					1200	263	253	0.8	99.8	409	0.310	0.960	62	242	284		111
					2376	263	268	0.2	99.9	411	0.170	0.900	66	244	281		110
					4176	201	257	0.4	99.9	384	0.190	0.590	61	195	228		90
				190	360	271	295	0.3	99.9	397	0.919	1.717	58				
				200	360	257	265	0.6	99.8	408	0.270	0.910	65	241	282		116
					1200	246	283	0.4	99.9	409	0.420	0.980	61	232	271		110
					2376	250	262	0.1	100.0	410	0.560	1.170	60	235	267		110
					4176	238	268	0.9	99.8	413	0.170	1.160	60	236	269		113
				205	360	268	262; 322	0.8	99.8	395	1.390	7.428	64	248	284		119
				220	360	260	259; 323	2.8	99.3	395	0.997	2.288	59	244	283		117
				225	360	241	267	1.9	99.5	413	0.310	0.870	61	222	262		111
					1200	188	264	0.3	99.9	406	0.380	0.680	57	178	214		100
					2376	146	268	0.2	99.9	395	0.100	0.760	52				
					4176	173	268	0.9	99.8	405	0.580	0.980	43				
				260	360	237	296	0.4	99.9	401	2.116	2.943	31				
	0.75	160	1	N/A		170	209; 322	59.2	84.2	394	0.152	0.717	59	162	201	293	105
			4	N/A		189	208; 321	46.2	87.7	392	0.201	0.655	57	187	207	291	104
			8	N/A		199	207; 322	42.3	88.8	391	0.136	0.615	56	195	213	290	107
	0.75	185	1	N/A		214	223; 322	32.3	91.4	396	0.182	0.800	70	193	230	290	122
			4	N/A		229	232; 323	22.5	94.0	396	0.166	0.722	70	220	239	288	113
			8	N/A		233	238; 323	17.2	95.4	397	0.041	0.064	63	231	252	287	115

Note:

☐	Under cured
🟩	Degree of cure higher than 99.5%
🟨	Potential thermal degradation

TABLE A.2.—SUMMARY OF THERMAL PROPERTIES OF EA9394C-2 EPOXY AS A FUNCTION OF CURE CONDITION FOR CURE PROCESS OPTIMIZATION

Adhesive type	Thick-ness, mm	Cure condition				mDSC				Standard TGA				DMA, single cantilever			
		Cure T, °C	Cure t, hr	Post-cure T, °C	Post-cure t, hr	T_g, °C	ExoPeak, T, °C	Residual ΔH, J/g	% Cure, %	T_d, °C	ΔWt%, RT-100 °C	Δ%Wt, 100-200 °C	ΔWt%, at 700°C	T_g, °C G'	T_{g1}, °C tan δ	T_{g2}, °C tan δ	T_β, °C G''
Hysol EA9394 C-2	0.1	93	1	N/A		131	143; 246	32.9	87.2	366	1.353	1.175	57				
				115	2	133	148; 250	17.7	93.1	378	0.612	1.127	60				
		115 after 1 hr at 93	2	130	360	175	212; 273	4.9	98.1	362	2.208	2.358	53				
				160	360	184	222; 296	2.2	99.1	358	2.470	5.580	56				
				175	360	200	206; 297	1.1	99.6	368	2.695	7.895	57				
				190	360	203	242; 299	0.9	99.6	382	3.360	39.810	65				
				205	360	193	296	0.7	99.7	366	4.120	10.090	66				
				220	360	198	220; 296	0.9	99.6	367	3.440	10.550	58				
				260	360	224	282	0.6	99.8	436	3.240	17.930	47				
				260	360	224	282	0.6	99.8	436	3.240	17.930	47				
				260	360	224	282	0.6	99.8	436	3.240	17.930	47				
				260	360	224	282	0.6	99.8	436	3.240	17.930	47				
				260	360	224	282	0.6	99.8	436	3.240	17.930	47				
				260	360	224	282	0.6	99.8	436	3.240	17.930	47				
	1.5	93	1	N/A		114	136; 261	52.8	79.5	363	0.629	1.045	58				
				115	2	142	153; 238	20.2	92.1	373	0.225	0.449	67				
						147	160	18.5	92.8	379	0.230	0.490	60	159	192		
				110	144	162	168; 241	16.7	93.5	372	0.466	0.021	64				
		115 after 1 hr at 93	2	N/A		142	153; 238	17.0	93.4	363	0.629	1.046	58				
				130	360	184	210; 283	10.0	96.1	365	0.695	2.373	59	174	224		
				160	360	201	203; 287	1.0	99.6	364	0.604	1.585	59	174	225		
				175	360	204	209; 298	0.6	99.8	368	0.937	9.939	66				
					360	189	265	3.2	98.8	378	0.350	0.810	59	185	234		
					1200	191	264	0.8	99.7	378	0.340	0.820	57	191	231		
					2376	197	267	1.1	99.6	382	0.330	1.060	61	192	227		
					4176	261	305	0.5	99.8	409	0.160	0.790	64	243	281		
					4176	261	305	0.5	99.8	409	0.160	0.790	64	243	281		
				190	360	193	260; 297	0.5	99.8	372	0.363	0.990	58	188	210		
				200	360	191	267	2.1	99.2	382	0.440	0.860	57	187	219		
					1200	188	264	0.9	99.7	384	0.430	0.780	57	171	207		
					2376	178	257	0.5	99.8	390	0.290	0.710	55	162	199		
					4176	178	255	0.5	99.8	399	0.360	0.570	55	170	208		
				205	360	196	205; 296	0.7	99.7	366	0.792	2.744	59	194		224	
				220	360	203	262; 295	0.6	99.8	366	0.576	1.216	58				
				225	360	157		0.5	99.8	392	0.460	0.790	54	159	180		
					1200	117	278	1.1	99.6	416	0.250	0.730	51	150	171		
					2376	135	269	0.5	99.8	424	0.320	0.610	50	123			
					4176	142		0.5	99.8	423	0.330	0.590	48				
				260	360	171	296	1.2	99.6	421	0.881	7.030	42	234		264	

TABLE A.2.—SUMMARY OF THERMAL PROPERTIES OF EA9394C-2 EPOXY AS A FUNCTION OF CURE CONDITION FOR CURE PROCESS OPTIMIZATION

Adhesive type	Thick-ness, mm	Cure condition				mDSC				Standard TGA				DMA, single cantilever			
		Cure T, °C	Cure t, hr	Post-cure T, °C	Post-cure t, hr	T_g, °C	ExoPeak, T, °C	Residual ΔH, J/g	% Cure, %	T_d, °C	ΔWt%, RT-100 °C	Δ%Wt, 100-200 °C	ΔWt%, at 700°C	T_g, °C G'	T_{g1}, °C tan δ	T_{g2}, °C tan δ	T_β, °C G''
	0.75	105	1	N/A		143	153; 257	17.5	93.2	372	0.222	0.443	58	137	165	233	
				115	6	158	163; 255	10.6	95.9	372	0.147	0.412	58				
				150	2	186	191; 251	7.0	97.3	375	0.028	0.213	61	183	208	239	
					6	195	202; 251	4.9	98.1	371	0.154	0.648	59	186	212		
			4	N/A		147	154; 254	16.9	93.4	372	0.156	0.513	59	139	168	231	
				115	6	158	164; 252	11.4	95.6	372	0.156	0.461	57	155	182	221	
				150	2	187	191; 252	6.6	97.4	371	0.103	0.405	59	176	198		
					6	197	200; 250	4.2	98.4	376	0.092	0.352	64	176	194		
		115	1	N/A		160	167; 256	12.8	95.0	372	0.145	0.491	58	138	158	231	
				150	2	189	191; 252	5.0	98.0	372	0.232	0.468	58	172	193	219	
					6	198	206; 251	3.4	98.7	372	0.196	0.530	59	174	213	225	
			4	N/A		159	165; 258	11.3	95.6	372	0.103	0.434	58	152	176	230	
				150	2	185	189; 256	4.2	98.3	373	0.221	0.403	58	180	204	224	
					6	198	254; 252	4.0	98.4	370	0.186	0.468	58	177	215	240	

Note:

⬜	Under cured
🟩	Degree of cure higher than 99.5%
🟨	Potential thermal degradation

TABLE A.3.—OVERALL TEST MATRIX FOR 15-DAY THERMAL AGING TESTS OF ADHESIVE/POTTING CANDIDATES

Aging *T*, °C			23	130	160	175	190	205	220	260
	Aging system		Baked control	Lunaire (Rm 145)	Lunaire Gruenberg	Blue M PC	Blue M N2	Blue M #6	Blue M #5	Blue M #5
Specimen	Properties			4/30/12 10:00 a.m.	4/30/12 10:00 a.m.	7/26/12 1:00 p.m.	4/30/12 10:00 a.m.	7/26/12 1:00 p.m.	7/26/12 1:00 p.m.	4/30/12 10:00 a.m.
Hysol EA9394 C-2				5/15/12 10:00 a.m.	5/15/12 10:00 a.m.	8/10/12 1:00 p.m.	5/15/12 10:00 a.m.	8/10/12 1:00 p.m.	8/10/12 1:00 p.m.	5/15/12 10:00 a.m.
Epoxy alone Thin, CN# Thick, CK#	Wt change, mDSC, TGA, DMA, FT-IR		(i) CN1, CN2, CN3, CN4 (ii) CK1, CK2	(i) CN5, CN6, CN7, CN8 (ii) CK3, CK4	(i) CN9, CN10, CN11, CN12 (ii) CK5, CK6	(i) CN17, CN18, CN19, CN20 (ii) CK9, CK10	(i) CN13, CN14, CN15, CN16 (ii) CK7, CK8	(i) CN21, CN22, CN23, CN24 (ii) CK11, CK12	(i) CN29, CN30, CN31, CN32 (ii) CK15, CK16	(i) CN25, CN26, CN27, CN28 (ii) CK13, CK14
Sandwich lap shear	Bond strength	120 °C	C3-1, C3-25, C4-9, C4-33, C4-36, C4-37,C4-38 C5-22, C6-1, C6-2, C6-33, C6-34, C6-35, C6-36, C6-37, C6-38, C6-39, C6-40, C6-41, C6-42, C6-43, C6-44	C3-2, C3-26, C4-10, C4-34, C5-23, C6-3	C3-3, C3-27, C4-11, C4-35, C5-24, C6-4	C3-5, C3-29, C4-13, C5-2, C5-26, C6-6	C3-4, C3-28, C4-12, C5-1, C5-25, C6-5	C3-6, C3-30, C4-14, C5-3, C5-27, C6-7	C3-8, C3-32, C4-16, C5-5, C5-29, C6-9	C3-7, C3-31, C4-15, C5-4, C5-28, C6-8
		170 °C	C3-9, C3-33, C4-17, C4-39, C4-40, C4-41, C5-6, C5-30, C6-10, C6-11	C3-10, C3-34, C4-18, C5-7, C5-31, C6-12	C3-11, C3-35, C4-19, C5-8, C5-32, C6-13	C3-13, C4-21, C5-10, C5-34, C6-15, C6-31	C3-12, C3-36, C4-20, C5-9, C5-33, C6-14	C3-14, C4-22, C5-11, C5-35, C6-16, C6-28	C3-16, C4-24, C5-13, C5-37, C6-18, C6-30	C3-15, C4-23, C5-12, C5-36, C6-17, C6-29
		200 °C	C3-17, C4-1, C4-25, C4-42, C4-43, C4-44, C5-14, C5-38, C6-19, C6-20	C3-18, C4-2, C4-26, C5-15, C5-39, C6-21	C3-19, C4-3, C4-27, C5-16, C5-40, C6-22	C3-21, C4-5, C4-29, C5-18, C5-42, C6-24	C3-20, C4-4, C4-28, C5-17, C5-41, C6-23	C3-22, C4-6, C4-30, C5-19, C5-43, C6-25	C3-24, C4-8, C4-32, C5-21, C6-27, C6-32	C3-23, C4-7, C4-31, C5-20, C5-44, C6-26
3M AF131-2										
Epoxy alone Thin, CN# Thick, CK#	Wt change, mDSC, TGA, DMA, FT-IR		(i) AN1, AN2, AN3 (ii) AK1, AK2	(i) AN4, AN5, AN6, (ii) AK3, AK4	(i) AN7, AN8, AN9 (ii) AK5, AK6	(i) AN13, AN14, AN15 (ii) AK9, AK10	(i) AN10, AN11, AN12 (ii) AK7, AK8	(i) AN16, AN17, AN18 (ii) AK11, AK12	(i) AN22, AN23, AN24 (ii) AK15, AK16	(i) AN19, AN20, AN21 (ii) AK13, AK14
Sandwich lap shear	Bond strength	120 °C	A1-1, A1-25, A2-12, A2-13, A4-2, A4-3, A4-4, A4-32, A5-23, A5-24, A5-40, A5-41, A5-42, A5-43, A5-44, A3-7, A3-8, A3-9	A1-2, A1-26, A2-14, A4-5, A4-33, A5-25	A1-3, A1-27, A2-15, A4-6, A4-34, A5-26	A1-5, A1-29, A2-17, A4-8, A4-36, A5-28	A1-4, A1-28, A2-16, A4-7, A4-35, A5-27	A1-6, A1-30, A2-18, A4-37, A5-29, A5-39	A1-7, A1-31, A2-19, A4-10, A4-38, A5-30	A1-8, A1-32, A2-20, A4-11, A4-39, A5-31
		170 °C	A1-9, A1-33, A2-21, A2-22, A4-12, A4-13, A4-14, A4-40, A5-32, A5-33	A1-10, A1-34, A2-23, A4-15, A4-41, A5-34	A1-11, A1-35, A2-24, A4-16, A4-42, A5-35	A1-13, A1-37, A2-26, A4-18, A4-44, A5-37	A1-12, A1-36, A2-25, A4-17, A4-43, A5-36	A1-14, A2-1, A2-27, A4-19, A5-1, A5-38	A1-15, A2-3, A2-28, A4-20, A5-2, A5-3	A1-16, A2-3, A2-29, A4-21, A5-4, A5-5
		200 °C	A1-17, A2-4, A2-30, A2-31, A4-22, A4-23, A4-24, A5-6, A5-7, A5-8	A1-18, A2-5, A2-32, A4-25, A5-9, A5-10	A1-19, A2-6, A2-33, A4-26, A5-11, A5-12	A1-21, A2-8, A2-35, A4-28, A5-15, A5-16	A1-20, A2-7, A2-34, A4-27, A5-13, A5-14	A1-22, A2-9, A2-36, A4-29, A5-17, A5-18	A1-23, A2-10, A2-37, A4-30, A5-19, A5-20	A1-24 A2-11, A4-1, A4-31, A5-21, A5-22

TABLE A.4.—SUMMARY OF LAP SHEAR BONDING PROPERTIES OF ADHESIVE CANDIDATES AFTER 15-DAY THERMAL AGING TESTS

Test temp.	Lap shear bond strength, psi										Lap shear strain-term ($dl/H/T$) at failure, in.$^{-1}$							
	Aging condition		15-days in nitrogen gas environment								15-days in nitrogen gas environment							
	Aging *T*, °C		23	130	160	175	190	205	220	260	23	130	160	175	190	205	220	260
120 °C 248 °F	EA 9394 C-2	Avg.	1707	1705	1696	1446	1262	1442	1136	743	11.4	10.9	7.6	14.2	5.6	12.0	10.8	5.8
		SD	187	134	305	417	409	209	384	197	3.2	1.1	2.3	4.6	1.7	2.2	4.3	1.2
		% change		0	–1	–15	–26	–16	–33	–56		–4.4	–33.3	24.2	–50.9	5.3	–5.3	–49.1
170 °C 338 °F		Avg.	1086	1337	1357	1243	1020	1394	1152	851	14.2	12.3	9.3	13.3	8.6	13.2	10.0	7.2
		SD	240	266	126	90	408	156	277	445	9.9	6.5	2.4	2.5	3.3	2.2	3.6	4.4
		% change		23	25	14	–6	28	6	–22		–13.4	–34.5	–6.2	–39.4	–6.7	–29.8	–49.3
200 °C 392 °F		Avg.	739	1248	1236	1041	932	1135	1023	32	5.1	7.9	8.9	17.7	8.1	10.9	13.3	10.2
		SD	48	157	126	186	222	222	357	39	1.5	2.0	2.7	3.9	4.8	4.0	3.6	4.5
		% change		69	67	41	26	54	38	–96		54.9	74.5	247.3	58.8	113.5	161.3	100.0
120 °C 248 °F	AF 131-2	Avg.	2526	2602	2262	1620	1342	1828	1792	6	15.2	16.6	13.0	15.0	8.6	15.1	12.0	0.5
		SD	657	698	443	401	543	530	730	2	4.5	6.4	4.7	6.2	2.1	4.5	3.6	0.5
		% change		3	–10	–36	–47	–28	–29	–100		9.2	–14.5	–1.3	–43.4	–0.5	–21.0	–96.7
170 °C 338 °F		Avg.	2144	2246	2238	1708	1089	1896	1450	5	22.8	20.6	14.7	12.7	12.2	16.2	13.0	0.5
		SD	422	722	599	495	331	655	637	2	6.5	10.6	1.8	4.6	4.5	5.9	4.2	0.5
		% change		5	4	–20	–49	–12	–32	–100		–9.6	–35.5	–44.3	–46.5	–29.0	–42.9	–97.8
200 °C 392 °F		Avg.	1740	2110	1941	1693	1524	1606	1491	9	16.7	21.7	17.9	17.6	12.1	16.1	15.7	11.9
		SD	291	348	466	690	605	766	430	9	9.1	3.9	7.0	6.3	3.2	4.4	5.9	2.6
		% change		21	12	–3	–12	–8	–14	–99		29.9	7.2	5.1	–27.5	–3.6	–6.2	–28.7

TABLE A.5.—OVERALL TEST MATRIX FOR 15-DAY THERMAL AGING TESTS OF THREAD LOCKER CANDIDATES

(a) Loctite 294

	Test conditions	Torque Test Specimens											
Aging conditions		23 °C			100 °C			150 °C			200 °C		
15-d aging under dry N_2	Unaged Control I	2-122 6-027 8-143	2-031 6-151 8-191	2-087 6-123 8-153	2-089 6-135 8-137	2-035 6-005 8-184	2-079 6-142 8-122	2-081 6-140 8-171	2-100 6-167 8-212	2-030 6-178 8-197	2-099 6-002 8-121	2-105 6-014 8-139	2-014 6-143 8-134
From 11/26/13 11:00 to 12/11/13 11:00	130 °C/266 °F Lunaire oven				2-096 6-023 8-221	2-066 6-152 8-144	2-040 6-136 8-195				2-054 6-168 8-168	2-029 6-006 8-011	2-049 6-004 8-185
	160 °C/320 °F Gruenberg oven				2-026 6-157 8-131	2-125 6-114 8-165	2-043 6-128 8-150				2-028 6-149 8-129	2-038 6-150 8-016	2-123 6-120 8-115
	190 °C/374 °F Blue M N_2 oven				2-052 6-118 8-030	2-084 6-109 8-014	2-064 6-008 8-133				2-037 6-153 8-118	2-061 6-028 8-008	2-041 6-203 8-005
	220 °C/428 °F Blue M #5 oven				2-027 6-011 8-223	2-121 6-195 8-177	2-017 6-130 8-018				2-098 6-147 8-015	2-085 6-129 8-013	2-053 6-250 8-189
	260 °C/500 °F Blue M #6 oven				2-076 6-013 8-120	2-015 6-189 8-020	2-056 6-007 8-176				2-077 6-126 8-110	2-042 6-145 8-194	2-083 6-155 8-136
# of specimen	#2 #6 #8	3	3	3	18	18	18	3	3	3	18	18	18

TABLE A.5.—OVERALL TEST MATRIX FOR 15-DAY THERMAL AGING TESTS OF THREAD LOCKER CANDIDATES

(b) Resbond 507TS

Aging conditions	Test conditions	Torque Test Specimens											
		23 °C			100 °C			150 °C			200 °C		
15-d aging under dry N_2	Unaged Control I	2-144 6-175 8-124	2-097 6-141 8-251	2-006 6-192 8-228	2-094 6-132 8-190	2-062 6-124 8-113	2-022 6-138 8-239	2-135 6-144 8-001	2-033 6-137 8-227	2-152 6-117 8-181	2-086 6-018 8-243	2-036 6-180 8-255	2-134 6-185 8-169
From 11/26/13 11:00 to 12/11/13 11:00	130 °C/266 °F Lunaire oven				2-153 6-001 8-180	2-068 6-127 8-225	2-156 6-191 8-241				2-018 6-183 8-111	2-095 6-184 8-232	2-163 6-169 8-163
	160 °C/320 °F Gruenberg oven				2-151 6-119 8-172	2-071 6-207 8-244	2-160 6-125 8-250				2-137 6-188 8-235	2-146 6-187 8-230	2-157 6-110 8-167
	190 °C/374 °F Blue M N_2 oven				2-133 6-016 8-216	2-047 6-181 8-234	2-148 6-030 8-156				2-073 6-173 8-236	2-050 6-003 8-240	2-131 6-159 8-256
	220 °C/428 °F Blue M #5 oven				2-102 6-170 8-125	2-080 6-165 8-237	2-162 6-194 8-141				2-075 6-009 8-158	2-124 6-017 8-233	2-165 6-134 8-178
	260 °C/500 °F Blue M #6 oven				2-058 6-193 8-155	2-078 6-148 8-154	2-016 6-139 8-214				2-065 6-115 8-128	2-143 6-196 8-160	2-107 6-176 8-224
# of specimen	#2 #6 #8	3	3	3	18	18	18	3	3	3	18	18	18

TABLE A.5.—OVERALL TEST MATRIX FOR 15-DAY THERMAL AGING TESTS OF THREAD LOCKER CANDIDATES

(c) Poly-Lok PET Patch

Test conditions / Aging conditions		Torque Test Specimens											
		23 °C			100 °C			150 °C			200 °C		
15-d aging under dry N_2	Unaged Control I	2-093 6-227 8-109	2-032 6-240 8-007	2-088 6-113 8-173	2-067 6-233 8-010	2-045 6-111 8-174	2-060 6-015 8-024	2-002 6-248 8-142	2-109 6-251 8-130	2-091 6-166 8-219	2-126 6-161 8-179	2-104 6-154 8-123	2-103 6-158 8-183
From 11/26/13 11:00 to 12/11/13 11:00	130 °C/266 °F Lunaire oven				2-072 6-164 8-127	2-063 6-156 8-210	2-010 6-179 8-114				2-011 6-012 8-182	2-048 6-238 8-152	2-039 6-029 8-217
	160 °C/320 °F Gruenberg oven				2-082 6-214 8-138	2-070 6-171 8-196	2-090 6-190 8-012				2-024 6-116 8-220	2-127 6-234 8-199	2-128 6-253 8-028
	190 °C/374 °F Blue M N_2 oven				2-044 6-249 8-029	2-012 6-010 8-215	2-059 6-112 8-119				2-025 6-133 8-211	2-051 6-131 8-200	2-055 6-210 8-209
	220 °C/428 °F Blue M #5 oven				2-046 6-223 8-025	2-057 6-024 8-132	2-034 6-160 8-198				2-092 6-121 8-187	2-101 6-122 8-218	2-074 6-165 8-112
	260 °C/500 °F Blue M #6 oven				2-106 6-231 8-140	2-129 6-236 8-151	2-021 6-213 8-204				2-023 6-226 8-193	2-013 6-146 8-213	2-108 6-237 8-126
# of specimen	#2 #6 #8	3	3	3	18	18	18	3	3	3	18	18	18

TABLE A.6.—SUMMARY OF TORQUE DATA UP TO 200 °C INLCUDING FAILURE MODE FROM UNAGED CONTROLS OF THREAD LOCKER CANDIDATES IN VARIOUS JOINT TYPES

Joint type		Torque strength, N-cm, and % installation torque																		
TL	Joint #	Sample ID	23 °C				Sample ID	100 °C				Sample ID	150 °C				Sample ID	200 °C		
			Break-loose	% Inst.	Prevail-ing	Maxi-mum		Break-loose	% Inst.	Prevail-ing	Maxi-mum		Break-loose	% Inst.	Prevail-ing	Maxi-mum		Break-loose	% Inst.	Prevail-ing	Maxi-mum
Loctite 294	2	2-122	29.8	81.0	2.0	2.0	2-089	27.2	73.9	2.2	2.2	2-081	29.5	80.2	1.9	2.0	2-099	22.0	59.8	3.5	3.7
		2-031	26.2	71.2	3.9	4.5	2-035	23.6	64.1	1.6	1.8	2-100	22.1	60.1	12.4	12.4	2-105	22.7	61.7	3.1	4.0
		2-087	38.9	105.7	21.9	22.0	2-079	29.5	80.2	1.9	2.0	2-030	26.1	70.9	4.8	5.0	2-014	20.1	54.6	1.9	2.5
		Avg.	31.6	86.0	9.3	9.5	Avg.	26.8	72.7	1.9	2.0	Avg.	25.9	70.4	6.4	6.5	Avg.	21.6	58.7	2.8	3.4
		SD	6.5	17.8	11.0	10.9	SD	3.0	8.1	0.3	0.2	SD	3.7	10.1	5.4	5.4	SD	1.3	3.7	0.8	0.8
	6	6-027	91.0	119.1	21.9	40.0	6-135	70.2	91.9	17.1	19.4	6-140	74.8	97.9	15.3	18.0	6-002	62.0	81.2	8.0	12.8
		6-151	97.8	128.0	35.7	57.4	6-005	78.3	102.5	23.4	24.9	6-167	53.8	70.4	14.8	17.1	6-014	49.8	65.2	8.6	9.4
		6-123	93.1	121.9	51.0	65.2	6-142	76.1	99.6	18.7	24.7	6-178	56.1	73.4	10.9	14.2	6-143	61.0	79.8	7.6	10.7
		Avg.	94.0	123.0	36.2	54.2	Avg.	74.9	98.0	19.7	23.0	Avg.	61.6	80.6	13.7	16.4	Avg.	57.6	75.4	8.1	11.0
		SD	3.5	4.6	14.6	12.9	SD	4.2	5.5	3.3	3.1	SD	11.5	15.1	2.4	2.0	SD	6.8	8.9	0.5	1.7
	8	8-143	21.9	168.5	44.5	45	8-137	13.8	106.2	19.8	25.9	8-171	13.4	103.1	7.8	8.2	8-121	15.5	119.2	9.4	10.0
		8-191	16.6	127.7	44.6	45	8-184	13.7	105.4	8.8	9.0	8-212	16.1	123.8	14.4	15.0	8-139	15.7	120.8	13.0	13.3
		8-153	27.3	210.0	44.5	45	8-122	17.5	134.6	29.9	37.3	8-197	13.8	106.2	11.9	12.6	8-134	16.3	125.4	11.0	11.1
		Avg.	21.9	168.7	44.5	45.0	Avg.	15.0	115.4	19.5	24.1	Avg.	14.4	111.0	11.4	11.9	Avg.	15.8	121.8	11.1	11.5
		SD	5.4	41.2	0.1	0.0	SD	2.2	16.7	10.6	14.2	SD	1.5	11.2	3.3	3.4	SD	0.4	3.2	1.8	1.7
Resbond 507TS	2	2-144	58.0	157.6	29.3	30.4	2-094	47.8	129.9	16.4	19.2	2-135	25.2	68.5	3.7	4.0	2-086	29.5	80.2	1.9	2.0
		2-097	71.7	194.8	37.3	63.1	2-062	52.8	143.5	14.4	19.0	2-033	33.7	91.6	5.5	7.5	2-036	29.4	79.9	2.1	2.9
		2-006	64.3	174.7	21.0	22.4	2-022	39.5	107.3	12.3	15.1	2-152	24.7	67.1	2.0	2.2	2-134	25.4	69.0	2.9	3.5
		Avg.	64.7	175.7	29.2	38.6	Avg.	46.7	126.9	14.4	17.8	Avg.	27.9	75.7	3.7	4.6	Avg.	28.1	76.4	2.3	2.8
		SD	6.9	18.6	8.2	21.6	SD	6.7	18.3	2.1	2.3	SD	5.1	13.7	1.8	2.7	SD	2.3	6.4	0.5	0.8
	6	6-175	141.9	185.7	12.7	26.7	6-132	93.9	122.9	12.9	31.8	6-144	62.1	81.3	3.8	10.7	6-018	60.9	79.7	3.4	7.4
		6-141	74.8	97.9	15.3	18.0	6-124	107.2	140.3	10.9	18.0	6-137	60.9	79.7	6.5	7.7	6-180	52.0	68.1	3.2	8.5
		6-192	135.6	177.5	28.7	38.6	6-138	100.7	131.8	8.0	13.5	6-117	64.7	84.7	8.3	14.7	6-185	56.1	73.4	3.1	4.1
		Avg.	117.4	153.7	18.9	27.8	Avg.	100.6	131.7	10.6	21.1	Avg.	62.6	81.9	6.2	11.0	Avg.	56.3	73.7	3.2	6.7
		SD	37.1	48.5	8.6	10.3	SD	6.7	8.7	2.5	9.5	SD	1.9	2.5	2.3	3.5	SD	4.5	5.8	0.2	2.3
	8	8-124	57.7	442.8	0.4	49.9	8-190	43.6	334.6	0.6	41.8	8-001	33.1	254.0	5.1	7.7	8-243	29.4	225.6	4.1	5.6
		8-251	69.2	531.1	1.0	1.2	8-113	48.6	373.0	32.7	49.6	8-227	30.4	233.3	5.9	7.5	8-255	28.4	218.0	3.6	4.9
		8-228	38.2	293.2	32	34.2	8-239	34.9	267.8	13.2	15.6	8-181	32.7	251.0	6.7	8.6	8-169	25.8	198.0	3.6	5.8
		Avg.	55.0	422.4	32.0	42.1	Avg.	42.4	325.1	23.0	35.7	Avg.	32.1	246.1	5.9	7.9	Avg.	27.9	213.9	3.8	5.4

TABLE A.6.—SUMMARY OF TORQUE DATA UP TO 200 °C INLCUDING FAILURE MODE FROM UNAGED CONTROLS OF THREAD LOCKER CANDIDATES IN VARIOUS JOINT TYPES

Joint type		Torque strength, N-cm, and % installation torque																			
TL	Joint #	Sample ID	23 °C				Sample ID	100 °C				Sample ID	150 °C				Sample ID	200 °C			
			Break-loose	% Inst.	Prevail-ing	Maxi-mum		Break-loose	% Inst.	Prevail-ing	Maxi-mum		Break-loose	% Inst.	Prevail-ing	Maxi-mum		Break-loose	% Inst.	Prevail-ing	Maxi-mum
		SD	15.7	120.3	18.1	24.9	SD	6.9	53.2	16.2	17.8	SD	1.5	11.2	0.8	0.6	SD	1.9	14.3	0.3	0.5
Poly-Lok PET Patch	2	2-093	22.8	62.0	7.1	12.8	2-067	15.4	41.8	5.4	5.8	2-002	13.2	35.9	1.5	1.6	2-126	11.5	31.3	1.8	2.0
		2-032	23.6	64.1	3.3	3.6	2-045	19.1	51.9	3.6	4.1	2-109	14.2	38.6	10.8	11.8	2-104	13.2	35.9	13.9	14.3
		2-088	22.3	60.6	14.1	14.8	2-060	18.1	49.2	2.4	2.5	2-091	17.6	47.8	18.2	18.7	2-103	13.0	35.3	18.5	18.8
		Avg.	22.9	62.2	8.2	10.4	Avg.	17.5	47.6	3.8	4.1	Avg.	15.0	40.8	10.2	10.7	Avg.	12.6	34.1	11.4	11.7
		SD	0.7	1.8	5.5	6.0	SD	1.9	5.2	1.5	1.7	SD	2.3	6.3	8.4	8.6	SD	0.9	2.5	8.6	8.7
	6	6-227	55.3	72.4	1.5	1.7	6-233	32.2	42.1	1.9	2.0	6-248	46.6	61.0	1.5	1.6	6-161	57.2	74.9	2.0	2.3
		6-240	54.7	71.6	2.2	2.4	6-111	54.5	71.3	2.3	2.4	6-251	54.9	71.9	1.7	2.2	6-154	17.1	22.4	2.4	2.5
		6-113	33.3	43.6	13.0	13.8	6-015	27.4	35.9	8.5	12.3	6-166	39.9	52.2	7.5	7.7	6-158	19.1	25.0	3.5	3.7
		Avg.	47.8	62.5	5.6	6.0	Avg.	38.0	49.8	4.2	5.6	Avg.	47.1	61.7	3.6	3.8	Avg.	31.1	40.8	2.6	2.8
		SD	12.5	16.4	6.4	6.8	SD	14.5	18.9	3.7	5.8	SD	7.5	9.8	3.4	3.4	SD	22.6	29.6	0.8	0.8
	8	8-109	21.6	67.5	26.4	27.4	8-010	11.8	36.9	5.3	7.5	8-142	15.5	48.4	2.6	3.7	8-179	11.9	37.2	2	2.8
		8-007	17.9	55.9	15.7	17.8	8-174	9.2	28.8	2.5	3.3	8-130	10.4	32.5	5.7	6.5	8-123	12.1	37.8	0.8	1.4
		8-173	35.8	111.9	28.5	29.1	8-024	8.8	27.5	7.7	7.7	8-219	6	18.8	4.0	5.4	8-183	11.7	36.6	1.5	1.7
		Avg.	25.1	78.4	23.5	24.8	Avg.	9.9	31.0	5.2	6.2	Avg.	10.6	33.2	4.1	5.2	Avg.	11.9	37.2	1.4	2.0
		SD	9.4	29.5	6.9	6.1	SD	1.6	5.1	2.6	2.5	SD	4.8	14.9	1.6	1.4	SD	0.2	0.6	0.6	0.7

🟥 Cohesive failure 🟦 Adhesive failure 🟨 Mixture mode 🟫 Thermally degraded or charred

TABLE A.7.—SUMMARY OF TORQUE DATA AT 100 AND 200 °C INCLUDING FAILURE MODE OF THREAD LOCKER CANDIDATES IN #2 JOINT AS A FUNCTION OF AGING TEMPERATURE

Aging T, °C	#2 Joint Torque Strengths, N-cm, and % installation torques																													
	Loctite 294 Installation torque = 36.8 N-cm										Resbond 507TS Installation torque = 36.8 N-cm										Poly-Lok PET Installation torque = 36.8 N-cm									
	100 °C					200 °C					100 °C					200 °C					100 °C					200 °C				
	Sample ID	Breakloose		Prevailing torque	Maximum torque	Sample ID	Breakloose		Prevailing torque	Maximum torque	Sample ID	Breakloose		Prevailing torque	Maximum torque	Sample ID	Breakloose		Prevailing torque	Maximum torque	Sample ID	Breakloose		Prevailing torque	Maximum torque	Sample ID	Breakloose		Prevailing torque	Maximum torque
		Torque	% Inst.				Torque	% Inst.				Torque	% Inst.				Torque	% Inst.				Torque	% Inst.				Torque	% Inst.		
23	🟨 2-089	27.2	74	2.2	2.2	🟦 2-099	22.0	60	3.5	3.7	🟨 2-094	47.8	130	16.4	19.2	🟨 2-086	29.5	80	1.9	2	🟨 2-067	15.4	42	5.4	5.8	🟨 2-126	11.5	31	1.8	2.0
	🟦 2-035	23.6	64	1.6	1.8	🟨 2-105	22.7	62	3.1	4.0	🟨 2-062	52.8	143	14.4	19.0	🟨 2-036	29.4	80	2.1	2.9	🟨 2-045	19.1	52	3.6	4.1	🟦 2-104	13.2	36	13.9	14.3
	🟨 2-079	29.5	80	1.9	2.0	🟨 2-014	20.1	55	1.9	2.5	🟨 2-022	39.5	107	12.3	15.1	🟨 2-134	25.4	69	2.9	3.5	🟨 2-060	18.1	49	2.4	2.5	🟦 2-103	13.0	35	18.5	18.8
	Avg.	26.8	73	1.9	2.0	Avg.	21.6	59	2.8	3.4	Avg.	46.7	127	14.4	17.8	Avg.	28.1	76	2.3	2.8	Avg.	17.5	48	3.8	4.1	Avg.	12.6	34	11.4	11.7
	SD	3.0	8	0.3	0.2	SD	1.3	4	0.8	0.8	SD	6.7	18	2.1	2.3	SD	2.3	6	0.5	0.8	SD	1.9	5	1.5	1.7	SD	0.9	3	8.6	8.7
130	🟦 2-096	24.1	65	15.4	19.5	🟦 2-054	20.7	56	1.9	2.4	2-153	34.0	92	4.6	17.3	🟨 2-018	21.5	58	3.1	3.4	2-072	12.9	35	15.4	16.6	🟨 2-011	8.0	22	0.6	1.0
	🟨 2-066	28.6	78	9.5	15.0	🟦 2-029	16.6	45	2.2	3.0	2-068	70.8	192	19.8	30.0	🟥 2-095	40.5	110	2.6	5.1	🟨 2-063	24.3	66	19.3	19.9	🟨 2-048	11.3	31	3.9	4.3
	🟦 2-040	27.6	75	5.0	6.3	🟦 2-049	11.0	30	0.5	0.8	2-156	34.4	93	7.6	13.8	2-163	26.6	72	2.4	2.6	🟨 2-010	16.2	44	2.2	2.3	🟨 2-039	11.6	32	4.9	6.1
	Avg.	26.8	73	10.0	13.6	Avg.	16.1	44	1.5	2.1	Avg.	46.4	126	10.7	20.4	Avg.	29.5	80	2.7	3.7	Avg.	17.8	48	12.3	12.9	Avg.	10.3	28	3.1	3.8
	SD	2.4	6	5.2	6.7	SD	4.9	13	0.9	1.1	SD	21.1	57	8.1	8.5	SD	9.8	27	0.4	1.3	SD	5.9	16	9.0	9.4	SD	2.0	5	2.3	2.6
160	🟦 2-026	26.3	71	3.4	4.0	🟦 2-028	12.2	33	2.6	3.0	🟨 2-151	27.8	76	1.4	1.8	2-137	24.6	67	1.4	1.8	🟨 2-082	18.0	49	11.7	12.5	🟨 2-024	8.7	24	0.6	1.3
	🟦 2-125	18.6	51	4.6	5.6	🟨 2-038	15.0	41	1.8	2.2	🟨 2-071	56.5	154	20.1	39.0	2-146	20.6	56	2.8	2.9	🟨 2-070	15.5	42	19.9	20.8	🟨 2-127	13.9	38	4.5	6.7
	2-043	19.8	54	5.0	5.4	🟦 2-123	20.5	56	1.4	1.9	🟨 2-160	28.2	77	3.4	5.3	2-157	25.3	69	0.9	4.1	🟨 2-090	14.7	40	5.7	7.1	🟨 2-128	17.3	47	20.0	2.7
	Avg.	21.6	59	4.3	5.0	Avg.	15.9	43	1.9	2.4	Avg.	37.5	102	8.3	15.4	Avg.	23.5	64	1.7	2.9	Avg.	16.1	44	12.4	13.5	Avg.	13.3	36	8.4	3.6
	SD	4.1	11	0.8	0.9	SD	4.2	11	0.6	0.6	SD	16.5	45	10.3	20.5	SD	2.5	7	1.0	1.2	SD	1.7	5	7.1	6.9	SD	4.3	12	10.3	2.8
190	🟨 2-052	18.3	50	15.6	15.6	🟦 2-037	15.2	41	7	8.4	2-133	35.4	96	6.3	9.2	2-073	15.3	42	1.3	11.4	🟨 2-044	8.6	23	8.9	10.1	🟨 2-025	6.2	17	1.9	2.3
	🟦 2-084	19.6	53	11.3	12.1	2-061	8.7	24	1.8	2.6	2-047	53.0	144	16.0	33.1	2-050	22.8	62	1.0	1.3	🟨 2-012	14.9	40	1.5	1.8	🟨 2-051	11.8	32	4.0	7.0
	🟦 2-064	21.2	58	19.2	20	🟨 2-041	16.7	45	2.7	3.2	2-148	42.5	115	2.6	2.9	2-131	16.2	44	0.9	1.2	🟨 2-059	12.0	33	17.6	22.1	🟨 2-055	5.2	14	8.1	11.7
	Avg.	19.7	54	15.4	15.9	Avg.	13.5	37	3.8	4.7	Avg.	43.6	119	8.3	15.1	Avg.	18.1	49	1.1	4.6	Avg.	11.8	32	9.3	11.3	Avg.	7.7	21	4.7	7.0
	SD	1.5	4	4.0	4.0	SD	4.3	12	2.8	3.2	SD	8.9	24	6.9	15.9	SD	4.1	11	0.2	5.9	SD	3.2	9	8.1	10.2	SD	3.6	10	3.2	4.7
220	🟨 2-027	21.1	57	1.9	2.0	🟨 2-098	15.4	42	6.4	8.0	🟨 2-102	47.0	128	3.5	4.6	2-075	2.7	7	2.7	3.0	🟨 2-046	13.6	37	3.4	3.6	🟨 2-092	5.1	14	6.0	7.8
	🟦 2-121	37.3	101	2.2	2.7	🟨 2-085	3.0	8	2.0	2.5	🟨 2-080	51.8	141	5.6	14.6	2-124	15.3	42	0.6	1.1	🟦 2-057	23.5	64	8.1	15.1	🟨 2-101	10.4	28	8.1	15.7
	🟨 2-017	17.0	46	5.9	6.5	🟦 2-053	4.0	11	0.9	1.4	2-162	46.3	126	4.7	8.1	2-165	28.0	76	2.4	4.7	🟦 2-034	8.7	24	1.8	1.8	🟨 2-074	10.4	28	12.3	13.0
	Avg.	25.1	68	3.3	3.7	Avg.	7.5	20	3.1	4.0	Avg.	48.4	131	4.6	9.1	Avg.	15.3	42	1.9	2.9	Avg.	15.3	41	4.4	6.8	Avg.	8.6	23	8.8	12.2
	SD	10.7	29	2.2	2.4	SD	6.9	19	2.9	3.5	SD	3.0	8	1.1	5.1	SD	12.7	34	1.1	1.8	SD	7.5	20	3.3	7.2	SD	3.1	8	3.2	4.0
260	🟨 2-076	26.4	72	5.3	5.3	🟫 2-077	2.1	6	0.9	1.8	🟫 2-058	40.9	111	6.7	9.2	🟫 2-065	11.0	30	0.3	0.6	2-106	16.7	45	2.3	2.4	🟫 2-023	6.6	18	1.6	1.8
	🟨 2-015	16.3	44	1.7	1.8	🟦 2-042	5.4	15	2.0	2.6	🟫 2-078	29.3	80	3.1	4.7	🟫 2-143	19.3	52	2.8	7.0	2-129	18.8	51	2.4	5.1	🟫 2-013	2.7	7	0.9	0.9
	🟦 2-056	25.3	69	6.3	8.2	🟦 2-083	14.8	40	3.2	3.8	🟫 2-016	26.1	71	1.6	2.0	🟫 2-107	20.7	56	0.5	0.8	2-021	23.1	63	1.2	1.5	🟫 2-108	5.5	15	2.3	2.6
	Avg.	22.7	62	4.4	5.1	Avg.	7.4	20	2.0	2.7	Avg.	32.1	87	3.8	5.3	Avg.	17.0	46	1.2	2.8	Avg.	19.5	53	2.0	3.0	Avg.	4.9	13	1.6	1.8
	SD	5.5	15	2.4	3.2	SD	6.6	18	1.2	1.0	SD	7.8	21	2.6	3.6	SD	5.2	14	1.4	3.6	SD	3.3	9	0.7	1.9	SD	2.0	5	0.7	0.9

🟥 Cohesive failure 🟦 Adhesive failure 🟨 Mixed failure 🟫 Thermally degraded or charred

TABLE A.8.—SUMMARY OF TORQUE DATA AT 100 AND 200 °C INCLUDING FAILURE MODE OF THREAD LOCKER CANDIDATES IN #6 JOINT AS A FUNCTION OF AGING TEMPERATURE

Aging *T*, °C	#6 Joint Torque Strengths, N-cm, and % installation torques																													
	Loctite 294 Installation torque = 76.4 N-cm										Resbond 507TS Installation torque = 76.4 N-cm										Poly-Lok PET Installation torque = 76.4 N-cm									
	100 °C					200 °C					100 °C					200 °C					100 °C					200 °C				
	Sample ID	Breakloose		Prevail-ing torque	Maxi-mum torque	Sample ID	Breakloose		Prevail-ing torque	Maxi-mum torque	Sample ID	Breakloose		Prevail-ing torque	Maxi-mum torque	Sample ID	Breakloose		Prevail-ing torque	Maxi-mum torque	Sample ID	Breakloose		Prevail-ing torque	Maxi-mum torque	Sample ID	Breakloose		Prevail-ing torque	Maxi-mum torque
		Torque	% Inst.				Torque	% Inst.				Torque	% Inst.				Torque	% Inst.				Torque	% Inst.				Torque	% Inst.		
23	🟥 6-135	70.2	92	17.1	19.4	🟥 6-002	62.0	81	8.0	12.8	🟥 6-132	93.9	123	12.9	31.8	🟥 6-018	60.9	80	3.4	7.4	🟨 6-233	32.2	42	1.9	2.0	🟨 6-161	57.2	75	2.0	2.3
	🟥 6-005	78.3	102	23.4	24.9	🟥 6-014	49.8	65	8.6	9.4	🟥 6-124	107.2	140	10.9	18.0	🟥 6-180	52.0	68	3.2	8.5	🟨 6-111	54.5	71	2.3	2.4	🟨 6-154	17.1	22	2.4	2.5
	🟥 6-142	76.1	100	18.7	24.7	🟥 6-143	61.0	80	7.6	10.7	🟨 6-138	100.7	132	8.0	13.5	🟥 6-185	56.1	73	3.1	4.1	🟨 6-015	27.4	36	8.5	12.3	🟨 6-158	19.1	25	3.5	3.7
	Avg.	74.9	98	19.7	23.0	Avg.	57.6	75	8.1	11.0	Avg.	100.6	132	10.6	21.1	Avg.	56.3	74	3.2	6.7	Avg.	38.0	50	4.2	5.6	Avg.	31.1	41	2.6	2.8
	SD	4.2	5	3.3	3.1	SD	6.8	9	0.5	1.7	SD	6.7	9	2.5	9.5	SD	4.5	6	0.2	2.3	SD	14.5	19	3.7	5.8	SD	22.6	30	0.8	0.8
130	🟥 6-023	73.7	96	18.2	25.8	🟥 6-168	55.8	73	8.8	15.9	🟥 6-001	113.5	149	25.2	25.4	🟥 6-183	64.7	85	5.0	10.7	🟨 6-164	47.6	62	1.4	1.8	🟨 6-012	79.1	104	2.3	2.5
	🟥 6-152	83.3	109	25.2	33.6	🟥 6-006	63.1	83	8.8	13.1	🟥 6-127	130.9	171	21.9	28.5	🟥 6-184	53.9	71	6.0	8.2	🟨 6-156	40.6	53	2.2	2.7	🟨 6-238	64.5	84	2.6	2.8
	🟥 6-136	82.6	108	19.4	24.4	🟥 6-004	58.5	77	8.5	9.9	🟥 6-191	135.5	177	22.0	42.3	🟥 6-169	65.6	86	4.4	10.9	🟨 6-179	48.7	64	10.2	10.8	🟨 6-029/174	28.4	37	5.3	5.9
	Avg.	79.9	105	20.9	27.9	Avg.	59.1	77	8.7	13.0	Avg.	126.6	166	23.0	32.1	Avg.	61.4	80	5.1	9.9	Avg.	45.6	60	4.6	5.1	Avg.	57.3	75	3.4	3.7
	SD	5.4	7	3.7	5.0	SD	3.7	5	0.2	3.0	SD	11.6	15	1.9	9.0	SD	6.5	9	0.8	1.5	SD	4.4	6	4.9	5.0	SD	26.1	34	1.6	1.9
160	🟥 6-157	85.0	111	25.5	42.2	🟥 6-149	62.2	81	6.1	7.8	🟥 6-119	140.0	183	9.3	27.6	🟥 6-188	62.9	82	4.0	7.5	🟨 6-214	57.2	75	1.4	1.9	🟨 6-116	50.6	66	2.3	2.4
	🟥 6-114	86.8	114	24.5	36.9	🟥 6-150	61.5	80	6.0	12.2	🟥 6-207	128.7	168	12.9	15.4	🟥 6-187	59.6	78	4.0	8.5	🟨 6-171	42.2	55	2.9	3.0	🟨 6-234	65.2	85	2.2	2.4
	🟥 6-128	71.7	94	27.0	39.4	🟥 6-120	56.8	74	11.4	15.4	🟥 6-125	121.7	159	15.9	20.0	🟥 6-110	62.0	81	3.0	10.6	🟨 6-190	50.8	66	2.6	5.1	🟨 6-253	53.1	70	8.7	9.3
	Avg.	81.2	106	25.7	39.5	Avg.	60.2	79	7.8	11.8	Avg.	130.1	170	12.7	21.0	Avg.	61.5	80	3.7	8.9	Avg.	50.1	66	2.3	3.3	Avg.	56.3	74	4.4	4.7
	SD	8.2	11	1.3	2.7	SD	2.9	4	3.1	3.8	SD	9.2	12	3.3	6.2	SD	1.7	2	0.6	1.6	SD	7.5	10	0.8	1.6	SD	7.8	10	3.7	4.0
190	🟥 6-118	78.5	103	25.9	39.3	🟥 6-153	67.4	88	13.0	13.4	🟥 6-016	109.5	143	9.8	20.9	🟫 6-173	56.6	74	2.2	3.5	🟨 6-249	71.2	93	2.4	2.4	🟨 6-133	79.9	105	1.9	2.5
	🟥 6-109	79.7	104	7.9	10.1	🟥 6-028	68.2	89	6.5	10.2	🟥 6-181	110.1	144	7.1	19.6	🟫 6-003	57.8	76	2.0	3.3	🟨 6-010	61.1	80	1.6	1.7	🟨 6-131	68.6	90	2.1	2.5
	🟥 6-008	80.2	105	23.0	23.1	🟥 6-203	63.7	83	7.4	10.6	🟥 6-030	108.9	143	5.8	12.9	🟫 6-159	67.1	88	2.2	7	🟨 6-112	32.9	43	6.3	9.9	🟨 6-210	28.9	38	3.7	3.9
	Avg.	79.5	104	18.9	24.2	Avg.	66.4	87	9.0	11.4	Avg.	109.5	143	7.6	17.8	Avg.	60.5	79	2.1	4.6	Avg.	55.1	72	3.4	4.7	Avg.	59.1	77	2.6	3.0
	SD	0.9	1	9.7	14.6	SD	2.4	3	3.5	1.7	SD	0.6	1	2.0	4.3	SD	5.7	8	0.1	2.1	SD	19.9	26	2.5	4.5	SD	26.8	35	1.0	0.8
220	🟥 6-011	81.2	106	18.9	20.2	6-147	64.1	84	8.4	10.6	🟫 6-170	97.1	127	5.0	7.5	6-009	53.5	70	2.0	2.4	🟨 6-223	51.7	68	2.1	2.1	🟨 6-121	66.1	87	0.6	1.2
	🟥 6-195	79.4	104	23.1	25.2	6-129	66.4	87	6.1	9.0	~~6-165~~					6-017	62.4	82	2.3	2.4	🟨 6-024	57.9	76	2.5	2.7	🟨 6-122	32.8	43	15.2	17.3
	🟥 6-130	69.7	91	19.6	29.7	6-250	59.8	78	7.4	11.8	🟫 6-194	88.8	116	4.7	7.9	6-134	65.8	86	2.2	2.7	🟨 6-160/165	49.3	65	7.9	9.1	🟨 6-239	53.7	70	6.7	7.4
	Avg.	76.8	100	20.5	25.0	Avg.	63.4	83	7.3	10.5	Avg.	93.0	122	4.9	7.7	Avg.	60.6	79	2.2	2.5	Avg.	49.8	65	5.8	7.2	Avg.	50.9	67	7.5	8.6
	SD	6.2	8	2.3	4.8	SD	3.4	4	1.2	1.4	SD	5.9	8	0.2	0.3	SD	6.4	8	0.2	0.2	SD	4.4	6	3.2	3.9	SD	16.8	22	7.3	8.1
260	🟫 6-013	77.6	102	3.7	3.7	🟫 6-126	70.9	93	0.7	1.0	🟫 6-193	108.0	141	6.7	9.6	🟫 6-115	62.2	81	13.8	14.8	🟫 6-231	70.3	92	1.4	1.8	🟫 6-226	53.3	70	1.1	1.4
	🟫 6-189	72.3	95	2.3	2.8	🟫 6-145	45.3	59	3.7	5.5	🟫 6-148	92.0	120	2.9	8.2	🟫 6-196	71.2	93	1.2	1.6	🟫 6-236	43.7	57	1.8	2.3	🟫 6-146	19.2	25	3.6	3.7
	🟫 6-007					🟫 6-155	62.6	82	1.4	2.0	🟫 6-139	78.3	102	1.9	3.6	🟫 6-176	68.9	90	0.6	3.9	🟫 6-213	36.8	48	3.8	3.8	🟫 6-237	33.2	43	2.6	3.4
	Avg.	75.0	98	3.0	3.3	Avg.	59.6	78	1.9	2.8	Avg.	92.8	121	3.8	7.1	Avg.	67.4	88	5.2	6.8	Avg.	50.3	66	2.3	2.6	Avg.	35.2	46	2.4	2.8
	SD	3.7	5	1.0	0.6	SD	13.1	17	1.6	2.4	SD	14.9	19	2.5	3.1	SD	4.7	6	7.5	7.1	SD	17.7	23	1.3	1.0	SD	17.1	22	1.3	1.3

🟥 Cohesive failure 🟦 Adhesive failure 🟨 Mixed failure 🟫 Thermally degraded or charred

TABLE A.9.—SUMMARY OF TORQUE DATA AT 100 AND 200 °C INCLUDING FAILURE MODE OF THREAD LOCKER CANDIDATES IN #8 JOINT AS A FUNCTION OF AGING TEMPERATURE

Aging *T*, °C	#8 Joint Torque Strengths, N-cm, and % installation torques																													
	Loctite 294 Installation torque = 13.03 N-cm										Resbond 507TS Installation torque = 13.03 N-cm										Poly-Lok PET Installation torque = 32.00 N-cm									
	100 °C					200 °C					100 °C					200 °C					100 °C					200 °C				
	Sample ID	Breakloose		Prevail-ing torque	Maxi-mum torque	Sample ID	Breakloose		Prevail-ing torque	Maxi-mum torque	Sample ID	Breakloose		Prevail-ing torque	Maxi-mum torque	Sample ID	Breakloose		Prevail-ing torque	Maxi-mum torque	Sample ID	Breakloose		Prevail-ing torque	Maxi-mum torque	Sample ID	Breakloose		Prevail-ing torque	Maxi-mum torque
		Torque	% Inst.				Torque	% Inst.				Torque	% Inst.				Torque	% Inst.				Torque	% Inst.				Torque	% Inst.		
23	🟥 8-137	13.8	106	19.8	25.9	🟥 8-121	15.5	119	9.4	10.0	🟥 8-190	43.6	335	0.6	41.8	🟥 8-243	29.4	226	4.1	5.6	🟨 8-010	11.8	37	5.3	7.5	🟨 8-179	11.9	37	2.0	2.8
	🟥 8-184	13.7	105	8.8	9.0	🟥 8-139	15.7	120	13.0	13.3	🟥 8-113	48.6	373	32.7	49.6	🟨 8-255	28.4	218	3.6	4.9	🟨 8-174	9.2	29	2.5	3.3	🟨 8-123	12.1	38	0.8	1.4
	🟥 8-122	17.5	134	29.9	37.3	🟥 8-134	16.3	125	11.0	11.1	🟦 8-239	34.9	268	13.2	15.6	🟨 8-169	25.8	198	3.6	5.8	🟨 8-024	8.8	28	7.7	7.7	🟨 8-183	11.7	37	1.5	1.7
	Avg.	15.0	115	19.5	24.1	Avg.	15.8	122	11.1	11.5	Avg.	42.4	325	15.5	35.7	Avg.	27.9	214	3.8	5.4	Avg.	9.9	31	5.2	6.2	Avg.	11.9	37	1.4	2.0
	SD	2.2	17	10.6	14.2	SD	0.4	3	1.8	1.7	SD	6.9	53	16.2	17.8	SD	1.9	14	0.3	0.5	SD	1.6	5	2.6	2.5	SD	0.2	1	0.6	0.7
130	🟥 8-221	18.3	140	43.3	43.3	🟥 8-168	17.4	134	13.3	14.8	🟥 8-180	54.4	417	1.6	47.6	🟥 8-111	34.5	265	4.5	8.2	🟨 8-127	13.0	41	8.3	11.0	🟨 8-182	10.5	33	6.1	7.1
	🟥 8-144	6.9	53	1.6	42.3	🟥 8-011	18.3	140	16.2	16.2	🟥 8-225	57.7	443	1.4	51.7	🟥 8-232	30.5	234	9.2	10.2	🟨 8-210	11.5	36	4.3	4.5	🟨 8-152	12.4	39	4.8	5.2
	🟥 8-195	19.1	147	43.1	43.1	🟥 8-185	15.8	121	12.5	12.5	🟥 8-241	61.7	474	1.2	54.1	🟥 8-163	23.3	179	7.2	8.9	🟨 8-114	17.2	54	8.6	9.5	🟦 8-217				
	Avg.	14.8	113	29.3	42.9	Avg.	17.2	132	14.0	14.5	Avg.	57.9	445	1.4	51.1	Avg.	29.4	226	7.0	9.1	Avg.	13.9	43	7.1	8.3	Avg.	11.5	36	5.5	6.2
	SD	6.8	52	24.0	0.5	SD	1.3	10	1.9	1.9	SD	3.7	28	0.2	3.3	SD	5.7	44	2.4	1.0	SD	3.0	9	2.4	3.4	SD	1.3	4	0.9	1.3
160	🟥 8-131	21.7	167	1.3	47.1	🟥 8-129	14.4	111	28.9	31.7	🟥 8-172	52.2	401	1.2	42.7	🟥 8-235					🟨 8-138	11.9	37	10.6	12.6	🟨 8-220	12.9	40	6.1	6.5
	🟥 8-165	22.4	172	1.3	51.4	🟥 8-016	20.8	160	22.0	23.7	🟥 8-244	58.3	447	1.4	51.3	🟥 8-230	41.0	315	17.3	23.6	🟨 8-196	14.9	47	5.5	6.1	🟨 8-199	15.1	47	4.9	5.5
	🟥 8-150	23.9	183	1.2	48.9	🟥 8-115	17.3	133	20.2	24.6	🟥 8-250	48.1	369	42.1	46.4	🟥 8-167	30.5	234	10.1	14.0	🟨 8-012	15.7	49	12.9	13.5	🟨 8-028	16.8	53	5.5	6.3
	Avg.	22.7	174	1.3	49.1	Avg.	17.5	134	23.7	26.7	Avg.	52.9	406	14.9	46.8	Avg.	35.8	274	13.7	18.8	Avg.	14.2	44	9.7	10.7	Avg.	14.9	47	5.5	6.1
	SD	1.1	9	0.1	2.2	SD	3.2	25	4.6	4.4	SD	5.1	39	23.6	4.3	SD	7.4	57	5.1	6.8	SD	2.0	6	3.8	4.0	SD	2.0	6	0.6	0.5
190	🟥 8-030	16.5	127	1.3	51.0	🟥 8-118	15.4	118	40.8	50.0	🟥 8-216					🟥 8-236	17.9	137	3.9	6.1	🟨 8-029	15.2	48	7.2	8.4	🟨 8-211	7.7	24	6.7	10.0
	🟥 8-014	20.7	159	1.6	46.4	🟥 8-008	16.4	126	30.8	33.7	🟥 8-234					🟥 8-240	20.9	160	4.9	8.4	🟨 8-215	11.1	35	13.1	15.0	🟨 8-200	11.6	36	5.0	6.7
	🟥 8-133	16.4	126	50.4	53.0	🟥 8-005	14.9	114	26.0	27.5	🟥 8-156					🟥 8-256					🟨 8-119	9.7	30	12.9	14.0	🟨 8-209	21.6	68	8.0	9.8
	Avg.	17.9	137	17.8	50.1	Avg.	15.6	119	32.5	37.1	Avg.					Avg.	19.4	149	4.4	7.3	Avg.	12.0	38	11.1	12.5	Avg.	13.6	43	6.6	8.8
	SD	2.5	19	28.3	3.4	SD	0.8	6	7.6	11.6	SD					SD	2.1	16	0.7	1.6	SD	2.9	9	3.4	3.6	SD	7.2	22	1.5	1.9
220	🟥 8-223	22.4	172	44.7	45.3	🟥 8-015	15.3	117	23.3	31.5	🟫 8-125	49.6	381	15.5	21.3	🟫 8-158	18.5	142	2.4	2.9	🟨 8-025	12.0	38	13.9	18.2	🟨 8-187	14.1	44	8.2	9.3
	🟥 8-177	28.8	221	1.5	45.5	🟥 8-013	19.1	147	29.7	31.2	🟫 8-237	39.9	306	8.6	12.2	🟫 8-233	16.6	127	2.7	3.1	🟨 8-132	7.5	23	4.2	4.6	🟨 8-218	16.5	52	9.2	12.2
	🟥 8-018	20.3	156	2.2	55.9	🟥 8-189	15.5	119	27.5	31.5	🟫 8-141	54.7	420	27.0	28.6	🟫 8-178	16.0	123	2.9	3.1	🟨 8-198	30.7	96	2.5	2.7	🟨 8-112	12.4	39	4.7	4.9
	Avg.	23.8	183	16.1	48.9	Avg.	16.6	128	26.8	31.4	Avg.	48.1	369	17.0	20.7	Avg.	17.0	131	2.7	3.0	Avg.	16.7	52	6.9	8.5	Avg.	14.3	45	7.4	8.8
	SD	4.4	34	24.7	6.1	SD	2.1	16	3.3	0.2	SD	7.5	58	9.3	8.2	SD	1.3	10	0.3	0.1	SD	12.3	38	6.2	8.5	SD	2.1	6	2.4	3.7
260	🟫 8-120	44.5	342	25.0	26.6	🟫 8-110	25.3	194	7.9	8.8	🟫 8-155	39.0	299	2.5	3.9	🟫 8-128	38.2	293	4.8	6.8	🟫 8-140	24.4	76	5.7	6.9	🟫 8-193	6.6	21	6.2	8.0
	🟫 8-020	35.7	274	19.4	21.2	🟫 8-194	21.7	167	12.6	14.0	🟫 8-154	38.3	294	2.7	6.1	🟫 8-160	33.0	253	2.2	3.4	🟫 8-151	8.7	27	3.3	3.8	🟫 8-213	3.2	10	4.6	5.4
	🟫 8-176	48.0	368	27.8	28.0	🟫 8-136	20.5	157	13.3	14.9	🟫 8-214	37.4	287	5.0	7.2	🟫 8-224	34.8	267	3.0	4.7	🟫 8-204	13.4	42	12.8	14.4	🟫 8-126	8.6	27	4.0	4.1
	Avg.	42.7	328	24.1	25.3	Avg.	22.5	173	11.3	12.6	Avg.	38.2	293	3.4	5.7	Avg.	35.3	271	3.3	5.0	Avg.	15.5	48	7.3	8.4	Avg.	6.1	19	4.9	5.8
	SD	6.3	49	4.3	3.6	SD	2.5	19	2.9	3.3	SD	0.8	6	1.4	1.7	SD	2.6	20	1.3	1.7	SD	8.1	25	4.9	5.5	SD	2.7	9	1.1	2.0

🟥 Cohesive failure 🟦 Adhesive failure 🟨 Mixed failure 🟫 Thermally degraded or charred

TABLE A.10.—OVERALL TEST MATRIX FOR 6-MONTH ACCELERATED THERMAL AGING TESTS OF ADHESIVE/POTTING CANDIDATES

Aging *T*, °C	Aging t, day			0: Controls							15							50						
	Sample	Test *T*, °C	Organics	1/23/14 2:00 p.m.							2/7/14 2:00 p.m.							3/18/14 2:00 a.m.						
175 (347 °F) Lunaire, R145	Epoxy thick sheet		AF131-2	A1	A2	A3	A4	A5	A6	A43-45	A7	A8	A9					A16	A17	A18				
			Hysol C-2	H1	H2	H3	H4	H5	H6		H7	H8	H9					H16	H17	H18				
	Epoxy lamination		AF131-2	1-2	27-28	53-54					3-4	29-30						9-10	35-36					
			Hysol C-2	61-62	87-88	113-114					63-64	89-90						69-70	95-96					
	Epoxy sandwich lap shear																							
	Static	23	AF131-2	A6A1	A7B14	A8A14	A9A14	A11A8	A12A9	A13B7	A6A2	A7B15	A8A15	A9A15	A11A9	A12A10	A13B8	A6A3	A7B16	A8A16	A9A16	A11A10	A12A11	A13B9
			Hysol C-2	C7A1	C8B18	C9A14	C10B14	C12B8	C13B1	C15B22	C7A2	C8B19	C9A15	C10B15	C12B9	C13B4	C15B23	C7A3	C8B20	C9A16	C10B16	C12B10	C13B7	C15B24
		150	AF131-2	A6A14	A7B27	A8A27	A9A27	A11A21	A12A14	A14A9	A6A15	A7B28	A8A28	A9A28	A11A22	A12A15	A14A11	A6A16	A7B29	A8A29	A9A29	A11A23	A12A16	A14A13
			Hysol C-2	C7A14	C8B31	C9A27	C10B27	C12B21	C13B2	C16A17	C7A15	C8B32	C9A28	C10B28	C12B22	C13B5	C16A15	C7A16	C8B33	C9A29	C10B29	C12B23	C13B8	C16A13
		200	AF131-2	A7B1	A8A1	A9A1	A9A39	A11A34	A12A27	A14A10	A7B2	A8A2	A9A2	A9A40	A11A35	A12A28	A14A12	A7B3	A8A3	A9A3	A9A41	A11A36	A12A29	A14A14
			Hysol C-2	C8B5	C9A1	C10B1	C10B39	C12B34	C13B3	C16A18	C8B6	C9A2	C10B2	C10B40	C12B35	C13B6	C16A16	C8B7	C9A3	C10B3	C10B41	C12B36	C13B9	C16A14
	Fatigue	175	AF131-2	A9B1 A10B40	A9B14 A11B9	A9B27 A11B18	A9B40 A11B31	A10B1 A12B17	A10B14 A12B18	A10B27 A12B32	A9B2 A10B41	A9B15 A11B10	A9B28 A11B17	A9B41 A11B32	A10B2 A12B19	A10B15 A12B20	A10B28 A12B33	A9B3 A10B42	A9B16 A11B11	A9B29 A11B16	A9B42 A11B33	A10B3 A12B21	A10B16 A12B22	A10B29 A12B34
			Hysol C-2	C11A1 C11B40	C11A14 C14A9	C11A27 C14A22	C11A40 C14A23	C11B1 C14A44	C11B14 C15B17	C11B27 C16A39	C11A2 C11B41	C11A15 C14A10	C11A28 C14A24	C11A41 C14A43	C11B2 C15A9	C11B15 C15B18	C11B28 C16A38	C11A3 C11B42	C11A16 C14A11	C11A29 C14A25	C11A42 C14A42	C11B3 C15A10	C11B16 C15B19	C11B29 C16A37
200 (392 °F) Blue M, #5, R244	Epoxy thick sheet		AF131-2								A10	A11	A12					A19	A20	A21				
			Hysol C-2								H10	H11	H12					H19	H20	H21				
	Epoxy lamination		AF131-2								5-6	31-32						11-12	37-38					
			Hysol C-2								65-66	91-92						71-72	97-98					
	Epoxy sandwich lap shear																							
	Static	23	AF131-2	A12A44	A13B22	A13B23	A13B24	A14A29	A14A30	A14A31	A6A6	A7B19	A8A19	A9A19	A11A13	A12A5	A13B14	A6A7	A7B20	A8A20	A9A20	A11A14	A12A6	A13B15
			Hysol C-2	C13B43	C13B44	C15A18	C15B36				C7A6	C8B23	C9A19	C10B19	C12B13	C13B16	C15B27	C7A7	C8B24	C9A20	C10B20	C12B14	C13B19	C15B28
		150	AF131-2								A6A19	A7B32	A8A32	A9A32	A11A26	A12A19	A14A19	A6A20	A7B7	A9A7	A11A1	A11A40	A12A24	A14A22
			Hysol C-2								C7A19	C8B36	C9A32	C10B32	C12B26	C13B17	C16A7	C7A20	C8B37	C9A33	C10B33	C12B27	C13B20	C16A5
		200	AF131-2								A7B6	A8A6	A9A6	A9A44	A11A39	A12A23	A14A19	A6A20	A7B33	A8A33	A9A33	A11A27	A12A20	A14A21
			Hysol C-2								C8B10	C9A6	C10B6	C10B44	C12B39	C13B18	C16A8	C8B11	C9A7	C10B7	C12B1	C12B40	C13B21	C16A6
	Fatigue	175	AF131-2								A9B6 A11B19	A9B19 A11B30	A9B32 A6B27	A10B6 A12B9	A10B19 A12B10	A10B32 A12B37	A11B1 A12B38	A9B7 A11B20	A9B20 A11B29	A9B33 A6A28	A10B7 A6B40	A10B20 A12B12	A10B33 A12B39	A11B2 A12B40
			Hysol C-2								C11A6 C14A14	C11A19 C14A28	C11A32 C14A35	C11B6 C15B4	C11B19 C15A1	C11B32 C15B13	C14A1 C16A34	C11A7 C14A16	C11A20 C14A29	C11A33 C14A34	C11B7 C15B5	C11B20 C15A2	C11B33 C15B14	C14A2 C16A33
225 (437 °F) Blue M, #6, R244	Epoxy thick sheet		AF131-2								A13	A14	A15					A22	A23	A24				
			Hysol C-2								H13	H14	H15					H22	H23	H24				
	Epoxy lamination		AF131-2								7-8	33-34						13-14	39-40					
			Hysol C-2								67-68	93-94						73-74	99-100					
	Epoxy sandwich lap shear																							
	Static	23	AF131-2	A13B25	A13B26	A14A32	A14A33				A6A10	A7B23	A8A23	A9A23	A11A17	A12A1	A13B12	A6A11	A7B24	A8A24	A9A24	A11A18	A12A2	A13B13
			Hysol C-2								C7A10	C8B27	C9A23	C10B23	C12B17	C13B28	C15B31	C7A11	C8B28	C9A24	C10B24	C12B18	C13B31	C15B32
		150	AF131-2								A6A23	A7B36	A8A36	A9A36	A11A30	A12A32	A14A4	A6A24	A7B37	A8A37	A9A37	A11A31	A12A33	A14A3
			Hysol C-2								C8B1	C8B40	C9A36	C10B36	C12B30	C13B29	C16A19	C8B2	C8B41	C9A37	C10B37	C12B31	C13B32	C16A21
		200	AF131-2								A7B10	A8A10	A9A10	A11A4	A11A43	A12A36	A14A5	A7B11	A8A11	A9A11	A11A5	A11A44	A12A37	A14A6
			Hysol C-2								C8B14	C9A10	C10B10	C12B4	C12B43	C13B30	C16A20	C8B15	C9A11	C10B11	C12B5	C12B44	C13B33	C16A22
	Fatigue	175	AF131-2								A9B10 A11B26	A9B23 A11B39	A9B36 A6A29	A10B10 A12B1	A10B23 A12B2	A10B36 A12B27	A11B5 A12B28	A9B11 A11B25	A9B24 A11B38	A9B37 A12B3	A10B11 A12B4	A10B24 A12B29	A10B37 A13B1	A11B6 A13B4
			Hysol C-2								C11A10 C14A15	C11A23 C14A39	C11A36 C15B5	C11B10 C15A5	C11B23 C15A13	C11B36 C15B9	C14A5 C16A30	C11A11 C14A17	C11A24 C14A38	C11A37 C15B6	C11B11 C15A6	C11B24 C15A14	C11B37 C15B10	C14A6 C16A29

TABLE A.10.—OVERALL TEST MATRIX FOR 6-MONTH ACCELERATED THERMAL AGING TESTS OF ADHESIVE/POTTING CANDIDATES

Aging *T*, °C	Aging t, day			99							174						
	Sample	Test *T*, °C	Organics	5/7/14 2:00 a.m.							7/24/14 2:00 a.m.						
175 (347 °F)	Epoxy thick sheet		AF131-2	A25	A26	A27					A34	A35	A36				
			Hysol C-2	H25	H26	H27					H34	H35	H36	H43			
	Epoxy lamination		AF131-2	15-16	41-42						21-22	47-48	55-56				
			Hysol C-2	75-76	101-102						81-82	107-108	115-116				
Lunaire, R145	Epoxy sandwich lap shear																
	Static	23	AF131-2	A6A4	A7B17	A8A17	A9A17	A11A11	A12A12	A13B10	A6A5	A7B18	A8A18	A9A18	A11A12	A12A13	A13B11
			Hysol C-2	C7A4	C8B21	C9A17	C10B17	C12B11	C13B10	C15B25	C7A5	C8B22	C9A18	C10B18	C12B12	C13B13	C15B26
		150	AF131-2	A6A17	A7B30	A8A30	A9A30	A11A24	A12A17	A14A15	A6A18	A7B31	A8A31	A9A31	A11A25	A12A18	A14A17
			Hysol C-2	C7A17	C8B34	C9A30	C10B30	C12B24	C13B11	C16A11	C7A18	C8B35	C9A31	C10B31	C12B25	C13B14	C16A9
		200	AF131-2	A7B4	A8A4	A9A4	A9A42	A11A37	A12A30	A14A16	A7B5	A8A5	A9A5	A9A43	A11A38	A12A31	A14A18
			Hysol C-2	C8B8	C9A4	C10B4	C10B42	C12B37	C13B12	C16A12	C8B9	C9A5	C10B5	C10B43	C12B38	C13B15	C16A10
	Fatigue	175	AF131-2	A9B4 A10B43	A9B17 A11B12	A9B30 A11B15	A9B43 A11B34	A10B4 A12B23	A10B17 A12B24	A10B30 A12B35	A9B5 A10B44	A9B18 A11B13	A9B31 A11B14	A9B44 A11B35	A10B5 A12B25	A10B18 A12B26	A10B31 A12B36
			Hysol C-2	C11A4 C11B43	C11A17 C14A12	C11A30 C14A26	C11A43 C14A41	C11B4 C15A11	C11B17 C15B20	C11B30 C16A36	C11A5 C11B44	C11A18 C14A13	C11A31 C14A27	C11A44 C14A40	C11B5 C15A12	C11B18 C15B21	C11B31 C16A35
200 (392 °F)	Epoxy thick sheet		AF131-2	A28	A29	A30					A37	A38	A39				
			Hysol C-2	H28	H29	H30					H37	H38	H39	H44			
	Epoxy lamination		AF131-2	17-18	43-44						23-24	49-50	57-58				
			Hysol C-2	77-78	103-104						83-84	109-110	117-118				
Blue M, #5, R244	Epoxy sandwich lap shear																
	Static	23	AF131-2	A6A8	A7B21	A8A21	A9A21	A11A15	A12A7	A13B18	A6A9	A7B22	A8A22	A9A22	A11A16	A12A8	A13B19
			Hysol C-2	C7A8	C8B25	C9A21	C10B21	C12B15	C13B22	C15B29	C7A9	C8B26	C9A22	C10B22	C12B16	C13B25	C15B30
		150	AF131-2	A6A21	A7B34	A8A34	A9A34	A11A28	A12A21	A14A23	A6A22	A7B35	A8A35	A9A35	A11A29	A12A22	A14A25
			Hysol C-2	C7A21	C8B38	C9A34	C10B34	C12B28	C13B23	C16A3	C7A22	C8B39	C9A35	C10B35	C12B29	C13B26	C16A1
		200	AF131-2	A7B8	A8A8	A9A8	A11A2	A11A41	A12A25	A14A24	A7B9	A8A9	A9A9	A11A3	A11A42	A12A26	A14A26
			Hysol C-2	C8B12	C9A8	C10B8	C12B2	C12B41	C13B24	C16A6	C8B13	C9A9	C10B9	C12B3	C12B42	C13B27	C16A2
	Fatigue	175	AF131-2	A9B8 A11B21	A9B21 A11B28	A9B34 A11B41	A10B8 A12B13	A10B21 A12B14	A10B34 A12B41	A11B3 A12B42	A9B9 A11B22	A9B22 A11B27	A9B35 A11B40	A10B9 A12B15	A10B22 A12B16	A10B35 A12B35	A11B4 A12B44
			Hysol C-2	C11A8 C14A18	C11A21 C14A30	C11A34 C14A33	C11B8 C15B2	C11B21 C15A3	C11B34 C15B15	C14A3 C16A32	C11A9 C14A20	C11A22 C14A31	C11A35 C14A32	C11B9 C8B44	C11B22 C15A4	C11B35 C15B16	C14A4 C16A31
225 (437 °F)	Epoxy thick sheet		AF131-2	A31	A32	A33					A40	A41	A42				
			Hysol C-2	H31	H32	H33					H40	H41	H42	H45			
	Epoxy lamination		AF131-2	19-20	45-46						25-26	51-52	59-60				
			Hysol C-2	79-80	105-106						85-86	111-112	119-120				
Blue M, #6, R244	Epoxy sandwich lap shear																
	Static	23	AF131-2	A6A12	A7B25	A8A25	A9A25	A11A19	A12A3	A13B16	A6A13	A7B26	A8A26	A9A26	A11A20	A12A4	A13B17
			Hysol C-2	C7A12	C8B29	C9A25	C10B25	C12B19	C13B34	C15B33	C7A13	C8B30	C9A26	C10B26	C12B20	C13B38	C15B34
		150	AF131-2	A6A25	A7B38	A8A38	A9A38	A11A32	A12A34	A14A2	A6A26	A7B39	A8A39	A8A40	A11A33	A12A35	A14A1
			Hysol C-2	C8B3	C8B42	C9A38	C10B38	C12B32	C13B35	C16A23	C8B4	C8B43	C9A39	C9A40	C12B33	C13B39	C16A25
		200	AF131-2	A7B12	A8A12	A9A12	A11A6	A12A38	A12A39	A14A7	A7B13	A8A13	A9A13	A11A7	A12A40	A12A41	A14A8
			Hysol C-2	C8B16	C9A12	C10B12	C12B6	C13B36	C13B37	C16A24	C8B17	C9A13	C10B13	C12B7	C13B40	C13B41	C16A26
	Fatigue	175	AF131-2	A9B12 A11B24	A9B25 A11B37	A9B38 A12B5	A10B12 A12B6	A10B25 A12B30	A10B38 A13B2	A11B7 A13B5	A9B13 A11B23	A9B26 A11B36	A9B39 A12B7	A10B13 A12B8	A10B26 A12B31	A10B39 A13B3	A11B8 A13B6
			Hysol C-2	C11A12 C14A19	C11A25 C14A37	C11A38 C15B7	C11B12 C15A7	C11B25 C15A15	C11B38 C15B11	C14A7 C16A28	C11A13 C14A21	C11A26 C14A36	C11A39 C15B8	C11B13 C15A8	C11B26 C15A16	C11BA39 C15B12	C14A8 C16A27

TABLE A.11.—SUMMARY OF STATIC LAP SHEAR BONDING PROPERTIES OF ADHESIVE CANDIDATES AFTER ACCELERATED THERMAL AGING TESTS

3M AF131-2 Film adhesive

Lap shear property			Bond strength, psi					Strain term $(\delta l/h/t)$-to-failure, in.$^{-1}$				
Test temp.	Aging T, °C	Aging t, day	0	15	50	99	174	0	15	50	99	174
23 °C (74 °F)	175	Avg.	1467	1160	456	782	862	8.1	5.5	4.0	5.1	4.7
		SD	375	386	219	302	248	2.0	1.1	1.3	0.9	1.5
		Δ%		–21	–69	–47	–41		–32	–51	–37	–42
	200	Avg.	1467	558	338	446	571	8.1	4.2	2.0	3.1	3.5
		SD	375	243	161	25	23	2.0	2.7	1.2	1.0	1.2
		Δ%		–62	–77	–70	–61		–48	–75	–62	–56
	225	Avg.	1467	342	257	24	20	8.1	3.4	3.5	1.5	2.8
		SD	375	243	161	25	23	2.0	1.3	1.6	1.2	2.7
		Δ%		–77	–83	–98	–99		–57	–57	–81	–66
150 °C (302 °F)	175	Avg.	1195	1192	976	721	634	6.7	5.8	7.7	4.8	7.3
		SD	316	222	204	240	474	1.2	1.4	1.9	1.2	2.3
		Δ%		–51	–67	–66	–67		–12	–16	–28	–9
	200	Avg.	1195	580	392	404	399	6.7	3.9	4.3	4.1	3.7
		SD	316	348	285	293	368	1.2	1.1	1.3	1.2	1.7
		Δ%		–51	–67	–66	–67		–41	–35	–38	–44
	225	Avg.	1195	485	92	14	17	6.7	2.8	4.5	4.6	4.4
		SD	316	249	106	10	15	1.2	1.0	1.8	3.5	4.7
		Δ%		–59	–92	–99	–99		–59	–32	–31	–35
200 °C (392 °F)	175	Avg.	1208	960	919	632	665	6.7	5.3	7.1	5.3	5.7
		SD	283	263	296	303	200	1.3	2.1	2.4	1.6	1.6
		Δ%		–20	–24	–48	–45		–21	7	–21	–14
	200	Avg.	1208	533	304	326	334	6.7	3.0	4.4	4.0	4.1
		SD	283	303	223	257	241	1.3	1.1	0.9	0.8	1.4
		Δ%		–56	–75	–73	–72		–54	–34	–40	–38
	225	Avg.	1208	708	80	26	18	6.7	4.2	4.4	1.8	1.8
		SD	283	364	65	6	13	1.3	2.3	1.8	0.4	1.4
		Δ%		–41	–93	–98	–99		–37	–33	–73	–73

Hysol EA9394C-2 Epoxy paste

Lap shear property			Bond strength, psi					Strain term $(\delta l/h/t)$-to-failure, in.$^{-1}$				
Test temp.	Aging T, °C	Aging t, day	0	15	50	99	174	0	15	50	99	174
23 °C (74 °F)	175	Avg.	1517	1251	1156	1118	1130	7.3	5.7	6.5	7.1	5.4
		SD	412	216	219	194	305	2.1	0.8	0.8	1.9	1.2
		Δ%		–17	–24	–26	–26		–22	–11	–3	–26
	200	Avg.	1517	1173	1242	1057	1070	7.3	4.1	7.1	6.1	5.2
		SD	412	296	272	248	473	2.1	0.3	2.0	2.0	0.8
		Δ%		–23	–18	–30	–29		–44	–3	–17	–29
	225	Avg.	1517	1240	1120	1022	958	7.3	6.3	7.2	5.4	5.6
		SD	412	189	295	221	285	2.1	1.5	1.7	1.2	1.9
		Δ%		–18	–26	–33	–37		–13	–2	–26	–24
150 °C (302 °F)	175	Avg.	917	1121	1014	944	855	7.0	6.4	6.8	7.7	7.4
		SD	378	145	206	197	271	1.8	1.2	1.4	1.9	2.5
		Δ%		22	11	3	–7		–9	–3	10	5
	200	Avg.	917	1113	1091	1206	1013	7.0	5.3	6.9	9.4	7.3
		SD	378	153	125	243	281	1.8	0.7	0.8	1.9	2.0
		Δ%		21	19	31	10		–25	–2	34	3
	225	Avg.	917	1143	1038	1052	1091	7.0	10.4	10.9	10.7	7.5
		SD	378	136	168	178	223	1.8	3.7	2.4	2.2	1.5
		Δ%		25	13	15	19		47	54	52	6
200 °C (392 °F)	175	Avg.	360	917	558	397	299	4.0	6.4	5.3	4.5	3.9
		SD	148	168	197	205	201	0.8	1.5	1.8	2.0	1.9
		Δ%		155	55	10	–17		60	32	11	–3
	200	Avg.	360	727	416	312	193	4.0	4.5	5.7	4.5	3.6
		SD	148	132	299	224	162	0.8	1.3	1.2	0.4	1.7
		Δ%		40	15	–13	–46		12	43	13	–10
	225	Avg.	360	460	289	191	290	4.0	4.9	4.8	3.9	3.9
		SD	148	113	114	194	238	0.8	2.1	1.4	3.1	1.9
		Δ%		28	–20	–47	–20		23	19	–3	–2

TABLE A.12.—SUMMARY OF FATIGUE LAP SHEAR BONDING PROPERTIES AT 175 °C OF ADHESIVE CANDIDATES AFTER ACCELERATED THERMAL AGING TEST

Aging *t*, day		0	15	50	100	180	0	15	50	100	180	0	15	50	100	180	0	15	50	100	180
Epoxy	Aging *T*, °C	Fatigue strength, psi					Fatigue to static strength ratio					Residual to static strength ratio					Residual to fatigue strength ratio				
AF131-2	175	470	500	280	290	320	0.39	0.46	0.29	0.43	0.50	0.57	0.60	0.68	1.05	0.94	1.44	1.32	2.35	2.48	1.88
	Δ%		6	–40	–38	–32		16	–26	8	27		6	20	85	65		–8	63	72	30
	200	470	295	220	260	280	0.39	0.53	0.62	0.71	0.76	0.57	0.58	1.18	2.22	1.99	1.44	1.10	1.90	3.14	2.62
	Δ%		–37	–53	–45	–40		34	58	79	93		2	107	291	251		–24	32	118	81
	225	470	200	190	75	20	0.39	0.34	2.31	3.97	1.20	0.57	0.61	4.58	20.7		1.44	1.78	1.98	5.20	
	Δ%		–57	–60	–84	–96		–13	487	908	205		7	707	3536			23	37	261	
EA9394 C-2	175	380	490	360	390	340	0.57	0.48	0.44	0.55	0.56	0.97	0.71	1.31	1.17	1.29	1.68	1.49	2.96	2.11	2.31
	Δ%		29	–5	3	–11		–17	–23	–4	–3		–27	36	21	33		–11	76	25	37
	200	380	460	440	400	430	0.57	0.49	0.55	0.48	0.65	0.97	0.69	1.35	1.67	2.01	1.68	1.43	2.44	3.46	3.08
	Δ%		21	16	5	13		–16	–4	–16	14		–28	39	73	108		–15	45	106	83
	225	380	300	320	285	320	0.57	0.35	0.45	0.42	0.43	0.97	1.00	1.69	1.68	1.41	1.68	2.83	3.75	4.03	3.31
	Δ%		–21	–16	–25	–16		–38	–22	–28	–26		4	74	73	46		68	123	139	97

Aging *t*, day		0	15	50	100	180	0	15	50	100	180	0	15	50	100	180
Epoxy	Aging *T*, °C	Residual to static strain-term ratio					SN slope/load sensitivity					Δσ, psi				
AF131-2	175	0.67	0.77	0.60	0.79	0.70	–39.2	–27.9	–20	–22	–23	60	200	286	63	–14
	Δ%		15	–10	19	5		–29	–48	–43	–41		232	374	4	–123
	200	0.67	0.75	1.08	1.34	1.07	–39.2	–15.2	–8.2	–14.5	–5.5	60	–27	–8	–92	–58
	Δ%		13	61	101	60		–61	–79	–63	–86		–145	–114	–253	–196
	225	0.67	1.52	1.38	0.66		–39.2	–10.0	–10.6			60	213	–287		
	Δ%		128	107	–1			–75	–73				253	–576		
EA9394 C-2	175	0.88	0.70	1.24	0.79	1.29	–35	–33.5	–22	–17	–19	–225	87	57	–20	–264
	Δ%		–20	41	–10	47		–4	–38	–51	–47		–139	–125	–91	17
	200	0.88	0.83	1.07	1.28	1.24	–35	–31.4	–31	–20	–32	–225	152	–97	–23	–353
	Δ%		–6	22	46	41		–10	–11	–42	–8		–168	–57	–90	57
	225	0.88	0.77	0.87	0.78	1.12	–35	–20.9	–50	–27	–25	–225	125	–224	–14	–11
	Δ%		–12	–1	–11	27		–40	42	–22	–28		–155	–1	–94	–95

TABLE A.13.—SUMMARY OF THERMAL PROPERTIES OF ADHESIVE CANDIDATES AFTER THE ACCELERATED THERMAL AGING EXPOSURES

Thermal properties			mDSC										TGA																			
Sample type	Aging T, °C	Aging t, day	T_g, °C					% Cure					T_d, °C					ΔWt%, RT-100 °C					ΔWt%, 100-200 °C					ΔWt% at 700 °C				
			0	15	50	99	174	0	15	50	99	174	0	15	50	99	174	0	15	50	99	174	0	15	50	99	174	0	15	50	99	174
3M AF131-2																																
Thick sheet	175	Avg.	200	261	263	263	201	84.3	98.6	99.6	100.0	99.9	408	410	409	411	384	0.22	0.28	0.31	0.17	0.19	0.72	0.95	0.96	0.90	0.59	62.0	62.0	62.0	65.5	61.2
		SD	9	5.9	3.6	0.0	2.4	0.3	1.0	0.1	0.0	0.1	1.4	0.7	3.5	4.9	1.5	0.06	0.05	0.01	0.11	0.19	0.12	0.09	0.08	0.14	0.21	0.0	0.0	0.0	4.9	4.0
		%Δ		30	31	31	0.1		17	18	19	18		0	0	1	–6		28	41	–24	–13		32	34	25	–18		0	0	6	–1
	200	Avg.	200	257	246	250	238	84.3	99.8	99.9	100.0	99.8	408	408	409	410	413	0.22	0.27	0.42	0.56	0.17	0.72	0.91	0.98	1.17	1.16	62.0	64.7	60.5	60.0	60.0
		SD	9	4.7	2.1	12.0	1.4	0.3	0.2	0.1	0.0	0.0	1.4	1.5	1.4	6.4	3.5	0.06	0.11	0.01	0.10	0.00	0.12	0.27	0.13	0.24	0.17	0.0	3.5	0.7	0.0	1.4
		%Δ		28	23	25	19		18	18	19	18		0	0	0	1		26	95	155	–23		26	35	62	60		4	–2	–3	–3
	225	Avg.	200	241	188	146	173	84.3	99.5	99.9	100.0	99.7	408	413	406	395	405	0.22	0.31	0.38	0.10	0.58	0.72	0.87	0.68	0.76	0.98	62.0	60.5	56.5	52.0	42.5
		SD	9	2.1	0	0.7	21.9	0.3	0.0	0.0	0.1	0.1	1.4	0.7	1.4	4.9	2.8	0.06	0.09	0.11	0.05	0.69	0.12	0.15	0.23	0.24	0.12	0.0	0.7	0.7	1.4	0.7
		% Δ		20	–6	–27	–14		18	19	19	18		1	0	–3	–1		41	76	–55	166		20	–6	5	35		–2	–9	–16	–31
Laminated thin film	175	Avg.	215	260	266	258	257	94.9	99.9	99.9	99.9	99.9	395	370	379	378	376	1.53	3.15	2.98	3.54	2.24	0.53	2.50	1.02	0.77	0.64	76.7	57.0	60.5	57.5	62.5
		SD	4	0.7	11.3	1.4	0.0	0.8	0.1	0.1	0.1	0.0	4.2	0.7	2.1	9.9	2.1	0.88	0.28	0.30	0.37	1.43	0.21	1.95	0.30	0.12	0.01	9.1	5.7	3.5	0.7	0.7
		%Δ		21	24	20	20		5	5	5	5		–7	–4	–4	–5		106	95	132	47		375	94	45	21		–26	–21	–25	–18
	200	Avg.	215	261	251	241	240	94.9	99.6	99.9	99.9	99.9	395	366	387	380	382	1.53	1.63	2.79	2.15	1.63	0.53	0.69	0.65	0.75	1.27	76.7	56.0	57.5	54.0	57.5
		SD	4	7.8	8.5	0.7	1.4	0.8	0.0	0.1	0.0	0.1	4.2	4.2	7.8	0.0	0.7	0.88	0.67	0.18	0.64	0.08	0.21	0.65	0.11	0.52	0.16	9.1	7.1	0.7	0.0	0.7
		%Δ		21	17	12	12		5	5	5	5		–7	–2	–4	–3		7	83	41	6		31	23	43	141		–27	–25	–30	–25
	225	Avg.	215	247	207	121	165	94.9	99.2	99.8	99.7	99.7	395	379	386	386	411	1.53	2.39	1.12	0.61	1.22	0.53	7.78	0.46	3.05	2.12	76.7	57.0	63.0	41.5	40.0
		SD	4	15.6	3.5	0.7	7.1	0.8	0.4	0.2	0.2	0.3	4.2	11.3	2.8	7.1	0.0	0.88	0.26	0.16	0.52	0.08	0.21	4.11	0.07	0.72	0.38	9.1	1.4	0.0	9.2	1.4
		%Δ		15	–4	–44	–23		4	5	5	5		–4	–2	–2	4		57	–27	–60	–20		1377	–13	478	302		–26	–18	–46	–48
Hysol EA9394 C-2																																
Thick sheet	175	Avg.	147	189	191	197	261	92.2	98.7	99.7	99.6	99.8	379	378	378	382	409	0.23	0.35	0.34	0.33	0.16	0.49	0.81	0.82	1.06	0.79	59.5	58.5	57.0	60.5	63.8
		SD	1	1.4	1.4	12.0	0.6	1.4	0.5	0.0	0.3	0.2	0.7	0.0	0.0	1.4	3.4	0.02	0.03	0.18	0.16	0.09	0.00	0.02	0.08	0.03	0.30	2.1	0.7	0.0	3.5	4.3
		%Δ		28	30	33	77		7	8	8	8		0	0	1	8		51	49	43	–29		64	67	116	61		–2	–4	2	7
	200	Avg.	147	191	188	178	178	92.2	99.2	99.7	99.8	99.8	379	382	384	390	399	0.23	0.44	0.43	0.29	0.36	0.49	0.86	0.78	0.71	0.57	59.5	56.5	57.0	55.0	54.5
		SD	1	2.8	3.5	4.7	7.1	1.4	0.8	0.0	0.1	0.0	0.7	2.1	4.2	4.2	1.4	0.02	0.19	0.14	0.03	0.23	0.00	0.06	0.19	0.05	0.11	2.1	0.7	1.4	0.0	0.7
		%Δ		30	27	21	21		8	8	8	8		1	1	3	5		90	88	25	54		76	58	44	16		–5	–4	–8	–8
	225	Avg.	147	157	117	135	142	92.2	99.8	99.6	99.8	99.8	379	392	416	424	423	0.23	0.46	0.25	0.32	0.33	0.49	0.79	0.73	0.61	0.59	59.5	54.0	51.0	49.5	47.5
		SD	1	0.0	4.5	6.4	0.7	1.4	0.0	0.1	0.0	0.1	0.7	0.0	2.8	2.1	0.0	0.02	0.11	0.02	0.01	0.06	0.00	0.12	0.15	0.09	0.06	2.1	1.4	1.4	0.7	0.7
		%Δ		7	–20	–9	–4		8	8	8	8		4	10	12	12		98	7	38	44		60	48	24	21		–9	–14	–17	–20
Laminated thin film	175	Avg.	150	209	210	204	212	93.4	99.9	99.9	99.6	99.8	357	366	355	342	352	1.06	1.42	1.33	1.77	0.90	0.44	0.25	0.58	0.83	0.85	51.0	54.5	50.5	47.5	52.0
		SD	1	2.1	2.8	6.4	12.7	0.1	0.0	0.2	0.4	0.1	5.7	16.3	4.2	5.7	17.7	0.32	0.18	0.62	0.35	0.36	0.08	0.00	0.68	0.08	0.21	1.4	7.8	0.7	0.7	1.4
		%Δ		39	40	36	41		7	7	7	7		2	–1	–4	–2		34	25	67	–15		–42	32	90	96		7	–1	–7	2
	200	Avg.	150	200	186	185	198	93.4	99.9	99.7	99.8	99.5	357	345	354	345	361	1.06	1.45	1.12	1.17	0.60	0.44	1.04	0.89	1.11	0.96	51.0	48.0	47.5	45.0	46.5
		SD	1	7.1	17.0	12.0	14.1	0.1	0.0	0.0	0.1	0.4	5.7	4.9	5.7	4.2	5.7	0.32	0.19	0.21	0.41	0.22	0.08	0.23	0.40	0.67	0.12	1.4	1.4	4.9	0.0	0.7
		%Δ		33	24	23	32		7	7	7	6		–4	–1	–3	1		36	5	10	–43		138	104	155	120		–6	–7	–12	–9
	225	Avg.	150	174	146	141	151	93.4	99.6	99.7	99.7	99.6	357	328	393	397	386	1.06	0.74	0.97	0.16	0.62	0.44	2.98	3.96	3.99	3.10	51.0	45.0	38.5	38.0	34.5
		SD	1	14.8	4.2	2.1	2.1	0.1	0.1	0.2	0.0	0.0	5.7	11.3	6.4	0.7	1.4	0.32	0.14	0.04	0.19	0.12	0.08	0.62	0.60	1.26	1.04	1.4	1.4	0.7	5.7	0.7
		%Δ		16	–3	–6	0		7	7	7	7		–8	10	11	8		–30	–8	–85	–41		584	810	815	611		–12	–25	–25	–32

TABLE A.13.—SUMMARY OF THERMAL PROPERTIES OF ADHESIVE CANDIDATES AFTER THE ACCELERATED THERMAL AGING EXPOSURES

Thermal Properties			DMA																					TMA				
Sample type	Aging T, °C	Aging t, day	T_g by G', °C					T_g by tan δ, °C					T_β by G'', °C					G' ratio (at 200 °C/at RT), %					T_g, °C				
			0	15	50	99	174	0	15	50	99	174	0	15	50	99	174	0	15	50	99	174	0	15	50	99	174
3M AF131-2																											
Thick sheet	175	Avg.	192	239	242	244	195	220	284	284	281	228	109	115	111	110	90	44	57	64	60	45	184				
		SD	0.7	3.5	1.4	2.1	0.0	1.4	1.4	2.1	1.4	0.7	0.7	0.7	1.4	2.8	2.8	1.6	4.2	0.7	0.9	1.3	1.4				
		%Δ		25	26	27	2		29	29	28	3		6	2	1	–17		29	46	37	2					
	200	Avg.	192	241	232	235	236	220	282	271	267	269	110	116	110	110	113	44	61	67	69	65	184	218			
		SD	0.7	1.4	0.0	2.8	3.5	1.4	0.7	0.7	0.0	2.1	0.0	0.7	3.5	2.1	2.1	1.6	2.8	5.6	0.4	1.0	1.4	0.0			
		%Δ		26	21	23	23		28	23	21	22		5	0	0	2		38	51	57	48		18			
	225	Avg.	192	222	173			220	262	214			110	111	100			44	66	32			184	225	180	141	168
		SD	0.7	0.0	2.8			1.4	1.4	0.7			0.0	4.2	1.4			1.6	3.9	6.1			1.4	6.2	4.2	0.0	3.6
		%Δ		16	–10				19	–3				1	–9				51	–27				22	–2	–23	–9
Hysol EA9394 C-2																											
Thick sheet	175	Avg.	159	185	191	192	243	192	234	231	227	281						24	36	42	41	62	142				
		SD	12.7	2.1	0.7	3.5	4.9	21.9	1.4	0.7	0.7	2.1						4.2	2.1	3.6	2.6	9.8	2.5				
		%Δ		16	20	20	53		22	20	18	46							47	72	66	153					
	200	Avg.	159	187	171	162	170	192	219	207	199	208						24	38	27	16	26	142		115		
		SD	12.7	0.7	4.0	1.3	0.7	21.9	0.7	1.7	1.8	1.4						4.2	2.1	2.4	2.9	3.4	2.5		0.0		
		%Δ		17	7	2	7		14	8	4	9							54	10	–36	6			–19		
	225	Avg.	159	150	123			192	180	171								24	6	4			142	142	123	128	139
		SD	12.7	5.7	0.0			21.9	1.4	0.0								4.2	0.0	0.0			2.5	4.0	0.0	0.7	1.5
		%Δ		–6	–23				–6	–11									–77	–36				0	–13	–10	–2

TABLE A.14.—OVERALL TEST MATRIX FOR 6-MONTH ACCELERATED THERMAL AGING EXPERIMENT OF THREAD LOCKER CANDIDATES

Aging conditions	Test conditions		Torque Test Specimens																	
			Loctite 294						Resbond 507TS						Poly-Lok PET Patch					
			100 °C			200 °C			100 °C			200 °C			100 °C			200 °C		
6-m accelerated aging under dry N_2	Unaged Control II		2-120	2-075	2-162	2-146	2-134	2-126	2-160	2-032	2-066	2-107	2-076	2-038	2-065	2-041	2-053	2-051	2-165	2-031
			6-015	6-039	6-233	6-111	6-123	6-160	6-177	6-070	6-200	6-005	6-154	6-012	6-145	6-014	6-146	6-168	6-112	6-052
			7-153	7-031	7-132	7-158	7-151	7-159	7-048	7-004	7-150	7-138	7-003	7-037	8-206	8-041	8-048	8-188	8-205	8-110
From 3/9/16 11:00	T1 = 190 °C Blue M N_2, R244	50 day 4/28/16 11:00	2-016	2-131	2-163	2-021	2-152	2-104	2-035	2-080	2-062	2-086	2-050	2-093	2-112	2-006	2-136	2-010	2-101	2-069
			6-059	6-024	6-053	6-164	6-041	6-220	6-113	6-231	6-072	6-130	6-221	6-212	6-058	6-147	6-092	6-091	6-028	6-178
			7-154	7-126	7-156	7-020	7-136	7-035	7-119	7-050	7-051	7-149	7-060	7-120	8-208	8-008	8-031	8-034	8-252	8-164
		100 day 6/16/16 15:48	2-030	2-043	2-106	2-055	2-122	2-034	2-137	2-105	2-085	2-071	2-148	2-111	2-070	2-028	2-019	2-026	2-064	2-011
			6-060	6-086	6-215	6-182	6-179	6-069	6-129	6-166	6-155	6-250	6-042	6-023	6-239	6-093	6-253	6-120	6-114	6-133
			7-033	7-143	7-036	7-014	7-042	7-106	7-029	7-057	7-007	7-144	7-058	7-012	8-059	8-060	8-192	8-178	8-047	8-124
		170 day 8/26/16 15:48	2-037	2-067	2-084	2-096	2-097	2-046	2-072	2-045	2-023	2-128	2-123	2-119	2-088	2-153	2-089	2-130	2-113	2-118
			6-068	6-085	6-035	6-006	6-043	6-045	6-234	6-095	6-140	6-161	6-236	6-131	6-087	6-008	6-038	6-066	6-152	6-071
			7-155	7-137	7-152	7-112	7-047	7-111	7-011	7-161	7-142	7-052	7-054	7-028	8-040	8-052	8-160	8-128	8-146	8-053
	T2 = 220 °C Gruenberg, R244	50 day 4/28/16 11:00	2-018	2-057	2-108	2-115	2-061	2-098	2-024	2-022	2-079	2-121	2-047	2-033	2-133	2-077	2-092	2-015	2-087	2-048
			6-088	6-011	6-174	6-236	6-135	6-050	6-118	6-198	6-213	6-156	6-089	6-249	6-061	6-055	6-063	6-122	6-158	6-219
			7-129	7-117	7-148	7-113	7-141	7-040	7-034	7-001	7-044	7-009	7-121	7-114	8-186	8-037	8-175	8-203	8-038	8-158
		100 day 6/16/16 15:48	2-094	2-116	2-059	2-039	2-040	2-144	2-125	2-117	2-013	2-124	2-036	2-014	2-020	2-056	2-058	2-017	2-138	2-091
			6-199	6-116	6-150	6-226	6-197	6-036	6-172	6-218	6-010	6-048	6-223	6-242	6-065	6-151	6-186	6-040	6-047	6-096
			7-146	7-157	7-059	7-008	7-039	7-016	7-002	7-043	7-032	7-025	7-123	7-124	8-046	8-207	8-222	8-136	8-035	8-224
		170 day 8/26/16 15:48	2-044	2-025	2-129	2-110	2-054	2-099	2-060	2-103	2-083	2-012	2-073	2-114	2-127	2-081	2-100	2-109	2-135	2-090
			6-195	6-149	6-044	6-049	6-027	6-157	6-168	6-094	6-142	6-237	6-051	6-227	6-121	6-143	6-054	6-029	6-057	6-238
			7-139	7-056	7-140	7-015	7-133	7-128	7-135	7-055	7-010	7-005	7-127	7-125	8-201	8-042	8-058	8-036	8-233	8-145
# of specimen	#2 #6 #7 or #8		21	21	21	21	21	21	21	21	21	21	21	21	21	21	21	21	21	21

TABLE A.15.—SUMMARY OF TORQUE DATA AT 100 AND 200 °C INCLUDING FAILURE MODE OF THREAD LOCKER CANDIDATES IN #2 JOINT AS A FUNCTION OF ACCELERATED AGING CONDITIONS

Aging *T*, °C	Aging *t*, day	#2 Joint Torque Strengths, N-cm, and % installation torques																													
		Loctite 294 Installation torque = 36.8 N-cm										Resbond 507TS Installation torque = 36.8 N-cm										Poly-Lok PET Installation torque = 36.8 N-cm									
		100 °C					200 °C					100 °C					200 °C					100 °C					200 °C				
		Sample ID	Breakloose Torque	Breakloose % Inst.	Prevail-ing torque	Maxi-mum torque	Sample ID	Breakloose Torque	Breakloose % Inst.	Prevail-ing torque	Maxi-mum torque	Sample ID	Breakloose Torque	Breakloose % Inst.	Prevail-ing torque	Maxi-mum torque	Sample ID	Breakloose Torque	Breakloose % Inst.	Prevail-ing torque	Maxi-mum torque	Sample ID	Breakloose Torque	Breakloose % Inst.	Prevail-ing torque	Maxi-mum torque	Sample ID	Breakloose Torque	Breakloose % Inst.	Prevail-ing torque	Maxi-mum torque
23	0	2-089	27.2	74	2.2	2.2	2-099	22.0	60	3.5	3.7	2-094	47.8	130	16.4	19.2	2-086	29.5	80	1.9	2	2-067	15.4	42	5.4	5.8	2-126	11.5	31	1.8	2.0
		2-035	23.6	64	1.6	1.8	2-105	22.7	62	3.1	4.0	2-062	52.8	143	14.4	19.0	2-036	29.4	80	2.1	2.9	2-045	19.1	52	3.6	4.1	2-104	13.2	36	13.9	14.3
		2-079	29.5	80	1.9	2	2-014	20.1	55	1.9	2.5	2-022	39.5	107	12.3	15.1	2-134	25.4	69	2.9	3.5	2-060	18.1	49	2.4	2.5	2-103	13.0	35	18.5	18.8
		Avg.	26.8	73	1.9	2.0	Avg.	21.6	59	2.8	3.4	Avg.	46.7	127	14.4	17.8	Avg.	28.1	76	2.3	2.8	Avg.	17.5	48	3.8	4.1	Avg.	12.6	34	11.4	11.7
		SD	3.0	8	0.3	0.2	SD	1.3	4	0.8	0.8	SD	6.7	18	2.1	2.3	SD	2.3	6	0.5	0.8	SD	1.9	5	1.5	1.7	SD	0.9	3	8.6	8.7
	0	2-120	34.1	93	23.2	23.8	2-146	20.2	55	0.8	3	2-160	59.2	161	10.9	20.7	2-107	37.4	102	5.5	18.6	2-065	19.8	54	1.8	2.4	2-051	18.2	49	0.9	1.4
		2-075	27.4	74	12.4	17.5	2-134	26.6	72	2.4	3.5	2-032	50.3	137	6.0	13.3	2-076	31.3	85	3.1	9.9	2-041	20.0	54	2.3	5	2-165	21.5	58	3.0	4.3
		2-162	25.2	68	2.9	3.5	2-126	21.8	59	2.1	5.1	2-066	41.3	112	8.5	18.5	2-038	22.6	61	1.9	3.7	2-053	23.5	64	9.4	14.3	2-031	2.0	5	1.4	1.4
		Avg.	28.9	79	12.8	14.9	Avg.	22.9	62	1.8	3.9	Avg.	50.3	137	8.5	17.5	Avg.	30.4	83	3.5	10.7	Avg.	21.1	57	4.5	7.2	Avg.	13.9	38	1.8	2.4
		SD	4.6	13	10.2	10.4	SD	3.3	9	0.9	1.1	SD	9.0	24	2.5	3.8	SD	7.4	20	1.8	7.5	SD	2.1	6	4.3	6.3	SD	10.4	28	1.1	1.7
190	15	2-052	18.3	50	15.6	15.6	2-037	15.2	41	7	8.4	2-133	35.4	96	6.3	9.2	2-073	15.3	42	1.3	11.4	2-044	8.6	23	8.9	10.1	2-025	6.2	17	1.9	2.3
		2-084	19.6	53	11.3	12.1	2-061	8.7	24	1.8	2.6	2-047	53.0	144	16.0	33.1	2-050	22.8	62	1.0	1.3	2-012	14.9	40	1.5	1.8	2-051	11.8	32	4.0	7.0
		2-064	21.2	58	19.2	20	2-041	16.7	45	2.7	3.2	2-148	42.5	115	2.6	2.9	2-131	16.2	44	0.9	1.2	2-059	12.0	33	17.6	22.1	2-055	5.2	14	8.1	11.7
		Avg.	19.7	54	15.4	15.9	Avg.	13.5	37	3.8	4.7	Avg.	43.6	119	8.3	15.1	Avg.	18.1	49	1.1	4.6	Avg.	11.8	32	9.3	11.3	Avg.	7.7	21	4.7	7.0
		SD	1.5	4	4.0	4.0	SD	4.3	12	2.8	3.2	SD	8.9	24	6.9	15.9	SD	4.1	11	0.2	5.9	SD	3.2	9	8.1	10.2	SD	3.6	10	3.2	4.7
		Δ %	–32		20	6	Δ %	–41		117	22	Δ %	–13		–2	–14	Δ %	–41		–70	–57	Δ %	–44		107	57	Δ %	–44		164	196
	50	2-016	16.8	46	8.8	9.2	2-021	24.6	67	5.1	5.6	2-035	42.2	115	7.5	16.8	2-086	21.8	59	1.2	2.2	2-112	10.3	28	2.0	2.1	2-010	10.8	29	8.3	9
		2-131	26.2	71	11.7	12.1	2-152	15.3	42	2.6	3.2	2-080	42.1	114	5.0	8.8	2-050	18	49	1.3	2.2	2-006	16.2	44	2.2	2.3	2-101	12.9	35	6.9	7.3
		2-163	33.2	90	10.7	11.2	2-104	21.5	58	17.0	18.6	2-062	32.8	89	7.0	10.6	2-093	19.8	54	1.7	4.9	2-136	21.7	59	2.8	3.1	2-069	14.6	40	31.2	32.4
		Avg.	25.4	69	10.4	10.8	Avg.	20.5	56	8.2	9.1	Avg.	39.0	106	6.5	12.1	Avg.	19.9	54	1.4	3.1	Avg.	16.1	44	2.3	2.5	Avg.	12.8	35	15.5	16.2
		SD	8.2	22	1.5	1.5	SD	4.7	13	7.7	8.3	SD	5.4	15	1.3	4.2	SD	1.9	5	0.3	1.6	SD	5.7	15	0.4	0.5	SD	1.9	5	13.6	14.0
		Δ %	–12		–19	–27	Δ %	–10		366	136	Δ %	–22		–23	–31	Δ %	–35		–60	–71	Δ %	–24		–48	–65	Δ %	–8		775	586
	100	2-030	13.3	36	12.9	13.9	2-055	18.4	50	11.8	17.4	2-137	55.1	150	3.6	7.6	2-071	12.6	34	1.2	2.6	2-070	22.1	60	8.9	9.9	2-026	5.5	15	9.3	10.2
		2-043	20.4	55	23.9	24.7	2-122	24.0	65	5.0	6.3	2-105	41.8	114	7.1	13.2	2-148	10.3	28	1.5	2.9	2-028	13.8	38	5.9	7.7	2-064	18.7	51	0.3	0.8
		2-106	28.1	76	7.7	11.1	2-034	17.0	46	2.4	2.9	2-085	44.1	120	3.4	10.3	2-111	16.3	44	2.4	4.8	2-019	4.7	13	8.3	8.3	2-011	7.5	20	10.6	11.8
		Avg.	20.6	56	14.8	16.6	Avg.	19.8	54	6.4	8.9	Avg.	47.0	128	4.7	10.4	Avg.	13.1	36	1.7	3.4	Avg.	13.5	37	7.7	8.6	Avg.	10.6	29	6.7	7.6
		SD	7.4	20	8.3	7.2	SD	3.7	10	4.9	7.6	SD	7.1	19	2.1	2.8	SD	3.0	8	0.6	1.2	SD	8.7	24	1.6	1.1	SD	7.1	19	5.6	5.9
		Δ %	–29		16	11	Δ %	–13		262	129	Δ %	–6		–44	–41	Δ %	–57		–51	–68	Δ %	–36		71	19	Δ %	–24		281	221
	180	2-037	25.8	70	11.5	14	2-096	18.9	51	7.7	10.2	2-072	54.8	149	3.9	15.3	2-128	10.6	29	1.6	3.9	2-088	7.1	19	8.2	10.2	2-130	12.4	34	2.2	2.6
		2-067	14.5	39	14.1	15.9	2-097	22.3	61	6.1	7.2	2-045	42.6	116	6.5	11.6	2-123	20.2	55	1.7	2.6	2-153	15.9	43	9.1	11.7	2-113	11.1	30	11.0	12
		2-084	25.4	69	9.2	14.5	2-046	16.0	43	1.4	3.4	2-023	51.1	139	3.8	15.3	2-119	9.1	25	0.6	1.5	2-089	17.2	47	17.9	17.9	2-118	14.0	38	10.0	10.9
		Avg.	21.9	60	11.6	14.8	Avg.	19.1	52	5.1	6.9	Avg.	49.5	135	4.7	14.1	Avg.	13.3	36	1.3	2.7	Avg.	13.4	36	11.7	13.3	Avg.	12.5	34	7.7	8.5
		SD	6.4	17	2.5	1.0	SD	3.2	9	3.3	3.4	SD	6.3	17	1.5	2.1	SD	6.0	16	0.6	1.2	SD	5.5	15	5.4	4.1	SD	1.5	4	4.8	5.1
		Δ %	–24		–10	–1	Δ %	–17		187	79	Δ %	–2		–44	–20	Δ %	–56		–63	–75	Δ %	–36		161	83	Δ %	–10		338	259

TABLE A.15.—SUMMARY OF TORQUE DATA AT 100 AND 200 °C INCLUDING FAILURE MODE OF THREAD LOCKER CANDIDATES IN #2 JOINT AS A FUNCTION OF ACCELERATED AGING CONDITIONS

Aging T, °C	Aging t, day	#2 Joint Torque Strengths, N-cm, and % installation torques																													
		Loctite 294 Installation torque = 36.8 N-cm										Resbond 507TS Installation torque = 36.8 N-cm										Poly-Lok PET Installation torque = 36.8 N-cm									
		100 °C					200 °C					100 °C					200 °C					100 °C					200 °C				
		Sample ID	Breakloose		Prevailing torque	Maximum torque	Sample ID	Breakloose		Prevailing torque	Maximum torque	Sample ID	Breakloose		Prevailing torque	Maximum torque	Sample ID	Breakloose		Prevailing torque	Maximum torque	Sample ID	Breakloose		Prevailing torque	Maximum torque	Sample ID	Breakloose		Prevailing torque	Maximum torque
			Torque	% Inst.				Torque	% Inst.				Torque	% Inst.				Torque	% Inst.				Torque	% Inst.				Torque	% Inst.		
220	15	2-027	21.1	57	1.9	2.0	2-098	15.4	42	6.4	8	2-102	47.0	128	3.5	4.6	2-075	2.7	7	2.7	3.0	2-046	13.6	37	3.4	3.6	2-092	5.1	14	6.0	7.8
		2-121	37.3	101	2.2	2.7	2-085	3.0	8	2.0	2.5	2-080	51.8	141	5.6	14.6	2-124	15.3	42	0.6	1.1	2-057	23.5	64	8.1	15.1	2-101	10.4	28	8.1	15.7
		2-017	17.0	46	5.9	6.5	2-053	4.0	11	0.9	1.4	2-162	46.3	126	4.7	8.1	2-165	28.0	76	2.4	4.7	2-034	8.7	24	1.8	1.8	2-074	10.4	28	12.3	13.0
		Avg.	25.1	68	3.3	3.7	Avg.	7.5	20	3.1	4.0	Avg.	48.4	131	4.6	9.1	Avg.	15.3	42	1.9	2.9	Avg.	15.3	41	4.4	6.8	Avg.	8.6	23	8.8	12.2
		SD	10.7	29	2.2	2.4	SD	6.9	19	2.9	3.5	SD	3.0	8	1.1	5.1	SD	12.7	34	1.1	1.8	SD	7.5	20	3.3	7.2	SD	3.1	8	3.2	4.0
		Δ%	–13		–74	–75	Δ%	–67		75	3	Δ%	–4		–46	–48	Δ%	–50		–46	–73	Δ%	–28		–1	–6	Δ%	–38		398	414
	50	2-018	34.6	94	8.8	12.2	2-115	13.9	38	1.7	1.9	2-024	46.6	127	2.5	6.5	2-121	16.7	45	2.2	3.2	2-133	34	92	5.7	8.9	2-015	11.3	31	3.7	6.4
		2-057	20	54	11.5	14.5	2-061	14.2	39	4.8	6.7	2-022	29.9	81	3.8	7.4	2-047	4.7	13	1.2	2.0	2-077	13.7	37	5.9	6.2	2-087	10.6	29	2.8	3.2
		2-108	34.1	93	15.0	15.5	2-098	21.4	58	7.7	8.3	2-079	31.3	85	2.4	7	2-033	15.0	41	0.7	2.1	2-092	17.9	49	19.1	27.7	2-048	14.1	38	1.9	3.0
		Avg.	29.6	80	11.8	14.1	Avg.	16.5	45	4.7	5.6	Avg.	35.9	98	2.9	7.0	Avg.	12.1	33	1.4	2.4	Avg.	21.9	59	10.2	14.3	Avg.	12.0	33	2.8	4.2
		SD	8.3	23	3.1	1.7	SD	4.2	12	3.0	3.3	SD	9.3	25	0.8	0.5	SD	6.5	18	0.8	0.7	SD	10.7	29	7.7	11.7	SD	1.9	5	0.9	1.9
		Δ%	2		–8	–6	Δ%	–28		168	46	Δ%	–29		–66	–60	Δ%	–60		–61	–77	Δ%	4		127	97	Δ%	–14		58	77
	100	2-094	35.8	97	17.2	17.5	2-039	25.2	68	7.1	8.8	2-125	53.8	146	4.3	15.8	2-124	8.9	24	0.7	1.4	2-020	14.8	40	2	2.4	2-017	9.9	27	6.7	7.2
		2-116	19.8	54	4.5	4.9	2-040	8.8	24	4.3	4.3	2-117	43.2	117	2.8	6.3	2-036	6.5	18	0.8	1.7	2-056	9.4	26	5.5	6.1	2-138	13.2	36	2.5	3.4
		2-059	34.9	95	17.8	30.8	2-144	14.4	39	2.5	3.6	2-013	52.0	141	8.1	18.6	2-014	19.0	52	0.5	1.1	2-058	13.0	35	3.4	5.1	2-091	9.9	27	5.0	7.1
		Avg.	30.2	82	13.2	17.7	Avg.	16.1	44	4.6	5.6	Avg.	49.7	135	5.1	13.6	Avg.	11.5	31	0.7	1.4	Avg.	12.4	34	3.6	4.5	Avg.	11.0	30	4.7	5.9
		SD	9.0	24	7.5	13.0	SD	8.3	23	2.3	2.8	SD	5.7	15	2.7	6.4	SD	6.6	18	0.2	0.3	SD	2.7	7	1.8	1.9	SD	1.9	5	2.1	2.2
		Δ%	4		3	19	Δ%	–29		162	44	Δ%	–1		–40	–22	Δ%	–62		–81	–87	Δ%	–41		–19	–37	Δ%	–21		168	149
	180	2-044	37.5	102	28.7	28.7	2-110	22.9	62	6.7	12	2-060	45.8	124	3.6	15.4	2-012	24.2	66	1.2	3.6	2-127	10	27	1.4	1.7	2-109	11.5	31	14	15.4
		2-025	21.8	59	6.1	7.8	2-054	16.4	45	11.0	11.3	2-103	49.8	135	6.7	16.2	2-073	17.3	47	1.5	3.9	2-081	10.1	27	10.4	12.6	2-135	18.2	49	5.7	6.4
		2-129	26	71	8.9	9.3	2-099	13.2	36	7.4	10	2-083	41.3	112	4.9	14	2-114	16.0	43	2.0	3	2-100	6.4	17	7.4	9.1	2-090	8.5	23	9.1	11.1
		Avg.	28.4	77	14.6	15.3	Avg.	17.5	48	8.4	11.1	Avg.	45.6	124	5.1	15.2	Avg.	19.2	52	1.6	3.5	Avg.	8.8	24	6.4	7.8	Avg.	12.7	35	9.6	11.0
		SD	8.1	22	12.3	11.7	SD	4.9	13	2.3	1.0	SD	4.3	12	1.6	1.1	SD	4.4	12	0.4	0.5	SD	2.1	6	4.6	5.6	SD	5.0	13	4.2	4.5
		Δ%	–2		14	2	Δ%	–23		374	187	Δ%	–9		–40	–13	Δ%	–37		–55	–67	Δ%	–58		42	8	Δ%	–8		443	363

🟥 Cohesive failure 🟦 Adhesive failure on fastener surface 🟨 Mixture of adhesive and cohesive mode 🟫 Thermally degraded or charred

TABLE A.16.—SUMMARY OF TORQUE DATA AT 100 AND 200 °C INCLUDING FAILURE MODE OF THREAD LOCKER CANDIDATES IN #6 JOINT AS A FUNCTION OF ACCELERATED AGING CONDITIONS

Aging T, °C	Aging t, day	#6 Joint torque strengths, N-cm, and % installation torques																													
		Loctite 294 Installation torques = 76.4 N-cm										Resbond 507TS Installation torques = 76.4 N-cm										Poly-Lok PET Installation torques = 76.4 N-cm									
		100 °C					200 °C					100 °C					200 °C					100 °C					200 °C				
		Sample ID	Breakloose		Prevail-ing torque	Maxi-mum torque	Sample ID	Breakloose		Prevail-ing torque	Maxi-mum torque	Sample ID	Breakloose		Prevail-ing torque	Maxi-mum torque	Sample ID	Breakloose		Prevail-ing torque	Maxi-mum torque	Sample ID	Breakloose		Prevail-ing torque	Maxi-mum torque	Sample ID	Breakloose		Prevail-ing torque	Maxi-mum torque
			Torque	% Inst.				Torque	% Inst.				Torque	% Inst.				Torque	% Inst.				Torque	% Inst.				Torque	% Inst.		
23	0	6-135	70.2	92	17.1	19.4	6-002	62.0	81	8.0	12.8	6-132	93.9	123	12.9	31.8	6-018	60.9	80	3.4	7.4	6-233	32.2	42	1.9	2.0	6-161	57.2	75	2.0	2.3
		6-005	78.3	102	23.4	24.9	6-014	49.8	65	8.6	9.4	6-124	107.2	140	10.9	18.0	6-180	52.0	68	3.2	8.5	6-111	54.5	71	2.3	2.4	6-154	17.1	22	2.4	2.5
		6-142	76.1	100	18.7	24.7	6-143	61.0	80	7.6	10.7	6-138	100.7	132	8.0	13.5	6-185	56.1	73	3.1	4.1	6-015	27.4	36	8.5	12.3	6-158	19.1	25	3.5	3.7
		Avg.	74.9	98	19.7	23.0	Avg.	57.6	75	8.1	11.0	Avg.	100.6	132	10.6	21.1	Avg.	56.3	74	3.2	6.7	Avg.	38.0	50	4.2	5.6	Avg.	31.1	41	2.6	2.8
		SD	4.2	5	3.3	3.1	SD	6.8	9	0.5	1.7	SD	6.7	9	2.5	9.5	SD	4.5	6	0.2	2.3	SD	14.5	19	3.7	5.8	SD	22.6	30	0.8	0.8
	0	6-015	77.5	101	27.5	40.1	6-111	57.6	75	5.3	9.9	6-177	86.2	113	7.5	19.6	6-005	78.6	103	0.7	4.3	6-145	32.4	42	4.9	8.0	6-168	25.6	34	2.8	3.3
		6-039	79.3	104	27.4	40.3	6-123	59.5	78	6.9	14.3	6-070	81.9	107	13.2	16.9	6-154	49.2	64	0.8	4.3	6-014	24.1	32	3.3	5.9	6-112	22.4	29	6.9	7.4
		6-233	67.6	88	27.4	32.9	6-160	52.4	69	9.0	15.5	6-200	86.7	113	5.7	14.2	6-012	59.9	78	1.3	4.4	6-146	31.2	41	2.1	2.6	6-052	22.9	30	6.0	8
		Avg.	74.8	98	27.4	37.8	Avg.	56.5	74	7.1	13.2	Avg.	84.9	111	8.8	16.9	Avg.	62.6	82	0.9	4.3	Avg.	29.2	38	3.4	5.5	Avg.	23.6	31	5.2	6.2
		SD	6.3	8	0.1	4.2	SD	3.7	5	1.9	2.9	SD	2.6	3	3.9	2.7	SD	14.9	19	0.3	0.1	SD	4.5	6	1.4	2.7	SD	1.7	2	2.2	2.6
190	15	6-118	78.5	103	25.9	39.3	6-153	67.4	88	13.0	13.4	6-016	109.5	143	9.8	20.9	6-173	56.6	74	2.2	3.5	6-249	71.2	93	2.4	2.4	6-133	79.9	105	1.9	2.5
		6-109	79.7	104	7.9	10.1	6-028	68.2	89	6.5	10.2	6-181	110.1	144	7.1	19.6	6-003	57.8	76	2.0	3.3	6-010	61.1	80	1.6	1.7	6-131	68.6	90	2.1	2.5
		6-008	80.2	105	23.0	23.1	6-203	63.7	83	7.4	10.6	6-030	108.9	143	5.8	12.9	6-159	67.1	88	2.2	7	6-112	32.9	43	6.3	9.9	6-210	28.9	38	3.7	3.9
		Avg.	79.5	104	18.9	24.2	Avg.	66.4	87	9.0	11.4	Avg.	109.5	143	7.6	17.8	Avg.	60.5	79	2.1	4.6	Avg.	55.1	72	3.4	4.7	Avg.	59.1	77	2.6	3.0
		SD	0.9	1	9.7	14.6	SD	2.4	3	3.5	1.7	SD	0.6	1	2.0	4.3	SD	5.7	8	0.1	2.1	SD	19.9	26	2.5	4.5	SD	26.8	35	1.0	0.8
		Δ%	6		–31	–36	Δ%	18		27	–14	Δ%	29		–14	5	Δ%	–3		129	6	Δ%	88		0	–15	Δ%	150		–51	–52
	50	6-059	74.3	97	27.6	27.6	6-164	51.9	68	14.3	16.3	6-113	103.8	136	2.7	7.3	6-130	51.7	68	0.8	6.5	6-058	29.6	39	1.0	4.1	6-091	35.7	47	8.4	8.7
		6-024	61.6	81	31.5	32.2	6-041	56.9	74	7.3	14.5	6-231	125.3	164	3.8	31.4	6-221	68	89	0.9	2.2	6-147	33.4	44	5.4	5.8	6-028	19.2	25	3.8	4.7
		6-053	60.4	79	16.0	18.3	6-220	69.5	91	8.4	14.9	6-072	86.8	114	7.6	18.1	6-212	74.6	98	0.8	1.6	6-092	36.6	48	8.2	8.5	6-178	24.4	32	9.4	9.5
		Avg.	65.4	86	25.0	26.0	Avg.	59.4	78	10.0	15.2	Avg.	105.3	138	4.7	18.9	Avg.	64.8	85	0.8	3.4	Avg.	33.2	43	4.9	6.1	Avg.	26.4	35	7.2	7.6
		SD	7.7	10	8.1	7.1	SD	9.1	12	3.8	0.9	SD	19.3	25	2.6	12.1	SD	11.8	15	0.1	2.7	SD	3.5	5	3.6	2.2	SD	8.4	11	3.0	2.6
		Δ%	–13		–9	–31	Δ%	5		42	15	Δ%	24		–47	12	Δ%	4		–11	–21	Δ%	14		42	12	Δ%	12		38	22
	100	6-060	85.6	112	4.5	9.2	6-182	54	71	13.7	14.2	6-129	95.5	125	2.2	7.7	6-250	75.1	98	1.1	3.6	6-239	29.9	39	5.2	6.2	6-120	30.4	40	7.7	8.1
		6-086	66.2	87	16.9	20.7	6-179	61.5	80	11.9	17.2	6-166	125	164	6.2	9.4	6-042	74.5	98	0.6	2.7	6-093	33	43	4.2	4.6	6-114	29.7	39	2.2	3.4
		6-215	62.8	82	5.4	8.8	6-069	69.0	90	18.1	18.4	6-155	119.4	156	5.2	9.9	6-023	61.4	80	1.0	2.0	6-253	30.9	40	11.1	13.1	6-133	29.7	39	9.8	9.9
		Avg.	71.5	94	8.9	12.9	Avg.	61.5	80	14.6	16.6	Avg.	113.3	148	4.5	9.0	Avg.	70.3	92	0.9	2.8	Avg.	31.3	41	6.8	8.0	Avg.	29.9	39	6.6	7.1
		SD	12.3	16	6.9	6.8	SD	7.5	10	3.2	2.2	SD	15.7	21	2.1	1.2	SD	7.7	10	0.3	0.8	SD	1.6	2	3.7	4.5	SD	0.4	1	3.9	3.4
		Δ%	–4		–67	–66	Δ%	9		106	25	Δ%	33		–48	–47	Δ%	12		–4	–36	Δ%	7		99	45	Δ%	27		25	14
	180	6-068	64.8	85	5.9	16	6-006	62.8	82	15.4	18.9	6-234	129.6	170	3.6	8	6-161	106.2	139	2.7	12.9	6-087	32.3	42	5.2	8.1	~~6-066~~				
		6-085	73.8	97	4.5	13.1	6-043	61.8	81	13.9	21.9	6-095	121.4	159	5.2	12.8	6-236	69.3	91	2.0	2.9	6-008	33.1	43	11.0	12.5	6-152	27.7	36	2.3	4.3
		6-035	69.3	91	5.3	12.6	6-045	50.7	66	8.5	15.4	6-140	81.5	107	2.8	6.5	6-131	62.8	82	1.2	2.2	6-038	30.4	40	0.7	1.9	6-071	28.8	38	6.9	7.4
		Avg.	69.3	91	5.2	13.9	Avg.	58.4	76	12.6	18.7	Avg.	110.8	145	3.9	9.1	Avg.	79.4	104	2.0	6.0	Avg.	31.9	42	5.6	7.5	Avg.	28.3	37	4.6	5.9
		SD	4.5	6	0.7	1.8	SD	6.7	9	3.6	3.3	SD	25.7	34	1.2	3.3	SD	23.4	31	0.8	6.0	SD	1.4	2	5.2	5.3	SD	0.8	1	3.3	2.2
		Δ%	–7		–81	–63	Δ%	3		78	42	Δ%	30		–56	–46	Δ%	27		111	38	Δ%	9		64	36	Δ%	20		–12	–6

TABLE A.16.—SUMMARY OF TORQUE DATA AT 100 AND 200 °C INCLUDING FAILURE MODE OF THREAD LOCKER CANDIDATES IN #6 JOINT AS A FUNCTION OF ACCELERATED AGING CONDITIONS

Aging T, °C	Aging t, day	#6 Joint torque strengths, N-cm, and % installation torques																							
		Loctite 294 Installation torques = 76.4 N-cm								Resbond 507TS Installation torques = 76.4 N-cm								Poly-Lok PET Installation torques = 76.4 N-cm							
		100 °C				200 °C				100 °C				200 °C				100 °C				200 °C			
		Sample ID	Breakloose		Prevail-ing torque	Maxi-mum torque	Sample ID	Breakloose		Prevail-ing torque	Maxi-mum torque	Sample ID	Breakloose		Prevail-ing torque	Maxi-mum torque	Sample ID	Breakloose		Prevail-ing torque	Maxi-mum torque	Sample ID	Breakloose		Prevail-ing torque	Maxi-mum torque
			Torque	% Inst.				Torque	% Inst.				Torque	% Inst.				Torque	% Inst.				Torque	% Inst.		
220	15	🟥 6-011	81.2	106	18.9	20.2	6-147	64.1	84	8.4	10.6	🟫 6-170	97.1	127	5.0	7.5	🟫 6-009	53.5	70	2.0	2.4	🟨 6-223	51.7	68	2.1	2.1	🟨 6-121	66.1	87	0.6	1.2
		🟥 6-195	79.4	104	23.1	25.2	6-129	66.4	87	6.1	9.0	~~6-165~~					🟫 6-017	62.4	82	2.3	2.4	🟨 6-024	57.9	76	2.5	2.7	🟨 6-122	32.8	43	15.2	17.3
		🟥 6-130	69.7	91	19.6	29.7	6-250	59.8	78	7.4	11.8	🟫 6-194	88.8	116	4.7	7.9	🟫 6-134	65.8	86	2.2	2.7	🟨 160/165	49.3	65	7.9	9.1	🟨 6-239	53.7	70	6.7	7.4
		Avg.	76.8	100	20.5	25.0	Avg.	63.4	83	7.3	10.5	Avg.	93.0	122	4.9	7.7	Avg.	60.6	79	2.2	2.5	Avg.	53.0	69	4.2	4.6	Avg.	50.9	67	7.5	8.6
		SD	6.2	8	2.3	4.8	SD	3.4	4	1.2	1.4	SD	5.9	8	0.2	0.3	SD	6.4	8	0.2	0.2	SD	4.4	6	3.2	3.9	SD	16.8	22	7.3	8.1
		Δ%	3		–25	–34	Δ%	12		3	-21	Δ%	9		–45	–54	Δ%	–3		132	–42	Δ%	81		21	–16	Δ%	115		43	39
	50	🟥 6-088	75.2	98	4.3	10.1	🟥 6-236	56.6	74	19.9	22.8	🟫 6-118	99.1	130	2.4	8.8	🟫 6-156	96.8	127	1.4	6.3	🟦 6-061	33.6	44	12.1	12.3	🟦 6-122	25.4	33	8	10
		🟥 6-011	63	82	6.5	7.1	🟥 6-135	60.3	79	11.5	13.4	🟫 6-198	103.9	136	5.4	15.7	🟥 6-089	85.4	112	2.6	7.5	🟦 6-055	31.6	41	9.2	12	🟦 6-158	26.5	35	3.7	4.9
		🟥 6-174	55.5	73	9.8	19.2	🟥 6-050	58.4	76	8.0	12.5	🟫 6-213	122.7	161	2.1	6	🟨 6-249	57.4	75	2.7	7	🟦 6-063	27.6	36	6.4	6.4	🟦 6-219	43.4	57	11.8	12.4
		Avg.	64.6	85	6.9	12.1	Avg.	58.4	76	13.1	16.2	Avg.	108.6	142	3.3	10.2	Avg.	79.9	105	2.2	6.9	Avg.	30.9	40	9.2	10.2	Avg.	31.8	42	7.8	9.1
		SD	9.9	13	2.8	6.3	SD	1.9	2	6.1	5.7	SD	12.5	16	1.8	5.0	SD	20.3	27	0.7	0.6	SD	3.1	4	2.9	3.3	SD	10.1	13	4.1	3.8
		Δ%	–14		–75	–68	Δ%	3		86	23	Δ%	28		–63	–40	Δ%	28		139	60	Δ%	6		169	86	Δ%	34		50	46
	100	🟥 6-199	66.5	87	1.9	2.4	🟥 6-226	56.4	74	7.5	10.1	🟫 6-172	106.7	140	4.6	11.5	🟨 6-048	72.6	95	2.9	8	🟦 6-065	21.8	29	8	8.0	🟦 6-040	30.2	40	4.6	6.8
		🟥 6-116	68.9	90	10.3	13.8	🟥 6-197	60.5	79	13.3	14.3	🟫 6-218	112.3	147	3	10.2	🟥 6-223	98.6	129	2.2	5.8	🟦 6-151	35.1	46	9.6	11.5	🟦 6-047	30.5	40	6.4	6.4
		🟥 6-150	72.7	95	11.5	11.9	🟥 6-036	60.5	79	12.5	13.2	🟫 6-010	70.8	93	3.3	12.4	🟫 6-242	85.8	112	2.9	7.0	🟦 6-186	46.6	61	3.3	5.9	🟦 6-096	30.3	40	5.3	6.8
		Avg.	69.4	91	7.9	9.4	Avg.	59.1	77	11.1	12.5	Avg.	96.6	126	3.6	11.4	Avg.	85.7	112	2.7	6.9	Avg.	34.5	45	7.0	8.5	Avg.	30.3	40	5.4	6.7
		SD	3.1	4	5.2	6.1	SD	2.4	3	3.1	2.2	SD	22.5	29	0.9	1.1	SD	13.0	17	0.4	1.1	SD	12.4	16	3.3	2.8	SD	0.2	0	0.9	0.2
		Δ%	–7		–71	–75	Δ%	5		57	–5	Δ%	14		–59	–33	Δ%	37		186	60	Δ%	18		103	54	Δ%	28		4	7
	180	🟥 6-195	61.2	80	17.1	17.4	🟥 6-049	76.8	101	10.9	14.9	🟫 6-168	94.1	123	5.3	8.2	🟫 6-237	91	119	1.5	4	🟦 6-121	42.9	56	6.8	7	🟦 6-029	24.3	32	7.5	9.7
		~~6-149~~					🟥 6-027	77.2	101	8.8	13.7	🟫 6-094	133.7	175	4.4	8.7	🟫 6-051	56.5	74	4.7	11.9	🟦 6-143	25.1	33	8.1	9.3	🟦 6-057	21.4	28	13.6	13.9
		🟫 6-044	68.2	89	2.6	11.4	🟥 6-157	65.4	86	7.2	11.5	🟫 6-142	102.6	134	4.5	7.7	🟫 6-227	99.5	130	3.5	7.8	🟦 6-054	30.9	40	4.6	11	🟦 6-238	32.5	43	2.9	4.2
		Avg.	64.7	85	9.9	14.4	Avg.	73.1	96	9.0	13.4	Avg.	110.1	144	4.7	8.2	Avg.	82.3	108	3.2	7.9	Avg.	33.0	43	6.5	9.1	Avg.	26.1	34	8.0	9.3
		SD	4.9	6	10.3	4.2	SD	6.7	9	1.9	1.7	SD	20.8	27	0.5	0.5	SD	22.8	30	1.6	4.0	SD	9.1	12	1.8	2.0	SD	5.8	8	5.4	4.9
		Δ%	–14		–64	–62	Δ%	29		27	1	Δ%	30		–46	–51	Δ%	32		246	82	Δ%	13		89	65	Δ%	10		53	49

🟥	Cohesive failure	🟦	Adhesive failure on fastener surface	🟨	Mixture of adhesive and cohesive mode	🟫	Thermally degraded or charred

TABLE A.17.—SUMMARY OF TORQUE DATA AT 100 AND 200 °C INCLUDING FAILURE MODE OF THREAD LOCKER CANDIDATES IN #7 OR #8 JOINT AS A FUNCTION OF ACCELERATED AGING CONDITIONS

Aging *T*, °C	Aging *t*, day	#7 or 8 Joint torque strengths, N-cm, and % installation torques																													
		Loctite 294 Installation torque = 74.51 N-cm										Resbond 507TS Installation torque = 74.51 N-cm										Poly-Lok PET Installation torque = 13.03 N-cm									
		100 °C					200 °C					100 °C					200 °C					100 °C					200 °C				
		Sample ID	Breakloose		Prevail -ing torque	Maxi- mum torque	Sample ID	Breakloose		Prevail- ing torque	Maxi- mum torque	Sample ID	Breakloose		Prevail- ing torque	Maxi- mum torque	Sample ID	Breakloose		Prevail- ing torque	Maxi- mum torque	Sample ID	Breakloose		Prevail- ing torque	Maxi- mum torque	Sample ID	Breakloose		Prevail- ing torque	Maxi- mum torque
			Torque	% Inst.				Torque	% Inst.				Torque	% Inst.				Torque	% Inst.				Torque	% Inst.				Torque	% Inst.		
23	0																					8-010	11.8	91	5.3	7.5	8-179	11.9	91	2.0	2.8
																						8-174	9.2	71	2.5	3.3	8-123	12.1	93	0.8	1.4
																						8-024	8.8	68	7.7	7.7	8-183	11.7	90	1.5	1.7
																						Avg.	9.9	76	5.2	6.2	Avg.	11.9	91	1.4	2.0
																						SD	1.6	13	2.6	2.5	SD	0.2	2	0.6	0.7
	0	7-153	78.4	105	35.1	45.1	7-158	92.5	124	22.7	24.8	7-048	204.5	274	64.5	88.3	7-138	129.2	173	7.8	11.6	8-206	6.2	48	2.3	3.2	8-188	3.4	26	3	3.3
		7-031	75.8	102	56.0	63.9	7-151	82.6	111	15.8	20.7	7-004	176.0	236	75.2	100	7-003	117.8	158	9.2	17.5	8-041	8.5	65	2.3	3	8-205	2.8	21	3.0	3.1
		7-132	89.4	120	57.8	71	7-159	72.0	97	21.0	22.8	7-150	119.6	161	42.4	43.3	7-037	103.9	139	6.7	10.1	8-048	5.3	41	0.9	1.9	8-110	3.3	25	1.8	2.6
		Avg.	81.2	109	49.6	60.0	Avg.	82.4	111	19.8	22.8	Avg.	166.7	224	60.7	77.2	Avg.	117.0	157	7.9	13.1	Avg.	6.7	51	1.8	2.7	Avg.	3.2	24	2.6	3.0
		SD	7.2	10	12.6	13.4	SD	10.3	14	3.6	2.1	SD	43.2	58	16.7	29.9	SD	12.7	17	1.3	3.9	SD	1.7	13	0.8	0.7	SD	0.3	2	0.7	0.4
190	15																					8-029	15.2	117	7.2	8.4	8-211	7.7	59	6.7	10.0
																						8-215	11.1	85	13.1	15.0	8-200	11.6	89	5.0	6.7
																						8-119	9.7	74	12.9	14.0	8-209	21.6	166	8.0	9.8
																						Avg.	12.0	92	11.1	12.5	Avg.	13.6	105	6.6	8.8
																						SD	2.9	22	3.4	3.6	SD	7.2	55	1.5	1.9
																						Δ%	80		504	362	Δ%	331		153	194
	50	7-154	94.1	126	99.5	112.3	7-020	95.7	128	34.3	42.1	7-119	206.9	278	16.6	36.3	7-149	90.3	121	5.6	5.6	8-208	10.9	84	7.2	8.2	8-034	3.5	27	3.2	3.6
		7-126	85.3	114	44.3	48.6	7-136	80.5	108	90.9	93.3	7-050	201.5	270			7-060	110.2	148	0.0	9.0	8-008	15.1	116	11.0	13.9	8-252	11.5	88	3.1	3.1
		7-156	102.7	138	127.0	141.2	7-035	83.4	112	58.6	73.6	7-051	212.3	285	63.8	77	7-120	87.1	117	6.7	8.9	8-031	14.9	114	11.4	17.9	8-164	15.7	120	0.9	1.1
		Avg.	94.0	126	90.3	100.7	Avg.	86.5	116	61.3	69.7	Avg.	206.9	278	40.2	56.7	Avg.	95.9	129	4.1	7.8	Avg.	13.6	105	9.9	13.3	Avg.	10.2	79	2.4	2.6
		SD	8.7	12	42.1	47.4	SD	8.1	11	28.4	25.8	SD	5.4	7	33.4	28.8	SD	12.5	17	3.6	1.9	SD	2.4	18	2.3	4.9	SD	6.2	48	1.3	1.3
		Δ%	16		82	68	Δ%	5		209	206	Δ%	24		–34	–27	Δ%	–18		–48	–40	Δ%	105		438	394	Δ%	223		–8	–13
	100	7-033	98.1	132	76.3	83.7	7-014	97	130	116.7	146.3	7-029	211.7	284			7-144	87	117	7.2	9.7	8-059	4.0	31	11.8	13.1	8-178	15.3	117	6.7	9.9
		7-143	105.2	141	144.1	159.4	7-042	88.1	118	105.8	112.1	7-057	222.1	298			7-058	88.3	119	4.8	5.8	8-060	14.3	110	7.6	7.8	8-047	12.7	97	2.6	2.8
		7-036	102.5	138	139.2	144.5	7-160	90.9	122	61.6	70.5	7-007	215.0	289			7-012	100.1	134	5.0	7.4	8-192	13.1	101	11.8	12.7	8-124	6.8	52	6.2	7.3
		Avg.	101.9	137	119.9	129.2	Avg.	92.0	123	94.7	109.6	Avg.	216.3	290	#DIV/0!	#DIV/0!	Avg.	91.8	123	5.7	7.6	Avg.	10.5	80	10.4	11.2	Avg.	11.6	89	5.2	6.7
		SD	3.6	5	37.8	40.1	SD	4.6	6	29.2	38.0	SD	5.3	7	#DIV/0!	#DIV/0!	SD	7.2	10	1.3	2.0	SD	5.6	43	2.4	3.0	SD	4.4	33	2.2	3.6
		Δ%	26		142	115	Δ%	12		377	382	Δ%	30		#DIV/0!	#DIV/0!	Δ%	–22		–28	–42	Δ%	57		467	315	Δ%	266		99	122
	180	7-155	103.5	139	160.4	160.9	7-112	89.2	120	89.5	103.9	7-011	222.5	299	Screw head failure		7-052	121.9	164	6.2	11.5	8-040	9.6	74	10.3	11.3	8-128	10.1	78	5.8	5.8
		7-137	107.4	144	122.4	149.8	7-047	93.6	126	56.6	60.2	7-161	218	293			7-054	89.5	120	6.9	9.6	8-052	14.5	111	8.5	10.2	8-146	20.6	158	6.8	8.2
		7-152	102	137	58.5	63.4	7-111	95.6	128	104.1	116.6	7-142	211.4	284			7-028	90.8	122	7.5	9.1	8-160	3.8	29	3.3	11.2	8-053	9.8	75	4.0	4.1
		Avg.	104.3	140	113.8	124.7	Avg.	92.8	125	83.4	93.6	Avg.	217.3	292	#DIV/0!	#DIV/0!	Avg.	100.7	135	6.9	10.1	Avg.	9.3	71	7.4	10.9	Avg.	13.5	104	5.5	6.0
		SD	2.8	4	51.5	53.4	SD	3.3	4	24.3	29.6	SD	5.6	7	#DIV/0!	#DIV/0!	SD	18.3	25	0.7	1.3	SD	5.4	41	3.6	0.6	SD	6.2	47	1.4	2.1
		Δ%	28		129	108	Δ%	13		321	311	Δ%	30		#DIV/0!	#DIV/0!	Δ%	–14		–13	–23	Δ%	40		302	304	Δ%	326		113	101

TABLE A.17.—SUMMARY OF TORQUE DATA AT 100 AND 200 °C INCLUDING FAILURE MODE OF THREAD LOCKER CANDIDATES IN #7 OR #8 JOINT AS A FUNCTION OF ACCELERATED AGING CONDITIONS

Aging T, °C	Aging t, day	#7 or 8 Joint torque strengths, N-cm, and % installation torques																													
		Loctite 294 Installation torque = 74.51 N-cm										Resbond 507TS Installation torque = 74.51 N-cm										Poly-Lok PET Installation torque = 13.03 N-cm									
		100 °C					200 °C					100 °C					200 °C					100 °C					200 °C				
		Sample ID	Breakloose		Prevail-ing torque	Maxi-mum torque	Sample ID	Breakloose		Prevail-ing torque	Maxi-mum torque	Sample ID	Breakloose		Prevail-ing torque	Maxi-mum torque	Sample ID	Breakloose		Prevail-ing torque	Maxi-mum torque	Sample ID	Breakloose		Prevail-ing torque	Maxi-mum torque	Sample ID	Breakloose		Prevail-ing torque	Maxi-mum torque
			Torque	% Inst.				Torque	% Inst.				Torque	% Inst.				Torque	% Inst.				Torque	% Inst.				Torque	% Inst.		
220	15																					🟨 8-025	12.0	92	13.9	18.2	🟨 8-187	14.1	108	8.2	9.3
																						🟨 8-132	7.5	58	4.2	4.6	🟨 8-218	16.5	127	9.2	12.2
																						🟨 8-198	30.7	236	2.5	2.7	🟨 8-112	12.4	95	4.7	4.9
																						Avg.	16.7	128	6.9	8.5	Avg.	14.3	110	7.4	8.8
																						SD	12.3	94	6.2	8.5	SD	2.1	16	2.4	3.7
																						Δ%	151		275	215	Δ%	353		183	193
	50	🟥 7-129	109.4	147	167.1	171.9	🟥 7-113	88.9	119	47.5	51.7	7-034	221.5	297	Screw head failure		🟨 7-009	129.6	174	8.5	17.7	🟦 8-186	16.1	124	6.4	6.7	🟦 8-203	13.7	105	5.3	6.2
		🟥 7-117	86.7	116	46.3	48.5	🟫 7-141	89.0	119	79.4	82.8	7-001	213.2	286			🟨 7-121	92	123	6.0	8.5	🟦 8-037	16.1	124	5.4	7.4	🟦 8-038	12.7	97	5.0	5.8
		🟥 7-148	84.6	114	90.7	94.2	🟥 7-040	79.0	106	53.9	54.2	7-044	199.7	268			7-114	107.3	144	7.7	9.4	🟦 8-175	11.3	87	11.4	11.6	🟦 8-158	14.5	111	5.3	9.0
		Avg.	93.6	126	101.4	104.9	Avg.	85.6	115	60.3	62.9	Avg.	211.5	284	#DIV/0!	#DIV/0!	Avg.	109.6	147	7.4	11.9	Avg.	14.5	111	7.7	8.6	Avg.	13.6	105	5.2	7.0
		SD	13.8	18	61.1	62.4	SD	5.7	8	16.9	17.3	SD	11.0	15	#DIV/0!	#DIV/0!	SD	18.9	25	1.3	5.1	SD	2.8	21	3.2	2.7	SD	0.9	7	0.2	1.7
		Δ%	15		104	75	Δ%	4		204	176	Δ%	27		#DIV/0!	#DIV/0!	Δ%	–6		–6	–9	Δ%	118		322	217	Δ%	331		100	133
	100	🟥 7-146	105.6	142	100.8	104.8	🟥 7-008	94.7	127	36.5	40.5	7-002	209	281			🟫 7-025	184.8	248	18.6	24.5	🟦 8-046	9.9	76	1	1.5	🟦 8-136	6.5	50	7.2	8.1
		🟥 7-157	87.3	117	40.4	42	🟥 7-039	90.1	121	48.1	48.2	7-043	218	293			🟫 7-123	121.5	163	8.1	10.1	🟦 8-207	13.7	105	5.3	7.3	🟦 8-035	15.3	117	2.6	3
		🟥 7-059	107.2	144	71.8	73	🟥 7-016	94.1	126	74.1	74.2	7-032	216.2	290			🟫 7-124	134.4	180	7.0	10.4	🟦 8-222	19.6	150	7.0	7.2	🟦 ~~8-224~~				
		Avg.	100.0	134	71.0	73.3	Avg.	93.0	125	52.9	54.3	Avg.	214.4	288	#DIV/0!	#DIV/0!	Avg.	146.9	197	11.2	15.0	Avg.	14.4	111	4.4	5.3	Avg.	10.9	84	4.9	5.6
		SD	11.1	15	30.2	31.4	SD	2.5	3	19.3	17.7	SD	4.8	6	#DIV/0!	#DIV/0!	SD	33.5	45	6.4	8.2	SD	4.9	38	3.1	3.3	SD	6.2	48	3.3	3.6
		Δ%	23		43	22	Δ%	13		167	139	Δ%	29		#DIV/0!	#DIV/0!	Δ%	26		42	15	Δ%	116		142	98	Δ%	244		88	85
	180	🟥 7-139	91.3	123	68.5	85.9	🟥 7-015	88.9	119	23.7	31.7	7-135	205.2	275	Screw head failure		🟫 7-005	228.5	307	23.2	46.4	🟦 8-201	16.9	130	10.2	10.4	🟦 8-036	13.7	105	4.8	5.9
		🟥 7-056	107.4	144	109.5	113.1	🟥 7-133	79	106	17.8	24	7-055	202.1	271			🟫 7-127	194.9	262	31.8	48.1	🟫 8-042	3.3	25	3.1	3.9	🟦 8-233	8.5	65	6.9	7.1
		🟥 7-140	104.5	140	66.6	69.5	🟥 7-128	93.2	125	60.9	67.4	7-010	207.5	279			🟫 7-125	186.2	250	11.9	23.7	🟦 8-058	16.7	128	4.9	5.6	🟦 8-145	9.6	74	2.9	5.1
		Avg.	101.1	136	81.5	89.5	Avg.	87.0	117	34.1	41.0	Avg.	204.9	275	#DIV/0!	#DIV/0!	Avg.	203.2	273	22.3	39.4	Avg.	12.3	94	6.1	6.6	Avg.	10.6	81	4.9	6.0
		SD	8.6	12	24.2	22.0	SD	7.3	10	23.4	23.2	SD	2.7	4	#DIV/0!	#DIV/0!	SD	22.3	30	10.0	13.6	SD	7.8	60	3.7	3.4	SD	2.7	21	2.0	1.0
		Δ%	24		64	49	Δ%	6		72	80	Δ%	23		#DIV/0!	#DIV/0!	Δ%	74		182	202	Δ%	85		231	146	Δ%	235		87	101

🟥	Cohesive failure	🟦	Adhesive failure on fastener surface	🟨	Mixture of adhesive and cohesive mode	🟫	Thermally degraded or charred

TABLE A.18.—OVERALL TEST MATRIX FOR 6-MONTH ACCELERATED THERMAL AGING EXPERIMENT OF O-RING AND SHRINK TUBING CANDIDATES

Aging *T*, °C	Aging *t*, day		0		15		50		100		180	
	Date		1/23/2014		2/7/2014		3/18/2014		5/7/2014		7/24/2014	
	Specimen	Organic	Specimen group ID and number of tube specimens									
175	O-ring	S1151	S1	10	S2	10	S5	10	S8	10	S11	10
(347 °F)		Z1028	Z1	10	Z2	10	Z5	10	Z8	10	Z11	10
Lunaire, R145	Shrink tubing	SRFR	R1	12	R2	11	R5	11	R8	12	R11	12
		ETFE	E1	15	E2	15	E5	15	E8	15	E11	15
200	O-ring	S1151			S3	10	S6	10	S9	10	S12	10
(392 °F)		Z1028			Z3	10	Z6	10	Z9	10	Z12	10
Blue M #5, R244	Shrink tubing	SRFR			R3	11	R6	11	R9	12	R12	12
		ETFE			E3	15	E6	15	E9	15	E12	15
225	O-ring	S1151			S4	10	S7	10	S10	10	S13	10
(437 °F)		Z1028			Z4	10	Z7	10	Z10	10	Z13	10
Blue M #6, R244	Shrink tubing	SRFR			R4	11	R7	12	R10	12	R13	12
		ETFE			E4	15	E7	15	E10	15	E13	15

TABLE A.19.—SUMMARY OF THERMAL PROPERTIES OF SRFR SHRINK TUBING AFTER THE ACCELERATED THERMAL AGING EXPOSURES

Sample type	Aging t, day		0	15	50	99	174	0	15	50	99	174	0	15	50	99	174	0	15	50	99	174	0	15	50	99	174	0	15	50	99	174
	Aging T, °C		mDSc, T_g, °C					mDSc, T_m, °C					mDSc, ΔH_{mR}, J/g					mDSC, ΔH_{mN}, J/g					mDSC, T_r, °C					TGA, T_d, °C				
SRFR	Avg.	175	101	99	99	86	94	–46	–47	–47	–46	–46	5.77	6.75	7.87	6.26	6.18	2.35	0.90	3.00	1.67	2.81	–47	–47	–48	–48	–49	400	426	429	425	429
		200	101	99	97	95	108	–46	–47	–47	–46	–47	5.77	7.27	9.84	7.15	5.90	2.35	2.49	2.98	0.88	2.24	–47	–48	–46	–49	–48	400	432	439	442	447
		225	101	104	110	87	101	–46	–46	–48	–47	–48	5.77	4.82	7.21	7.56	6.44	2.35	0.70	1.59	2.58	1.50	–47	–48	–49	–48	–50	400	444	455	451	458
	SD	175	0.5	3.0	1.9	1.9	13.2	0.0				0.1	0.4				4.9	0.0				2.3	0.0				0.5	3.0	0.8	0.6	0.3	0.4
		200	0.5	0.6	8.7	6.9	7.6	0.0		1.4			0.4		2.4			0.0		0.3			0.0		1.6			3.0	1.6	0.8	1.1	1.7
		225	0.5	3.1	4.0	4.5	9.0	0.0			1.0		0.4			4.0		0.0			1.4		0.0			0.8		3.0	0.9	4.4	1.4	0.8
	%Δ	175	0	–2	–1	–14	–7	0	2	3	1	0	0	17	36	8	7	0	–62	27	–29	20	0	0	0	2	3	0	7	7	6	7
		200	0	–2	–4	–6	7	0	4	4	2	4	0	26	70	24	2	0	6	27	–62	–5	0	1	–3	3	1	0	8	10	11	12
		225	0	3	0	–14	9	0	1	5	3	5	0	–16	25	31	12	0	–70	–32	10	–36	0	1	3	2	5	0	11	14	13	14

Sample type	Aging t, day		0	15	50	99	174	0	15	50	99	174	0	15	50	99	174	0	15	50	99	174	0	15	50	99	174
	Aging T, °C		TGA, Δwt%, RT-100 °C					TGA, Δwt%, 100-200 °C					TGA, Δwt%, at 700 °C					Iso-TGA at 200 °C, 7 hr, Initial wt loss, wt%					Iso-TGA at 200 °C, 7 hr, Dwell wt loss, wt%				
SRFR	Avg.	175	0.20	0.32	0.28	0.22	0.15	0.19	0.22	0.14	0.42	0.25	16.5	19.1	19.5	19.0	19.4	1.08	0.87	0.45	0.62	0.51	1.85	0.72	0.49	0.27	0.28
		200	0.20	0.29	0.38	0.25	0.43	0.19	0.19	0.14	0.21	0.15	16.5	20.9	21.6	22.3	22.7	1.08	0.42	0.66	0.48	0.40	1.85	0.40	0.34	0.16	0.26
		225	0.20	0.33	0.24	0.19	0.09	0.19	0.09	0.32	0.16	0.53	16.5	24.0	25.7	24.6	25.3	1.08	0.35	0.42	0.54	0.46	1.85	0.19	0.29	0.22	0.22
	SD	175	0.20	0.04	0.17	0.09	0.11	0.02	0.06	0.04	0.15	0.03	0.3	0.1	0.3	0.6	0.1	0.41	0.08	0.19		0.24	0.41	0.11	0.09		0.05
		200	0.20	0.03	0.08	0.04	0.28	0.02	0.07	0.01	0.08	0.00	0.3	0.1	0.2	1.0	0.7	0.41	0.05	0.41	0.11	0.01	0.41	0.03	0.18	0.03	0.02
		225	0.20	0.06	0.15	0.13	0.07	0.02	0.06	0.07	0.03	0.01	0.3	0.6	0.6	4.5	0.4	0.41	0.09	0.19	0.10	0.14	0.41	0.01	0.17	0.02	0.02
	%Δ	175	0	65	41	15	–24	0	16	–25	124	32	0	15	18	15	17	0	–20	–58	–43	–53	0	–61	–74	–85	–85
		200	0	48	92	28	118	0	4	–24	11	–20	0	26	30	35	37	0	–62	–39	–56	–63	0	–78	–82	–91	–86
		225	0	68	23	–4	–54	0	–53	74	–13	184	0	45	55	49	53	0	–68	–61	–50	–57	0	–90	–84	–88	–88

Sample type	Aging t, day		0	15	50	99	174	0	15	50	99	174	0	15	50	99	174	0	15	50	99	174	0	15	50	99	174
	Aging T, °C		Iso-TGA at 200 °C, 7 hr, Loss rate, [(wt%/min)×1000]					DMA-axail, T_{t1}, °C tan δ					DMA-axail, T_{t2}, °C tan δ					DMA-axail, E' ratio, (150/23 °C) %					DMA-axail, E' ratio, (200/23 °C) %				
SRFR	Avg.	175	–2.80	–0.90	–0.83	–0.07	–0.26	137	144	148	149	150						28	22	23	26	23	20	14	14	16	14
		200	–2.80	–0.48	–0.30	–0.10	–0.45	137	147	146	153	153						28	26	22	27	25	20	16	15	15	14
		225	–2.80	–0.12	–0.23	–0.09	0.00	137	151	152	157	160						28	26	25	27	26	20	14	13	13	12
	SD	175	1.84	0.23	0.01		0.07	7	1	3	1	6						4	4	3	4	4	4	1	3	3	2
		200	1.84	0.00	0.32	0.03	0.03	7	0	0	1	2						4	6	4	4	5	4	3	2	4	2
		225	1.84	0.10	0.21	0.10	0.00	7	0	2	1	2						4	5	3	4	4	4	3	2	2	3
	%Δ	175	0	–68	–70	–97	–91	0	5	8	8	9						0	–20	–19	–8	–19	0	–33	–31	–22	–33
		200	0	–83	–89	–96	–84	0	7	6	11	12						0	–7	–22	–3	–10	0	–20	–28	–24	–33
		225	0	–96	–92	–97	–100	0	10	11	15	17						0	–9	–9	–2	–7	0	–31	–39	–35	–42

Sample type	Aging t, day		0	15	50	99	174	0	15	50	99	174	0	15	50	99	174	0	15	50	99	174
	Aging T, °C		DMA-radial, T_{t1}, °C tanδ					DMA-radial, T_{t2}, °C tanδ					DMA-radial, E' ratio, (150/23 °C) %					DMA-radial, E' ratio, (200/23 °C) %				
SRFR	Avg.	175	155	155	159	153	159	258	230	236			35	40	38	37	46	19	24	21	20	26
		200	155	160	160	159	166	258	311				35	40	47	38	43	19	21	25	20	25
		225	155	163	167	171	170	258					35	42	44	37	41	19	24	27	21	21
	SD	175		2	2								5	11	7			1	10	4		
		200											5	2	4	17	17	1	2	4	8	18
		225											5	1	15	9	12	1	5	15	1	7
	%Δ	175	0	0	3	–1	3	0	–11	–9			0	15	9	5	30	0	22	10	1	34
		200	0	3	3	3	7	0	21	–100			0	15	35	7	22	0	8	31	5	32
		225	0	5	8	10	10	0	–100	–100			0	19	25	6	18	0	26	42	9	11

TABLE A.20.—SUMMARY OF THERMAL PROPERTIES OF ETFE SHRINK TUBING AFTER THE ACCELERATED THERMAL AGING EXPOSURES

Sample type	Aging *t*, day		0	15	50	99	174	0	15	50	99	174	0	15	50	99	174	0	15	50	99	174	0	15	50	99	174	0	15	50	99	174
	Aging *T*, °C		mDSC, T_g, °C					mDSC, T_m, °C					mDSC, ΔH_{mR}, J/g					mDSC ΔH_{mN}, J/g					mDCS, T_r, °C					TGA, T_d, °C				
ETFE	Avg.	175	–5	–4	–5	–5	–5	217	218	219	219	219	6.16	4.53	5.33	3.41	5.84	8.89	13.46	14.42	12.88	13.39	216	216	216	217	217	481	480	485	482	483
		200	–5	–4	–4	–5	–5	217	225	226	228	228	6.16	1.62	3.81	3.94	4.76	8.89	12.61	11.27	11.86	10.84	216	223	225	226	226	481	481	478	479	478
		225	–5	–4	–5	–4	–5	217	213	215	210	209	6.16	3.39	2.95	5.19	5.60	8.89	9.32	8.71	7.81	7.36	216	212	213	209	208	481	481	481	480	482
	SD	175	0.8	0.2	1.0	0.5	0.2	0.0	0.8	0.3	0.0	0.1	1.1	1.0	2.8	0.2	0.5	1.9	0.7	2.5	0.9	0.1	0.6	0.7	0.6	0.3	0.6	0.8	0.2		1.3	0.1
		200	0.8	0.6	0.3	0.2	0.8	0.0	2.1	1.4	0.8	0.9	1.1	1.3	0.3	0.6	0.0	1.9	0.6	2.0	0.3	0.1	0.6	0.9	0.5	0.3	0.0	0.8	0.5	0.6	1.8	0.2
		225	0.8	0.5	0.4	0.5	0.4	0.0	0.8	3.5	0.4	0.9	1.1	1.6	1.3	0.5	0.7	1.9	1.4	2.1	2.0	0.8	0.6	0.8	3.2	1.0	0.7	0.8	1.4	0.2	1.3	1.0
	%Δ	175	0	–15	–1	–1	8	0	0	1	1	1	0	–27	–14	–45	–5	0	51	62	45	51	0	0	0	1	1	0	0	1	0	0
		200	0	–7	–6	6	4	0	4	4	5	5	0	–74	–38	–36	–23	0	42	27	33	22	0	3	4	5	5	0	0	–1	0	–1
		225	0	–7	–1	–9	2	0	–2	–1	–3	–4	0	–45	–52	–16	–9	0	5	–2	–12	–17	0	–2	–1	–3	–3	0	0	0	0	0

Sample type	Aging *t*, day		0	15	50	99	174	0	15	50	99	174	0	15	50	99	174	0	15	50	99	174	0	15	50	99	174
	Aging *T*, °C		TGA, Δwt%, RT-100 °C					TGA, Δwt%, 100-200 °C					TGA, Δwt%, at 700 °C					Iso-TGA at 200 °C, 7 hr, Initial wt loss, wt%					Iso-TGA at 200 °C, 7 hr, Dwell wt loss, wt%				
ETFE	Avg.	175	0.08	0.07	0.06	0.11	0.03	0.04	0.07	0.04	0.08	0.05	94.3	94.1	90.5	92.2	88.8	0.24	0.07	0.10	0.06	0.12	0.11	0.04	0.02	0.04	0.02
		200	0.08	0.06	0.13	0.04	0.20	0.04	0.04	0.07	0.05	0.13	94.3	93.9	93.9	93.0	94.0	0.24	0.07	0.08	0.09	0.10	0.11	0.01	0.03	0.01	0.01
		225	0.08	0.06	0.06	0.07	0.07	0.04	0.05	0.07	0.02	0.10	94.3	92.0	91.6	94.3	93.6	0.24	0.04	0.08	0.05	0.19	0.11	0.10	0.01	0.04	0.03
	SD	175	0.03	0.04		0.08	0.01	0.03	0.03		0.08	0.07	0.5	0.0	0.0	1.6	2.1	0.19	0.05	0.12	0.02	0.03	0.15	0.02	0.02	0.04	0.01
		200	0.03	0.03	0.01	0.06	0.12	0.03	0.02	0.02	0.05	0.06	0.5	0.1	0.1	2.0	0.1	0.19	0.06	0.01	0.00	0.02	0.15	0.01	0.03	0.01	0.01
		225	0.03	0.04	0.08	0.03	0.02	0.03	0.01	0.00	0.02	0.02	0.5	1.5	2.7	0.4	0.5	0.19	0.01	0.03	0.04	0.03	0.15	0.08	0.01	0.03	0.00
	%Δ	175	0	–11	–28	41	–57	0	50	2	89	23	0	0	–4	–2	–6	0	–72	–58	–76	–52	0	–59	–85	–67	–86
		200	0	–24	67	–44	160	0	–13	70	4	203	0	0	0	–1	0	0	–73	–67	–61	–58	0	–88	–77	–87	–93
		225	0	–23	–17	–12	–13	0	17	–46	18	117	0	–2	–3	0	–1	0	–84	–68	–79	–22	0	–10	–87	–61	–72

Sample type	Aging *t*, day		0	15	50	99	174	0	15	50	99	174	0	15	50	99	174	0	15	50	99	174	0	15	50	99	174
	Aging *T*, °C		Iso-TGA at 200 °C, 7 hr, Loss rate, [(wt%/min)×1000]					DMA-axail, T_{t1}, °C tanδ					DMA-axail, T_{t2}, °C tanδ					DMA-axail, *E′* ratio, (150/23 °C) %					DMA-axail, *E′* ratio, (200/23 °C) %				
ETFE	Avg.	175	–0.011	–0.06	–0.02	–0.09	–0.013	85	84	82	85	86	233	233	229	234	238	12	20	15	16	14	6	13	9	12	10
		200	–0.011	–0.03	0.01	–0.01	–0.014	85	85	83	87	88	233	239	241	243	246	12	15	12	17	12	6	7	7	10	7
		225	–0.011	–0.17	0.00	0.00	–0.054	85	82	81	84	85	233	222	227	224	223	12	15	19	11	12	6	7	11	5	7
	SD	175	0.02	0.05	0.03	0.13	0.02	3	4	1	1	2	1	4	1	3	0	3	8	9	7	9	1	5	5	6	7
		200	0.02	0.04	0.02	0.01	0.01	3	1	3	1	2	1	2	1	1	3	3	8	3	11	3	1	3	2	7	3
		225	0.02	0.04	0.08	0.04	0.08	3	0	2	7	0	1	5	1	4	4	3	12	7	4	5	1	6	5	2	3
	%Δ	175	0	489	98	768	23	0	–1	–4	0	1	0	0	–2	1	2	0	72	32	41	25	0	125	62	103	78
		200	0	182	–215	–45	29	0	1	–2	3	4	0	3	3	4	6	0	31	7	48	2	0	31	19	72	19
		225	0	1463	–113	–82	391	0	–3	–4	0	0	0	–4	–2	–4	–4	0	28	68	–4	7	0	27	91	–6	15

Sample type	Aging *t*, day		0	15	50	99	174	0	15	50	99	174	0	15	50	99	174	0	15	50	99	174
	Aging *T*, °C		DMA-radial, T_{t1}, °C tanδ					DMA-radial, T_{t2}, °C tanδ					DMA-radial, *E′* ratio, (150/23 °C) %					DMA-radial, *E′* ratio, (200/23 °C) %				
ETFE	Avg.	175	91	93	93	95	84	243	243	248	251	267	24	17	21	16	14	15	10	14	8	8
		200	91	92	96	95	90	243	248	248	252	249	24	15	22	24	20	15	10	15	14	13
		225	91	88	93	89	92	243	238	254	244	228	24	21	20	30	23	15	12	9	19	14
	SD	175			2									3	21	6			5	16	2	
		200												15	24	4	14		12	16	2	11
		225				2								6	11	6	2		4	3	6	3
	%Δ	175	0	2	2	4	–8	0	0	2	4	10	0	–31	–13	–36	–43	0	–34	–8	–46	–49
		200	0	1	6	5	–1	0	2	2	4	3	0	–39	–8	0	–16	0	–35	0	–8	–9
		225	0	–3	2	–2	1	0	–2	5	0	–6	0	–14	–17	24	–5	0	–20	–39	27	–4

TABLE A.21.—OVERALL NOTCHED TENSILE PROPERTIES OF SHRINK TUBING CANDIDATES AS A FUNCTION OF ACCELERATED AGING CONDITION

Material direction	Aging *T*, °C	Properties Aging *t*, day	Notched tensile strength at 25 °C, psi					Notched tensile strength at 200 °C, psi					Ultimate Elongation at 25 °C, in./in.					Ultimate elongation at 200 °C, in./in.				
			0	15	50	99	174	0	15	50	99	174	0	15	50	99	174	0	15	50	99	174
SRFR - Axial (radially notched)	175	Avg.	461	436	360	312	311	160	128	101	103	85	10.9	4.9	3.3	2.3	2.0	7.9	4.0	2.5	2.6	1.9
		SD	65	87	34	24	16	19	24	10	18	12	3.4	1.2	0.5	0.3	0.1	1.5	0.8	0.3	0.4	0.3
		Δ%	0	−5	−22	−32	−33	0	−20	−37	−35	−47	0	−56	−70	−78	−82	0	−49	−68	−67	−76
	200	Avg.	461	357	335	283	339	160	116	83	111	96	10.9	3.6	2.7	1.6	1.7	7.9	3.3	2.1	2.5	2.0
		SD	65	43	66	29	58	19	10	9	27	19	3.4	0.9	1.1	0.2	0.4	1.5	0.4	0.3	0.6	0.4
		Δ%	0	−23	−27	−39	−26	0	−28	−48	−31	−40	0.0	−67	−75	−85	−84	0.0	−59	−73	−68	−75
	225	Avg.	461	278	315	245	208	160	85	96	70	61	10.9	2.2	2.5	1.4	1.1	7.9	2.6	2.7	1.9	1.8
		SD	65	21	105	40	17	19	14	36	11	9	3.4	0.3	1.5	0.4	0.1	1.5	0.4	1.0	0.2	0.2
		Δ%	0	−40	−32	−47	−55	0	−47	−40	−56	−62	0.0	−80	−77	−87	−90	0.0	−67	−66	−76	−77
SRFR - Radial (axially notched)	175	Avg.	313	267	229	302	272	81	83	72	80	68	2.2	1.3	1.3	1.0	0.9	1.3	0.9	0.8	0.9	0.9
		SD	62	37	42	53	15	15	8	8	9	6	0.7	0.2	0.3	0.2	0.0	0.2	0.1	0.1	0.1	0.1
		Δ%	0	−15	−27	−4	−13	0	2	−11	−2	−17	0.0	−43	−43	−53	−61	0.0	−27	−40	−29	−34
	200	Avg.	313	230	237	213	239	81	83	65	69	72	2.2	1.1	1.0	0.7	0.7	1.3	0.9	0.7	0.9	0.8
		SD	62	30	36	24	29	15	10	8	17	14	0.7	0.1	0.1	0.1	0.1	0.2	0.1	0.0	0.1	0.1
		Δ%	0	−27	−24	−32	−24	0	2	−21	−15	−12	0.0	−50	−55	−68	−66	0.0	−33	−47	−33	−37
	225	Avg.	313	193	213	198	151	81	80	72	55	44	2.2	0.8	0.9	0.6	0.5	1.3	0.9	0.8	0.8	0.8
		SD	62	22	59	18	41	15	16	41	5	11	0.7	0.0	0.5	0.1	0.1	0.2	0.2	0.2	0.1	0.1
		Δ%	0	−38	−32	−37	−52	0	−2	−11	−33	−46	0.0	−64	−58	−75	−79	0.0	−29	−39	−40	−41
ETFE - Axial (radially notched)	175	Avg.	1657	1697	1704	1690	1747	228	291	251	310	335	3.1	4.2	3.2	3.8	2.9	5.6	3.0	2.1	2.3	1.9
		SD	106	158	305	137	77	36	50	34	16	25	0.4	0.7	0.3	0.9	0.1	1.6	0.6	0.5	0.7	0.1
		Δ%	0	2	3	2	5	0	28	10	36	47	0.0	34	3	22	−8	0.0	−47	−63	−58	−66
	200	Avg.	1657	1537	1655	1903	1680	228	245	242	319	231	3.1	3.1	4.2	4.5	2.3	5.6	2.4	2.3	2.5	1.5
		SD	106	143	148	191	142	36	23	37	20	14	0.4	0.3	1.5	1.3	0.5	1.6	0.4	0.9	0.3	0.1
		Δ%	0	−7	0	15	1	0	8	6	40	1	0.0	−1	35	45	−28	0.0	−58	−59	−54	−73
	225	Avg.	1657	1626	1602	1719	1770	228	161	171	199	156	3.1	2.9	3.1	2.5	2.3	5.6	1.8	2.0	1.8	1.5
		SD	106	46	100	102	95	36	12	31	44	18	0.4	0.2	0.6	0.5	0.5	1.6	0.1	0.3	0.3	0.3
		Δ%	0	−2	−3	4	7	0	−29	−25	−13	−32	0.0	−9	−2	−20	−25	0.0	−67	−64	−67	−72
ETFE - Radial (axially notched)	175	Avg.	1553	1460	1504	1540	1586	372	420	417	385	388	2.5	2.5	2.3	2.2	2.1	1.9	1.3	1.1	1.2	1.3
		SD	168	59	77	167	128	17	26	28	33	55	0.4	0.2	0.1	0.2	0.5	0.1	0.1	0.1	0.1	0.2
		Δ%	0	−6	−3	−1	2	0	13	12	4	4	0.0	0	−9	−13	−18	0.0	−28	−41	−34	−32
	200	Avg.	1553	1578	1450	1612	1778	372	406	366	350	339	2.5	2.5	2.3	2.3	2.0	1.9	1.1	1.0	1.0	0.9
		SD	168	164	127	86	121	17	23	19	27	29	0.4	0.2	0.2	0.2	0.2	0.1	0.1	0.0	0.1	0.1
		Δ%	0	2	−7	4	14	0	9	−2	−6	−9	0.0	16	−8	−11	−23	0.0	−40	−45	−47	−53
	225	Avg.	1553	1640	1515	1603	1794	372	392	374	310	322	2.5	2.2	1.9	1.8	1.4	1.9	1.0	0.8	1.0	0.7
		SD	168	96	61	202	124	17	42	59	54	48	0.4	0.2	0.1	0.3	0.2	0.1	0.2	0.1	0.3	0.1
		Δ%	0	6	−2	3	15	0	5	1	−17	−13	0.0	−14	−23	−29	−45	0.0	−49	−57	−45	−63

TABLE A.22.—SUMMARY OF THERMAL PROPERTIES OF O-RING CANDIDATES AFTER THE ACCELERATED THERMAL AGING EXPOSURES

Sample type	Aging *t*, day		0	15	50	99	174	0	15	50	99	174	0	15	50	99	174	0	15	50	99	174	0	15	50	99	174	0	15	50	99	174	0	15	50	99	174
	Aging *T*, °C		mDSC/DSC, T_g, °C					mDSC/DSC, T_m, °C					mDSC/DSC, ΔH_m, J/g					mDSC/DSC, T_{exo}, °C					mDSC, ΔH_{exo}, J/g					TGA, T_d, °C					TGA, Δwt%, RT-100 °C				
S1151	Avg.	175						–43	–43	–43	–43	–43	3.5	3.8	3.2	3.0	2.4	375	372	376	374	375	79.9	73.3	72.3	71.8	58.9	503	498	490	498	492	0.74	0.61	0.74	0.77	0.73
		200						–43	–43	–43	–43	–44	3.5	4.0	3.3	2.5	3.3	375	375	378	379	389	79.9	55.6	62.3	57.3	51.1	503	498	492	492	491	0.74	0.79	0.71	0.91	0.94
		225						–43	–44	–44	–45	–46	3.5	5.0	3.3	2.9	3.0	375	385	388	397	430	79.9	57.3	60.3	60.3	31.8	503	485	485	488	489	0.74	0.60	0.68	0.99	0.92
	SD	175						0.5	0.3	0.0	0.3	0.3	0.9	0.1	1.7	0.9	1.2	0.0	0.0	0.0	0.7	0.0	2.3	4.5	9.3	4.6	6.8	3.5	2.1	4.2	0.7	0.7	0.08	0.01	0.07	0.09	0.03
		200						0.5	0.0	0.2	0.1	0.5	0.9	1.1	1.5	1.0	0.7	0.0	0.7	1.4	0.7	2.1	2.3	9.4	2.8	19.9	8.1	3.5	0.7	3.5	1.4	2.8	0.08	0.15	0.05	0.01	0.05
		225						0.5	0.2	0.2	0.2	0.2	0.9	0.3	1.8	0.6	1.7	0.0	0.7	0.7	2.1	7.1	2.3	0.6	4.3	13.6	23.3	3.5	3.5	4.9	0.7	0.7	0.08	0.02	0.05	0.03	0.02
	%Δ	175						0	0	0	1	0	0	6	–9	–15	–33	0	–1	0	0	0	0	–8	–10	–10	–26	0	–1	–2	–1	–2	0	–18	0	4	–1
		200						0	–1	0	0	2	0	14	–6	–29	–6	0	0	1	1	4	0	–30	–22	–28	–36	0	–1	–2	–2	–2	0	7	–4	22	27
		225						0	1	3	4	8	0	41	–7	–18	–15	0	3	3	6	15	0	–28	–25	–25	–60	0	–4	–4	–3	–3	0	–19	–9	33	24
Z1028	Avg.	175	6.8	7.0	6.9	6.8	6.9											288	289	289	295	288	5.4	2.8	2.4	4.1	2.5	471	469	468	469	470	0.08	0.06	0.10	0.14	0.08
		200	6.8	7.1	7.0	7.1	7.0											288	292	291	289	289	5.4	5.2	2.0	4.1	3.7	471	469	468	469	469	0.08	0.09	0.09	0.08	0.11
		225	6.8	6.9	7.2	6.9	6.9											288	289	285	295	290	5.4	5.4	2.2	3.1	2.6	471	470	470	469	469	0.08	0.11	0.16	0.13	0.06
	SD	175	0.1	0.2	0.2	0.1	0.2											0.7	2.1	0.0	7.1	0.0	0.1	0.9	0.6	2.4	0.3	1.4	7.8	0.7	2.1	2.1	0.00	0.02	0.05	0.02	0.00
		200	0.1	0.3	0.2	0.2	0.3											0.7	1.4	4.2	0.0	1.4	0.1	1.1	0.2	0.8	0.8	1.4	1.4	1.4	0.0	0.7	0.00	0.02	0.01	0.00	0.05
		225	0.1	0.2	0.1	0.2	0.3											0.7	0.7	5.7	7.8	1.4	0.1	1.0	1.1	2.0	0.4	1.4	2.1	0.7	2.1	0.0	0.00	0.00	0.07	0.00	0.02
	%Δ	175	0	3	1	0	1											0	0	1	3	0	0	–48	–55	–24	–54	0	–1	–1	–1	0	0	–25	19	69	–4
		200	0	4	2	4	2											0	2	1	1	1	0	–5	–63	–25	–32	0	0	–1	0	–1	0	11	15	–5	41
		225	0	1	5	1	2											0	0	–1	2	1	0	1	–59	–43	–53	0	0	0	–1	0	0	39	101	59	–27

Sample type	Aging *t*, day		0	15	50	99	174	0	15	50	99	174	0	15	50	99	174	0	15	50	99	174	0	15	50	99	174
	Aging *T*, °C		TGA, Δwt%, 100-200 °C					TGA, Δwt%, at 700 °C					Iso-TGA at 200 °C, 7 hr, Initial wt loss, wt%					Iso-TGA at 200 °C, 7 hr, Dwell wt loss, wt%					Iso-TGA at 200 °C, 7 hr, Loss rate, [(wt%/min)×1000]				
S1151	Avg.	175	1.32	1.19	1.30	1.36	1.35	55.3	58.0	54.9	53.7	54.5	2.11	1.85	1.90	1.94	1.88	1.56	0.75	0.47	0.28	0.31	–1.31	–0.66	–0.57	–0.24	–0.33
		200	1.32	1.27	1.35	1.36	1.44	55.3	54.9	57.7	58.3	53.9	2.11	1.90	1.87	1.80	1.71	1.56	0.55	0.36	0.23	0.23	–1.31	–0.61	–0.44	–0.24	–0.13
		225	1.32	1.37	1.31	1.32	1.50	55.3	53.5	54.0	53.8	57.1	2.11	1.71	1.77	1.90	1.78	1.56	0.38	0.27	0.21	0.31	–1.31	–0.41	–0.22	–0.18	–0.26
	SD	175	0.16	0.00	0.13	0.04	0.02	0.3	3.9	0.1	1.1	0.1	0.45	0.02	0.02	0.03	0.06	0.19	0.02	0.03	0.04	0.01	0.32	0.16	0.01	0.03	0.06
		200	0.16	0.07	0.02	0.06	0.01	0.3	0.4	3.7	6.1	2.0	0.45	0.05	0.00	0.14	0.28	0.19	0.05	0.03	0.04	0.07	0.32	0.03	0.00	0.02	0.04
		225	0.16	0.03	0.04	0.03	0.02	0.3	1.5	0.1	0.2	5.8	0.45	0.04	0.15	0.03	0.24	0.19	0.00	0.01	0.04	0.03	0.32	0.09	0.06	0.03	0.03
	%Δ	175	0	–10	–2	3	2	0	5	–1	–3	–1	0	–12	–10	–8	–11	0	–52	–70	–82	–80	0	–50	–56	–82	–75
		200	0	–4	3	3	9	0	–1	4	5	–3	0	–10	–11	–15	–19	0	–65	–77	–85	–85	0	–53	–66	–81	–90
		225	0	3	–1	0	14	0	–3	–2	–3	3	0	–19	–16	–10	–16	0	–76	–83	–86	–80	0	–68	–83	–86	–80
Z1028	Avg.	175	0.15	0.12	0.18	0.18	0.18	87.7	85.4	89.1	88.7	84.6	0.20	0.28	0.27	0.32	0.31	0.04	0.07	0.06	0.06	0.04	–0.04	–0.06	–0.07	–0.07	–0.04
		200	0.15	0.14	0.15	0.17	0.17	87.7	85.7	89.2	87.9	88.0	0.20	0.29	0.32	0.32	0.32	0.04	0.06	0.04	0.03	0.04	–0.04	–0.06	–0.06	–0.02	–0.02
		225	0.15	0.17	0.18	0.19	0.18	87.7	86.1	89.7	88.8	87.1	0.20	0.30	0.34	0.34	0.35	0.04	0.03	0.02	0.03	0.06	–0.04	0.04	0.02	–0.01	–0.07
	SD	175	0.00	0.03	0.01	0.02	0.03	0.2	4.5	0.6	0.4	3.7	0.09	0.00	0.01	0.02	0.01	0.01	0.00	0.01	0.01	0.01	0.06	0.02	0.05	0.05	0.02
		200	0.00	0.00	0.01	0.01	0.00	0.2	4.3	0.8	0.2	1.6	0.09	0.03	0.01	0.02	0.02	0.01	0.00	0.01	0.01	0.01	0.06	0.01	0.03	0.04	0.02
		225	0.00	0.03	0.02	0.00	0.00	0.2	4.4	1.0	0.1	0.5	0.09	0.01	0.02	0.02	0.01	0.01	0.01	0.01	0.01	0.00	0.06	0.00	0.01	0.04	0.03
	%Δ	175	0	–19	22	23	18	0	–3	2	1	–4	0	40	35	64	56	0	–78	55	63	1	0	31	56	62	5
		200	0	–7	0	12	13	0	–2	2	0	0	0	44	63	61	61	0	63	2	–20	9	0	33	38	–61	–47
		225	0	10	23	26	18	0	–2	2	1	–1	0	51	72	74	77	0	–10	–34	–6	73	0	–191	–150	–67	55

TABLE A.23.—SUMMARY OF HARDNESS OF O-RING CANDIDATES AFTER THE ACCELERATED THERMAL AGING EXPOSURES

O-ring type		S1151						Z1028						
Aging *t*, day		t_o, in.	0	15	50	99	174	Sample ID	t_o, in.	0	15	50	99	174
Aging *T*, °C	Sample ID		Durometer hardness, Shore A							Durometer hardness, Shore A				
175	1-1	0.0690	78.4	81.4	83.2	78.6	83.2	1-1	0.0710	86.6	87.6	87.8	88.2	87.4
	1-2		80.2	82.4	82.6	82.8	82.0	1-2		87.4	87.2	86.6	85.8	84.0
	1-3		75.2	80.4	83.4	82.6	83.6	1-3		84.4	86.8	86.4	87.6	83.8
	2-1		81.8	81.8	83.0	84.2	83.2	2-1		86.6	81.8	87.2		86.6
	2-2		80.8	81.0	81.6	82.4	82.0	2-2		87.4	87.4	87.0		86.8
	2-3		82.0	81.4	83.4	83.4	81.4	2-3		87.4	86.8	87.2		85.4
	Avg.		79.7	81.4	82.9	82.3	82.6	Avg.		86.6	86.3	87.0	87.2	85.7
	SD		2.6	0.7	0.7	1.9	0.9	SD		1.2	2.2	0.5	1.2	1.5
	Δ%			2.1	3.9	3.3	3.6	Δ%			–0.4	0.5	0.7	–1.1
200	1-1			80.8	82.4	84.8	85.6	1-1			85.8	87.8	87.8	86.4
	1-2			80.8	82.8	82.6	85.4	1-2			86.8	87.8	86.2	86.6
	1-3			81.0	82.6	85.0	87.2	1-3			86.0	86.4	87.0	86.2
	2-1			83.2	82.8	84.6	85.0	2-1			88.0	88.2	86.2	85.0
	2-2			81.8	82.8	84.0	83.4	2-2			85.4	87.4	86.6	86.6
	2-3			81.0	82.8	84.2	84.6	2-3			85.6	87.2	86.2	87.6
	Avg.		79.7	81.4	82.7	84.2	85.2	Avg.		86.6	86.3	87.5	86.7	86.4
	SD		2.6	0.9	0.2	0.9	1.3	SD		1.2	0.98	0.63	0.64	0.84
	Δ%			2.1	3.7	5.6	6.9	Δ%			–0.4	1.0	0.0	–0.3
225	1-1			80.8	83.4	85.0	87.6	1-1			85.6	86.6	88.2	88.6
	1-2			82.6	84.4	82.6	86.8	1-2			86.4	86.2	87.8	85.4
	1-3			82.0	84.2	84.4	87.0	1-3			84.0	87.2	87.6	86.8
	2-1			84.0	83.2	85.2	88.0	2-1			87.0	85.8	88.0	87.8
	2-2			83.8	84.6	85.0	85.6	2-2			87.0	87.2	86.6	87.4
	2-3			82.6	83.8	85.6	85.8	2-3			87.2	87.6	87.0	88.0
	Avg.		79.7	82.6	83.9	84.6	86.8	Avg.		86.6	86.2	86.8	87.5	87.3
	SD		2.6	1.18	0.56	1.07	0.95	SD		1.2	1.2	0.7	0.6	1.1
	Δ%			3.6	5.3	6.1	8.9	Δ%			–0.5	0.2	1.0	0.8

TABLE A.24.—OVERALL TENSILE PROPERTIES OF S1151 O-RING AS FUNCTIONS OF TEST TEMPERATURE AND ACCELERATED AGING CONDITIONS

Test, *T*, °C	Aging, *T*, °C	Properties	Tensile strength, psi					Ultimate elongation1, %					Young's modulus1, ea., psi					Tangent modulus at ε = ~20%, ea., psi				
		Aging time, days	0	15	50	99	174	0	15	50	99	174	0	15	50	99	174	0	15	50	99	174
24	175	Avg.	1044	1101	891	1050	1132	176	134	102	117	115	759	1006	889	1010	1023	492	717	676	785	823
		SD	96	64	309	41	61	27	18	43	12	6	85	185	62	52	96	129	136	47	66	50
		Δ%	0	5	–15	1	8	0	–24	–42	–33	–35	0	33	17	33	35	0	46	37	60	67
	200	Avg.	1044	877	796	844	1067	176	108	82	78	91	759	950	929	1067	1031	492	723	754	1022	1001
		SD	96	263	273	179	113	27	45	46	30	8	85	96	62	61	61	129	4	28	15	42
		Δ%	0	–16	–24	–19	2	0	–39	–53	–56	–48	0	25	22	41	36	0	47	53	108	103
	225	Avg.	1044	821	591	540	455	176	98	39	25	1	759	990	1037	1147	1384	492	735	956	1008	1718
		SD	96	235	132	105	98	27	44	15	17	10	85	37	69	186	319	129	64	96	124	129
		Δ%	0	–21	–43	–48	–56	0	–44	–78	–86	–100	0	30	37	51	82	0	49	94	105	249
150	175	Avg.	635	641	665	673	743	121	88	64	66	57	579	805	942	836	1179	418	549	756	696	879
		SD	17	20	19	32	107	5	9	10	7	18	19	47	106	28	48	28	59	96	66	76
		Δ%	0	1	5	6	17	0	–27	–47	–45	–52	0	39	63	45	104	0	31	81	66	110
	200	Avg.	635	474	598	593	687	121	47	63	50	60	579	790	816	968	1034	418	583	649	704	850
		SD	17	131	81	54	14	5	24	13	11	5	19	7	12	55	94	28	24	46	16	11
		Δ%	0	–25	–6	–7	8	0	–61	–48	–59	–51	0	37	41	67	79	0	40	55	68	103
	225	Avg.	635	505	352	244	330	121	56	19	–5	–2	579	749	804	977	1173	418	617	766	888	1068
		SD	17	155	216	118	141	5	30	36	22	18	19	47	47	163	184	28	108	65	180	85
		Δ%	0	–20	–45	–62	–48	0	–54	–84	–104	–101	0	29	39	69	103	0	48	83	112	156
200	175	Avg.	577	452	350	488	536	45	34	23	31	43	840	761	666	808	729	722	722	624	779	693
		SD	64	60	44	2	78	5	11	12	1	14	15	45	48	30	48	48	14	84	23	19
		Δ%	0	–22	–39	–15	–7	0	–25	–48	–30	–4	0	–9	–21	–4	–13	0	0	–14	8	–4
	200	Avg.	577	356	287	343	447	45	28	5	4	21	840	615	738	920	815	722	734	712	784	823
		SD	64	297	147	166	10	5	44	12	18	1	15	133	132	16	30	48	90	251	205	57
		Δ%	0	–38	–50	–41	–22	0	–38	–89	–91	–54	0	–27	–12	9	–3	0	2	–1	9	14
	225	Avg.	577	469	440	361	399	45	28	26	2	11	840	732	738	1016	888	722	827	819	933	963
		SD	64	139	70	142	118	5	20	5	18	16	15	32	179	154	45	48	24	196	122	48
		Δ%	0	–19	–24	–37	–31	0	–37	–41	–94	–75	0	–13	–12	21	6	0	15	13	29	33

TABLE A.25.—OVERALL TENSILE PROPERTIES OF Z1028 O-RING AS FUNCTIONS OF TEST TEMPERATURE AND ACCELERATED AGING CONDITIONS

Test, *T*, °C	Aging, *T*, °C	Properties	Tensile strength, psi					Ultimate elongation1, %					Young's modulus1, ea., psi					Tangent modulus at ε = ~20%, ea., psi				
		Aging time, days	0	15	50	99	174	0	15	50	99	174	0	15	50	99	174	0	15	50	99	174
24	175	Avg.	2740	2544	2738	2802	2803	140	111	120	127	123	1056	1063	1085	1141	1121	1624	1700	1681	1768	2066
		SD	172	283	144	75	36	19	19	13	10	2	80	47	21	28	24	53	21	25	164	96
		Δ%	0	–7	0	2	2	0	–21	–14	–10	–12	0	1	3	8	6	0	5	4	9	27
	200	Avg.	2740	2695	2884	2854	2857	140	121	114	113	108	1056	1042	1200	1149	1115	1624	1679	1826	2000	2039
		SD	172	121	267	212	44	19	9	15	10	4	80	32	156	77	14	53	130	172	184	60
		Δ%	0	–2	7	–1	0	0	–14	–19	–19	–23	0	–1	14	9	6	0	3	12	23	26
	225	Avg.	2740	2894	2726	3041	2829	140	122	98	112	97	1056	1091	1334	1121	1151	1624	1598	1908	2249	2286
		SD	172	55	224	127	477	19	4	7	7	15	80	55	182	36	93	53	29	264	57	143
		Δ%	0	6	–1	11	3	0	–13	–30	–20	–31	0	3	26	6	9	0	–2	18	39	41
150	175	Avg.	593	553	606	574	644	86	72	73	57	78	538	556	577	619	566	415	452	470	559	463
		SD	128	48	63	59	75	15	5	3	7	6	6	3	21	29	23	43	56	33	37	44
		Δ%	0	–7	2	–3	9	0	–17	–15	–34	–10	0	3	7	15	5	0	9	13	35	12
	200	Avg.	593	606	702	604	673	86	79	90	60	73	538	540	529	604	565	415	436	438	547	495
		SD	128	27	45	18	117	15	3	6	5	8	6	13	9	20	47	43	50	8	41	39
		Δ%	0	2	19	2	14	0	–8	4	–31	–15	0	0	–2	12	5	0	5	5	32	19
	225	Avg.	593	617	560	662	708	86	84	68	72	79	538	506	523	578	542	415	400	451	490	477
		SD	128	28	57	68	80	15	4	2	5	7	6	30	27	57	15	43	25	27	59	5
		Δ%	0	4	–6	12	20	0	–3	–21	–17	–9	0	–6	–3	7	1	0	–4	9	18	15
200	175	Avg.	712	631	402	572	544	77	70	37	63	56	646	631	629	594	621	559	533	556	547	555
		SD	19	1	95	29	1	13	1	13	4	1	23	3	30	13	36	48	3	32	7	1
		Δ%	0	–11	–44	–20	–24	0	–8	–52	–18	–27	0	–2	–3	–8	–4	0	–5	–1	–2	–1
	200	Avg.	712	537	568	609	704	77	61	52	64	67	646	592	654	627	648	559	508	606	543	591
		SD	19	86	70	61	70	13	9	5	11	1	23	21	17	23	15	48	21	24	25	75
		Δ%	0	–25	–20	–14	–1	0	–21	–33	–17	–13	0	–8	1	–3	0	0	–9	8	–3	6
	225	Avg.	712	474	542	646	606	77	53	53	64	70	646	586	639	611	558	559	521	558	568	490
		SD	19	44	148	142	141	13	6	19	7	3	23	9	28	30	65	48	12	2	58	82
		Δ%	0	–33	–24	–9	–15	0	–31	–31	–17	–9	0	–9	–1	–5	–14	0	–7	0	1	–12

References

1. Dudzinski, L.A., Hamley, J.A., McCallum, P.W., Sutliff, T.J., Zakrajsek, J.F., NASA's Radioisotope Power Systems Program Status. In: 11th International Energy Conversion Engineering Conference (IECEC) proceedings. 14-17 Jul. 2013; San Jose, California
2. Hibbard, K.E., Mason, L.S., Ndu, O., Smith, C., Withrow, J.P., Stirling to Flight Initiative. In: Proceedings of IEEE Aerospace Conference 2016. 5-12 Mar. 2016; Big Sky, MT.
3. Chan, J., Wood, J.G., Schreiber, J.G., Development of Advanced Stirling Radioisotope Generator for Space Exploration. NASA/TM—2007-214806, NASA Glenn Research Center. May 2007.
4. Wilson, S.D., Wong W.A., NASA Glenn Research Center Support of the Advanced Stirling Radioisotope Generator Project. NASA/TM—2015-218462, NASA Glenn Research Center. April 1, 2015.
5. Wong, W.A., Wilson, S.D., Collins J., and Wilson, K., Advanced Stirling Convertor (ASC) Technology Maturation. NASA/TM—2016-218908. NASA Glenn Research Center. August 2016.
6. Shin, E.E., Evaluation and Validation of Organic Materials for Advanced Stirling Convertors (ASCs): Overview. In: 13th International Energy Conversion Engineering Conference (IECEC) Proceedings. AIAA Propulsion and Energy Forum and Exposition 2015, ECD-02, Stirling Components session, 27-29 July 2015, Orlando, Florida.
7. Shin, E.E., Sutter J.K., Thieme L., Organics Evaluated for Advanced Stirling Convertor (ASC), R&T Research and Technology 2006, NASA/TM—2007-214479, GRC, Cleveland, OH, p252-253, 2006.
8. Shin, E.E., Pepper, S., Sutter, J., and Thieme, L., Compilation of Monthly Reports (October/November 2000 through December 2005) for the Evaluation of Key Organic Materials in the SRG110 Stirling Convertor. NASA-GRC Preliminary Information Release (PIR) PIR # ST-06-006, Feb 2006.
9. Shin, E.E., Scheiman, D., Cybulski, M., Quade, D., Inghram, L., and Burke, C., Validation of Organics for Advanced Stirling Convertor (ASC). In: Proceedings of Space Technology and Application International Forum (STAIF)-2008, Albuquerque, NM, Feb 10 – 14, 2008, AIP Conference Proceedings, Vol. 969, Edited by Mohamed S. El-Genk, pp 570-581.
10. Mireles, O.R., Shin, E.E., Bowman, C., Vesudevan, L., Mixed Neutron & Gamma-Ray Testing of Stirling-Alternator Candidate Organic Materials. In: Proceedings of IECEC 2010, 8th Annual International Energy Conversion Engineering Conference, Paper# 769917, 25 – 28 July 2010, Nashville, TN.
11. Mireles, O.R., Shin, E.E., and Bowman, C., Post-Irradiation Evaluation of the Stirling Alternator Radiation Test Article. IN: Proceedings of ICAPP 10, San Diego, CA, USA, June 13-17, 2010, Paper 10008